

Functional renormalization group in Floquet space applied to periodically driven quantum dots

Von der Fakultät für Mathematik, Informatik und Naturwissenschaften
der RWTH Aachen University zur Erlangung des akademischen Grades
einer Doktorin der Naturwissenschaften genehmigte Dissertation

vorgelegt von

Anna Katharina Eissing, M.Sc.

aus Papenburg



Berichter:

Universitätsprofessor Dr. rer. nat. Volker Meden

Universitätsprofessor Dr. rer. nat. Herbert Schoeller

Tag der mündlichen Prüfung:

21. Februar 2017

Diese Dissertation ist auf den Internetseiten der Universitätsbibliothek online verfügbar.

Contact Information:

Anna Katharina Eissing

**Institut für Theorie der Statistischen Physik
Physikzentrum, RWTH Aachen
52056 Aachen**

phone: +49 241 8027032

email: eissing (at) physik.rwth-aachen.de

Preface

The present thesis has greatly benefited from numerous discussions with my colleagues and I would like to express my gratitude for their help during my PhD studies.

First of all, I would like to thank Volker Meden for giving me the opportunity to work and learn in his group. I enjoyed writing my PhD thesis under his supervision and highly appreciate that he always made time for my questions.

Further I owe a great debt of gratitude to Dante Kennes, who supported the project from the first minute. We had countless discussions, in which he shared a lot of his knowledge of the quantum many-body physics with me.

I would like to thank Herbert Schoeller for answering my questions about the Floquet-Liouville space and for co-refereeing this thesis.

The work has further benefited from discussions with Janine Splettstoesser, Thilo Plücker and Takafumi Suzuki. Takafumi has visited the group in spring 2015 and introduced us to his work about photon-assisted current noise in quantum dots.

Financial support from the Deutsche Forschungsgemeinschaft via the Research Training Group 'Quantum Many-Body Methods in Condensed Matter Systems' (RTG 1995) is acknowledged.

Contents

Preface	iii
Introduction	1
1 Short Summary	3
2 Introduction	5
3 Model: Interacting Resonant Level Model	9
3.1 Open quantum dot system	9
3.2 Field theoretical IRLM	10
3.3 Three site IRLM	10
3.4 Transformation of the time dependency of the chemical potential	12
3.5 The equilibrium IRLM	13
Methods	17
4 Floquet-Green's Function	19
4.1 Keldysh Green's function	20
4.1.1 Green's function	20
4.1.2 Keldysh formalism	20
4.1.3 Dyson equation	22
4.2 Generating Functionals	24
4.2.1 Grassmann algebra and Functional integrals	24
4.2.2 Functional Integral Representation of the Keldysh Green's functions	25
4.2.3 Generating Functionals	27
4.3 Floquet theory	29
4.4 Floquet-Green's function	30
4.4.1 Transformation to Floquet space	30
4.4.2 Symmetries	31
4.4.3 Dyson equation	31
4.5 Reservoir self-energy: Dressed Green's function	32
4.5.1 Reservoir Green's functions	32
4.5.2 Projection Technique: Reservoir self-energy	32
4.5.3 Dissipation Fluctuation Theorem for Reservoir Self-energy	33
4.6 Observables	34
4.6.1 Occupancy	34
4.6.2 Charge susceptibility	34
4.6.3 Current	35
4.6.4 Pumped charge	35
4.6.5 Linear conductance	36
4.6.6 Spectral function	36

5	Functional Renormalization Group in Floquet space	37
5.1	Fundamental idea	37
5.2	Flow equation	38
5.2.1	Derivation	38
5.2.2	Initial condition	41
5.2.3	Truncation	42
5.3	Flow equation in Floquet space	43
5.3.1	Cutoff scheme: Auxiliary reservoirs	43
5.3.2	Flow Equation	44
5.3.3	Symmetries: A short discussion	44
5.3.4	Renormalized parameters	45
5.3.5	Numerical implementation	45
6	Perturbation Theory in Floquet-Liouville Space	49
6.1	Liouville space and its kinetic equation	49
6.1.1	Liouville space	49
6.1.2	Kinetic equation	50
6.1.3	Diagrammatics	51
6.1.4	Observable: Current	54
6.2	Floquet-Liouville space	54
6.2.1	Diagrammatic in Floquet space	54
6.2.2	General form of the RLM Liouvillian	56
6.3	Markov approximation and Perturbation Theory	57
6.3.1	Perturbation Theory in RLM: First order diagramm	57
6.3.2	Markov approximation in Floquet space	58
6.3.3	Quantum Master equation in Floquet Space	60

Dynamics in Periodically Driven Quantum Dots 61

7	Renormalization in Periodically Driven Quantum Dots	63
7.1	The equilibrium IRLM	64
7.2	The time independent non-equilibrium IRLM	65
7.3	The time dependent non-equilibrium IRLM	68
7.4	From transient behavior to the periodic steady state	69
7.5	Time periodically driven IRLM in the limit of small driving amplitude	70
7.5.1	Setup and Protocols	70
7.5.2	Keldysh Green's function in the limit of small driving amplitudes	71
7.5.3	Mean value: $k = 0$ component	73
7.5.4	Protocol 1: Time periodic $\tau_L(t)$	75
7.5.5	Protocol 2: Time periodic $\tau_L(t)$ and $\tau_R(t)$	79
7.5.6	Protocol 3: Time periodic $\epsilon(t)$	80
7.5.7	Protocol 4: Time periodic $\tau_L(t)$ and $\epsilon(t)$	84
7.6	Tuning the effective reservoir distribution function	85
7.6.1	Setup and Illustration of the physical situation	85
7.6.2	Effect on the Renormalization flow	86
7.7	Conclusion	88
8	Transport in Periodically Driven Quantum Dots	91
8.1	Transport in the time independent non-equilibrium IRLM	92
8.2	Transport in the adiabatic limit	92
8.2.1	Dot Occupancy	93
8.2.2	Current for a varying onsite energy	93
8.2.3	Parametric quantum pumps	94

8.3	Quantum pumps: Two parameter pump	95
8.4	Quantum pumps: Single parameter pump	98
8.4.1	Susceptibility	99
8.4.2	Pumping power	102
8.4.3	Perturbation Theory in Liouville space: Mean current	104
8.5	Current and Conductance of non-sinusoidal signals	105
8.6	Conclusion	108
Conclusion & Outlook		111
9	Conclusion & Outlook	113
Supplements		117
	Bibliography	119
	List of Publications	125
	Curriculum Vitae	127
Thank You!		129

Introduction

Chapter 1

Short Summary

Quantum dot systems controlled by external fields which are periodic in time with a frequency Ω have been subject of a lot of experimental research [Pot92, Swi99, Kae15], lately. At the same time a broad range of theoretical approaches for its description have been developed [Tho83, Bru94, Bro98, Spl06, Mos02, Pla04]. These systems exhibit interesting effects such as pump mechanisms, where charge is transported due to the periodic oscillation of the confining potentials without any applied bias voltage [Swi99, Bro98]. The adiabatic limit of a small driving frequency Ω (compared to all other energy scales of the system) is a well studied regime, where it can be explicitly taken advantage of the small parameter Ω [Mos04a, Spl06]. Equally, a very large driving frequency (anti-adiabatic limit) can be exploited to set up an efficient approach [Het95, Bra08, Cro12b]. However, also the intermediate regime shows intriguing physics [Mos02, Cav09, Bra08, Cro12b, Cro12a, Kas12]. In any regime treating a two-particle Coulomb interaction still is an obstacle when describing time periodic quantum systems [Bru97, Spl06].

The functional renormalization group (FRG) has proved to be an unbiased tool to study correlation effects for small to intermediate interactions in a wide range of low-dimensional systems [Met12]. Relying on the Wilsonian renormalization group (RG) idea [Wil74], it constitutes a very flexible tool to be set up in various bases or formulations. The main goal of the present thesis is to set up the FRG formalism in Floquet space to treat interacting, time periodic quantum dots and to investigate the consequential renormalization of the parameters and the transport through the dot.

Functional renormalization group in Floquet space

Building upon the time independent, steady state description in frequency space [Kar06, Kar10a, Jak09] and a time dependent FRG formulation [Ken11, Ken14], we tackle the steady state of periodically driven quantum dots. We focus on the long time behavior where all transients have died out, and therefore the entire system is characterized by the same periodicity as given by the driven external fields. As a consequence, we can transform the according time dependent flow equation to Floquet space using Floquet-Green's functions [Arr05, Arr06, Tsu08, Ste08, Gen15]. It allows us to study quantum dot systems in the whole range of driving frequency and amplitude in the presence of a small Coulomb interaction.

We exemplify the potential of our approach by applying it to the interacting resonant level model (IRLM), describing an idealized single level quantum dot dominated only by charge fluctuations. It constitutes an interesting model which is well known for its intriguing renormalization physics resulting in power law behavior in the renormalized parameters and transport observables [Sch80a, Sch82a, Bor07, Doy07, Bou08, Kar10c].

Renormalization in time periodic systems: Role of the driving frequency

We investigate the role of the driving frequency Ω in the RG flows of the time periodic parameters of the IRLM. The small driving amplitude limit allows to complement our numerical solution by analytic expressions of the renormalization of all dot parameters to the leading order of driving

amplitude over mean value. Four different configurations are studied, where distinct combinations of the hopping and/or onsite energy of the dot are chosen to be time periodic. The transparent structure of the renormalization of the parameters in this limit, allows for an analytic treatment of all higher harmonics, where $k\Omega$ is identified as the relevant energy scale in the k th harmonic, rendering the mean value independent of the time periodicity. The various protocols reveal very different RG flows. It ranges from a transparent infrared cutoff $k\Omega$ yielding an according power law in the driving frequency to RG flows, which are characterized by an involved interplay of all present energy scales. Even beyond the small driving amplitude limit the RG flow is discussed with the help of an effective reservoir distribution function which can be defined in this setup and its form is defined by the ratio of driving amplitude and frequency [Suz15].

Transport through the interacting time periodic quantum dot

The second focus is directed to the transport in the time periodic quantum dot systems and how it is affected by the Coulomb interaction. Based on the well studied parameter pump in the adiabatic limit [Bro98], where two parameters are varied periodically and phase shifted, we like to investigate the pumped charge in the whole regime of driving frequency and amplitude including interaction in such a setup. Further a single parameter pump is realized and the charge susceptibility as well as the mean current are studied. The latter reveals power law behavior on the driving frequency. A quantum master equation calculation in Floquet-Liouville space complements the FRG results to study the requirements of such a single parameter quantum pump. Finally, the conductance and the current are considered for several time periodic hoppings of non-sinusoidal form.

Chapter 2

Introduction

Quantum information processing has recently gained a lot of interest. Its key idea is to exploit quantum mechanical properties such as e.g. the superposition of states to perform certain numerical tasks in a more efficient way [DiV95]. Those quantum computers are built of quantum mechanical bits, so called qubits. One possible realization of such a qubit is a quantum dot, a nanodevice, which constitutes a spatial confinement in all three dimensions and is therefore considered to be a zero dimensional system [Han07]. The realization of a quantum computer, which consists of more than a few qubits and which performs a numerical computation with a certain fidelity still poses a major challenge asking for further theoretical and experimental research [DiV95]. Among others a detailed understanding of the transport properties of a quantum dot is required, in particular if Coulomb interaction is included. Thus, quantum dot systems have been subject of extensive research in the last years, theoretically as well as experimentally [Han07], and a comprehensive insight of their physical properties is a step on the route of the development of more complicated components for possible quantum processing devices.

Time periodically driven systems

One active field of research concentrates on setups with time periodically varying external fields with a driving frequency Ω [Pla04, Roc13]. A possible application is the quantum pump, where charge is transported by periodic oscillations of the confining potentials without any applied bias voltage. Thouless suggested an analogon of the classical peristaltic pump such that by an adiabatic variation of the external fields, where the driving frequency is small compared to all other energy scales in the system, quantized particle transport can be observed [Tho83]. This has stimulated further theoretical research of pumping mechanism in the adiabatic limit [Bro98] as well as beyond it [Bru94, Het95, Bru97]. According experiments have been realized in the adiabatic limit [Swi99] or for larger driving frequency [Kae15, Roc13]. The quantization of the transported charge ne has then led to the idea of a single electron pump [Pot92, Kae15] as well as single electron currents which could be used as a new standard of the current [Pek13].

The theoretical description of time periodic systems relies mainly on the Floquet theory. It is based on the Floquet theorem that specifies the class of solutions to periodic linear differential equation [Flo83]. Using this theorem, the time dependent Schrödinger equation can be brought to an effective, time independent form in the long-time limit; simplifying the solution significantly [Shi65, Gri98, Pla04]. This renders the underlying Fourier basis the appropriate basis for the description of time periodic problems.

One possible route to describe transport through these systems uses the scattering matrix approach of Büttiker, Thomas and Prêtre [Büt94]. It has been applied to the parameter pump by Brouwer [Bro98] in the adiabatic limit. Employing Floquet theory, it is extended to the Floquet scattering theory for arbitrary driving frequency and amplitude [Mos02]. The so-called 'Floquet engineering' constitutes an approach with which the effective, time independent Floquet Hamiltonians are calculated to describe the dynamics of the system, including transient behavior [Buk15].

Especially the adiabatic regime of a small driving frequency is well studied, since it can be explicitly taken advantage of the driving frequency as a small parameter [Ale98, Spl05, Spl06, Riw10, Mos04a, Mos04b, Riw13]. In the opposite, anti-adiabatic limit the driving frequency constitutes the largest energy scale, which can be used for an efficient description [Het95, Bra08, Cro12b]. Yet, the intermediate regime also shows interesting effects such as single parameter pumping and reversion of the pump direction [Cit03, Cav09, Bra08, Cro12b, Cro12a, Kas12, Kae08].

However, to include Coulomb interaction in the description of the many body problem, still poses a major challenge [Bru94, Het95, Bru97, Cit03, Spl06, Win13, Hil10, Hil11, Her09, Suz15]. We thus aim to develop a method with which one can approach interacting, low-dimensional quantum systems, where the driving amplitude and frequency are not subject to any constraints.

Method Development: Functional Renormalization Group in Floquet Space

The functional renormalization group (FRG) has proven to be a versatile tool to treat low-dimensional systems with interaction [Met12]. It provides us with an infinite hierarchy of flow equations describing the complete many body problem and which - when solved exactly - would provide the exact solution. Only due to the necessary truncation of this hierarchy, the method is restricted to small to intermediate interactions. FRG has been extended recently to explicitly time dependent Hamiltonians [Ken12a]. With this method it is feasible to tackle the transient as well as the long time behavior of time dependent quantum systems, including time periodic ones. However, to reach the steady state is numerically costly in this approach as each time step is calculated explicitly and the treatment is too involved to derive analytic expressions from this formulation. In this thesis, we aim at the long time behavior, where all transient dynamics has died out, such that the whole system has inherited the given periodicity. It is taken explicitly advantage of the time periodicity of the steady state by using Floquet-Green's functions [Arr05, Arr06, Tsu08, Ste08, Gen15], such that the flow equation is transformed from its explicitly time dependent formulation to Floquet space.

The quantum dot is modeled as an idealized, single level quantum dot by the interacting resonant level model (IRLM). The influence of the time periodically varied external fields is represented as usually by time dependent parameters $p(t)$ (referred to as 'signal' in the following) in this microscopic model [Bro98, Spl05, Spl06, Hil10, Her09, Hau13, Cav09, Cro12b, Kas12, Mos02, Koh05]. These signals can be of arbitrary form, e.g. sinusoidal or triangular form, without any restrictions on the driving amplitude.

One advantage of the method employed in the present work is the opportunity to consider the renormalization of the dot parameters explicitly and even derive analytic expressions for them in certain limits. This way we can first understand the renormalization of the parameters, and only subsequently consider the resulting transport properties. The dependency of the observables on the renormalized parameters is not always transparent, but the discovered renormalization can guide the understanding. On the other hand, some observables can even be computed analytically. Here we benefit from the details of the utilized truncation of the FRG which allows to derive analytic expressions in the non-interacting setup and afterwards substitute the parameters by their renormalized equivalents. As a consequence, the presentation of the results is twofold: First the renormalization of the parameters is discussed, the second part illuminates the transport in the interacting setups.

Renormalization physics

The unbiased approach without any assumptions concerning the time periodicity allows to tackle the renormalization physics of the periodically driven IRLM. Since it allows to consider the whole range of driving frequency, the role of the energy scale Ω in the RG flow can be examined. Earlier studies show that the IRLM provides intriguing physics of competing energy scales, where power law behavior can be observed in the limit of one energy scale much larger than the oth-

ers [Sch80a, Sch82a, Bor07, Bor08, Bou08, Doy07, Kar10c]. Based on this, the role of the driving frequency Ω as an additional energy scale in the renormalization flow is approached.

First the small amplitude limit is analyzed, which allows to complement the full numerical solution of the truncated flow equations by analytic expressions for the renormalization of hopping and onsite energy in four different driving protocols. It makes it feasible to identify the role of Ω and detect a new power law depending on the driving frequency in one protocol.

Next, the onsite energy is driven periodically with arbitrary driving frequency and amplitude. To illustrate the physical situation at hand an effective reservoir distribution function is defined: It is of staircase form with steps at multiples of Ω , the ratio of driving amplitude and driving frequency defines the height of each step. As a consequence, different physical situations can be created by a certain choice of the ratio, which enable us to examine the influence of the reservoir distribution function and with this the driving frequency on the RG flow beyond the small amplitude limit.

Transport in periodically driven quantum dots

In the second part we focus on transport in time periodic and interacting dot systems. Transport in the adiabatic and small amplitude limit is considered in the beginning. It is studied which of the known physics in the time-independent steady state can be found in the time periodic setup. Starting from the peristaltic pump [Bro98], where analytic expressions are available in the small amplitude limit [Spl07], we explore the pumping setup in the whole regime of frequency and amplitude. We focus mainly on the pumped charge Q , comparing results in the interacting and non-interacting regime.

Based on the rich renormalization physics observed for the hopping when only this parameter is periodically varied, transport in this setup is considered. The charge susceptibility as well as the mean current are examined here for a single parameter pump realized by an harmonic driving. The dc current is calculated in two different ways: FRG calculations are supplemented by quantum master equation calculations in Floquet space for a finite temperature. With this we demonstrate that a finite current can be obtained already via quantum master equations. Finally, conductance and current are regarded for non-sinusoidal signals of the hopping.

Outline

The outline of the present thesis is as follows: The subsequent Chapter 3 introduces the interacting resonant level model as the main model of interest. A short introduction in the known equilibrium physics is given. The Keldysh Green's functions are introduced and their generating functionals are defined in Chapter 4. Subsequently, these Green's functions are transformed to Floquet space, using the Fourier basis as a convenient basis to treat time periodically driven systems. This is complemented by an explanation of the reservoir dressed Green's function to treat the open system and finally the single-particle observables are defined. Next, the functional renormalization group is introduced and the flow equations derived in Chapter 5. The truncation is chosen and the resulting flow equation from the explicit time dependent formulation transformed to Floquet space. The methodical part of the thesis is finished by the presentation of the perturbation theory calculation in Floquet-Liouville space with the Markov approximation of Chapter 6. Thereafter the functional renormalization group in Floquet space is used to examine the renormalization in periodically driven quantum dots (Chapter 7) and the transport in interacting quantum dot systems is considered (Chapter 8). In Chapter 9 we draw a conclusion and a short outlook is given.

Chapter 3

Model: Interacting Resonant Level Model

Contents

3.1	Open quantum dot system	9
3.2	Field theoretical IRLM	10
3.3	Three site IRLM	10
3.4	Transformation of the time dependency of the chemical potential	12
3.5	The equilibrium IRLM	13

The present chapter starts with introducing a general few level quantum dot model which can be investigated employing the method devised within our work. We then focus on the interacting resonant level model (IRLM), the main model tackled in the present thesis. It is a prototype model of a single level quantum dot dominated by charge fluctuations. This rather simple model shows divergencies in the wide band limit when tackled by ordinary perturbation theory, requiring for alternative methods. Several approaches have been employed [Noz69, Fil81, Sch80a, Sch80b, Sch82a, Sch82b, Sch82c, Doy07, Bor07, Bou08] including the FRG [Kar10c, Ken12a] utilized here. It has been demonstrated that the IRLM is characterized by intriguing power law behavior in the equilibrium as well as the non-equilibrium.

After the introduction of the well known field-theoretical realization of the IRLM, it is discussed how it can be realized by a three site model to include the interaction as an on-dot parameter, as necessary for our approach. For this, the wide band limit of a large structureless band is employed. This is followed by an explanation of a gauge transformation to shift the time-dependency of the chemical potentials of the reservoirs to a phase of the hopping elements in the wide band limit. Finally the known physics in equilibrium is reviewed including a short discussion of the failure of the perturbation theory and the power law behavior in equilibrium yielding to the definition of a low-energy scale T_K .

3.1 Open quantum dot system

The method devised in the present thesis is applicable to any few level quantum dot with a Hamiltonian of the form

$$H(t) = H_{\text{dot}}(t) + \sum_{\alpha} [H_{\text{coup},\alpha}(t) + H_{\text{res},\alpha}], \quad (3.1.1)$$

with a general dot Hamiltonian, which consists of a single particle term and the properly anti-symmetrized matrix element of the two-particle interaction,

$$H_{\text{dot},0}(t) = \sum_{ij} \epsilon_{ij}(t) d_i^{\dagger} d_j, \quad (3.1.2)$$

$$H_{\text{dot},\text{int}}(t) = \sum_{ijkl} \bar{u}_{ijkl}(t) d_i^{\dagger} d_j^{\dagger} d_l d_k. \quad (3.1.3)$$

ϵ_{ij} describes the on dot hopping terms as well as the onsite energy, while the two-particle interaction describes the Coulomb interaction. Here $d^{(\dagger)}$, d are annihilation (creation) operators on the dot and the i, j, k, l label the levels of the dot. The two leads ($\alpha \in R, L$) are modeled as non-interacting and are tunnel-coupled to the dot

$$H_{\text{coup},\alpha}(t) = \sum_{i,q_\alpha} v_{q_\alpha,i}(t) d_i^\dagger c_{q_\alpha} + \text{H.c.}, \quad (3.1.4)$$

$$H_{\text{res},\alpha} = \sum_{q_\alpha} \epsilon_{q_\alpha} c_{q_\alpha}^\dagger c_{q_\alpha}, \quad (3.1.5)$$

with annihilation (creation) operators $c_{q_\alpha}^{(\dagger)}$ of reservoir electrons. Any of the parameters indicated by the argument t can be assumed to be time periodic with the same period T .

Initial statistics

The initial density matrix at time t_0 is assumed to be of the form

$$\rho_0 = \rho(t = t_0) = \rho_0^{\text{dot}} \otimes \rho_{\alpha_1,0}^{\text{res}} \otimes \rho_{\alpha_2,0}^{\text{res}} \otimes \dots \otimes \rho_{\alpha_n,0}^{\text{res}}, \quad (3.1.6)$$

with the reservoirs in grand-canonical equilibrium

$$\rho_{\alpha,0}^{\text{res}} = e^{-(H_{\text{res},\alpha} - \mu_\alpha N_\alpha)/T_\alpha} / \text{Tr} e^{-(H_{\text{res},\alpha} - \mu_\alpha N_\alpha)/T_\alpha}, \quad (3.1.7)$$

with temperature T_α , particle number operator $N_\alpha = \sum_{q_\alpha} c_{q_\alpha}^\dagger c_{q_\alpha}$ and chemical potential μ_α . For $t < t_0$ the dot is assumed to be empty and decoupled.

3.2 Field theoretical IRLM

The interacting resonant level model is characterized by the following dot and coupling Hamiltonian

$$H_{\text{dot}} = \epsilon d^\dagger d, \quad (3.2.1)$$

$$H_{\text{coup}} = \sum_{q,\alpha=L,R} \frac{t_\alpha(t)}{\sqrt{\rho_\alpha^{(0)}}} (d^\dagger c_{q,\alpha} + \text{H.c.}) + \left(d^\dagger d - \frac{1}{2}\right) \sum_{q,q',\alpha=L,R} \frac{\tilde{u}_\alpha(t)}{\rho_\alpha^{(0)}} : c_{q,\alpha}^\dagger c_{q',\alpha} :, \quad (3.2.2)$$

where the dot and reservoir creation (annihilation) operators are denoted by $d(d^\dagger)$ and $c_{q,\alpha}(c_{q,\alpha}^\dagger)$, respectively. $: \dots :$ indicates normal ordering, $\rho_\alpha^{(0)}$ is the reservoir density of states at the Fermi level and is specified in Eq. (3.3.5). We define the mean tunneling rate as

$$\Gamma_{\alpha,0} = \pi |t_{\alpha,0}|^2 \rho_\alpha(\omega), \quad (3.2.3)$$

where $t_{\alpha,0}$ indicates the time averaged mean value of $t_\alpha(t)$, $\rho_\alpha(\omega)$ is the reservoir density of states and is specified for the wide band limit in Eq. (3.3.4).

3.3 Three site IRLM

The field theoretical model is *not* of the form proposed in Eqs. (3.1.1) to (3.1.5), such that an appropriate realization of the model is necessary. Hence, we define a dot Hamiltonian

$$H_{\text{dot},0} = \epsilon(t) n_2 - \left[\tau_L(t) d_1^\dagger d_2 + \tau_R(t) d_2^\dagger d_3 + \text{H.c.} \right], \quad (3.3.1)$$

$$H_{\text{dot}, \text{int}} = U(t) \left[\left(n_1 - \frac{1}{2}\right) \left(n_2 - \frac{1}{2}\right) + \left(n_2 - \frac{1}{2}\right) \left(n_3 - \frac{1}{2}\right) \right]. \quad (3.3.2)$$

The IRLM is thus modeled by a three site central region where the site with index 2 models the quantum dot and the first and third site model the first site of the left and right reservoir,

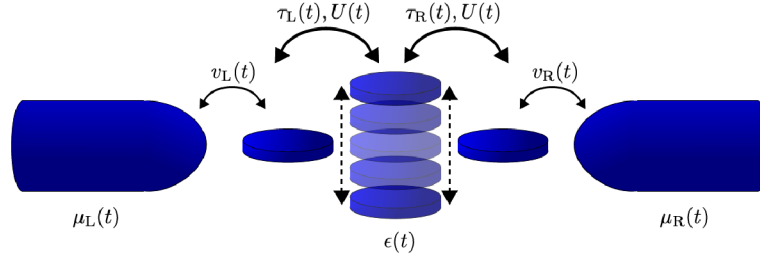


Figure 3.1: The three site realization of the interacting resonant level model employing the wide band limit by $v \gg \tau_{L/R}, \epsilon$. Any of the parameter as indicated can be chosen time periodic.

respectively. The quantum dot might be subject to a gate voltage determining the onsite energy ϵ , where $\epsilon = 0$ defines the particle hole symmetric point. The Coulomb interaction is introduced as a density-density interaction between the electron on the dot and one on the first site of the left/right reservoir, written in a particle hole symmetric form. We consider both cases of positive and negative interaction. A possible realization of the latter might be a quantum dot coupled to phonons, with the phonon frequency in the adiabatic limit [Eid13]. The bandwidth in this model is defined by

$$D = D_\alpha = |v|^2 \pi \rho_\alpha(\omega), \quad (3.3.3)$$

where v is the k_α independent coupling and $\rho_\alpha(\omega)$ is the reservoir density of states. The field theoretical model can be realized properly by the three site model in the so-called wide band limit.

Wide band limit

We are not interested in the details of the reservoirs and employ the wide band limit of a structureless, large band as well as couplings independent of the wave vector k_α . The local density of states in the reservoirs is

$$\rho_\alpha(\omega) = \frac{1}{\rho_\alpha^{(0)}} \sum_k \delta(\omega - \epsilon_{\alpha k} - \mu_\alpha), \quad (3.3.4)$$

which for convenience can be chosen as a symmetric Lorentzian

$$\rho_\alpha(\omega) = \frac{D^2}{D^2 + \omega^2} \quad \text{with} \quad \rho_\alpha^{(0)} = \frac{1}{\pi D} \quad (3.3.5)$$

and subsequently apply the limit of $D \rightarrow \infty$. In the three site model this corresponds to setting $v \gg \tau_{L/R}, |\epsilon|$.

Relation to the field theoretical model

Next, the parameters of both models are examined to understand their relation and to demonstrate that indeed the three site model correctly reproduces the field theoretical IRLM, when employing the wide band limit $v \rightarrow \infty$ ($D \rightarrow \infty$). The hopping elements of the two models are related as follows

$$\tau_\alpha = t_\alpha \sqrt{\pi D} \xrightarrow{D \rightarrow \infty} \infty. \quad (3.3.6)$$

However, inserting this into the definition of the hybridization of Eq.(3.2.3), the **effective hybridization** Γ_{1d} between the dot and the first site of left/right reservoir of the (effective) one dot structure can be defined as

$$\Gamma_{1d,\alpha} = \frac{\tau_\alpha^2}{D} = \frac{(t_\alpha)^2 \pi D}{D} \xrightarrow{D \rightarrow \infty} \text{const.}, \quad (3.3.7)$$

which stays constant in this limit. As a consequence, the effective reservoir density of states when regarding the site 2 as the dot, is of Lorentzian shape with a width of $4\Gamma_{1d}$. The relation of the two

particle interaction in both realizations of the model is $U = \frac{\tilde{u}_\alpha}{\rho_\alpha^{(0)}}$ such that

$$U/D = \frac{\tilde{u}_\alpha}{\rho_\alpha^{(0)}D} = \frac{\tilde{u}_\alpha \pi D}{D} \xrightarrow{D \rightarrow \infty} \text{const.} \quad (3.3.8)$$

Throughout the present work all functional renormalization group calculations are employed for the three site model, while the perturbative calculation in Liouville space presented in Chapter 6 are made in the field theoretical model. One might wonder at this point that the factors $\frac{t_\alpha(t)}{\sqrt{\rho_\alpha^{(0)}}}$ and $\frac{\tilde{u}_\alpha(t)}{\rho_\alpha^{(0)}}$ of the Hamiltonian in Eq. (3.2.2) diverge in the wide band limit. However, it still allows for a sensible (and even perturbative) approach, which becomes apparent, when defining the according reservoir field operator in Eq. (6.1.20).

If the three site model is considered to be deep in the wide band limit (with a finite, but large enough D), both models yield consistent results.

3.4 Transformation of the time dependency of the chemical potential

Even though in general a time dependent onsite energy in the leads is not treatable, the wide band limit allows to perform a gauge transformation that shifts the time periodicity of the reservoir onsite energy to a phase of the hopping elements to the dot

$$\tau_0 \rightarrow \tau_0 e^{i \int_0^t \mu(t') dt'} . \quad (3.4.1)$$

As a consequence, for the IRLM in the wide band limit the reservoir onsite energy can be driven time periodically as well.

The transformation follows the idea as presented in Ref. [Ken12b], and is equivalent to the approaches of Refs. [Spl07, Kam00, Str05, Kwa10]. In the wide band limit raising the filling of the lead, i.e. the chemical potential is equivalent to raising the energy levels. We rewrite the reservoir Hamiltonian in the Wannier basis [Jak09, Ken11] and include the first and third site to the effective left/right reservoir

$$H_{\alpha, \text{eff res}} = \sum_{m=0}^{\infty} (\epsilon_\alpha + \mu_\alpha(t)) a_{m,\alpha}^\dagger a_{m,\alpha} - (v_\alpha a_{m+1,\alpha}^\dagger a_{m,\alpha} + \text{H.c.}) , \quad (3.4.2)$$

with $d_L = d_1$ and $d_R = d_3$ as well as $a_{0,\alpha} = d_\alpha$ and $a_{m+1,\alpha} = c_{m,\alpha}$.

The gauge transformation is defined as

$$\bar{H} = G(t) H(t) G^\dagger(t) + i \dot{G}(t) G^\dagger(t) , \quad (3.4.3)$$

with

$$G(t) = e^{i \sum_\alpha \sum_m \phi_\alpha(t) a_{m,\alpha}^\dagger a_{m,\alpha}} = \prod_\alpha \prod_m \sum_l \frac{(\phi_\alpha(t) n_{m,\alpha})^l}{l!} , \quad (3.4.4)$$

where $n_{m,\alpha} = a_{m,\alpha}^\dagger a_{m,\alpha}$, $\phi_\alpha(0) = 0$ and $\dot{\phi}_\alpha(t) = \mu_\alpha(t)$.

We need to calculate the commutators

$$[G(t), H(t)] = [G(t), H_{\text{dot},0}(t)] + [G(t), H_{\text{dot},\text{int}}(t)] + [G(t), H_{\text{lead},\alpha}(t)] , \quad (3.4.5)$$

assuming the known fermionic relations $\{a_{m,\alpha}, a_{n,\alpha'}^\dagger\} = \delta_{mn} \delta_{\alpha\alpha'}$ with $\{\cdot, \cdot\}$ denoting the anti-commutator. Because

$$[n_{m,\alpha}, n_{j,\alpha'}] = 0 \quad (3.4.6)$$

for all $m, j \in \mathbb{N}$ and $\alpha, \alpha' \in \{L, R\}$, the only non-vanishing commutators are of the form

$$\begin{aligned} [G(t), \tau_R(t) d_2^\dagger d_3] &= \left[\prod_{\alpha} \prod_m \sum_l \frac{(\Phi_{\alpha}(t) n_{m,\alpha})^l}{l!}, \tau_R(t) d_2^\dagger d_3 \right] \\ &= e^{i \sum_m \Phi_L(t) n_{m,L}} e^{i \sum_{m=1} \Phi_R(t) n_{m,R}} \left[\sum_l \frac{(\Phi_R(t) n_{0,R})^l}{l!}, \tau_R(t) d_2^\dagger d_3 \right], \end{aligned} \quad (3.4.7)$$

with the left hand side as well as the hermitian conjugate terms behaving analogously. Concentrating on the commutator with $n_{0,R} = n_3$ leads to

$$\begin{aligned} \left[\sum_l \frac{(\Phi_R(t) n_3)^l}{l!}, \tau_R(t) d_2^\dagger d_3 \right] &= \tau_R(t) \sum_l \frac{(\Phi_R(t))^l}{l!} \sum_{k=0}^{l-1} (n_3)^k [n_3, d_2^\dagger d_3] (n_3)^{l-k-1} \\ &= \tau_R(t) \sum_l \frac{(\Phi_R(t))^l}{l!} \sum_{k=0}^{l-1} (n_3)^k (-d_2^\dagger d_3) (n_3)^{l-k-1} \\ &= \tau_R(t) \sum_l \frac{(\Phi_R(t))^l}{l!} \sum_{k=0}^{l-1} \sum_{p=0}^k \binom{k}{p} (-d_2^\dagger d_3) (-n_3)^{k-p} (n_3)^{l-k-1} \\ &= \tau_R(t) \sum_l \frac{(\Phi_R(t))^l}{l!} [(n_3 - 1)^l + n_3^l] \\ &= \tau_R(t) d_2^\dagger d_3 \left(e^{i \Phi_R(n_3+1)} - e^{i \Phi_R(n_3)} \right). \end{aligned} \quad (3.4.8)$$

As a result the transformed Hamiltonian reads

$$\begin{aligned} \bar{H} &= G(t) H_{\text{dot},0}(t) G^\dagger(t) + H_{\text{dot,int}}(t) + H_{\text{lead},\alpha}(t) + H_{\text{coup},\alpha}(t) - \sum_{\alpha} \sum_m \dot{\Phi}_{\alpha}(t) n_m \\ &= \epsilon(t) n_2 + \left(\tau_L e^{i \Phi_L(t)} d_1^\dagger d_2 + \tau_R e^{-i \Phi_R(t)} d_2^\dagger d_3 + \text{H.c.} \right) \\ &\quad + U \left[\left(n_1 - \frac{1}{2} \right) \left(n_2 - \frac{1}{2} \right) + \left(n_2 - \frac{1}{2} \right) \left(n_3 - \frac{1}{2} \right) \right] \\ &\quad + \sum_{\alpha} \sum_m \epsilon_{\alpha} a_m^\dagger a_m - (v_{\alpha} a_{m+1,\alpha}^\dagger a_{m,\alpha} + \text{H.c.}), \end{aligned} \quad (3.4.9)$$

where the last term in the first line cancels the time periodic chemical potentials in the leads and the hopping elements have gathered a phase, which can be understood as a phase acquired by an electron when traversing an electrical field created by the chemical potentials in the leads [Spl07].

3.5 The equilibrium IRLM

Already now the basic equilibrium renormalization physics of the IRLM is discussed. An ordinary perturbation theory calculation motivates the application of a RG method to this model, and the known equilibrium physics is sketched in order to define the low energy scale T_K . A more detailed discussion is presented after the FRG is introduced in Section 7.1, Sections 7.2 and 7.3 introduce the renormalization physics of the non-equilibrium and time-dependent IRLM, accordingly.

Perturbation theory fails in the wide band limit

A naive perturbation theory calculation to the first order in the interaction U reveals why a renormalization group approach is necessary to treat the IRLM in the wide band limit. Calculating the first order self-energy contribution to the hopping element $\tau_L = \tau_R = \tau_0$ results

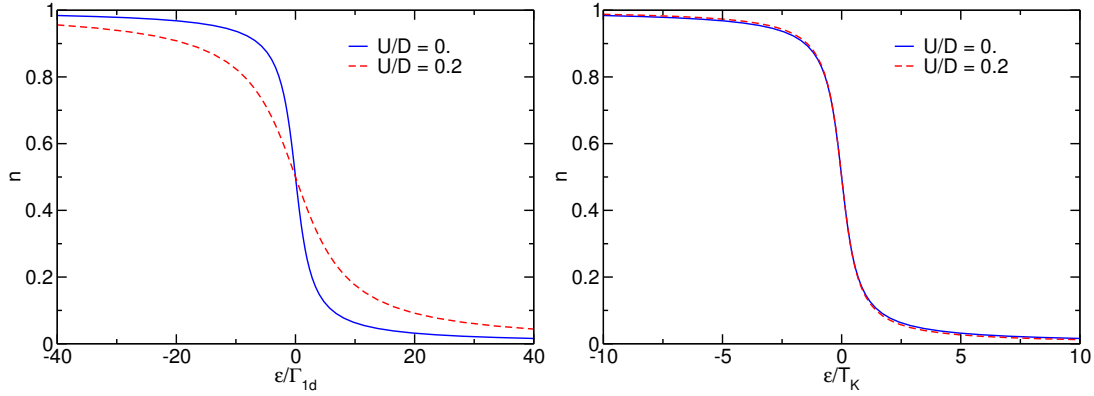


Figure 3.2: The dot occupancy as a function of the onsite energy ϵ . In the left panel ϵ is scaled in microscopic parameters, which is compared to ϵ scaled with the renormalized, equilibrium energy scale T_K in the right panel. Rescaling ϵ with T_K recovers for the interacting system the form of the non-interacting system, such that the main effect of the interaction is encoded in the low energy scale T_K . For vanishing interaction $T_K = 4\Gamma_{1d}$. We choose $U/D = \{0., 0.2\}$ with $T_K = \{2.5 \cdot 10^{-5}, 7.93 \cdot 10^{-5}\}$.

in [Noz69, Fil81, Sch80b, Sch82a, Ken14]

$$\begin{aligned} \tau_0^{\text{PT}} &= \tau_0 - \frac{U}{\pi D} \frac{\tau_0}{\sqrt{1 - 8\tau_0^2/D^2}} \ln \left(\frac{1 - \sqrt{1 - 8\tau_0^2/D^2}}{1 + \sqrt{1 - 8\tau_0^2/D^2}} \right) \\ &\approx \tau_0 - \frac{U}{\pi D} \tau_0 \ln \left(\frac{2\tau_0^2}{D^2} \right). \end{aligned} \quad (3.5.1)$$

While employing the wide band limit $D \rightarrow \infty$ results in a logarithmic divergency, already a large, but finite bandwidth D restricts the valid interaction regime to a minimum. Several methods have been devised to circumvent it [Noz69, Fil81, Sch80b, Sch82a, Sch82b, Sch82c], where one possibility is the functional RG approach. It employs the renormalization group idea [Kar10c], where leading logarithmic terms are summed up throughout the renormalization flow yielding power law behavior characteristic for the IRLM.

Low-energy scale T_K

In the equilibrium setup a renormalized hopping element can be defined and follows a power law [Bor07, Doy07, Bor08, Kar10c]

$$\frac{\tau_0^{\text{ren}}}{\tau_0} = \left(\frac{2\tau_0^2}{D^2} \right)^{-\frac{U}{\pi D} + \mathcal{O}(U^2)} \quad \text{for } |\epsilon| \ll T_K \ll D, \quad (3.5.2)$$

where we have already used the energy scale T_K , which is defined next.

Calculating the charge susceptibility

$$\chi = \left. \frac{dn}{d\epsilon} \right|_{\epsilon=0}, \quad (3.5.3)$$

with the dot occupancy defined in Eq. (4.6.3) in a non-interacting setup and substituting the parameters by the renormalized equivalents¹ reveals that the charge susceptibility is mainly characterized by the renormalized hoppings [Kar10c]. It hence reflects their power-law behavior

$$\chi \sim \left(\frac{\tau_0}{D} \right)^{\frac{2U}{\pi D} + \mathcal{O}(U^2)} \quad (3.5.4)$$

¹We will show at a later stage that in the formulation of the approach employed here, non-interacting expressions for observables still hold true for the interacting setup, when the parameters are substituted by the renormalized ones.

and can be used to define a renormalized, low-energy scale T_K for the equilibrium setup as

$$T_K = \frac{-\pi}{2\chi}, \quad (3.5.5)$$

which proved to be a useful definition [Kar10b, And11a, And11b, Ken12a]. To illustrate the benefit of this low-energy scale the occupancy is displayed in Fig. 3.2 for the setup with and without interaction. To obtain this figure the method employed in the present thesis is used already here, where further details are explained in Chapters 4 and 5. The dot occupancy n is depicted as a function of onsite energy ϵ scaled by the microscopic parameters on the one hand and scaled by the low-energy scale T_K on the other hand. While in the former case, the characteristic step is broadened by the influence of the interaction, rescaling with the renormalized energy scale recovers the form of the non-interacting setup. Hence, the main effect of the interaction in the equilibrium setup is encoded in T_K . This renormalized energy scale is the emergent low energy scale of the model.

Methods

Chapter 4

Floquet-Green's Function

Contents

4.1	Keldysh Green's function	20
4.1.1	Green's function	20
4.1.2	Keldysh formalism	20
4.1.3	Dyson equation	22
4.2	Generating Functionals	24
4.2.1	Grassmann algebra and Functional integrals	24
4.2.2	Functional Integral Representation of the Keldysh Green's functions	25
4.2.3	Generating Functionals	27
4.3	Floquet theory	29
4.4	Floquet-Green's function	30
4.4.1	Transformation to Floquet space	30
4.4.2	Symmetries	31
4.4.3	Dyson equation	31
4.5	Reservoir self-energy: Dressed Green's function	32
4.5.1	Reservoir Green's functions	32
4.5.2	Projection Technique: Reservoir self-energy	32
4.5.3	Dissipation Fluctuation Theorem for Reservoir Self-energy	33
4.6	Observables	34
4.6.1	Occupancy	34
4.6.2	Charge susceptibility	34
4.6.3	Current	35
4.6.4	Pumped charge	35
4.6.5	Linear conductance	36
4.6.6	Spectral function	36

The functional renormalization group (FRG) method we employ in the present thesis relies on the Green's function formalism. This chapter is thus dedicated to revisit the concept of Green's functions, explain the Keldysh formalism necessary for the non-equilibrium setups and introduces coherent states and the functional integral representation of Green's functions. Subsequently the generating functionals of the time dependent Green's functions are introduced, necessary for the derivation of the FRG in the next chapter. In the second half of the chapter the Floquet theory is introduced and the resulting transformation of the Green's functions to Floquet space is presented for an efficient description of the steady state of the time periodically driven system. It will be used at a later point to transform the flow equation accordingly. The projection method is discussed to calculate the reservoir self-energy to obtain a reservoir dressed Green's functions that includes the

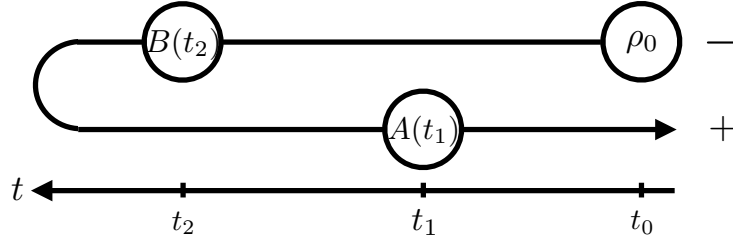


Figure 4.1: The Keldysh contour combines the forward and backward propagation to a joint one, where the according branches are labelled by $-$ and $+$, respectively.

influence of the reservoirs on the dot parameter. We conclude the chapter with the discussion of the single-particle observables derivable of the Green's function. Similar introductions to Green's functions can also be found in [Jak14, Sch11, Kar10a, Ken14].

4.1 Keldysh Green's function

4.1.1 Green's function

Initially, we focus on the dot part of the Hamiltonian $H_{\text{dot}} = H_0 + H_{\text{int}}$ only, as defined in Eqs. (3.1.2) and (3.1.3). For this system the n -point Green's function is defined as an expectation value of n different operators as

$$\begin{aligned} G_{A_1, A_2, \dots, A_n}(t_1, t_2, \dots, t_n) &= -i \text{Tr} [A_1[t_1]_H A_2[t_2]_H \dots A_n[t_n]_H \rho] \\ &= -i \langle A_1[t_1]_H A_2[t_2]_H \dots A_n[t_n]_H \rangle_\rho, \end{aligned} \quad (4.1.1)$$

where $A[t]_H$ denotes the time dependent operators in the Heisenberg picture and ρ is the density matrix.

We focus on two-point Green's function $G_{A,B}(t_1, t_2)$ in the following, from which all objects of relevance here can be computed. For illustration purposes we start with a simple example and choose A and B to be $A = A^\dagger$ and $B = 1$. The Green's function reduces to the expectation value of an arbitrary observable $\langle A \rangle(t)$ which is defined as

$$\langle A \rangle(t) = \text{Tr} [A(t) \rho(t)] = \text{Tr} [U(t_0, t) A(t) U(t, t_0) \rho_0] = \text{Tr} [A[t]_H \rho_0], \quad (4.1.2)$$

with $A[t]_H \equiv U(t_0, t) A(t) U(t, t_0)$, $\rho_0 = \rho(t_0)$ and the time evolution operator defined as

$$U(t, t') = \begin{cases} T \exp[-i \int_{t'}^t H(\tau) d\tau] & t > t' \\ \tilde{T} \exp[-i \int_t^{t'} H(\tau) d\tau] & t' > t, \end{cases} \quad (4.1.3)$$

where T is the time order operator, \tilde{T} is the anti-time order operator. The expectation value of Eq. (4.1.2) thus consists of a forward and a backward propagation, which constitutes a problem when generalizing the treatment to more than one operator. A useful definition of a diagrammatic language includes among others a single particle propagation from one state into another, which can only be defined properly if it consists of a single propagation in time. While in the equilibrium situation the time translation of the system as well as the vanishing commutator of density and Hamilton operator, makes the definition of a single propagation in time feasible, the non-equilibrium situation is indeed more complicated and requires the so called Keldysh formalism.

4.1.2 Keldysh formalism

Main idea of the Keldysh formalism is the definition of a **Keldysh contour** γ as depicted in Fig. 4.1 to combine forward and backward propagation to a single propagation. The contour starts at the

initial time t_0 , propagates to ∞ and subsequently propagates back in time. This joint propagation in time requires however an extra single particle like Keldysh index, labeling the forward propagation with $-$ and the backward propagation in time with $+$.

Using this notation the expectation value can be rewritten

$$\begin{aligned}\langle A \rangle(t) &= \text{Tr } T_\gamma e^{i \int_{t_0}^t H^+} A^- e^{-i \int_{t_0}^t H^-} \rho_0 \\ &= \text{Tr } T_\gamma e^{-i \int_{t_0}^t [H^- - H^+]} A^- \rho_0 ,\end{aligned}\quad (4.1.4)$$

where in the latter step a unity of the form

$$1 = U(t, \infty) U(\infty, t) = e^{-i \int_{t_0}^t H^-} e^{i \int_{t_0}^t H^+} \quad (4.1.5)$$

has been introduced. The Keldysh index of H^p indicates the direction of the propagation. In this specific example, where A is the only operator in the propagation, its Keldysh index can be chosen as desired, since its branch is irrelevant.

Only when generalizing this idea to two arbitrary operators A and B

$$G_{AB}^{pp'}(t_1, t_2) = -i \langle T_\gamma A[t_1]_H B[t_2]_H \rangle_{\rho_0} , \quad (4.1.6)$$

with p (p') indicating the Keldysh index of $A[t_1]_H$ ($B[t_2]_H$) and T_γ being the time ordering with respect to the contour, the benefit becomes apparent: Even though $t_1 < t_2$, the operators are ordered along one contour propagating from ρ_0 through B to A (see Fig. 4.1).

For the specific case of the single-particle Green's functions with $A = a_q$ and $B = a_{q'}^\dagger$ (where a/a^\dagger are fermionic annihilation/creation operator) four possible combinations arise

$$\text{Chronological : } G_{qq'}^{--}(t, t') = G_{qq'}^c(t, t') = -i \left\langle T a_q[t]_H a_{q'}^\dagger[t']_H \right\rangle_{\rho_0} , \quad (4.1.7)$$

$$\text{Lesser : } G_{qq'}^{-+}(t, t') = G_{qq'}^<(t, t') = i \left\langle a_{q'}^\dagger[t']_H a_q[t]_H \right\rangle_{\rho_0} , \quad (4.1.8)$$

$$\text{Larger : } G_{qq'}^{+-}(t, t') = G_{qq'}^>(t, t') = -i \left\langle a_q[t]_H a_{q'}^\dagger[t']_H \right\rangle_{\rho_0} , \quad (4.1.9)$$

$$\text{Anti - Chronological : } G_{qq'}^{++}(t, t') = G_{qq'}^{\tilde{c}}(t, t') = -i \left\langle \tilde{T} a_q[t]_H a_{q'}^\dagger[t']_H \right\rangle_{\rho_0} . \quad (4.1.10)$$

For a compact notation, they are condensed to a matrix in Keldysh space (only respective indices shown)

$$\hat{G} = \begin{pmatrix} G^{--} & G^{-+} \\ G^{+-} & G^{++} \end{pmatrix} . \quad (4.1.11)$$

Multiplying two operators in Keldysh space is defined as [Sch11]

$$\hat{A}\hat{B} = \hat{A}\sigma_z\hat{B} , \quad (4.1.12)$$

where σ_z is the Paulimatrix and with integration over the internal time argument

$$(\hat{A}\hat{B})(t, t') \equiv \int_{t_0}^{\infty} dt_1 \hat{A}(t, t_1) \hat{B}(t_1, t') . \quad (4.1.13)$$

The commutator relations under the action of T_γ are

$$\{a_q^p, a_{q'}^{p'}\} = 0 \quad \{a_q^p, a_{q'}^{p'\dagger}\} = \delta_{qq'} \delta_{pp'} , \quad (4.1.14)$$

where $\{\cdot, \cdot\}$ indicates the anticommutator, confirming the single particle like nature of the extra Keldysh index. The anti-symmetrized two-particle matrix element including the Keldysh indices becomes

$$\bar{u}_{\{q_1 p_1\}\{q_2 p_2\}\{q_3 p_3\}\{q_4 p_4\}} = \bar{u}_{q_1 q_2 q_3 q_4} \times (-p_1) \delta(p_1 = p_2 = p_3 = p_4) . \quad (4.1.15)$$

The fact that the four Green's functions are not independent, but are linked due to causality as

$$G^c(t, t') + G^{\tilde{c}}(t, t') = G^<(t, t') + G^>(t, t') \quad t \neq t' \quad (4.1.16)$$

renders one Green's function redundant and allows to perform a rotation in Keldysh space [Lar75]

$$\hat{G} = \begin{pmatrix} G^{\text{ret}} & G^K \\ 0 & G^{\text{adv}} \end{pmatrix} = \underbrace{\frac{1}{\sqrt{2}} \begin{pmatrix} 1 & 1 \\ 1 & -1 \end{pmatrix}}_{R_A} \begin{pmatrix} G^c & G^< \\ G^> & G^{\tilde{c}} \end{pmatrix} \underbrace{\frac{1}{\sqrt{2}} \begin{pmatrix} 1 & 1 \\ -1 & 1 \end{pmatrix}}_{R_B}. \quad (4.1.17)$$

The resulting three different Green's functions are defined as

$$\begin{aligned} \text{Retarded : } G_{qq'}^{\text{ret}}(t, t') &= \Theta(t - t')(G_{qq'}^>(t, t') - G_{qq'}^<(t, t')) \\ &= -i \Theta(t - t') \left\langle \{a_q[t]_H, a_{q'}^\dagger[t']_H\} \right\rangle_{\rho_0}, \end{aligned} \quad (4.1.18)$$

$$\begin{aligned} \text{Advanced : } G_{qq'}^{\text{adv}}(t, t') &= -\Theta(t' - t)(G_{qq'}^>(t, t') - G_{qq'}^<(t, t')) \\ &= i \Theta(t' - t) \left\langle \{a_q[t']_H, a_{q'}^\dagger[t]_H\} \right\rangle_{\rho_0}, \end{aligned} \quad (4.1.19)$$

$$\begin{aligned} \text{Keldysh : } G_{qq'}^K(t, t') &= (G_{qq'}^>(t, t') + G_{qq'}^<(t, t')) \\ &= -i \left\langle [a_q[t]_H, a_{q'}^\dagger[t]_H] \right\rangle_{\rho_0}, \end{aligned} \quad (4.1.20)$$

with $(\{\cdot, \cdot\})$ $[\cdot, \cdot]$ being the (anti)commutator. The retarded Green's function is known from linear response theory, where the cause preceding the effect is expressed by the according Θ -function and in equilibrium it is directly connected to the Matsubara Green's function [Jak14]. The advanced Green's function is the according counterpart, both contain the spectral information [Sch11]. While $G^<$ describes the statistics of the particles ($G^>$ accordingly for the holes), G^K is a combination of both [Jak14] and is used to calculate e.g. the occupancy. Besides the reduction by one Green's function, another main advantage of the rotation will become obvious when the Dyson equation is discussed.

4.1.3 Dyson equation

The non-interacting and the full Green's function are defined as

$$\text{Non - interacting : } g_{qq'}^{pp'}(t, t') = -i \left\langle T_\gamma a_q[t]_{H_0} a_{q'}^\dagger[t']_{H_0} \right\rangle_{\rho_0}, \quad (4.1.21)$$

$$\text{Full : } G_{qq'}^{pp'}(t, t') = -i \left\langle T_\gamma a_q[t]_H a_{q'}^\dagger[t']_H \right\rangle_{\rho_0}, \quad (4.1.22)$$

with only the non-interacting part or the full dot Hamiltonian included in the time propagation, respectively.

The non-interacting Green's function fulfills the following differential equation (for a proof see Ref. [Sch11] or [Ken11])

$$\left(i \frac{\partial}{\partial t} - \hat{\epsilon}(t) \right) \hat{g}(t, t') = \sigma_z \delta(t - t'), \quad (4.1.23)$$

with

$$\hat{\epsilon} \equiv \begin{pmatrix} \epsilon(t) & 0 \\ 0 & \epsilon(t) \end{pmatrix} \quad (4.1.24)$$

and $\epsilon(t)$ is the single-particle part of the Hamiltonian. Rotating Eq. (4.1.23) as defined in Eq. (4.1.17) yields

$$\left(i \frac{\partial}{\partial t} - \hat{\epsilon}(t) \right) \hat{g}(t, t') = \delta(t - t') \mathbb{1}, \quad (4.1.25)$$

when noting that $R_A \sigma_z R_B = \mathbb{1}$.

The full Green's function can be calculated from the non-interacting Green's function via the **Dyson equation**

$$\hat{\hat{G}}(t, t') = \hat{\hat{g}}(t, t') + [\hat{\hat{g}} \sigma_z \hat{\hat{\Sigma}} \sigma_z \hat{\hat{G}}](t, t') \quad (4.1.26)$$

with the **self-energy** Σ , which is the sum of all connected, one particle irreducible diagrams [Neg88]. The concept of the self-energy can be equally extended to the Keldysh space, yielding an object with two Keldysh indices. It hence can also be represented by a matrix structure in the Keldysh basis as

$$\hat{\hat{\Sigma}} = \begin{pmatrix} \Sigma^c & \Sigma^< \\ \Sigma^> & \Sigma^{\bar{c}} \end{pmatrix}. \quad (4.1.27)$$

Analogously as for the Green's function, also for the self-energies hold

$$\Sigma^c(t, t') + \Sigma^{\bar{c}}(t, t') = \Sigma^<(t, t') + \Sigma^>(t, t') \quad t \neq t', \quad (4.1.28)$$

which allows to apply the same transformation for the self-energy to rotate in the {ret, adv, Keldysh} basis.

Applying the transformation to the complete Dyson equation and noting that $R_B^{-1} \sigma_z R_A^{-1} = \mathbb{1}$ yields

$$\hat{G}(t, t') = \hat{g}(t, t') + [\hat{g} \hat{\Sigma} \hat{G}](t, t'). \quad (4.1.29)$$

Examining each entry independently

$$G^{\text{ret}} = g^{\text{ret}} + g^{\text{ret}} \Sigma^{\text{ret}} G^{\text{ret}}, \quad (4.1.30)$$

$$G^{\text{adv}} = g^{\text{adv}} + g^{\text{adv}} \Sigma^{\text{adv}} G^{\text{adv}}, \quad (4.1.31)$$

$$G^K = g^K + g^{\text{ret}} \Sigma^{\text{ret}} G^K + g^{\text{ret}} \Sigma^K G^{\text{adv}} + g^K \Sigma^{\text{adv}} G^{\text{adv}}, \quad (4.1.32)$$

where contraction over internal indices and time arguments is assumed, another benefit of the rotation is revealed: It decouples the retarded and advanced Green's function from the Keldysh one.

Finally, we rewrite the Dyson equation of Eq. (4.1.29) by multiplying by g^{-1} from the left and integrate over the entire time regime [Ken11], leading to

$$\left(i \frac{\partial}{\partial t} - \hat{\epsilon}(t) \right) \hat{G}(t, t') - [\hat{\Sigma} \hat{G}](t, t') = \delta(t - t'), \quad (4.1.33)$$

a reformulation which will prove to be convenient at a later stage.

Keldysh Green's function

The Keldysh component of the Dyson equation is of more complicated form compared to the retarded/advanced entries, namely

$$G^K(t, t') = g^K(t, t') + [g^{\text{ret}} \Sigma^{\text{ret}} G^K](t, t') + [g^{\text{ret}} \Sigma^K G^{\text{adv}}](t, t') + [g^K \Sigma^{\text{adv}} G^{\text{adv}}](t, t'). \quad (4.1.34)$$

Resolving for all G^K on the left hand side and utilizing $g^K(t, t') = -ig^{\text{ret}}(t, t_0)(1 - 2\bar{n})g^{\text{adv}}(t_0, t')$ as well as the Dyson equation for the retarded/advanced component, it can be reduced to [Ken11, Ken12a]

$$G^K(t, t') = -iG^{\text{ret}}(t, t_0)(1 - 2\bar{n})G^{\text{adv}}(t_0, t') + [G^{\text{ret}} \Sigma^K G^{\text{adv}}](t, t'), \quad (4.1.35)$$

where $\bar{n}_{ij} = \text{Tr} \rho_0^{\text{dot}} d_i^\dagger d_j$ is the initial occupancy of the dot. While the first part describes the transient behavior off the initial dot state, only the second term survives in the long time limit $t_0 \rightarrow -\infty$. Hence, the steady state Keldysh Green's function reads as

$$G_{\text{steady}}^K(t, t') = [G^{\text{ret}} \Sigma^K G^{\text{adv}}](t, t'). \quad (4.1.36)$$

4.2 Generating Functionals

Generating functionals play an important role in the derivation of the functional renormalization group, which is the main method of the present thesis presented in the next chapter. They are set up in the coherent state functional integral formulation introduced now. We thus start with revisiting the basics of Grassmann algebra, coherent states and functional integrals and subsequently derive the generating functionals of Green's and vertex functions. Equal introductions into the topic can be found e.g. in [Neg88, Kar10a, Ken14, Jak14].

4.2.1 Grassmann algebra and Functional integrals

Path integrals for single particle problems formulated with eigenstates of the position and momentum operator have been introduced originally in 1933 by Paul Dirac [Dir33] and extensively developed by Richard Feynman [Fey48, Fey49, Fey50] (thus also widely known as Feynman path integrals). The generalization to many-particle functional integrals allow for a convenient representation of Green's and vertex functions and form the basis of the diagrammatic language.

The main idea is to divide the finite time interval between an initial time t_i and the final time t_f into infinitesimal steps. The evolution operator can be calculated at each step and the matrix elements are subsequently chained together [Neg88]. For non-interacting terms of the Hamiltonian (quadratic in creation/annihilation operator) the resulting Gaussian integral can be even solved exactly. For interacting terms which are of higher order (in creation/annihilation operator) the functional integral formalism provides the possibility to set up consistent calculations perturbative in the interaction, which among others allows to formulate a RG procedure.

The functional integrals are formulated here by coherent states which are a convenient choice if the initial Hamiltonian is written with operators in the second quantization notation. Coherent states are defined as the right eigenstates of the annihilation operator

$$a_q |\psi\rangle = \psi_q |\psi\rangle, \quad \langle\psi| a_q^\dagger = \langle\psi| \bar{\psi}_q, \quad (4.2.1)$$

and are constructed as

$$|\psi\rangle = |\psi_{q_1}, \psi_{q_2}, \dots\rangle = e^{-\sum_q \psi_q a_q^\dagger} |\text{vac}\rangle, \quad (4.2.2)$$

$$\langle\psi| = \langle\psi_{q_1}, \psi_{q_2}, \dots| = \langle\text{vac}| e^{-\sum_q \bar{\psi}_q a_q}. \quad (4.2.3)$$

where the scalar product is given by

$$\langle\psi|\phi\rangle = e^{\sum_q \bar{\psi}_q \phi_q} = 1 + \sum_q \bar{\psi}_q \phi_q. \quad (4.2.4)$$

The eigenvalues ψ_q are Grassmann numbers, which fulfill fermionic commutation relations

$$\{\psi_{q_1}, \psi_{q_2}\} = \{\psi_{q_1}, \bar{\psi}_{q_2}\} = \{\psi_{q_1}, a_{q_2}^{(\dagger)}\} = 0 \quad \text{and thus} \quad \psi_q^2 = 0, \quad (4.2.5)$$

i.e. anticommute. We only state the following important relations here and refer the interested reader to [Neg88] for the according proofs and if necessary more details. The unity operator can be represented by the coherent state as

$$\mathbb{1} = \int \prod_q d\bar{\psi}_q d\psi_q |\psi\rangle \langle\psi| e^{-\sum_q \bar{\psi}_q \psi_q}, \quad (4.2.6)$$

and the trace of an arbitrary operator O is defined as

$$\text{Tr} O = \int \prod_q d\bar{\psi}_q d\psi_q \langle -\psi| O |\psi\rangle e^{-\sum_q \bar{\psi}_q \psi_q}. \quad (4.2.7)$$

The 'Gaussian integral' reads as

$$\int \prod_q d\bar{\psi}_q d\psi_q e^{-\sum_{q_1, q_2} \bar{\psi}_{q_1} O_{q_1, q_2} \psi_{q_2} + \sum_q \bar{\psi}_q \phi_q + \bar{\phi}_q \psi_q} = \det O e^{\sum_{q_1, q_2} \bar{\phi}_{q_1} [O^{-1}]_{q_1, q_2} \phi_{q_2}}, \quad (4.2.8)$$

which is used to describe the quadratic, i.e. non-interacting terms of the Hamiltonian.

The subdivision in infinitesimal parts - needed for the functional integral representation - is justified by the **Trotter formula** stating that

$$e^{-\lambda H} = \lim_{N \rightarrow \infty} \left(: e^{-\lambda H/N} : \right)^N, \quad (4.2.9)$$

where H is the known, normal ordered Hamiltonian and $: \cdot :$ indicates normal ordering. The unity operator $\mathbb{1}$ is introduced N times between each of the infinite steps. It allows to change from operator representation to coherent states. This procedure is now demonstrated for the Green's function.

4.2.2 Functional Integral Representation of the Keldysh Green's functions

Restating the Green's functions definition

$$G_{q, q'}^{p, p'}(t, t') = -i \left\langle T_\gamma a_q^p[t] a_{q'}^{\dagger, p'}[t'] \right\rangle_{\rho_0} = -i \left\langle T_\gamma a_q^{\{t, p\}} a_{q'}^{\dagger, \{t', p'\}} e^{-i \oint_\gamma d\tau H(\tau)} \right\rangle_{\rho_0}, \quad (4.2.10)$$

where in the second step the time evolution is just rewritten with the integral to be read as

$$\oint_\gamma dt_i = \sum_{p=\pm} (-p) \int_{t_0}^t dt_i \mid_{t_i \in \gamma_p}. \quad (4.2.11)$$

It is then convenient to define [Ken14]

$$a_q^{\max} = \begin{cases} a_q^{\{t, p\}} & \text{if } t_p >_\gamma t'_{p'} \\ -a_{q'}^{\dagger, \{t', p'\}} & \text{if } t_p \leq_\gamma t'_{p'} \end{cases}, \quad a_q^{\min} = \begin{cases} a_q^{\{t, p\}} & \text{if } t_p \leq_\gamma t'_{p'} \\ a_{q'}^{\dagger, \{t', p'\}} & \text{if } t_p >_\gamma t'_{p'} \end{cases}, \quad (4.2.12)$$

$$t^{\max} = \begin{cases} t_p & \text{if } t_p >_\gamma t'_{p'} \\ t'_{p'} & \text{if } t_p \leq_\gamma t'_{p'} \end{cases}, \quad t^{\min} = \begin{cases} t_p & \text{if } t_p \leq_\gamma t'_{p'} \\ t'_{p'} & \text{if } t_p >_\gamma t'_{p'} \end{cases}, \quad (4.2.13)$$

where the \leq_γ is to be understood with respect the contour γ . This allows to rewrite the Green's functions as

$$G_{q, q'}^{p, p'}(t, t') = -i \text{Tr} \left[T_\gamma e^{-i \int_{t^{\max}}^{\{t_0, +\}} d\tau H(\tau)} a_q^{\max} T_\gamma e^{-i \int_{t^{\min}}^{t^{\max}} d\tau H(\tau)} a_q^{\min} T_\gamma e^{-i \int_{\{t_0, -\}}^{t^{\min}} d\tau H(\tau)} \rho_{t_0}^- \right]. \quad (4.2.14)$$

Using Eq. (4.2.7) the trace can be carried out, yielding to

$$G_{q, q'}^{p, p'}(t, t') = -i \int \prod_{q''} d\bar{\psi}_{q'', 0}^- d\psi_{q'', 0}^- \langle -\psi_0^- \mid T_\gamma e^{-i \int_{t^{\max}}^{\{t_0, +\}} d\tau H(\tau)} a_q^{\max} T_\gamma e^{-i \int_{t^{\min}}^{t^{\max}} d\tau H(\tau)} a_q^{\min} \\ \times T_\gamma e^{-i \int_{\{t_0, -\}}^{t^{\min}} d\tau H(\tau)} \rho_{t_0}^- \mid \psi_0^- \rangle e^{-\sum_{q''} \bar{\psi}_{q'', 0}^- \psi_{q'', 0}^-}. \quad (4.2.15)$$

At this point the key step towards a functional integral representation is employed: the Trotter decomposition. Unity operators as defined in Eq. (4.2.6) are inserted at $N-1$ positions in the upper branch and N position in the lower branch of the Keldysh contour. Subsequently applying the limit

$N \rightarrow \infty$, leads to

$$\begin{aligned}
G_{q,q'}^{p,p'}(t, t') = & -i \lim_{N \rightarrow \infty} \int \prod_{n=0}^{N-1} \prod_{p''=\pm} \prod_{q''} d\bar{\psi}_{q'',n}^{p''} d\psi_{q'',n}^{p''} \psi_{q,n}^p \psi_{q',n}^{p'} \langle \psi_1^- | \rho_{t_0}^- | \psi_0^- \rangle \\
& \times \exp \left\{ - \sum_{n=1}^{N-1} \left[\sum_{q''} \bar{\psi}_{q'',n+1}^- \left(\psi_{q'',n+1}^- - \psi_{q'',n}^- \right) + i\Delta t \mathcal{H} \left(\{ \bar{\psi}^- \}_{n+1}, \{ \psi^- \}_n \right) \right] \right. \\
& - \sum_{n=0}^{N-1} \left[\sum_{q''} \bar{\psi}_{q'',n+1}^+ \left(\psi_{q'',n+1}^+ - \psi_{q'',n}^+ \right) - i\Delta t \mathcal{H} \left(\{ \bar{\psi}^+ \}_{n+1}, \{ \psi^+ \}_n \right) \right] \\
& \left. - \sum_{q''} \bar{\psi}_{q'',1}^- \psi_{q'',1}^- + \sum_{q''} \bar{\psi}_{q'',N}^+ \psi_{q'',N}^+ - \sum_{q''} \bar{\psi}_{q'',0}^- \psi_{q'',0}^- \right\}, \quad (4.2.16)
\end{aligned}$$

with the boundary conditions as

$$\psi_N^- \equiv \psi_0^+, \quad \psi_N^+ \equiv -\psi_0^-. \quad (4.2.17)$$

The Hamiltonian has been rewritten in terms of Grassmann variables as

$$\mathcal{H} \left(\{ \bar{\psi}^\pm \}_{n+1}, \{ \psi^\pm \}_n \right) = H(a_q^\dagger \rightarrow \bar{\psi}_{q,n+1}^\pm, a_q \rightarrow \psi_{q,n}^\pm). \quad (4.2.18)$$

Without loss of generality the density matrix can be brought into a quadratic form, which allows to calculate [Kar10a]

$$\begin{aligned}
\langle \psi | \rho | \psi' \rangle &= \langle \psi | e^{\sum_{q''} \rho_{q''} a_{q''}^\dagger a_{q''}} | \psi' \rangle = \langle \psi | \prod_{q''} \left[1 + \sum_{m=1}^{\infty} \frac{\rho_{q''}^m}{m!} \underbrace{(a_{q''}^\dagger a_{q''} \dots a_{q''}^\dagger a_{q''})}_{m\text{-pairs}} \right] | \psi' \rangle \\
&\stackrel{(4.2.1)}{=} \langle \psi | \prod_{q''} \left[1 + \bar{\psi}_{q''} \psi_{q''}' \sum_{m=1}^{\infty} \frac{\rho_{q''}^m}{m!} \underbrace{(a_{q''} \dots a_{q''}^\dagger)}_{\substack{(\psi_{q''}^2=0) \\ \rightarrow 1}} \right] | \psi' \rangle \\
&= \langle \psi | \prod_{q''} \left[1 + e^{\rho_{q''}} \bar{\psi}_{q''} \psi_{q''}' - \bar{\psi}_{q''} \psi_{q''}' \right] | \psi' \rangle \\
&= \prod_{q''} \left[1 + e^{\rho_{q''}} \bar{\psi}_{q''} \psi_{q''}' - \bar{\psi}_{q''} \psi_{q''}' \right] \left(1 + \sum_{\bar{q}''} \bar{\psi}_{\bar{q}''} \psi_{\bar{q}''}' \right) \\
&= e^{\sum_{q''} \exp(\rho_{q''}) \bar{\psi}_{q''} \psi_{q''}'}. \quad (4.2.19)
\end{aligned}$$

Identifying the quadratic (non-interacting) terms and terms in higher order of the Grassmann variables, the Green's function is rewritten in a continous representation [Neg88]

$$\begin{aligned}
G_{q,q'}^{p,p'}(t, t') = & -i \int \mathcal{D}\bar{\psi} \psi \psi_q^p(t) \bar{\psi}_{q'}^{p'}(t') \\
& \times \exp \left\{ i \int_{t_0}^{\infty} d\tau \sum_{q_1 q_2} \sum_{p_1 p_2} \bar{\psi}_{q_1}^{p_1}(\tau + \eta) [\hat{g}(\tau, \tau)^{-1}]_{q_1, q_2}^{p_1, p_2} \psi_{q_2}^{p_2}(\tau) - i S_{\text{int}} \right\}, \quad (4.2.20)
\end{aligned}$$

with $\mathcal{D}\bar{\psi} \psi = \lim_{N \rightarrow \infty} \int \prod_{n=0}^{N-1} \prod_{p''=\pm} \prod_{q''} d\bar{\psi}_{q'',n}^{p''} d\psi_{q'',n}^{p''}$.

The non-interacting terms are combined to \hat{g}^{-1} and the interaction terms are described by S_{int} . In case of only two-particle interaction, the respective action S_{int} becomes

$$S_{\text{int}} = \frac{1}{4} \sum_{1,2,1',2'} \bar{u}_{1,2,1',2'} \bar{\psi}_1 \bar{\psi}_2 \psi_{2'} \psi_{1'}, \quad (4.2.21)$$

with the multiindex $1 = \{t, p, q\}$ and the two particle interaction defined as

$$\bar{u}_{1,2,1',2'} = \delta(t_1 - t'_1)\delta(t_1 - t_2)\delta(t_1 - t'_2) \times \bar{u}_{\{q_1 p_1\}, \{q_2 p_2\}, \{q'_1 p'_1\}, \{q'_2 p'_2\}}(t_1). \quad (4.2.22)$$

The notation g^{-1} in the first term already implies that the quadratic parts sum up to the inverse of the non-interacting Green's functions. To verify this Eq. (4.2.20) is calculated with $S_{\text{int}} = 0$

$$\begin{aligned} [g]_{q,q'}^{p,p'}(t, t') &= -i \int \mathcal{D}\bar{\psi}\psi \psi_q^p(t) \bar{\psi}_{q'}^{p'}(t') \exp \left\{ i \int_{t_0}^{\infty} d\tau \sum_{q_1 q_2} \sum_{p_1 p_2} \bar{\psi}_{q_1}^{p_1}(\tau + \eta) [\hat{g}(\tau, \tau)^{-1}]_{q_1, q_2}^{p_1, p_2} \psi_{q_2}^{p_2}(\tau) \right\} \\ &= \left[\frac{\delta}{\delta \bar{\phi}_{q'}^{p'}}(t') \frac{\delta}{\delta \phi_q^p(t)} - i \int \mathcal{D}\bar{\psi}\psi \exp \left\{ i \int_{t_0}^{\infty} d\tau \sum_{q_1 q_2} \sum_{p_1 p_2} \bar{\psi}_{q_1}^{p_1}(\tau + \eta) [\hat{g}(\tau, \tau)^{-1}]_{q_1, q_2}^{p_1, p_2} \psi_{q_2}^{p_2}(\tau) \right. \right. \\ &\quad \left. \left. + \int_{t_0}^{\infty} d\tau \sum_{q_1, p_1} [\bar{\psi}_{q_1}^{p_1}(\tau) \phi_{q_1}^{p_1}(\tau) + \bar{\phi}_{q_1}^{p_1}(\tau) \psi_{q_1}^{p_1}(\tau)] \right\} \right]_{\bar{\phi}=\phi=0} \\ &= [\hat{g}]_{q,q'}^{p,p'}(t, t'), \end{aligned} \quad (4.2.23)$$

showing that it is indeed correct.

With these definitions at hand, we will use the following shorthand notations in the following

$$(\psi, \phi) = i \sum_1 \psi_1 \phi_1, \quad (\bar{\psi}, X\psi) = i \sum_{12} \bar{\psi}_1 X_{12} \psi_2, \quad (4.2.24)$$

$$S_0 = \left(\bar{\psi}, [\hat{g}]^{-1}, \psi \right) = i \sum_{1,2} \bar{\psi}_1 [\hat{g}]^{-1}_{1,2} \psi_2. \quad (4.2.25)$$

4.2.3 Generating Functionals

With the functional integral formalism introduced, generating functionals for the Green's and vertex function can be set up and relations between them are derived. The generating functionals are obtained by adding additional terms to the physical Hamiltonian in which field operators are coupled to external sources [Neg88]. From these Green's and vertex functions are obtained by taking the derivative with respect to the external field and subsequently setting the fields to zero. We follow here the presentation as employed in Ref. [Med02, Kar10a, Ken14].

Green's functions

The general m -particle Green's function is defined as

$$G_m(1 \dots m; 1' \dots m') = (-i)^m \left\langle T_{\gamma} a_{q_1}^{p_1'}[t_1']_H \dots a_{q_m}^{p_m'}[t_m']_H a_{q_m}^{p_m, \dagger}[t_m]_H \dots a_{q_1}^{p_1, \dagger}[t_1]_H \right\rangle. \quad (4.2.26)$$

The associated generating functional is

$$\mathcal{W}(\{\bar{\eta}\}, \{\eta\}) = \frac{1}{Z} \int \mathcal{D}\bar{\psi}\psi \exp \{ S_0 - iS_{\text{int}} - (\bar{\psi}, \eta) - (\bar{\eta}, \psi) \}, \quad (4.2.27)$$

such that the m -particle Green's function is generated by

$$G_m(1 \dots m; 1' \dots m') = (-i)^m \frac{\delta^m}{\delta \bar{\eta}_{1'} \dots \delta \bar{\eta}_{m'}} \frac{\delta^m}{\delta \eta_1 \dots \delta \eta_m} \mathcal{W}(\{\bar{\eta}\}, \{\eta\}) \Big|_{\eta=\bar{\eta}=0}. \quad (4.2.28)$$

The general m -particle Green's function also includes unconnected diagrams, i.e. contributions consisting of two or more diagrams which are not linked to each other at all. These unlinked diagrams are of no relevance for the propagation. Thus only **connected Green's functions** are necessary, the associated generating functional is defined via

$$\mathcal{W}^c(\{\bar{\eta}\}, \{\eta\}) = \ln [\mathcal{W}(\{\bar{\eta}\}, \{\eta\})], \quad (4.2.29)$$

where again the respective derivative is necessary

$$G_m^c(1 \dots m; 1' \dots m') = (-i)^m \frac{\delta^m}{\delta \bar{\eta}_{1'} \dots \delta \bar{\eta}_{m'}} \frac{\delta^m}{\delta \eta_1 \dots \delta \eta_m} \mathcal{W}^c(\{\bar{\eta}\}, \{\eta\}) \Big|_{\eta=\bar{\eta}=0}. \quad (4.2.30)$$

Vertex functions

The m -particle **vertex function** is defined as the sum of all one-particle irreducible diagrams with $2m$ amputated, external legs. The corresponding generating functional is the Legendre transformation of \mathcal{W}^c , the effective action

$$\Gamma(\{\bar{\phi}\}, \{\phi\}) = -\mathcal{W}^c(\{\bar{\eta}\}, \{\eta\}) - (\bar{\phi}, \eta) - (\bar{\eta}, \phi) + (\bar{\phi}, [g]^{-1}, \phi), \quad (4.2.31)$$

where the last term including the bare Green's function g has been added compared to textbook definition which proves to be convenient [Med02]. The conjugated fields are defined via

$$\phi = i \frac{\delta}{\delta \bar{\eta}} \mathcal{W}^c(\{\bar{\eta}\}, \{\eta\}) \quad \bar{\phi} = -i \frac{\delta}{\delta \eta} \mathcal{W}^c(\{\bar{\eta}\}, \{\eta\}), \quad (4.2.32)$$

The m -particle vertex functions is generated by the m th derivative of the effective action as

$$\gamma_m(1 \dots m, 1' \dots m') = (-i)^m \frac{\delta^m}{\delta \bar{\phi}_1 \dots \delta \bar{\phi}_m} \frac{\delta^m}{\delta \phi_{m'} \dots \delta \phi_{1'}} \Gamma(\{\bar{\phi}\}, \{\phi\}) \Big|_{\phi=\bar{\phi}=0}. \quad (4.2.33)$$

Relation between Green's and vertex functions

Before the generating functionals for Green's and vertex function can be used to derive the FRG, we discuss some relations between them, which prove to be useful at a later stage. By plugging in the definition of the effective action (Eq. (4.2.31)) and the generating fields, it is a straightforward calculation to show [Kar06]

$$\begin{aligned} \frac{\delta \Gamma}{\delta \phi_1} &= \sum_2 \left[-\frac{\delta \mathcal{W}^c}{\delta \eta_2} \frac{\delta \eta_2}{\delta \phi_1} - \frac{\delta \mathcal{W}^c}{\delta \bar{\eta}_2} \frac{\delta \bar{\eta}_2}{\delta \phi_1} + i \left(\bar{\phi}_2 \frac{\delta \eta_2}{\delta \phi_1} - \frac{\delta \bar{\eta}_2}{\delta \phi_1} \phi_2 - \bar{\phi}_2 [(g)^{-1}]_{21} \right) \right] + i \bar{\eta}_1 \\ &= i \left[\bar{\eta}_1 - \sum_2 \bar{\phi}_2 [(g)^{-1}]_{21} \right], \end{aligned} \quad (4.2.34)$$

$$\begin{aligned} \frac{\delta \Gamma}{\delta \bar{\phi}_1} &= \sum_2 \left[-\frac{\delta \mathcal{W}^c}{\delta \eta_2} \frac{\delta \eta_2}{\delta \bar{\phi}_1} - \frac{\delta \mathcal{W}^c}{\delta \bar{\eta}_2} \frac{\delta \bar{\eta}_2}{\delta \bar{\phi}_1} + i \left(\bar{\phi}_2 \frac{\delta \eta_2}{\delta \bar{\phi}_1} - \frac{\delta \bar{\eta}_2}{\delta \bar{\phi}_1} \phi_2 + [(g)^{-1}]_{12} \phi_2 \right) \right] - i \eta_1 \\ &= i \left[-\eta_1 + \sum_2 [(g)^{-1}]_{12} \phi_2 \right], \end{aligned} \quad (4.2.35)$$

where one needs to keep in mind that the fields $\bar{\phi}$ and ϕ are independent, i.e. $\frac{d\bar{\phi}}{d\phi} = 0$. We consider

$$\begin{aligned} i \delta_{11'} &= i \frac{\delta \phi_1}{\delta \phi_{1'}} = -\frac{\delta}{\delta \phi_{1'}} \frac{\delta \mathcal{W}^c}{\delta \bar{\eta}_1} = -\sum_2 \left[\frac{\delta \eta_2}{\delta \phi_{1'}} \frac{\delta^2 \mathcal{W}^c}{\delta \eta_2 \delta \bar{\eta}_1} + \frac{\delta \bar{\eta}_2}{\delta \phi_{1'}} \frac{\delta^2 \mathcal{W}^c}{\delta \bar{\eta}_2 \delta \bar{\eta}_1} \right] \\ &= \sum_2 \left[\left(\frac{-i \delta^2 \Gamma}{\delta \phi_{1'} \delta \bar{\phi}_2} - [(g)^{-1}]_{21'} \right) \frac{\delta^2 \mathcal{W}^c}{\delta \eta_2 \delta \bar{\eta}_1} - \frac{-i \delta^2 \Gamma}{\delta \phi_{1'} \delta \phi_2} \frac{\delta^2 \mathcal{W}^c}{\delta \bar{\eta}_2 \delta \bar{\eta}_1} \right], \end{aligned} \quad (4.2.36)$$

where the Eqs. (4.2.34) and (4.2.35) are utilized. Analog relations can be derived using $\frac{d\bar{\phi}_1}{d\phi_{1'}} = \delta_{11'}$ and $\frac{d\phi_1}{d\phi_{1'}} = \frac{d\bar{\phi}_1}{d\phi_{1'}} = 0$, which is combined to

$$\begin{pmatrix} -i \frac{\delta^2 \Gamma}{\delta \bar{\phi} \delta \phi} + (g)^{-1} & -i \frac{\delta^2 \Gamma}{\delta \bar{\phi} \delta \bar{\phi}} \\ -i \frac{\delta^2 \Gamma}{\delta \phi \delta \phi} & -i \frac{\delta^2 \Gamma}{\delta \phi \delta \bar{\phi}} - (g)^{-1, T} \end{pmatrix} \times \begin{pmatrix} -i \frac{\delta^2 \mathcal{W}^c}{\delta \bar{\eta} \delta \eta} & i \frac{\delta^2 \mathcal{W}^c}{\delta \bar{\eta} \delta \bar{\eta}} \\ i \frac{\delta^2 \mathcal{W}^c}{\delta \eta \delta \eta} & -i \frac{\delta^2 \mathcal{W}^c}{\delta \eta \delta \bar{\eta}} \end{pmatrix} = 1. \quad (4.2.37)$$

Rearranging the equation allows for the definition

$$\begin{aligned} \mathcal{V}(\{\bar{\phi}\}, \{\phi\}) &= \begin{pmatrix} -i \frac{\delta^2 \mathcal{W}^c}{\delta \bar{\eta} \delta \eta} & i \frac{\delta^2 \mathcal{W}^c}{\delta \bar{\eta} \delta \bar{\eta}} \\ i \frac{\delta^2 \mathcal{W}^c}{\delta \eta \delta \eta} & -i \frac{\delta^2 \mathcal{W}^c}{\delta \eta \delta \bar{\eta}} \end{pmatrix} \\ &= \begin{pmatrix} -i \frac{\delta^2 \Gamma}{\delta \bar{\phi} \delta \phi} + [\mathbf{g}]^{-1} & -i \frac{\delta^2 \Gamma}{\delta \bar{\phi} \delta \bar{\phi}} \\ -i \frac{\delta^2 \Gamma}{\delta \phi \delta \phi} & -i \frac{\delta^2 \Gamma}{\delta \phi \delta \bar{\phi}} - [\mathbf{g}]^{-1, T} \end{pmatrix}^{-1}. \end{aligned} \quad (4.2.38)$$

While we have only stated the definitions of the Green's and vertex functions and their associated generating functionals so far, we can now relate the full and the bare single particle Green's function to the one-particle vertex function γ_1 by considering the (1,1) element of Eq. (4.2.38) at vanishing fields

$$G_1(1'; 1) = G_1^c(1'; 1) = -i \frac{\delta^2 \mathcal{W}^c}{\delta \bar{\eta}_{1'} \delta \eta_1} \Big|_{\eta=\bar{\eta}=0} = \left[-i \frac{\delta^2 \Gamma}{\delta \bar{\phi} \delta \phi} \Big|_{\phi=\bar{\phi}=0} + \mathbf{g}^{-1} \right]_{1'1}^{-1}, \quad (4.2.39)$$

where it is used that there is no unconnected part in a single particle Green's function. The resulting expression is a well known relation namely the Dyson equation, which allows to identify the one-particle vertex function

$$\gamma_1 = -i \frac{\delta^2 \Gamma}{\delta \bar{\phi} \delta \phi} \Big|_{\phi=\bar{\phi}=0} = -\Sigma, \quad (4.2.40)$$

as the self-energy up to a minus sign. This proves all the definitions of this section as correct and meaningful.

4.3 Floquet theory

For the calculation of the long-time behavior of time periodically driven quantum dot systems Floquet-Green's functions can be employed [Shi65, Win93, Arr05, Arr06, Wu08, Tsu08, Ren14, Gen15, Wu08]. Here the Floquet theory is reviewed [Gri98] to justify the required transformations. The **Floquet theorem** states that any differential equation of the form [Flo83]

$$\frac{d}{dt} \Psi(t) = A(t) \Psi(t) \quad (4.3.1)$$

with a time periodic operator $A(t) = A(t + T)$ and the period T has a solution

$$\Psi_\alpha(t) = e^{-i\epsilon_\alpha t/\hbar} \phi_\alpha(t), \quad (4.3.2)$$

where the Floquet modes $\phi_\alpha(t)$ have the same periodicity as the operator $A(t)$: $\phi_\alpha(t) = \phi_\alpha(t + T)$. This theorem equals the Bloch theorem used to describe space periodic structures.

The structure of the periodic solution renders it convenient to define a **Floquet Hamiltonian**

$$\mathcal{H}(t) = H(t) - i\hbar \frac{\partial}{\partial t}, \quad (4.3.3)$$

such that the Floquet modes $\phi_\alpha(t)$ are its eigenfunction with the respective eigenenergy ϵ_α . The resulting quasienergy eigenvalue equation has the form of the time-independent Schrödinger equation [Gri98], which constitutes one of the main advantage of the Floquet theory based approaches.

It then becomes useful to define the **Floquet space** as a composite space of the real space \mathcal{R} and the space of time periodic functions \mathcal{T} . Its basis is given by

$$|i, k\rangle = |i\rangle \otimes |k\rangle, \quad (4.3.4)$$

with $|i\rangle = c_i^\dagger |0\rangle$ and the Fourier basis $|k\rangle$ with $k \in \mathbb{Z}$. The respective elements of the time periodic Hamiltonian in the space of time periodic functions are

$$\langle k | H | k' \rangle = H_{k,k'} = \frac{1}{T} \int_0^T dt e^{i(k-k')\Omega t} H(t), \quad (4.3.5)$$

defined via the Fourier transformation. The Fourier series of the single time dependent parameters

$$\epsilon_{ij}(t) = \sum_k \epsilon_{ij;k} e^{ik\Omega t} \quad (4.3.6)$$

leads to a single-particle part of the Floquet Hamiltonian of the form

$$\langle i, k | \mathcal{H} | j, k' \rangle = (\epsilon_{ij;0} - k\Omega \delta_{ij}) \delta_{kk'} + \epsilon_{ij;k'-k}. \quad (4.3.7)$$

Time independent parameters are diagonal in \mathcal{T} , while off-diagonal elements are given by the respective Fourier coefficients.

The Floquet theorem thus states that the solution of the Dyson equation (4.1.23) in the long time limit, where all transient behavior has died out, is of periodic form with the same period T as given. This justifies the following transformation.

4.4 Floquet-Green's function

4.4.1 Transformation to Floquet space

We here present the transformation of the initially double time dependent Green's function to Floquet space [Wu08]. First one of the time dependence is Fourier transformed to the energy space

$$G_{ij}^X(t, \omega) = \int_{-\infty}^{\infty} dt' e^{i\omega(t-t')} G_{ij}^X(t, t'), \quad (4.4.1)$$

with the respective backtransform

$$G_{ij}^X(t, t') = \frac{1}{2\pi} \int_{-\infty}^{\infty} d\omega e^{i\omega(t'-t)} G_{ij}^X(t, \omega). \quad (4.4.2)$$

The remaining time dependency can be Fourier expanded

$$G_{ij}^X(t, \omega) = \sum_k G_{ij;k}^X(\omega) e^{-ik\Omega t}, \quad (4.4.3)$$

with the according Fourier coefficients defined as

$$G_{ij;k}^X(\omega) = \frac{|\Omega|}{2\pi} \int_0^T dt e^{ik\Omega t} G_{ij}^X(t, \omega). \quad (4.4.4)$$

The initial single dependency on the new Fourier coefficient is artificially extended as

$$G_{ij;k}^X = G_{ij;k0}^X, \quad (4.4.5)$$

which by using the relation

$$G_{ij;kk'}^X(\omega) = G_{ij;k-k'0}^X(\omega + k'\Omega) \quad (4.4.6)$$

can be generalized to

$$G_{ij;kk'}^X(\omega) = \langle i, k | G^X(\omega) | j, k' \rangle \quad (4.4.7)$$

in Floquet space for $X \in \{c, \tilde{c}, <, >, \text{ret}, \text{adv}, K\}$. It allows for a convenient matrix multiplication in Floquet space. Nevertheless, the physical Fourier coefficient is the difference $k_1 = k - k'$. All these transformation apply equally to the self-energy.

The here presented transform is a convenient reformulation of the transform presented in Ref. [Tsu08, Gen15, Ren14] for the special case of only two time dependent Green's functions. A generalization to objects depending on more than two times requires the definition of relative/average times and an according transformation of these.

4.4.2 Symmetries

The symmetries of the Green's functions as well as the self-energies known from the explicitly time dependent case [Ken12a]

$$G_{ij}^{\text{adv}}(t, t') = [G_{ji}^{\text{ret}}(t', t)]^* \quad G_{ij;kk'}^{\text{K}}(t, t') = -[G_{ji;k'k}^{\text{K}}(t', t)]^* \quad (4.4.8)$$

$$\Sigma_{ij}^{\text{adv}}(t, t') = [\Sigma_{ji}^{\text{ret}}(t', t)]^* \quad \Sigma_{ij;kk'}^{\text{K}}(t, t') = -[\Sigma_{ji;k'k}^{\text{K}}(t', t)]^* \quad (4.4.9)$$

transform to

$$G_{ij;kk'}^{\text{adv}}(\omega) = [G_{ji;k'k}^{\text{ret}}(\omega)]^* \quad G_{ij;kk'}^{\text{K}}(\omega) = -[G_{ji;k'k}^{\text{K}}(\omega)]^* \quad (4.4.10)$$

$$\Sigma_{ij;kk'}^{\text{adv}}(\omega) = [\Sigma_{ji;k'k}^{\text{ret}}(\omega)]^* \quad \Sigma_{ij;kk'}^{\text{K}}(\omega) = -[\Sigma_{ji;k'k}^{\text{K}}(\omega)]^* \quad (4.4.11)$$

in Floquet space.

4.4.3 Dyson equation

First, we apply the transformations of Eqs. (4.4.1 - 4.4.4) to the differential equation of the non-interacting Green's function

$$\left(i \frac{\partial}{\partial t} - \hat{\epsilon}(t)\right) \hat{g}(t, t') = \delta(t - t') \mathbb{1}, \quad (4.4.12)$$

and consider only the retarded component, which results in

$$(\omega + k\Omega) \underline{\underline{g}}_{kk'}^{\text{ret}}(\omega) - \sum_{k_1} \epsilon_{k_1-k} \underline{\underline{g}}_{k_1 k'}^{\text{ret}}(\omega) = \delta_{kk'}, \quad (4.4.13)$$

where ϵ_{k_1-k} are the entries of the one particle dot Hamiltonian. This is converted to

$$\underline{\underline{g}}^{\text{ret}}(\omega) = \frac{1}{\omega - \mathcal{H} + i0^+}. \quad (4.4.14)$$

The double underlines indicate the objects as a matrix in Floquet space. The retarded Green's function can be identified as the resolvent of the Floquet Hamiltonian.

In order to transform the Dyson equation

$$\left[i \frac{\partial}{\partial t} - \hat{\epsilon}(t)\right] \hat{G}(t, t') - \int_{t_0}^{\infty} dt_1 \hat{\Sigma}(t, t_1) \hat{G}(t_1, t') = \delta(t - t') \mathbb{1}, \quad (4.4.15)$$

to Floquet space, we employ the long time limit $t_0 \rightarrow \infty$ and subsequently Green's function and self-energy can be transformed by Eqs. (4.4.1 - 4.4.4) and the single particle part of the Hamiltonian by Eq. (4.3.7).

Retarded/Advanced Green's function

This results in

$$\left[(\omega + k\Omega) \underline{\underline{1}} - (\underline{\underline{\epsilon}} + \underline{\underline{\Sigma}}^{\text{ret(adv)}}(\omega))\right] \underline{\underline{G}}^{\text{ret(adv)}} = \underline{\underline{1}} \quad (4.4.16)$$

for the retarded (advanced) component. Summation over the real space quantum numbers as well as the Floquet index is assumed. The identity is defined accordingly as $\underline{\underline{1}}_{ij, kk'} = \delta_{ij} \delta_{kk'}$ and $\underline{\underline{\epsilon}}$ indicates the matrix of the single particle part of the Hamiltonian with the coefficients defined in Eq. (4.3.7).

Keldysh Green's function

The Keldysh Green's function is given by ($t_0 \rightarrow \infty$)

$$G^K(t, t') = \int dt_1 \int dt_2 G^{\text{ret}}(t, t_1) [\Sigma^K(t_1, t_2)] G^{\text{adv}}(t_2, t') \quad (4.4.17)$$

which transform with Eqs. (4.4.1 - 4.4.4) and the relation Eq. (4.4.6) to

$$\underline{\underline{G}}^{\text{K}}(\omega) = \underline{\underline{G}}^{\text{ret}}(\omega) \underline{\underline{\Sigma}}^{\text{K}}(\omega) \underline{\underline{G}}^{\text{adv}}(\omega), \quad (4.4.18)$$

assuming summation over all internal indices.

4.5 Reservoir self-energy: Dressed Green's function

Up to now only the dot system has been considered, but we aim at the description of an open system. In this section we thus now discuss the non-interacting reservoir Green's functions and subsequently calculate the reservoir self-energy. The projection method is then presented to define a reservoir dressed Green's function, which includes the influence of the reservoirs on the dot parameters exact.

4.5.1 Reservoir Green's functions

The reservoirs are assumed to be time independent, semi-infinite baths of noninteracting electrons. The resulting free retarded/advanced reservoir Green's functions are calculated via Eq. (4.1.25) and can quite generally be expressed in terms of the reservoir density of states [Kar10a, Jak09]

$$g_{\text{res},\alpha}^{\text{ret(adv)}}(\omega) = \mp i\pi\rho_{\text{res},\alpha}(\omega) + \mathcal{P} \int \frac{\rho_{\text{res},\alpha}(\omega')}{\omega - \omega'} d\omega', \quad (4.5.1)$$

with \mathcal{P} indicating the principal value. Due to the missing time dependency the non-interacting Green's functions are diagonal in Floquet space, such that

$$g_{\text{res},\alpha, kk'}^{\text{ret(adv)}}(\omega) = g_{\text{res},\alpha}^{\text{ret(adv)}}(\omega) \delta_{k,k'}, \quad (4.5.2)$$

and Keldysh Green's function can be calculated by employing a dissipation-fluctuation theorem like relation valid in equilibrium for Floquet space

$$g_{\text{res},\alpha, kk'}^{\text{K}}(\omega) = [1 - 2f_{\alpha}(\omega + k\Omega)] [g_{\text{res},\alpha, kk'}^{\text{ret}}(\omega) - g_{\text{res},\alpha, kk'}^{\text{adv}}(\omega)], \quad (4.5.3)$$

where $f_{\alpha}(\omega)$ is the Fermi function of the reservoir α . The retarded/advanced Green's function can thus be calculated as in the time translational case.

Tight-binding chain

One possibility to model the semi-infinite bath is a tight-binding chain defined as

$$H_{\text{res},\alpha} = -\nu_{\alpha} \sum_{n=0}^{\infty} c_n^{\dagger} c_{n+1} + \text{H.c.}, \quad (4.5.4)$$

with annihilation (creation) operator c_n (c_n^{\dagger}) on the n th side of chain. The respective free Green's functions are calculated to [Jak09]

$$g_{\text{res},\alpha}^{\text{ret}}(\omega) = \frac{1}{2\nu_{\alpha}^2} \begin{cases} -\text{sgn}(\omega) \sqrt{\omega^2 - 4\nu_{\alpha}^2} & |\omega| > 2\nu_{\alpha} \\ \omega - i\sqrt{4\nu_{\alpha}^2 - \omega^2} & |\omega| \leq 2\nu_{\alpha} \end{cases} = [g_{\text{res},\alpha}^{\text{adv}}(\omega)]^*, \quad (4.5.5)$$

where ν_{α} is the bandwidth of the reservoir α .

4.5.2 Projection Technique: Reservoir self-energy

We like to find now a Green's function which describes the local quantum system including the effect of the coupled reservoirs. The Hamiltonian as defined in Section 3.1 is of the following form

$$H = H_{\text{dot},0} + H_{\text{dot,int}} + H_{\text{coupl}} + H_{\text{res}} \quad (4.5.6)$$

where the sum over the different reservoirs α have been absorbed into the definition of the coupling and reservoir Hamiltonian compared to Eq. (3.1.1). No direct link between the reservoirs is assumed. The projection technique as described in Ref. [Tay72] is employed here [Kar10a, Ken14]. Key idea is to divide the whole system into a local system (P) and the reservoir part (Q) such that symbolically $1 = P + Q$ with P and Q as the respective projectors on the different parts of the system. Introducing the identities in the Dyson equation yields

$$1G1 = 1g1 + 1g11\Sigma11G1 \quad (4.5.7)$$

where all indices are suppressed. From this we can derive

$$G_{PP} = g_{PP} + g_{PP} \Sigma_{PP} G_{PP} + g_{PP} \Sigma_{PQ} G_{QP} \quad (4.5.8)$$

$$G_{QP} = g_{QQ} \Sigma_{QP} G_{PP} \quad (4.5.9)$$

because $g_{QP} = g_{PQ} = \Sigma_{QQ} = 0$. Solving this for G_{PP} yields

$$G_{PP} = [(g_{PP})^{-1} - \Sigma_{PQ} g_{QQ} \Sigma_{QP} - \Sigma_{PP}]^{-1} \quad (4.5.10)$$

where $\Sigma_{PQ} g_{QQ} \Sigma_{QP} = \Sigma_{\text{res}}$, which can be calculated exactly, since Σ_{PQ} originates from the coupling between reservoir and system only. Σ_{PP} covers the two-particle interaction on the dot. As a result, we distinguish the following Green's functions (GF):

$$\begin{aligned} \text{Non-interacting local GF : } g &= g_{PP}, \\ \text{Non-interacting reservoir GF : } g_{\text{res}} &= g_{QQ}, \\ \text{Reservoir dressed, non-interacting GF : } G^0 &= G_{PP}^0 = [(g_{PP})^{-1} - \Sigma_{PQ} g_{QQ} \Sigma_{QP}]^{-1}, \\ \text{Full (reservoir dressed, interacting) GF : } G &= G_{PP} = [(g_{PP})^{-1} - \Sigma_{PQ} g_{QQ} \Sigma_{QP} - \Sigma_{PP}]^{-1}, \end{aligned} \quad (4.5.11)$$

The reservoir dressed, non-interacting Green's function will be used as bare Green's function in the following, including the reservoir's effect on the dot parameters. The Dyson equation like form of the calculation of the reservoir dressed Green's function from the non-interacting, dot Green's function and the reservoir self-energy can also be deduced from a physical interpretation: The propagation between two dot states can contain an arbitrary number of temporal excursions into each of the reservoirs, where one excursion consists of tunneling into a single particle state of the reservoir, free propagation in the reservoir and tunneling back into the dot regime [Jak09]. Summing all these contributions by a geometric series results in the same expression.

The expression $\Sigma_{PQ} g_{QQ} \Sigma_{QP}$ can either be evaluated in Floquet space directly, or one transforms the known time dependent equivalent [Ken12a] to Floquet space. Either way, the reservoir self-energy is in general given by

$$\begin{pmatrix} [\Sigma_{\text{res}}^{\text{ret}}]_{ij;kk'} & [\Sigma_{\text{res}}^{\text{K}}]_{ij;kk'} \\ 0 & [\Sigma_{\text{res}}^{\text{adv}}]_{ij;kk'} \end{pmatrix} = \sum_{q_\alpha, k_1} v_{q_\alpha, i, k-k_1}^* \begin{pmatrix} g_{\text{res}, \alpha}^{\text{ret}} & g_{\text{res}, \alpha}^{\text{K}} \\ 0 & g_{\text{res}}^{\text{adv}, \alpha} \end{pmatrix}_{q_\alpha, k_1, k_1} v_{q_\alpha, j, k_1-k'}. \quad (4.5.12)$$

with the respective non-interacting reservoir Green's functions.

4.5.3 Dissipation Fluctuation Theorem for Reservoir Self-energy

Since for the noninteracting reservoir Green's functions the dissipation-fluctuation theorem holds, the Keldysh self-energy follows as

$$\Sigma_{\text{res}, ij, kk'}^{\alpha, \text{K}}(\omega) = \sum_{k_1, q_\alpha} v_{q_\alpha, i, k-k_1}^* [1 - 2 f_\alpha(\omega + k_1 \Omega)] [g_{\text{res}}^{\alpha, \text{ret}}(\omega) - g_{\text{res}}^{\alpha, \text{adv}}(\omega)] v_{q_\alpha, j, k_1-k'}. \quad (4.5.13)$$

Only if all time dependency is on the dot, i.e. the coupling is time independent, we can find a dissipation fluctuation like relation for the reservoir self-energy in Floquet space as

$$\underline{\Sigma}_{\text{res}}^{\alpha, \text{K}}(\omega) = [\underline{\mathbf{1}} - 2 \underline{F}^\alpha(\omega)] [\underline{\Sigma}_{\text{res}}^{\alpha, \text{ret}}(\omega) - \underline{\Sigma}_{\text{res}}^{\alpha, \text{adv}}(\omega)], \quad (4.5.14)$$

with $\underline{F}^\alpha(\omega)_{kk'} = f_\alpha(\omega + k \Omega) \delta_{k, k'}$. In order to shift the time dependency of the chemical potential to the hopping on the dot, a gauge transformation can be employed (see Section 3.4).

Wide band limit

In the present thesis, all results are obtained in the wide band limit modeling a flat, structureless band

$$g_{\text{res},\alpha}^{\text{ret}}(\omega) = -i/\nu_\alpha = -i\pi\rho_{\text{res}} = [g_{\text{res},\alpha}^{\text{adv}}(\omega)]^* . \quad (4.5.15)$$

If all time dependency is on the dot, the resulting reservoir self-energies are

$$\Sigma_{ij,kk'}^{\text{ret/adv}}(\omega) = \mp iD\delta_{kk'}\delta_{ij}(\delta_{i1} + \delta_{i3}), \quad (4.5.16)$$

$$\Sigma_{ij,kk'}^{\text{K}}(\omega) = -2iD[1 - 2f_{\text{L}}(\omega + k\Omega)]\delta_{kk'}\delta_{ij}\delta_{i1} - 2iD[1 - 2f_{\text{R}}(\omega + k\Omega)]\delta_{kk'}\delta_{ij}\delta_{i3}, \quad (4.5.17)$$

with D defined in Eq. (3.3.3) and $f_\alpha(\omega)$ is the Fermi function of reservoir α .

The wide band limit is employed by setting $v_\alpha \rightarrow \infty$ and $\nu_\alpha \rightarrow \infty$, such that $D = (v_\alpha)^2/\nu_\alpha$ remains constant. Only subsequently the limit $D \rightarrow \infty$ is applied, as described in Section 3.3 to model the single level quantum dot.

4.6 Observables

We aim at describing the transport in time periodically driven systems. It is described by the following single particle observables which can be calculated from the full Green's functions. We focus here on the most simple case of only two reservoirs coupled, namely a right (R) and a left (L) one.

4.6.1 Occupancy

The dot occupancy is defined as

$$\bar{n}_i(t) = \langle c_i^\dagger(t)c_i(t) \rangle = \frac{1}{i} G_{ii}^<(t, t) . \quad (4.6.1)$$

Expressing it in terms of Keldysh Green's functions and employing the Fourier series as

$$\bar{n}_i(t) = \sum_k n_{i,k} e^{ik\Omega t} , \quad (4.6.2)$$

the Fourier coefficients are given by

$$n_{i,k} = \frac{1}{4\pi i} \left[\int d\omega G_{ii,-k0}^{\text{K}}(\omega) \right] + \frac{1}{2} \delta_{k,0} . \quad (4.6.3)$$

4.6.2 Charge susceptibility

For the sake of completeness, we restate the definition of the charge susceptibility

$$\chi = \left. \frac{dn}{d\epsilon} \right|_{\epsilon=0} , \quad (4.6.4)$$

with ϵ as the dot onsite energy. The respective higher harmonics are defined as

$$\chi_k = \left. \frac{dn_k}{d\epsilon} \right|_{\epsilon=0} . \quad (4.6.5)$$

4.6.3 Current

Another important observable is the charge current flowing from reservoir α into the dot, which is defined as [Mei92]

$$J_\alpha(t) = \mp \partial_t N_\alpha(t) = -i \text{Tr} \rho_0 [H(t), N_\alpha(t)] , \quad (4.6.6)$$

where N_α is the particle number operator of the reservoir α . We illustrate the calculation for the current flowing from the left reservoir, but the right current can be calculated analogously (with c_R and d_3).

$$J_L(t) = -iT_L^* \left\langle \left[d_1^\dagger c_L, c_L^\dagger d_1 \right] [t] - \text{h.c.} \right\rangle_{\rho_{t_0}} = -T_L^* G_{L,1}^<(t, t) + \text{c.c.} \quad (4.6.7)$$

We again employ the projection method to compute $G_{L,1}^<(t, t')$.

$$\begin{aligned} J_L(t) &= -v_L^* \int_{t_0}^{\infty} \begin{pmatrix} g_{\text{res},L}^c(t, t') & g_{\text{res},L}^<(t, t') \\ g_{\text{res},L}^>(t, t') & g_{\text{res},L}^c(t, t') \end{pmatrix} \begin{pmatrix} v_L & 0 \\ 0 & -T_L \end{pmatrix} \begin{pmatrix} G_{11}^c(t', t) & G_{11}^<(t', t) \\ G_{11}^>(t', t) & G_{11}^c(t', t) \end{pmatrix} \Big|_{<} dt' + \text{c.c.} \\ &= -|v_L|^2 \int_{t_0}^{\infty} [g_{\text{res},L}^c(t, t') G_{11}^<(t', t) - g_{\text{res},L}^<(t, t') G_{11}^c(t', t)] dt' + \text{c.c.} \\ &= -|v_L|^2 \int_{t_0}^{\infty} [g_{\text{res},L}^{\text{ret}}(t, t') G_{11}^<(t', t) - g_{\text{res},L}^<(t, t') G_{11}^{\text{adv}}(t', t)] dt' + \text{c.c.} \\ &= \frac{-|v_L|^2}{2} \int_{t_0}^{\infty} [g_{\text{res},L}^{\text{ret}}(t, t') G_{11}^K(t', t) + g_{\text{res},L}^K(t, t') G_{11}^{\text{adv}}(t', t)] dt' + \text{c.c.} \quad (4.6.8) \end{aligned}$$

where the expression is recasted only by the utilization of known relations between the Green's functions and $G^{\text{ret}}(t, t') \sim \Theta(t - t')$.

Using Eq. (4.5.12), it can be rewritten to

$$J_\alpha(t) = -\text{Re} \int dt' \Sigma_\alpha^{\text{ret}}(t, t') G^K(t', t) - G^{\text{ret}}(t, t') \Sigma_\alpha^K(t', t) , \quad (4.6.9)$$

for the steady state ($t_0 \rightarrow -\infty$) and with a summation over the dot indices assumed.

Applying the transformation to Floquet space yields

$$J_\alpha(t) = \frac{1}{4\pi} \sum_k e^{ik\Omega t} \int_{-\infty}^{\infty} d\omega \left[\underline{\Sigma}_\alpha^{\text{ret}}(\omega) \underline{G}^K(\omega) - \underline{G}^{\text{ret}}(\omega) \underline{\Sigma}_\alpha^K(\omega) \right]_{-k,0} + [\dots]_{k,0}^* . \quad (4.6.10)$$

If the Fourier series of the currents is

$$J_\alpha(t) = \sum_k J_{\alpha,k} e^{ik\Omega t} , \quad (4.6.11)$$

the respective coefficients can be identified as

$$J_{\alpha,k} = \frac{1}{4\pi} \sum_{k'} \int_{-\infty}^{\infty} d\omega \left[\hat{\Sigma}_{\alpha,-k-k'}^{\text{ret}}(\omega + k'\Omega) \hat{G}_{k'}^K(\omega) - \hat{G}_{-k-k'}^{\text{ret}}(\omega + k'\Omega) \hat{\Sigma}_{\alpha,k'}^K(\omega) \right] + [-k \rightarrow k]^* . \quad (4.6.12)$$

The mean value of the current $J_{k=0} = J_{L,k=0} = J_{R,k=0}$ indicates the pumping power, i.e. the average amount of pumped charge per unit time.

4.6.4 Pumped charge

For the discussion of quantum pumps in periodically driven systems the pumped charge per period is of great interest and defined as

$$Q = \frac{1}{2} \int_0^T dt (J_L(t) - J_R(t)) . \quad (4.6.13)$$

It is connected to the pumping power via $Q = J_{k=0} T$.

4.6.5 Linear conductance

To study the linear response of the current to a small static bias voltage, the linear conductance can be calculated as

$$G_{\alpha}(t) = \lim_{V \rightarrow 0} \frac{dJ_{\alpha}(t)}{dV}, \quad (4.6.14)$$

with the Fourier coefficients defined as

$$G_{\alpha,k} = \lim_{V \rightarrow 0} \frac{dJ_{\alpha,k}}{dV}. \quad (4.6.15)$$

4.6.6 Spectral function

In order to examine the influence of the time periodicity on the spectrum, the time averaged spectral function is calculated by

$$A_0(\omega) = -\frac{1}{\pi} \text{Im} G_{11,00}^{\text{ret}}(\omega) \quad (4.6.16)$$

from the zeroth component of the reservoir dressed, dot Green's function.

Chapter 5

Functional Renormalization Group in Floquet space

Contents

5.1	Fundamental idea	37
5.2	Flow equation	38
5.2.1	Derivation	38
5.2.2	Initial condition	41
5.2.3	Truncation	42
5.3	Flow equation in Floquet space	43
5.3.1	Cutoff scheme: Auxiliary reservoirs	43
5.3.2	Flow Equation	44
5.3.3	Symmetries: A short discussion	44
5.3.4	Renormalized parameters	45
5.3.5	Numerical implementation	45

The present chapter introduces the functional renormalization group (FRG) as the main method used in this thesis. After the introduction of the general idea, the flow equations are derived, as well as initial conditions and truncation schemes of the infinite hierarchy are discussed. Subsequently the flow equation in Floquet space is discussed with the concrete, utilized cutoff scheme. After a short discussion of the preservation of symmetries, the main flow equation describing the renormalization of the hopping matrix elements as well as the onsite energy for a time independent interaction are stated. We conclude the chapter with a few comments on the numerical implementation.

5.1 Fundamental idea

The functional renormalization group is based on the RG idea developed by Wilson [Wil74] to tackle problems where the contributing energy scales are separated by several orders of magnitude. The key idea is to treat the degrees of freedom with different energy scales successively to avoid possible infrared divergencies, which perturbative approaches are often plagued when tackling low-dimensional systems [Met12]. Even though earlier version of RG methods set up on a functional level are known [Weg73, Pol84, Wie88], the formulation of the 'exact' RG with a flow equation for the effective action by Wetterich [Wet93] is the origin of the FRG formulation used in the present thesis.

In this FRG framework the successive treatment of energy scales is realized by inserting an artificial energy scale Λ into the bare Green's function

$$G^0 \rightarrow G^{0,\Lambda} \quad \text{such that} \quad G^{0,\Lambda=\infty} = 0, \quad G^{0,\Lambda=0} = G^0. \quad (5.1.1)$$

As a consequence, the effective action also depends on the flow parameter. It allows to derive an according flow equation for the effective action. Expansion in the external fields leads to an infinite hierarchy of differential equation for the m -particle vertex functions γ_m of the form

$$\frac{d}{d\Lambda} \gamma_m^\Lambda = \mathcal{F}(\gamma_1^\Lambda, \gamma_2^\Lambda, \dots, \gamma_{m+1}^\Lambda, \Lambda). \quad (5.1.2)$$

This a priori exact reformulation of the many-body problem would yield exact results if one could solve the whole hierarchy of differential equations. The flow parameter is integrated from an exactly solvable starting point to an effective physical system at the end of the flow, where contributions of all energy scales are summed up throughout the flow regularizing possible infrared divergencies. Differently than in the original Wilsonian RG not only contributions below the flow parameter are kept, but informations on properties of all energy scales are accessible [Met12].

While it is not possible to solve the infinite hierarchy exactly (or only for anyway exactly solvable models), different truncation schemes can be employed adjusted to the considered problem. The main advantage of the method is that besides the truncation no approximations or assumptions need to be plugged in, rendering it a very flexible method, where the flow equations can be set up for very diverse problems in an according basis. The physical (comparatively) transparent flow equation automatically handle the different energy scales successively and allow under some conditions even for analytical insights.

5.2 Flow equation

The derivations presented here follow the route as applied in Ref. [Med02, Kar10a, Ken14, Met12].

5.2.1 Derivation

Flow of the generating functional of the Green's function

For the derivation of the flow equation, we redefine the functional \mathcal{W} of Eq. (4.2.27)

$$\mathcal{W}^\Lambda(\{\bar{\eta}\}, \{\eta\}) = \frac{1}{Z_0^\Lambda} \int \mathcal{D}\bar{\psi}\psi \exp \{S_0^\Lambda - iS_{\text{int}} - (\bar{\psi}, \eta) - (\bar{\eta}, \psi)\}, \quad (5.2.1)$$

by substituting Z by Z_0 for convenience, which changes \mathcal{W}^c and Γ only by a constant and thus does not change the connected Green's and vertex functions $G_{m \geq 1}^c$ and $\gamma_{m \geq 1}$. The introduction of the flow parameter Λ in the Green's function (where the exact implementation is discussed in Section 5.3.1), yields a Λ dependent bare action

$$S_0^\Lambda = \left(\bar{\psi}, [G^{0,\Lambda}]^{-1} \psi \right). \quad (5.2.2)$$

Taking the derivative of $\mathcal{W}^c = \ln \mathcal{W}$ results in the flow equation

$$\dot{\mathcal{W}}^{c,\Lambda} = \frac{1}{\mathcal{W}^\Lambda} \partial_\Lambda \left[\frac{1}{Z_0^\Lambda} \int \mathcal{D}\bar{\psi}\psi \exp \{S_0^\Lambda - iS_{\text{int}} - (\bar{\psi}, \eta) - (\bar{\eta}, \psi)\} \right]. \quad (5.2.3)$$

To evaluate it further, we take a closer look at the Λ dependent part

$$\begin{aligned} \partial_\Lambda \frac{e^{S_0^\Lambda}}{Z_0^\Lambda} &= \frac{e^{S_0^\Lambda}}{Z_0^\Lambda} \left[(\bar{\psi}, \partial_\Lambda [G^{0,\Lambda}]^{-1} \psi) - i \sum_{1,1'} \left\{ \int \frac{\mathcal{D}\bar{\psi}\psi}{Z_0^\Lambda} \bar{\psi}_1 \psi_{1'} e^{S_0^\Lambda} [\partial_\Lambda [G^{0,\Lambda}]^{-1}]_{1,1'} \right\} \right] \\ &= \frac{e^{S_0^\Lambda}}{Z_0^\Lambda} \{ (\bar{\psi}, \partial_\Lambda [G^{0,\Lambda}]^{-1} \psi) - \text{Tr} [G^{0,\Lambda} \partial_\Lambda [G^{0,\Lambda}]^{-1}] \}, \end{aligned} \quad (5.2.4)$$

which simplifies the flow equation to

$$\dot{\mathcal{W}}^{c,\Lambda} = -\text{Tr} [G^{0,\Lambda} \partial_\Lambda [G^{0,\Lambda}]^{-1}] + \frac{1}{\mathcal{W}^\Lambda} \left(\frac{\delta}{\delta \eta}, \{ \partial_\Lambda [G^{0,\Lambda}]^{-1} \} \frac{\delta}{\delta \bar{\eta}} \right) \mathcal{W}^\Lambda. \quad (5.2.5)$$

We aim at a closed expression only explicitly depending on \mathcal{W}^c , and hence rewrite

$$\begin{aligned}
\frac{1}{\mathcal{W}^\Lambda} \left(\frac{\delta}{\delta \eta}, \partial_\Lambda [G^{0,\Lambda}]^{-1} \frac{\delta}{\delta \bar{\eta}} \right) \mathcal{W}^\Lambda &= e^{-\mathcal{W}^{c,\Lambda}} \left(\frac{\delta}{\delta \eta}, \partial_\Lambda [G^{0,\Lambda}]^{-1} \frac{\delta}{\delta \bar{\eta}} \right) e^{\mathcal{W}^{c,\Lambda}} \\
&= \left(\frac{\delta \mathcal{W}^{c,\Lambda}}{\delta \eta}, \partial_\Lambda [G^{0,\Lambda}]^{-1} \frac{\delta \mathcal{W}^{c,\Lambda}}{\delta \bar{\eta}} \right) + \left(\frac{\delta}{\delta \eta}, \partial_\Lambda [G^{0,\Lambda}]^{-1} \frac{\delta}{\delta \bar{\eta}} \right) \mathcal{W}^{c,\Lambda} \\
&= \left(\frac{\delta \mathcal{W}^{c,\Lambda}}{\delta \eta}, \partial_\Lambda [G^{0,\Lambda}]^{-1} \frac{\delta \mathcal{W}^{c,\Lambda}}{\delta \bar{\eta}} \right) + i \sum_{1,1'} \left[\frac{\delta^2 \mathcal{W}^{c,\Lambda}}{\delta \eta_1 \delta \bar{\eta}_{1'}} [\partial_\Lambda [G^{0,\Lambda}]^{-1}]_{1,1'} \right] \\
&= \left(\frac{\delta \mathcal{W}^{c,\Lambda}}{\delta \eta}, \partial_\Lambda [G^{0,\Lambda}]^{-1} \frac{\delta \mathcal{W}^{c,\Lambda}}{\delta \bar{\eta}} \right) - i \text{Tr} \left[\partial_\Lambda [G^{0,\Lambda}]^{-1} \frac{\delta^2 \mathcal{W}^{c,\Lambda}}{\delta \bar{\eta} \delta \eta} \right].
\end{aligned} \tag{5.2.6}$$

Finally, we obtain a flow equation for the generating functional of the connected Green's functions

$$\begin{aligned}
\dot{\mathcal{W}}^{c,\Lambda} &= -\text{Tr} [G^{0,\Lambda} \partial_\Lambda [G^{0,\Lambda}]^{-1}] + i \text{Tr} \left[\partial_\Lambda [G^{0,\Lambda}]^{-1} \frac{\delta^2 \mathcal{W}^{c,\Lambda}}{\delta \bar{\eta} \delta \eta} \right] \\
&\quad + \left(\frac{\delta \mathcal{W}^{c,\Lambda}}{\delta \eta}, \partial_\Lambda [G^{0,\Lambda}]^{-1} \frac{\delta \mathcal{W}^{c,\Lambda}}{\delta \bar{\eta}} \right).
\end{aligned} \tag{5.2.7}$$

Flow of the generating functional of the vertex function

For the FRG frame employed in this thesis, this is only one step on the route to the flow equation of the vertex functions. Next we consider the flow equation of the effective action, which generates the vertex functions. The effective action is a Legendre transform of \mathcal{W}^c , where the conjugated fields are defined via Eq. (4.2.32). While ϕ and $\bar{\phi}$ are the variables of the effective action, η and $\bar{\eta}$ acquire a Λ dependency. Taking the derivative of Eq. (4.2.31) thus yields

$$\begin{aligned}
\dot{\Gamma}^\Lambda(\{\bar{\phi}\}, \{\phi\}) &= -\frac{d}{d\Lambda} \mathcal{W}^{c,\Lambda}(\{\bar{\eta}^\Lambda\}, \{\eta^\Lambda\}) - (\bar{\phi}, \dot{\eta}^\Lambda) - (\dot{\bar{\eta}}^\Lambda, \phi) + (\bar{\phi}, \partial_\Lambda [G^{0,\Lambda}]^{-1} \phi) \\
&= -\dot{\mathcal{W}}^{c,\Lambda} - \sum_1 \left[\dot{\eta}_1^\Lambda \frac{\delta \mathcal{W}^{c,\Lambda}}{\delta \eta_1^\Lambda} + \dot{\bar{\eta}}_1^\Lambda \frac{\delta \mathcal{W}^{c,\Lambda}}{\delta \bar{\eta}_1^\Lambda} \right] - (\bar{\phi}, \dot{\eta}^\Lambda) - (\dot{\bar{\eta}}^\Lambda, \phi) + (\bar{\phi}, \partial_\Lambda [G^{0,\Lambda}]^{-1} \phi) \\
&= -\dot{\mathcal{W}}^{c,\Lambda}(\{\bar{\eta}^\Lambda\}, \{\eta^\Lambda\}) + (\bar{\phi}, \partial_\Lambda [G^{0,\Lambda}]^{-1} \phi) \\
&= \text{Tr} [G^{0,\Lambda} \partial_\Lambda [G^{0,\Lambda}]^{-1}] \mp i \text{Tr} \left[\partial_\Lambda [G^{0,\Lambda}]^{-1} \frac{\delta^2 \mathcal{W}^{c,\Lambda}}{\delta \bar{\eta}^\Lambda \delta \eta^\Lambda} \right] \\
&= \text{Tr} [G^{0,\Lambda} \partial_\Lambda [G^{0,\Lambda}]^{-1}] - \text{Tr} [\partial_\Lambda [G^{0,\Lambda}]^{-1} \mathcal{V}_{11}^\Lambda(\{\bar{\phi}\}, \{\phi\})] .
\end{aligned} \tag{5.2.8}$$

where the flow equation (5.2.7) has been used. In order to indicate the relation to the derivative of Γ in a compact way, \mathcal{V}_{11}^Λ has been used in the last step, which is the upper right element of the matrix defined in Eq. (4.2.38), which relates the derivatives of \mathcal{W}^c and Γ . The resulting expression is the flow equation of the effective action.



Figure 5.1: First two flow equations for the self-energy (grey circle) and the two-particle vertex function (grey square). Green dot/line indicates the derivative with respect to the flow parameter Λ , the grey hexagon is the three-particle vertex function.

Flow of the vertex function

To extract the flow equation of the vertex functions, Eq. (4.2.38) is reshaped to

$$\begin{aligned}
 \mathcal{V}^\Lambda &= \begin{pmatrix} -i \frac{\delta^2 \Gamma^\Lambda}{\delta \bar{\phi} \delta \phi} + [G^{0,\Lambda}]^{-1} & -i \frac{\delta^2 \Gamma^\Lambda}{\delta \bar{\phi} \delta \phi} \\ -i \frac{\delta^2 \Gamma^\Lambda}{\delta \phi \delta \bar{\phi}} & -i \frac{\delta^2 \Gamma^\Lambda}{\delta \phi \delta \phi} - [G^{0,\Lambda}]^{-1, T} \end{pmatrix}^{-1} \\
 &= \left[\begin{pmatrix} [G^\Lambda]^{-1} & 0 \\ 0 & -[G^\Lambda]^{-1, T} \end{pmatrix} + \begin{pmatrix} \mathcal{U}^\Lambda & -i \frac{\delta^2 \Gamma^\Lambda}{\delta \bar{\phi} \delta \phi} \\ -i \frac{\delta^2 \Gamma^\Lambda}{\delta \phi \delta \bar{\phi}} & -\mathcal{U}^\Lambda \end{pmatrix} \right]^{-1} \\
 &= - \underbrace{\left[1 - \begin{pmatrix} -G^\Lambda & 0 \\ 0 & [G^\Lambda]^T \end{pmatrix} \cdot \begin{pmatrix} \mathcal{U}^\Lambda & -i \frac{\delta^2 \Gamma^\Lambda}{\delta \bar{\phi} \delta \phi} \\ -i \frac{\delta^2 \Gamma^\Lambda}{\delta \phi \delta \bar{\phi}} & -\mathcal{U}^\Lambda \end{pmatrix} \right]^{-1}}_{=\tilde{\mathcal{V}}^\Lambda} \cdot \begin{pmatrix} -G^\Lambda & 0 \\ 0 & [G^\Lambda]^T \end{pmatrix}, \quad (5.2.9)
 \end{aligned}$$

where \mathcal{U}^Λ is the difference of the one-particle vertex functions and the second derivative of Γ^Λ with respect to its fields

$$\mathcal{U}^\Lambda = -i \frac{\delta^2 \Gamma^\Lambda}{\delta \bar{\phi} \delta \phi} - (-i) \frac{\delta^2 \Gamma^\Lambda}{\delta \bar{\phi} \delta \phi} \Big|_{\phi=\bar{\phi}=0} = -i \frac{\delta^2 \Gamma^\Lambda}{\delta \bar{\phi} \delta \phi} - \gamma_1^\Lambda = -i \frac{\delta^2 \Gamma^\Lambda}{\delta \bar{\phi} \delta \phi} - [G^\Lambda]^{-1} + [G^{0,\Lambda}]^{-1}. \quad (5.2.10)$$

With $\tilde{\mathcal{V}}^\Lambda = \hat{\mathcal{V}}_{11}^\Lambda$ the flow equation reads as

$$\dot{\Gamma}^\Lambda = \text{Tr} [G^{0,\Lambda} \partial_\Lambda [G^{0,\Lambda}]^{-1}] - \text{Tr} [G^\Lambda \partial_\Lambda [G^{0,\Lambda}]^{-1} \tilde{\mathcal{V}}^\Lambda]. \quad (5.2.11)$$

which allows to expand $\tilde{\mathcal{V}}^\Lambda$ in a geometric series

$$\tilde{\mathcal{V}}^\Lambda = 1 - G^\Lambda \mathcal{U}^\Lambda + \left[G^\Lambda \mathcal{U}^\Lambda G^\Lambda \mathcal{U}^\Lambda - G^\Lambda \frac{-i \delta^2 \Gamma^\Lambda}{\delta \bar{\phi} \delta \bar{\phi}} [G^\Lambda]^T \frac{-i \delta^2 \Gamma^\Lambda}{\delta \phi \delta \phi} + \dots \right]. \quad (5.2.12)$$

If this is compared to the series expansion of the derivative of effective action around $\phi = \bar{\phi} = 0$

$$\partial_\Lambda \Gamma^\Lambda(\{\bar{\phi}\}, \{\phi\}) = \sum_{m=0}^{\infty} \frac{(-1)^m (i)^m}{(m!)^2} \sum_{1 \dots m} \sum_{1' \dots m'} \partial_\Lambda \gamma_m^\Lambda(1 \dots m, 1' \dots m') \bar{\phi}_1 \dots \bar{\phi}_m \phi_{m'} \dots \phi_{1'}, \quad (5.2.13)$$

and sorted by the order of external fields, the flow equation for each of the vertex function can be read off. Since the flow of γ_0 decouples from the rest of the hierarchy, we disregard its flow equation in the following and begin with the flow of the self-energy as the lowest order equation.

Flow of the Self-Energy

In order to extract the flow equation for γ_1 , we consider the terms of \mathcal{U} , which are linear in $\phi \bar{\phi}$

$$\mathcal{U}^{\Lambda, \text{lin}} = \frac{(-i)(i)^2}{(2!)^2} \frac{\delta^2}{\delta \bar{\phi}_3 \delta \phi_3} \sum_{1'2'12} \gamma_2^\Lambda(1'2'; 12) \bar{\phi}_{1'} \bar{\phi}_{2'} \phi_2 \phi_1 = -i \sum_{2'2} \gamma_2^\Lambda(2'3'; 23) \bar{\phi}_{2'} \phi_2, \quad (5.2.14)$$

where it is utilized that

$$\gamma_2^\Lambda(1'2'; 12) = -\gamma_2^\Lambda(2'1'; 12), \quad \gamma_2^\Lambda(1'2'; 12) = -\gamma_2^\Lambda(1'2'; 21). \quad (5.2.15)$$

The resulting flow equation reads as

$$\partial_\Lambda \gamma_1^\Lambda(1'; 1) = \sum_{22'} [G^\Lambda \partial_\Lambda [G^{0,\Lambda}]^{-1} G^\Lambda]_{22'} \gamma_2^\Lambda(1'2'; 12) = \sum_{22'} S_{22'}^\Lambda \gamma_2^\Lambda(1'2'; 12). \quad (5.2.16)$$

where we have defined the single-scale propagator

$$S_{1'1}^\Lambda = S^\Lambda(1'; 1) = \sum_{22'} G_{1'2}^\Lambda [\partial_\Lambda [G^{0,\Lambda}]^{-1}]_{22'} G_{2'1}^\Lambda = -\partial_\Lambda^* G_{1'1}^\Lambda = -\partial_\Lambda^* G^\Lambda(1'; 1). \quad (5.2.17)$$

The resulting flow equation is depicted on the left hand side of Fig.5.1, where the grey circle illustrates the self-energy, the grey square the two-particle vertex function and the single-scale propagator is depicted by the crossed out line.

Flow of the effective Interaction

The flow of the effective interaction γ_2 is analogously identified as

$$\begin{aligned} \partial_\Lambda \gamma_2^\Lambda(1'2'; 12) = & \sum_{33'} S_{33'}^\Lambda \gamma_3^\Lambda(1'2'3'; 123) \\ & - \sum_{33'44'} S_{33'}^\Lambda \gamma_2^\Lambda(3'4'; 12) G_{4'4}^\Lambda \gamma_2^\Lambda(1'2'; 4'3) \\ & - \left[\sum_{33'44'} S_{33'}^\Lambda \gamma_2^\Lambda(1'3'; 14) G_{44'}^\Lambda \gamma_2^\Lambda(2'4'; 23) \right. \\ & \quad \left. - (1' \leftrightarrow 2') - (1 \leftrightarrow 2) + (1' \leftrightarrow 2', 1 \leftrightarrow 2) \right], \end{aligned} \quad (5.2.18)$$

by collecting all terms quadratic in $\phi\bar{\phi}$. The structure of the flow equation reveals that it conserves the anti-symmetrization of the bare interaction \bar{u}_{ijkl} . A diagrammatic representation of the resulting flow equation is shown on the right hand side of Fig.5.1, where the grey square indicates the two-particle vertex function and the grey hexagon the three-particle vertex function.

Higher orders

One can now proceed further to end up with an infinite hierarchy of differential equations. All differential equations are of the structure as stated in Eq. (5.1.2) and thus coupled. A solution of the complete set of differential equation would yield an exact solution of the many-body problem. This is obviously impossible and a truncation needs to be employed. The truncation employed here is discussed in Section 5.2.3.

5.2.2 Initial condition

The initial conditions for the vertex functions need to be defined. It is of course possible to derive them analytically rigorous as it is presented in Ref. [Med02]. We here like to follow the simple, diagrammatic argument as employed in Refs. [Ken11, Kar10a, Ken14]. The bare Green's function vanishes at the beginning of the flow, i.e. $G^{0,\Lambda=\infty} = 0$ such that the effective action simplifies to

$$\Gamma^{\Lambda=\infty}(\{\bar{\phi}\}, \{\phi\}) = i S_{\text{int}} = \frac{i}{4} \sum_{121'2'} \bar{u}_{1'2'12} \psi_{1'} \psi_{2'} \psi_2 \psi_1. \quad (5.2.19)$$

All possible diagrams include at least one propagation and are thus suppressed except the lowest order diagram of γ_2 , which is only the bare interaction. Thus, it results in the following initial condition

$$\gamma_2^{\Lambda=\infty} = -i \bar{u}_{1'2'12} \quad \gamma_{m \neq 2}^{\Lambda=\infty} = 0. \quad (5.2.20)$$



Figure 5.2: The lowest order truncation keeps only the first flow equation for the self-energy (grey circle), where the two particle vertex (grey square) has been substituted by the bare interaction (dark blue dot). Green dot/line indicates the derivative with respect to the flow parameter Λ .

We focus now on a Coulomb, density-density type interaction between neighboring sites in the central dot region of our model. It is of the form $U d_n^\dagger d_n d_m^\dagger d_m$ and leads to the bare antisymmetrized vertex

$$\bar{u}_{1'2'12} = U \times \delta(t'_1 = t'_2 = t_3 = t_4) \times (-i)(-\nu_1)\delta(\nu'_1 = \nu'_2 = \nu_1 = \nu_2) . \quad (5.2.21)$$

Rotating to the RKA-basis yields (with all other indices suppressed)

$$\begin{aligned} \bar{u}_{n'_1 n'_2 n_1 n_2} &= \sum_{\nu'_1 \nu'_2 \nu_1 \nu_2} [R_B^{-1}]_{n'_1 \nu'_1} [R_B^{-1}]_{n'_2 \nu'_2} \times [(-\nu_1)\delta(\nu'_1 = \nu'_2 = \nu_1 = \nu_2)] \times [R_A^{-1}]_{\nu_1 n_1} [R_A^{-1}]_{\nu_2 n_2} \\ &= \frac{\bar{u}}{2} \times \begin{cases} 1 & n'_1 = n_1 \wedge n'_2 \neq n_2 \vee n'_1 \neq n_1 \wedge n'_2 = n_2 \\ 0 & \text{otherwise} . \end{cases} \end{aligned} \quad (5.2.22)$$

5.2.3 Truncation

From the afore discussed initial conditions it can be derived that each m -particle vertex function γ_m is generated by the interaction at least of the order $\mathcal{O}(U^m)$ with U as the amplitude of the interaction. Assuming the bare interaction to be a small parameter justifies a truncation of the hierarchy, where a maximal order m_c is chosen. The resulting truncation is defined as

$$\gamma_{m_c+1}^\Lambda = \gamma_{m_c+1}^{\Lambda=\infty} \Rightarrow \partial_\Lambda \gamma_{m \leq m_c}^\Lambda = f(\{\gamma_n^\Lambda : n \leq m_c\}, \gamma_{m_c+1}^{\Lambda=\infty}) , \quad \partial_\Lambda \gamma_{m > m_c}^\Lambda = 0 . \quad (5.2.23)$$

Only the self-energy flows: $m_c = 1$

If we truncate the hierarchy already after the first differential equation by choosing $m_c = 1$, we set

$$\gamma_2(1, 2, 1', 2') = -i\bar{u}_{1,2,1',2'} \quad \gamma_{m>2} = 0 . \quad (5.2.24)$$

The resulting differential equation describes a frequency independent self-energy which flows, but the vertex \bar{u} remains unrenormalized (and static). All terms to the leading order of U are included, but due to the feedback of the self-energy into the loop, also higher order contributions are captured partially. The physical consequence of this truncation is an effective non-interacting system with renormalized parameters at the end of the flow.

Earlier studies have shown that the self-energy already provides the main physics in the IRLM, and the FRG with this truncation is able to capture power-law behavior with U dependent exponents correct to its leading order [Kar10c, Met12, Ken12a]. This is also confirmed by the results presented in Chapter 7, which are obtained with this lowest order truncation as well.

Next higher order truncation: $m_c = 2$

In the next higher order truncation (choosing $m_c = 2$) the effective interaction flows additionally, such that the resulting self-energy acquires a frequency dependence [Kar10a, Jak09]. This already requires a much higher numerical effort and is beyond the scope of this thesis.

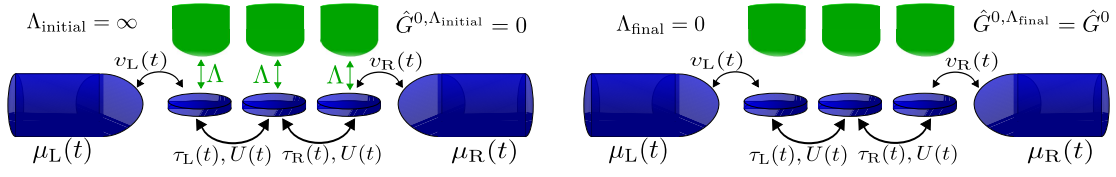


Figure 5.3: Auxiliary reservoir cutoff: At the beginning of the flow auxiliary reservoirs (green) are coupled to the three sites with $\Lambda = \infty$, which renders all other energy scales irrelevant and the bare Green's function vanishes (left panel). Integrating down to a final, vanishing flow parameter the initial, physical system is recovered, where the auxiliary reservoirs are completely decoupled (right panel).

5.3 Flow equation in Floquet space

5.3.1 Cutoff scheme: Auxiliary reservoirs

In order to introduce the flow parameter, we use the known hybridization cut-off scheme as developed by Ref. [Jak09] and extended by Refs. [Kar10a] and [Ken11]. The flow parameter is the hybridization of auxiliary wide band reservoirs which are connected to each of the three sites. While there are several distinct possibilities to choose the temperature and chemical potential of the auxiliary reservoirs, we assume the temperature of the reservoirs to be infinite, which renders the chemical potential irrelevant. The resulting reservoir distribution functions are structureless, which avoids any imprint of an artificial energy structure [Ken12a]. It has been shown by Ref. [Ken11] that this yields consistent results for the steady state of the IRLM. The respective self-energies can be calculated as

$$\Sigma_{\text{cut},ij}^{\text{ret/adv}}(t, t') = \mp i\Lambda\delta(t - t')\delta_{ij}, \quad (5.3.1)$$

$$\Sigma_{\text{cut},ij}^{\text{K}}(t, t') = -\Lambda T_{\text{cut}} e^{-i\mu_{\text{cut}}(t-t')} \sum_{\pm} \frac{1}{\sinh[T_{\text{cut}}\pi(t-t' \pm i\delta)]} \xrightarrow{T_{\text{cut}} \rightarrow \infty} 0, \quad (5.3.2)$$

which for the $T_{\text{cut}} = \infty$ case are transformed to

$$\Sigma_{\text{cut},ij;k,k'}^{\Lambda,\text{ret/adv}}(\omega) = \mp i\Lambda\delta_{ij}\delta_{kk'}, \quad (5.3.3)$$

$$\Sigma_{\text{cut},ij;k,k'}^{\Lambda,\text{K}}(\omega) = 0. \quad (5.3.4)$$

The according physical situation is sketched in Fig. 5.3. At the beginning of the flow the auxiliary leads are coupled infinitely strong to the three sites, rendering all other energy scales irrelevant and the bare Green's function is zero. Throughout the flow the couplings are weakened, such that at the end of the flow the auxiliary reservoirs are completely decoupled. This way the initial physical system is recovered, but with renormalized parameters. The cutoff is thus implemented by simply extending the initial configuration, i.e. by a physical meaningful setup. As a consequence, it preserves causality, which makes it a reasonable choice for non-equilibrium situations [Jak09, Jak10b, Kar10a].

Initial condition

After the specification of the exact form of the cut-off scheme, a reconsideration of the initial condition is necessary. We have argued in Section 5.2.2 that the bare propagator vanishes in the limit $\Lambda \rightarrow \infty$, as it is exponentially suppressed by the infinite coupling to the auxiliary reservoirs. But this is indeed not true for equal time Green's functions as it appears in the Hartree-Fock diagram of γ_1 [Jak10a, Kar10a, Ken11, Ken14]. The correct initial condition reads as [Ken12a]

$$\lim_{\Lambda \rightarrow \infty} \Sigma_{ij}^{\text{ret,adv}}(t, t') = \frac{1}{2}\delta(t - t') \sum_l \bar{u}_{il,jl}(t), \quad (5.3.5)$$

$$\Sigma_{ij}^{\text{K},\Lambda=\infty}(t, t') = 0, \quad (5.3.6)$$

in the time dependent form and can be transformed straightforwardly to

$$\Sigma_{ij,k0}^{\text{ret},\Lambda=\infty}(0) = \frac{1}{2} \sum_l \bar{u}_{ijl;-k000}, \quad (5.3.7)$$

$$\Sigma_{ij,k0}^{\text{K},\Lambda=\infty}(0) = 0. \quad (5.3.8)$$

The initial condition for the particle-hole symmetric Hamiltonian of Eq. (3.3.2) is

$$\Sigma^{\text{ret},\Lambda=\infty} = 0 \quad (5.3.9)$$

as the U dependent contribution to the onsite energy cancels the initial condition stated in Eq. (5.3.7).

5.3.2 Flow Equation

The starting point is now Eq. (5.2.16), which needs to be considered with the bare interaction defined in Eq. (5.2.22). We use the single-scale propagator defined via Eq. (5.2.17), which with

$$\partial_\Lambda G^{0,\Lambda} = G^{0,\Lambda} \frac{\partial \Sigma_{\text{cut}}^\Lambda}{\partial \Lambda} G^{0,\Lambda} \quad (5.3.10)$$

becomes

$$S^\Lambda = G^\Lambda \frac{\partial \Sigma_{\text{cut}}^\Lambda}{\partial \Lambda} G^\Lambda. \quad (5.3.11)$$

With the cutoff self-energy defined in Eqs. (5.3.1) and (5.3.2) it thus reads

$$\hat{S}^\Lambda(t, t') = \begin{pmatrix} iG^{\text{ret},\Lambda} G^{\text{ret},\Lambda} & iG^{\text{ret},\Lambda} G^{\text{K},\Lambda} - iG^{\text{K},\Lambda} G^{\text{adv},\Lambda} \\ 0 & -iG^{\text{adv},\Lambda} G^{\text{adv},\Lambda} \end{pmatrix} (t, t'). \quad (5.3.12)$$

Equal time single-scale propagator

For the first flow equation (5.2.16), the equal time single-scale propagator needs to be evaluated. It is then easy to see that [Ken11]

$$S^{\text{ret},\Lambda}(t, t) = \int dt_1 \underbrace{G^{\text{ret},\Lambda}(t, t_1)}_{\sim \Theta(t-t_1)} \underbrace{G^{\text{ret},\Lambda}(t_1, t)}_{\sim \Theta(t_1-t)} = 0 = S^{\text{adv},\Lambda}(t, t) \quad (5.3.13)$$

such that the Keldysh component of the self-energy does not flow

$$\partial_\Lambda \Sigma^{\text{K},\Lambda}(t, t') = 0. \quad (5.3.14)$$

As a result the whole problem reduces to a single differential equation of the form [Ken12a]

$$\partial_\Lambda \Sigma_{ij}^{\text{ret},\Lambda}(t', t) = \sum_{n,m} S_{nm}^{\text{K},\Lambda}(t, t) \left[-\frac{i}{2} \bar{u}_{imjn}(t) \right] \delta(t' - t). \quad (5.3.15)$$

Transforming it to Floquet space yields

$$\partial_\Lambda \Sigma_{ij;k0}^{\text{ret},\Lambda}(0) = -i \sum_{n,m,k'} \int \frac{d\omega}{4\pi} S_{nm;k'+k0}^{\text{K},\Lambda}(\omega) (\bar{u}_{imjn;k'000}), \quad (5.3.16)$$

which is the central differential equation of the presented work. The structure of the equation directly reveals that the resulting self-energy does not acquire any frequency dependence.

5.3.3 Symmetries: A short discussion

Finally, we shortly review the important symmetries and their conservation, further discussions can be found in Refs. [Kar10a, Ken14].

Antisymmetrization of the effective interaction

The effective interaction is antisymmetrized to ensure the anticommutation under the exchange of fermions,

$$\gamma_2(1', 2'; 1, 2) = -\gamma_2(2', 1'; 1, 2) = -\gamma_2(1', 2'; 2, 1). \quad (5.3.17)$$

By exploiting these symmetries to the vertex function in the fRG equations, it can be shown that the equations preserve the symmetry.

Complex conjugation

The symmetries presented in the section 4.4.2 are conserved within the lowest order truncation of the functional RG employed here.

Causality

Causality is the base of the applied rotation in the Keldysh formalism and hence should not be broken by the flow equation. This is one of the main reasons of the choice of the hybridization cutoff scheme as discussed in Section 5.3.1. This has been investigated extensively in Ref. [Jak09, Kar10a], where it is contrasted to the sharp frequency cutoff, which violates causality.

5.3.4 Renormalized parameters

Throughout the present work we focus on time independent interaction amplitudes. The resulting flow equations for the renormalization of the hoppings $\tau_{L(R)}(t)$ and the onsite energy $\epsilon(t)$ are

$$\partial_\Lambda \tau_{L(R),k}^\Lambda = -\frac{U}{4\pi i} \partial_\Lambda^* \int d\omega G_{12/23;0k}^{K,\Lambda}(\omega), \quad (5.3.18)$$

$$\partial_\Lambda \epsilon_k^\Lambda = -\frac{U i}{4\pi} \partial_\Lambda^* \int d\omega \left(G_{11;0k}^{K,\Lambda}(\omega) + G_{33;0k}^{K,\Lambda}(\omega) \right) \quad (5.3.19)$$

where the notation ∂_Λ^* is used as defined in Eq. (5.2.17). Compared to the known flow equation for the time independent steady state [Kar10c], they only differ by an extra single-particle like index k , indicating the Floquet channel.

In the chosen, lowest order truncation as discussed in Section 5.2.3, we obtain frequency independent, renormalized parameters at the end of the RG procedure

$$\tau_{L,k}^{\text{ren}} = \tau_{L,k}^{\text{init}} + \Sigma_{12,0k}^{\text{ret},\Lambda=0}, \quad (5.3.20)$$

$$\tau_{R,k}^{\text{ren}} = \tau_{R,k}^{\text{init}} + \Sigma_{23,0k}^{\text{ret},\Lambda=0}, \quad (5.3.21)$$

$$\epsilon_k^{\text{ren}} = \epsilon_k^{\text{init}} + \Sigma_{22,0k}^{\text{ret},\Lambda=0}. \quad (5.3.22)$$

Superscript 'init' or 'ren' mark here the parameter at the beginning ($\Lambda = \infty$) or at the end of the flow ($\Lambda = 0$), respectively.

As a consequence of the frequency independent renormalization, the resulting setup at the end of the flow is an effective, non-interacting system with parameters renormalized by the interaction. This in turn, has an important implication: We can derive expressions for the single-particle observables in the non-interacting system, which still hold true in the interacting setup, when substituting the parameters by their renormalized equivalents. This is exact in the lowest order truncation and does not include any further approximation.

5.3.5 Numerical implementation

The flow equations defined in Eqs. (5.3.18) and (5.3.19) need to be solved to compute the renormalization of the parameters. The Floquet channels are in general all coupled, rendering it necessary to solve the full flow equation numerically with an appropriate number of higher harmonics.

The number of included higher harmonics depends crucially on the exact form and amplitude of the applied signal for the time periodic parameters. Besides the fact that already in a non-interacting

setup the most common signals of a sine function ($k_{\max} = 1$), a triangular signal ($k_{\max} = 100$) and a square signal ($k_{\max} = 200$) need a different amount of included higher harmonics for a proper signal form, the finite interaction might create further higher harmonics throughout the flow.

We will show in Chapter 7 that for small driving amplitudes $\Delta\tau \ll \tau_0$ and $\Delta\epsilon \ll T_K$, the Floquet channels decouple to the leading order of $\frac{\Delta\tau}{\tau_0}$ or $\frac{\Delta\epsilon}{T_K}$. As a result, it is sufficient to include $k_{\max} = 5$ (sin), $k_{\max} = 120$ (triangular) and $k_{\max} = 250$ (square) higher harmonics to obtain converged results for the respective signals.

With increasing driving amplitude the included higher harmonics need to be raised accordingly, e.g. up to $k_{\max} = 50$ for a sinusoidal signal with e.g. $\Delta\tau/\tau_0 = 0.9$ (as depicted in Fig. 8.3).

While the integral from $\Lambda = \infty$ to $\Lambda = 0$ can be performed with a standard integrator for ordinary differential equations as e.g. "integrate.ode" from the SciPy library, the energy integral on the right hand side of the flow equations (5.3.18) and (5.3.19) poses a numerical obstacle.

Analytic solution of the energy integral

The spectral function of a time periodically driven system shows several sidebands (see Fig. 7.15), which render the numerical energy integration on the right hand side of Eqs. (5.3.18) and (5.3.19) more involved. To avoid the numerical problems of a slowly converging frequency integral in the periodically driven setups, the respective integral is rewritten and solved analytically. We here focus on the case of undriven reservoirs (all time dependency is on the dot), the resulting reservoir self-energies are diagonal in the Fourier space.

The relevant integrands on the right hand site of the flow equations are either the Keldysh Green's function (occupancy, current) or the Keldysh single-scale propagator (flow equation). By diagonalizing the retarded/advanced Green's function with respect to a combined index, which is introduced next, the according integrals can be brought into a simple form, which can be solved analytically.

Calculating the eigenvalues and -vectors of the retarded Green's function allows to rewrite it

$$G^{\text{ret}} = T^{-1} D^{\text{ret}} T = (G^{\text{adv}})^{\dagger} \quad (5.3.23)$$

where T^{-1} includes the eigenvectors as columns. Inserted in Eq. (4.4.18), this leads to

$$\underline{\underline{G}}^K = \underline{\underline{T}}^{-1} \underline{\underline{D}}^{\text{ret}} \underline{\underline{T}} \underline{\underline{\Sigma}}^K \underline{\underline{T}}^{\dagger} (\underline{\underline{D}}^{\text{ret}})^{\dagger} (\underline{\underline{T}}^{-1})^{\dagger} \quad (5.3.24)$$

$$\underline{\underline{S}}^K = \underline{\underline{T}}^{-1} [\underline{\underline{D}}^{\text{ret}}]^2 \underline{\underline{T}} \underline{\underline{\Sigma}}^K \underline{\underline{T}}^{\dagger} (\underline{\underline{D}}^{\text{ret}})^{\dagger} (\underline{\underline{T}}^{-1})^{\dagger} - \underline{\underline{T}}^{-1} \underline{\underline{D}}^{\text{ret}} \underline{\underline{T}} \underline{\underline{\Sigma}}^K \underline{\underline{T}}^{\dagger} [(\underline{\underline{D}}^{\text{ret}})^{\dagger}]^2 (\underline{\underline{T}}^{-1})^{\dagger}. \quad (5.3.25)$$

To simplify the following, we merge the site and the Floquet index to a joint index $p(i, k) = 3(k + k_{\max}) + i$ with i as site index and k as Floquet index, such that $k(p, i) = (p - i)/3 - k_{\max}$. With the diagonal form of the reservoir self-energy, the Keldysh Green's function can be rewritten to

$$\begin{aligned} G_{pq}^K &= \sum_{n,m,l} v_{pm} d_{mm}(\omega) \bar{v}_{mn} v_{pl}^* d_{ll}^*(\omega) \bar{v}_{ln} [2f_n(\omega) - 1] iD \\ &= \sum_{n(j),m,l} v_{pm} \bar{v}_{mn} [2F(m, l, n) - G(m, l)] v_{pl}^* \bar{v}_{ln}^* iD \quad \text{with } j \in \{1, 3\}. \end{aligned} \quad (5.3.26)$$

where v_{im} is the i th entry of the m th eigenvector (\bar{v}_{im} the respective entry of T) and the integrals $F(m, l, n)$ and $G(m, l)$ are defined in Eqs. (5.3.29) and (5.3.31). The joined index n is summed only over those numbers resulting from a site index $j \in \{1, 3\}$ (as a consequence of the structure of the

reservoir self-energy). The single-scale propagator is rewritten equivalently to

$$\begin{aligned}
S_{pq}^K &= \sum_{n(j),m,l} v_{pm} [d_{mm}(\omega)]^2 \bar{v}_{mn} v_{pl}^* d_{ll}^*(\omega) \bar{v}_{ln}^* [2f_n(\omega) - 1] iD \\
&\quad - \sum_{n(j),m,l} v_{pm} d_{mm}(\omega) \bar{v}_{mn} v_{pl}^* [d_{ll}^*(\omega)]^2 \bar{v}_{ln}^* [2f_n(\omega) - 1] iD \\
&= \sum_{n(j),m,l} v_{pm} \bar{v}_{mn} [2H(m, l, n) - K(m, l)] v_{pl}^* \bar{v}_{ln}^* iD \\
&\quad - \sum_{n(j),m,l} v_{pm} \bar{v}_{mn} [2H(\bar{l}, \bar{m}, n) - K(\bar{l}, \bar{m})] v_{pl}^* \bar{v}_{ln}^* iD \quad \text{with } j \in \{1, 3\}, \tag{5.3.27}
\end{aligned}$$

where \bar{l} indicates that the respective eigenvalue λ_l in the integrals of Eqs. (5.3.30) and (5.3.32) needs to be complex conjugated. For $T = 0$ the Fermi function is

$$f_n(\omega) = \Theta[\omega + k(n)\Omega + \mu_n], \tag{5.3.28}$$

resulting in the following integrals

$$\begin{aligned}
F(m, l, n) &= \int_{-\infty}^{\mu_n - k(n)\Omega} \frac{1}{\omega - \lambda_m} \frac{1}{\omega - \lambda_l^*} d\omega \\
&= \frac{1}{\lambda_m - \lambda_l^*} [-2\pi i + \ln(\mu_n - k(n)\Omega - \lambda_m) - \ln(\mu_n - k(n)\Omega - \lambda_l^*)] \tag{5.3.29}
\end{aligned}$$

$$\begin{aligned}
H(m, l, n) &= \int_{-\infty}^{\mu_n - k(n)\Omega} \frac{1}{(\omega - \lambda_m)^2} \frac{1}{\omega - \lambda_l^*} d\omega \\
&= -\frac{(\lambda_m - \lambda_l^*)(\mu_n + k(n)\Omega - \lambda_m)}{(\lambda_m - \lambda_l^*)^2} \\
&\quad + \frac{1}{(\lambda_m - \lambda_l^*)^2} [(2\pi i + \ln(\mu_n - k(n)\Omega - \lambda_l^*) - \ln(\mu_n - k(n)\Omega - \lambda_m))] \tag{5.3.30}
\end{aligned}$$

$$G(m, l) = \int_{-\infty}^{\infty} \frac{1}{\omega - \lambda_m} \frac{1}{\omega - \lambda_l^*} d\omega = \frac{2\pi i}{\lambda_m - \lambda_l^*} \tag{5.3.31}$$

$$K(m, l) = \int_{-\infty}^{\infty} \frac{1}{(\omega - \lambda_m)^2} \frac{1}{\omega - \lambda_l^*} d\omega = \frac{2\pi i}{(\lambda_m - \lambda_l^*)^2} \tag{5.3.32}$$

where λ_m / λ_l^* are the respective eigenvalues of the retarded/advanced Green's function.

Chapter 6

Perturbation Theory in Floquet-Liouville Space

Contents

6.1	Liouville space and its kinetic equation	49
6.1.1	Liouville space	49
6.1.2	Kinetic equation	50
6.1.3	Diagrammatics	51
6.1.4	Observable: Current	54
6.2	Floquet-Liouville space	54
6.2.1	Diagrammatic in Floquet space	54
6.2.2	General form of the RLM Liouvillian	56
6.3	Markov approximation and Perturbation Theory	57
6.3.1	Perturbation Theory in RLM: First order diagramm	57
6.3.2	Markov approximation in Floquet space	58
6.3.3	Quantum Master equation in Floquet Space	60

In this chapter a formalism is introduced which is based on superoperators acting on the Liouville space. The method is a powerful tool to describe the time evolution of open quantum dot systems. The central idea is to devise a kinetic equation for a reduced density matrix, where the reservoir degrees of freedom are integrated out. An effective Liouville operator is defined, which acts only on the local dot system, but includes information of the reservoir as well as the system-reservoir coupling. The latter is included perturbatively in the kernel, which can be calculated in a very transparent and efficient way with the corresponding diagrammatic rules. In general this makes it feasible to calculate non-Markovian dynamics of open dot systems, including the computation of typical relaxation and decoherence rates. While this formalism has led to the development of an involved, non-equilibrium RG scheme to tackle the system in an even more comprehensive way, we only focus on a perturbation theory calculation in the Markov approximation.

The introduction here follows very strongly the presentation as depicted in Ref. [Sch09], as well as Ref. [Sch12, Sch14]. First, we introduce the Liouville space as well as its kinetic equation and diagrammatics for time independent Hamiltonians are discussed. Subsequently the Floquet-Liouville space is introduced [Sch12], where it is elaborated how to extend the diagrammatics for the time periodic case. The Markov approximation is devised in order to set up the quantum master equation with a kernel calculated to the first order in tunneling rate.

6.1 Liouville space and its kinetic equation

6.1.1 Liouville space

We consider Hamiltonians of the general form

$$H_{\text{tot}}(t) = H_S(t) + H_{\text{res}}(t) + H_V(t) , \quad (6.1.1)$$

where H_S is the Hamiltonian of the local quantum system, H_{res} is the Hamiltonian of the non-interacting reservoirs and H_V is the system reservoir coupling. The **von Neumann equation** describes the time evolution of the total density matrix $\rho_{\text{tot}}(t)$

$$i\dot{\rho}_{\text{tot}}(t) = [H_{\text{tot}}(t), \rho_{\text{tot}}(t)] = L_{\text{tot}}(t)\rho_{\text{tot}}(t), \quad (6.1.2)$$

with the total Hamiltonian $H_{\text{tot}}(t)$ of Eq. (6.1.1). In the second step the **Liouville operator** of the whole system $L_{\text{tot}}(t)$ is introduced. It is a quantum field superoperator, i.e. a linear map on an operator, which is defined as

$$L_{\text{tot}}(t)A = [H_{\text{tot}}(t), A], \quad (6.1.3)$$

where A is any operator and $[\cdot, \cdot]$ indicates the commutator. The full, effective Liouville operator can be decomposed into the respective three parts

$$L_{\text{tot}}(t) = L_S(t) + L_{\text{res}}(t) + L_V(t), \quad (6.1.4)$$

with

$$L_i(t) = [H_i(t), \cdot] \quad (6.1.5)$$

and $i \in \{S, \text{res}, V\}$. The Liouville operator (also called Liouvillian) acts on the Liouville space, a linear space of operators. With $\{|n\rangle\}_n$ as a complete, orthonormal basis of the Hilbert space, the respective Liouville space basis vectors are defined as

$$|nm\rangle \equiv |n\rangle \langle m| \quad \langle nm|A\rangle \equiv A_{nm}, \quad (6.1.6)$$

where A is again any operator in the Hilbert space. The matrix elements of the Liouvillian are thus defined as

$$\begin{aligned} L_{nm, n'm'} &= \langle nm|L|n'm'\rangle \\ &= H_{nn'}\delta_{mm'} - H_{mm'}\delta_{nn'}. \end{aligned} \quad (6.1.7)$$

6.1.2 Kinetic equation

To find a formally exact kinetic equation for the local density matrix, the reservoir degrees of freedom are integrated out

$$\rho(t) = \text{Tr}_{\text{res}} \rho_{\text{tot}}(t). \quad (6.1.8)$$

We assume an initial total density matrix of the form

$$\rho_{\text{tot}}(t_0) = \rho(t_0)\rho_{\text{res}}^{\text{eq}}, \quad (6.1.9)$$

with reservoir density matrices

$$\rho_{\text{res}}^{\text{eq}} = \prod_{\alpha} \rho_{\alpha}^{\text{eq}} \quad \text{and} \quad \rho_{\alpha}^{\text{eq}} = \frac{1}{Z_{\alpha}} e^{-(H_{\alpha} - \mu_{\alpha} N_{\alpha})/T_{\alpha}} \quad (6.1.10)$$

which are in the grand-canonical equilibrium with the respective Hamiltonian H_{α} , temperature T_{α} , chemical potential μ_{α} , particle number operator N_{α} and partition function Z_{α} of reservoir α .

The time evolution of the reduced density matrix $\rho(t)$ can be described by

$$i\dot{\rho}(t) = \int_{t_0}^t dt' L^{\text{eff}}(t, t')\rho(t'), \quad (6.1.11)$$

where $L^{\text{eff}}(t, t')$ is the effective Liouville operator acting on the local system, but containing information of the reservoir degrees of freedom as well as the reservoir-system interaction. It is only defined for $t > t'$ as a response function related to $\rho(t')$. The formal solution of the von Neumann equation shows one advantage of the Liouville formalism

$$\rho_{\text{tot}}(t) = T e^{-i \int_{t_0}^t dt' H_{\text{tot}}(t')} \rho_{\text{tot}}(t_0) T e^{i \int_{t_0}^t dt' H_{\text{tot}}(t')} = T e^{-i \int_{t_0}^t dt' L_{\text{tot}}(t')} \rho_{\text{tot}}(t_0), \quad (6.1.12)$$

where T indicates the time ordering operator. While in the Hamilton formalism a forward and a backward propagation on the Keldysh contour is necessary, the Liouville operator only requires one forward propagation taking care of both branches of the Keldysh contour, hiding the Keldysh index in the larger dimension of Liouville space compared to the one of the quantum system. Rewriting Eq. (6.1.8) yields

$$\rho(t) = \text{Tr}_{\text{res}} T e^{-i \int_{t_0}^t dt' L_{\text{tot}}(t')} \rho_{\text{tot}}(t_0). \quad (6.1.13)$$

The effective Liouvillian $L^{\text{eff}}(t, t') = L_S(t, t') + \Sigma(t, t')$ is composed of the local system Liouvillian and a kernel containing the information of the reservoir-system coupling. The kinetic equation can thus be put to

$$i\dot{\rho}(t) - \int_{t_0}^t dt' L_S(t, t')\rho(t') = \int_{t_0}^t dt' \Sigma(t, t')\rho(t'), \quad (6.1.14)$$

where the left hand side is the von Neumann equation of the isolated system, whereas the right hand side of the equation describes the non-Markovian influence of the coupling to the reservoirs on the dot [Sch09]. In case of a time independent Hamiltonian, it further simplifies to

$$i\dot{\rho}(t) - L_S\rho(t) = \int_{t_0}^t dt' \Sigma(t - t')\rho(t'). \quad (6.1.15)$$

It is then beneficial to Laplace transform the reduced density matrix

$$\tilde{\rho}(E) = \int_{t_0}^{\infty} e^{iE(t-t_0)} \rho(t), \quad (6.1.16)$$

where E is the Laplace variable with a positive imaginary part to ensure convergence. Using the formal solution of the kinetic equation yields for a time independent Hamiltonian

$$\begin{aligned} \tilde{\rho}(E) &= \text{Tr}_{\text{res}} \frac{i}{E - L} \rho(t_0) = \text{Tr}_{\text{res}} \frac{i}{E - L_{\text{res}} - L_S - L_V} \rho(t_0) \\ &\approx i \text{Tr}_{\text{res}} \frac{1}{E - L_{\text{res}} - L_S} L_V \frac{1}{E - L_{\text{res}} - L_S} L_V \dots L_V \frac{1}{E - L_{\text{res}} - L_S} \rho(t_0) \end{aligned} \quad (6.1.17)$$

where in the second step the expression has been expanded in L_V by a geometric series.

In the next section, a diagrammatics is introduced, which allows to specify $\Sigma(E)$ and to calculate it. The goal here is to set up a perturbation theory calculation by expanding in system reservoir coupling, but as shown in Ref. [Sch09, Kas13] the diagrammatics can straightforwardly be extended to an involved RG scheme in the Liouville space. We start with the diagrammatics for the time-independent Hamiltonian, and show later how these diagrammatics are extended to the time-periodic case.

6.1.3 Diagrammatics

We will focus on fermionic systems in the following (for the bosonic expressions see e.g. Refs. [Sch14, Sch12, Sch09]). For a compact notation a superindex is defined for the reservoir field operators as

$$i \equiv \eta\alpha\sigma\omega, \quad i = 1, 2, \dots \quad (6.1.18)$$

including $\eta = +(-)$ for creation (annihilation) operator, reservoir index α , channel index σ (e.g. spin) and the energy of the reservoir states measured with respect to the chemical potential $\omega = \epsilon_{\alpha\sigma k} - \mu_{\alpha}$ with a unique relation between ω and the reservoir energy quantum number k assumed. This compact notation will be used in the following.

The general form of the coupling between reservoir and local system can be rewritten to

$$H_V = \frac{1}{n!} \{ \eta_1 \dots \eta_n \} : a_1 a_2 \dots a_n : g_{12\dots n} \rightarrow \frac{1}{n!} g_{12\dots n} : a_1 a_2 \dots a_n : \quad (6.1.19)$$

where

$$a_i \equiv \frac{1}{\sqrt{\rho_\alpha^{(0)}}} \sum_k \delta(\omega - \epsilon_{\alpha\sigma k} + \mu_\alpha) a_{\eta\alpha\sigma k} \quad (6.1.20)$$

is a general reservoir field operator, which needs to be scaled properly by the reservoir density of states at the Fermi level $\sqrt{\rho_\alpha^{(0)}}$. $\frac{1}{n!}$ takes care of all possible permutations of the reservoir operators, $g_{12...n}$ is an arbitrary, anti-symmetrized operator acting on the local system, where n is any integer, implicit summation/integration is assumed over the multi-indices and $: \dots :$ denotes normal ordering w.r.t. the equilibrium distribution of the reservoirs. In the second step (indicated by the arrow) the expression is significantly simplified for the further usage. While this is not an exact reformulation, it can be shown that it is correct for the calculation of the reduced density matrix and local observables (for a detailed derivation, see Appendix of Ref. [Sch09]). Hence, it is used in the following.

From this a general form of the respective Liouvillian is derived

$$L_V = \frac{1}{n!} \sum_{p=\pm} G_{1...n}^{(0)p\dots p} : A_1^p \dots A_n^p : . \quad (6.1.21)$$

The according superoperators of the reservoir are

$$A_1^p b = \sigma_{\text{res}}^p \begin{cases} a_1 b & \text{for } p = + \\ b a_1 & \text{for } p = - \end{cases} , \quad (6.1.22)$$

as well as of the dot system are

$$G_{1...n}^{(0)p_1\dots p_n} b = \delta_{pp_1}\dots\delta_{pp_n} \begin{cases} 1 & \text{for } n \text{ even} \\ \sigma^p & \text{for } n \text{ odd} \end{cases} \begin{cases} g_{1...n} b & \text{for } p = + \\ -b g_{1...n} & \text{for } p = - \end{cases} , \quad (6.1.23)$$

which includes a sign superoperator, defined as

$$\sigma^+ = 1, \quad \sigma_{s_1, s_2, s'_1, s'_2}^- = \delta_{s_1, s'_1} \delta_{s_2, s'_2} (-)^{N_{s_1} - N_{s_2}} . \quad (6.1.24)$$

The product of reservoir field operators as it appears in Eq. (6.1.21) acts as

$$: A_1^p \dots A_n^p : b = \begin{cases} 1 & \text{for } n \text{ even} \\ \sigma_{\text{res}}^p & \text{for } n \text{ odd} \end{cases} \begin{cases} a_1 \dots a_n : b & \text{for } p = + \\ b : a_1 \dots a_n : & \text{for } p = - \end{cases} \quad (6.1.25)$$

in Liouville space.

In order to perform the trace over the reservoir degrees of freedom, Eq. (6.1.17) needs to be brought to a form where it decomposes in a part of the local quantum system and a part of the reservoir. For this the reservoir field operators are commuted through the resolvents $\frac{1}{E - L_{\text{res}} - L_S}$ using the commutation relation

$$A_1^p L_{\text{res}} = (L_{\text{res}} - x_1) A_1^p , \quad (6.1.26)$$

with $x_i = \eta_i(\omega_i + \mu_{\alpha_i}) = \bar{\omega}_i + \bar{\mu}_i$. The relation follows directly from the commutation relation of the normal operators $[a_1, H_{\text{res}, \alpha}] = -\eta(\omega + \mu_\alpha) a_1$. As a result, all reservoir field superoperators are moved to the right

$$: A_1^p \dots A_n^p : \frac{1}{E - L_{\text{res}} - L_S} = \frac{1}{E + x_1 + \dots + x_n - L_{\text{res}} - L_S} : A_1^p \dots A_n^p : . \quad (6.1.27)$$

Also the trace is moved to the right subsequently, where $\text{Tr}_{\text{res}} L_{\text{res}} = 0$ holds, which allows to set all $L_{\text{res}} \rightarrow 0$. Consequently, Eq. (6.1.17) is decomposed in a system and a reservoir part, where the latter can now be tackled using Wick's theorem, obeying the following rules [Sch09]:

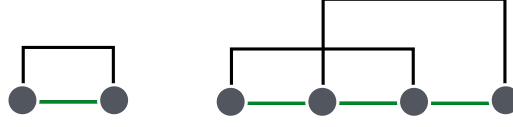


Figure 6.1: First and second order diagrams contributing to the kernel $\Sigma(E)$: Black lines indicate the contractions, green line the resolvents, dark grey dots indicate the coupling vertices.

- Contract all operators A such that no contractions occur within the normal-ordered parts.
- Disentangle the contractions into a product of pairs and give a minus sign for each interchange of a reservoir operator.
- Sum over all possibilities to contract the reservoir operators.

We explain this with a simple example

$$\begin{aligned} \langle : A_1^{p_1} A_2^{p_2} :: A_3^{p_3} A_4^{p_4} : \rangle_{\rho_{\text{res}}} &= \overbrace{A_1^{p_1} A_2^{p_2} A_3^{p_3} A_4^{p_4}} + \overbrace{A_1^{p_1} A_2^{p_2} A_3^{p_3} A_4^{p_4}} \\ &= -\gamma_{13}^{p_1 p_3} \gamma_{24}^{p_2 p_4} + \gamma_{14}^{p_1 p_4} \gamma_{23}^{p_2 p_3}. \end{aligned} \quad (6.1.28)$$

The contractions are then calculated using

$$\begin{aligned} \gamma_{11'}^{pp'} &= \overbrace{A_1^p A_{1'}^{p'}} = \text{Tr}_{\text{res}} A_1^p A_{1'}^{p'} \rho_{\text{res}}^{\text{eq}} \\ &= \delta_{1\bar{1}'} p' \rho_{\alpha\sigma}(\omega) f_{\alpha}^{p'\eta}(\omega) = \delta_{1\bar{1}'} p' \rho_{\alpha\sigma}(\omega) f_{\alpha}(p'\eta\omega), \end{aligned} \quad (6.1.29)$$

where $\bar{i} \equiv -\eta\alpha\sigma\omega$, $\delta_{12} = \delta_{\eta_1\eta_2} \delta_{\alpha_1\alpha_2} \delta_{\sigma_1\sigma_2} \delta(\omega_1 - \omega_2)$ and $f_{\alpha}^{+}(\omega) = f_{\alpha}(\omega)$ as well as $f_{\alpha}^{-}(\omega) = 1 - f_{\alpha}(\omega)$. $f_{\alpha}(\omega)$ is the Fermi function of reservoir α .

Finally the resolvents are defined

$$\Pi^{X_1} \equiv \frac{1}{E + X_1 - L_S}, \quad (6.1.30)$$

with X_1 as the sum of all x_k to the left of the resolvent.

The reduced density operator in Laplace space reads then

$$\tilde{\rho}(E) \rightarrow \frac{i}{S} (-1)^{N_p} (\Pi\gamma) G \frac{1}{E + X_1 - L_S} G \dots G \frac{1}{E + X_r - L_S} G \frac{1}{E - L_S} \rho(t_0) \quad (6.1.31)$$

$$= \frac{i}{E - L_S - \Sigma(E)} \rho(t_0), \quad (6.1.32)$$

where the kernel $\Sigma(E)$ is identified as

$$\Sigma(E) \rightarrow \frac{1}{S} (-1)^{N_p} (\Pi\gamma)_{\text{irr}} G \frac{1}{E + X_1 - L_S} G \dots G \frac{1}{E + X_r - L_S} G, \quad (6.1.33)$$

only including irreducible diagrams. The arrows indicate here the symbolically equivalence. Accordingly, the following diagrammatic rules hold [Sch09]

- $S = \Pi_{i < j} m_{ij}!$ is a symmetry factor, where m_{ij} is the number of contractions between vertex i and j . Two diagrams are considered to be different if they can not be mapped on each other permuting only the field operators of each vertex.
- $(-1)^{N_p}$ is a fermionic sign factor, where N_p is the number of interchanges of fermionic field operators A_i^p in Liouville space which are needed to write the contractions in product form.

- $(\Pi\gamma)_{\text{irr}}$ stands for the product of all contractions which lead to irreducible diagrams. If A_1^p and $A_1^{p'}$ are contracted, and A_1^p stands left to $A_1^{p'}$, the contraction is given by $\gamma_{11'}^{pp'}$ (Eq. (6.1.29)). The contractions are indicated by the upper conjunctions in a diagram (see Fig. 6.1).
- To determine the energy argument X_i of resolvent i , we draw an auxiliary vertical cut at the position of that resolvent. X_i is the sum of all x -variables of the contraction, which cross the vertical cut. The x variable of a contraction $\gamma_{11'}^{pp'}$ is defined as $x = \eta(\omega + \mu_\alpha)$, i.e. refers to the left A_1^p -operator of the contraction. Resolvents are drawn as green, lower lines between the dots in a diagram (see Fig. 6.1).
- $G \equiv G_{1\dots n}^{p_1\dots p_n}$ are the coupling vertices acting on the local quantum system, defined by Eq. (6.1.23). Each field operator is indicated by a black dot in the diagram (see Fig. 6.1).

In Figure 6.1 the first two diagrams contributing to the kernel $\Sigma(E)$ are depicted exemplary with coupling vertices which consist of a single field operator.

6.1.4 Observable: Current

The time evolution of the average of any observable R is

$$\begin{aligned}\langle R \rangle(t) &= \text{Tr}_{\text{tot}} R \rho_{\text{tot}}(t) \\ &= \text{Tr}_{\text{tot}} e^{iH_{\text{tot}}(t-t_0)} R e^{-iH_{\text{tot}}(t-t_0)} \rho_{\text{tot}}(t_0) \\ &= -i \text{Tr} \text{Tr}_{\text{res}} L_R e^{-iL_{\text{tot}} t} \rho(t_0) \rho_{\text{res}}^{\text{eq}},\end{aligned}\quad (6.1.34)$$

for a time-independent H_{tot} . L_R is the respective Liouvillian defined as

$$L_R = \frac{i}{2} \{R, \cdot\}, \quad (6.1.35)$$

with $\{\cdot, \cdot\}$ indicating the anticommutator. Due to the similar form, this expression can be brought to an analogous form as Eq. (6.1.11)

$$\langle R \rangle(t) = -i \text{Tr} \left(\int_{t_0}^t \Sigma_R(t-t') \rho(t') \right), \quad (6.1.36)$$

where the only difference between kernel Σ and observable kernel Σ_R is that the first vertex $G^{(0)}$ is substituted by the vertex $R^{(0)}$ in the latter.

The main observable of interest within the present work is the particle current flowing from reservoir α into the local system. It is defined as

$$I_\gamma(t) = -\partial_t N_\alpha(t) = -i[H_V, N_\alpha(t)], \quad (6.1.37)$$

where N_α is the particle number operator of reservoir α . One can show that

$$(i_\gamma)_{1\dots n} = i \sum_{k=1}^n \eta_k \delta_{\alpha_k, \gamma} g_{1\dots n}, \quad (I_\gamma)_{1\dots n}^{(0)p\dots p} = -\frac{1}{2} \sum_{k=1}^n \eta_k \delta_{\alpha_k, \gamma} p G_{1\dots n}^{(0)p\dots p}. \quad (6.1.38)$$

The current kernel $\Sigma_\gamma(E)$ can then be computed perturbatively in an analogous way as $\Sigma(E)$ for a time-independent Hamiltonian.

6.2 Floquet-Liouville space

6.2.1 Diagrammatic in Floquet space

We are interested in the steady-state of a time-periodically driven system, assuming that all operators as well as the derived observables are time periodic and thus fulfill the relation

$$A(t+T, t'+T) = A(t, t'). \quad (6.2.1)$$

The goal is to transform all objects in a combined space of Liouville space and Fourier space, which is denoted as Floquet-Liouville space. The periodicity of the double time dependent operators allows to rewrite them - equally as the two-time dependent Green's function in the former chapters - as

$$A(t, t') = \sum_k e^{-ik\Omega t} A^k(\tau = t - t'), \quad (6.2.2)$$

$$A^k(E) = \int d\tau e^{iE'\tau} A^k(\tau). \quad (6.2.3)$$

Fourier transforming Eq. (6.2.2) yields

$$A(E, E') = \sum_k \delta(E - E' - k\Omega) A^k(E), \quad (6.2.4)$$

which relates the double energy dependent objects to the ones in the Floquet-Liouville space.

One needs to start with the general time dependent expressions of the objects of interest. We only state them here and refer the interested reader to Ref. [Sch12, Kas13]. The general expression for the propagator in Laplace space is

$$\Pi(E, E') = \frac{i}{E} \delta(E, E') + \frac{1}{E} \int dE_1 L(E, E_1) \Pi(E_1, E'), \quad (6.2.5)$$

which can be transformed to

$$\underline{\Pi}(E) = \frac{1}{E - \underline{\tilde{L}}(E)} \underline{e}_0, \quad (6.2.6)$$

using the relations of Eqs. (6.2.2, 6.2.3, 6.2.4). Here $\underline{\tilde{L}}$ is a matrix and $\underline{\Pi}$ as well as \underline{e}_0 are vectors in the combined space of Fourier space and Liouville space, i.e. defined as [Sch12]

$$\langle ks_1 s_2 | \underline{\tilde{L}}^{\text{eff}}(E) | k' s'_1 s'_2 \rangle = \langle s_1 s_2 | L_{\text{eff}}^{k-k'}(E + k'\Omega) - k\Omega \delta_{k,k'} | s'_1 s'_2 \rangle, \quad (6.2.7)$$

$$\langle ks_1 s_2 | \underline{\Pi}(E) | s'_1 s'_2 \rangle = \langle s_1 s_2 | \Pi_k(E) | s'_1 s'_2 \rangle, \quad (6.2.8)$$

$$\langle ks_1 s_2 | \underline{e}_0 | s'_1 s'_2 \rangle = \delta_{k0} \delta_{s_1, s'_1} \delta_{s_2, s'_2}. \quad (6.2.9)$$

Eq. (6.2.7) defines here the relation between the full matrix $\underline{\tilde{L}}$ and $L^k(E)$. The reduced density matrix for the time periodic case reads then

$$\begin{aligned} \rho(t) &= \Pi(t, t_0) \rho(t_0) \\ &= \sum_n e^{-in\Omega t} \frac{i}{2\pi} \int dE e^{-iE(t-t_0)} \left(\frac{1}{E - \underline{\tilde{L}}(E)} \right)_{n0} \rho(t_0) \end{aligned} \quad (6.2.10)$$

in Floquet space. In order to compute the time evolution of the reduced density matrix, $\underline{\tilde{L}}$ needs to be diagonalized, solving

$$\underline{\tilde{L}}(E) |x_k(E)\rangle = \lambda_k |x_k(E)\rangle, \quad (6.2.11)$$

$$\langle \bar{x}_k(E) | \underline{\tilde{L}}(E) = \langle \bar{x}_k(E) | \lambda_k. \quad (6.2.12)$$

Since we only aim at the steady state of the system, only real eigenvalues need to be considered. Imaginary eigenvalues yield to an exponential decay, which has died out already in the long-time limit. The real eigenvalues are given by $-k\Omega$. The resulting eigenvalue equations for the right and left eigenvectors are

$$L_{ns_1 s_2, n' s'_1 s'_2}^{\text{eff}}(E) x_{n' s'_1 s'_2}^k(E) | ns_1 s_2 \rangle = -k\Omega x_{ns_1 s_2}^k(E) | ns_1 s_2 \rangle, \quad (6.2.13)$$

$$L_{ns_1 s_2, n' s'_1 s'_2}^{\text{eff}}(E) x_{ns_1 s_2}^k(E) \langle ns_1 s_2 | = -k\Omega x_{n' s'_1 s'_2}^k(E) \langle ns_1 s_2 |. \quad (6.2.14)$$

The left eigenvectors are

$$\langle \bar{x}_k | = \langle k00 | + \langle k11 |, \quad (6.2.15)$$

where the k th eigenvector belongs to the eigenvalue $-k\Omega$.

Calculating the right eigenvectors is more complicated, because they depend on the energy argument E . Moreover, in order to evaluate the energy integral of Eq. (6.2.10), poles and branch cuts of the right eigenvectors in the upper complex plane need to be located carefully. This is a difficult task independent of the order to which the effective Liouvillian is calculated. We avoid a further discussion of this, because the present study will employ a further approximation later on, rendering also the right eigenvector energy independent.

The general expression of the double energy dependent kernel in Laplace space

$$\begin{aligned} \Sigma(E, E') \rightarrow & (-i)^{m-1} (-1)^{N_p} \frac{1}{S} (\Pi\gamma)_{irr} \int \mathcal{D}\{E, E'\} G(E, E_1) \Pi^{X_1}(E'_1, E_1) \\ & \times G(E_1, E'_2) \Pi^{X_2}(E'_2, E_2) \dots G(E_{m-2}, E'_{m-1}) \Pi^{X_m}(E'_{m-1}, E_{m-1}) G(E_{m-1}, E'_m) \end{aligned} \quad (6.2.16)$$

can be transformed to Floquet space by employing Eqs. (6.2.2, 6.2.3, 6.2.4)

$$\begin{aligned} \Sigma^k(E - k\Omega) \rightarrow & (-i)^{m-1} (-1)^{N_p} \frac{1}{S} (\Pi\gamma)_{irr} \sum_{k'_1 \dots k'_m} \sum_{k_1 \dots k_{m-1}} G^{k'_1} \Pi^{k_1, X_1}(E - k'_1\Omega - k_1\Omega) G^{k'_2} \\ & \times \Pi^{k_2, X_2}(E - k'_1\Omega - k_1\Omega - k'_2\Omega - k_2\Omega) G^{k'_3} \dots G^{k'_{m-1}} \\ & \times \Pi^{k_{m-1}, X_{m-1}}(E - k'_{1, \dots, m-1}\Omega - k_{1, \dots, m-2}\Omega) G^{k'_m} \delta k, k'_{1, \dots, m} + k_{1, \dots, m-1}. \end{aligned} \quad (6.2.17)$$

The resulting expressions depend on one energy argument E and an extra Fourier index (analogously as the Green's function in Floquet space). This allows to use the diagrammatics derived in Sec. 6.1.3 for the time independent case and complement them by the following rules [Kena]:

- Add $\sum_{k'_m}$ for each vertex G and $G \rightarrow G^{k'_m}$.
- Add \sum_{k_m} for each propagator Π and $\Pi^X(E) \rightarrow \Pi^{k_m, X}(E - \sum_{j'} j' \Omega - \sum_j j \Omega)$, where j' runs over all Floquet indices of G s to the left and j runs over all Floquet indices of Π s to the left as well as the index of the current Π itself.
- On the left hand side add to the object an additional index k and shift the energy argument E by $-k\Omega$ as well as add a $\delta_{k, \sum k' + \sum k}$ to the right hand side.

6.2.2 General form of the RLM Liouvillian

We concentrate now on the resonant level model as defined in Eq. (3.2.2) with $U = 0$ in the wide band limit. The local Hilbert space is spanned by $|0\rangle, |1\rangle$, such that the Liouville space is spanned by the basis $|00\rangle, |11\rangle, |10\rangle, |01\rangle$. The k th component of the effective Liouvillian in its general form in this basis is

$$\mathbf{L}_{eff}^k = \begin{pmatrix} i\Gamma_0^k(E) & -i\Gamma_1^k(E) & 0 & 0 \\ -i\Gamma_0^k(E) & i\Gamma_1^k(E) & 0 & 0 \\ 0 & 0 & \epsilon^k(E) & 0 \\ 0 & 0 & 0 & -[\epsilon^k(-E^*)]^* \end{pmatrix}. \quad (6.2.18)$$

From the two properties

$$\text{Tr } \rho(t) = 0 \quad (\text{conservation of probability}) \quad (6.2.19)$$

$$\text{and} \quad \rho(t) = \rho^\dagger(t) \quad (\text{hermiticity}) \quad (6.2.20)$$

of the reduced density matrix follow for the general Liouvillian

$$\text{Tr } L^{eff}(t, t') = 0 \quad (6.2.21)$$

$$(L^{eff})^c(t, t') = -L(t, t') \quad (6.2.22)$$

where the 'c-transformation' is defined as $(A^c)_{ss',\bar{s}\bar{s}'} = A_{s's,\bar{s}'\bar{s}}^*$. This in turn directly yields the properties

$$\text{Tr} [L^{(k)}(E)] = 0 \quad (6.2.23)$$

$$[L^{(k)}(E)]^c = -L^{(-k)}(-E^*). \quad (6.2.24)$$

The entries Γ_0^k and Γ_1^k of the upper left corner are the Fourier coefficients of the rates from the dot state $|0\rangle$ to $|1\rangle$ and vice versa, respectively. Due to the simplicity of the model, where the charge is the only quantum number, the off-diagonal blocks vanish, i.e. upper right block and the lower left block decouple. This allows to focus on the the upper right block, which with

$$\rho_{00} \equiv p_0 \quad (6.2.25)$$

$$\rho_{11} \equiv p_1, \quad (6.2.26)$$

and Eq. (6.2.19) reduces to a master equation which only calculates the probabilities of the dot being empty p_0 or full p_1 .

6.3 Markov approximation and Perturbation Theory

6.3.1 Perturbation Theory in RLM: First order diagramm

For the resonant level model, the superindex reduces to

$$i \equiv \eta\alpha\omega, \quad i = 1, 2, \dots \quad (6.3.1)$$

i.e. omitting the spin index and $\alpha \in \{R, L\}$. The coupling between system and reservoir is

$$g_i^k = t_k^\alpha \begin{cases} c & \text{for } \eta = + \\ c^\dagger & \text{for } \eta = - \end{cases}. \quad (6.3.2)$$

where $t_\alpha(t) = \sum_k t_k^\alpha e^{ik\Omega t}$. With this definition, we can now apply the derived diagrammatics to calculate the kernel to first order in the tunnel rates, i.e. evaluating the first diagram in Fig. 6.1. The first diagram is

$$\begin{aligned} \Sigma^k(E) &= \gamma_{12}^{p_1 p_2} G_{k_1,1}^{p_1} \Pi_{00}^{s_1}(E + k\Omega - k_1\Omega) G_{k_2,2}^{p_2} \delta_{k_1+k_2,k} \\ &= (p_2 \gamma_1^s + \gamma_1^a) \delta_{12} G_{k_1,1}^{p_1} \Pi_{00}^{s_1}(E + k\Omega - k_1\Omega) G_{k_2,2}^{p_2} \delta_{k_1+k_2,k} \\ &= \Sigma^{s,k}(E) + \Sigma^{a,k}(E), \end{aligned} \quad (6.3.3)$$

with the contraction divided into a symmetric and an antisymmetric part

$$\gamma_{11'}^{pp'} = \delta_{11'} (p' \gamma_1^s + \gamma_1^a), \quad (6.3.4)$$

$$\gamma_1^s = \frac{1}{2} \bar{\rho}_{\alpha\sigma}(\bar{\omega}), \quad (6.3.5)$$

$$\begin{aligned} \gamma_1^a &= \bar{\rho}_{\alpha\sigma}(\bar{\omega}) \left(f_\alpha(\bar{\omega}) + \frac{1}{2} \right) \\ &= \bar{\rho}_{\alpha\sigma}(\bar{\omega}) T_\alpha \frac{1}{2} \sum_n \left(\frac{1}{\bar{\omega} - i\omega_n^\alpha} + \frac{1}{\bar{\omega} + i\omega_n^\alpha} \right). \end{aligned} \quad (6.3.6)$$

The Fermi distribution has been decomposed accordingly and is represented in terms of the Matsubara frequencies $\omega_n^\alpha = (2n+1)\pi T_\alpha$. The spectral function $\bar{\rho}_{\alpha\sigma}(\bar{\omega}) = \rho_{\alpha\sigma}(\omega)$ with $\bar{\omega} = \eta\omega$ is defined by the wide band limit in Eq. (3.3.5). These two parts are calculated separately. The antisymmetric

part reads

$$\begin{aligned}
\Sigma^{a,k}(E) &= \gamma_1^a \delta_{1\bar{2}} G_{k_1,1}^{p_1} \Pi_{00}^{s_1}(E + k\Omega - k_1\Omega) G_{k_2,2}^{p_2} \delta_{k_1+k_2,k} \\
&= \gamma_1^a \delta_{1\bar{2}} \langle rs | G_{k_1,1}^{p_1} | il \rangle \Pi_{00,ilmn}^{s_1}(E + k\Omega - k_1\Omega) \langle mn | G_{k_2,2}^{p_2} | pq \rangle \delta_{k_1+k_2,k} \\
&= \lim_{D \rightarrow \infty} \int d\bar{\omega} \frac{D^2}{D^2 + \bar{\omega}^2} \left[T_\alpha \frac{1}{2} \sum_n \frac{1}{\bar{\omega} - i\omega_n^\alpha} + \frac{1}{\bar{\omega} + i\omega_n^\alpha} \right] \frac{1}{\bar{\omega} - z} \\
&\quad \times \delta_{ln} \delta_{im} \delta_{1\bar{2}} \delta_{k_1+k_2,k} \langle rs | G_{k_1,1}^{p_1} | il \rangle \langle mn | G_{k_2,2}^{p_2} | pq \rangle \delta_{k_1+k_2,k} \\
&= \lim_{D \rightarrow \infty} \left[\sum_n \frac{T_\alpha \pi}{iD + E + k_2\Omega \pm \epsilon} \frac{D^2}{D^2 - (\omega_n^\alpha)^2} - \sum_{n \geq 0} \frac{iT_\alpha \pi}{i\omega_n^\alpha - z} \frac{D^2}{D^2 - (\omega_n^\alpha)^2} \right] \\
&\quad \times \delta_{ln} \delta_{im} \delta_{1\bar{2}} \langle rs | G_{k_1,1}^{p_1} | il \rangle \langle mn | G_{k_2,2}^{p_2} | pq \rangle \delta_{k_1+k_2,k} \\
&= \sum_{\alpha, k_2} |00\rangle \langle 00| t_{k-k_2}^\alpha t_{k_2}^\alpha \left[\sum_{n \geq 0} \frac{iT_\alpha \pi}{E + k_2\Omega + \epsilon + i\omega_n^\alpha} - \sum_{n \geq 0} \frac{iT_\alpha \pi}{E + k_2\Omega - \epsilon + i\omega_n^\alpha} \right] \\
&\quad + |11\rangle \langle 11| t_{k-k_2}^\alpha t_{k_2}^\alpha \left[\sum_{n \geq 0} \frac{iT_\alpha \pi}{E + k_2\Omega - \epsilon + i\omega_n^\alpha} - \sum_{n \geq 0} \frac{iT_\alpha \pi}{E + k_2\Omega + \epsilon + i\omega_n^\alpha} \right] \\
&\quad + |00\rangle \langle 11| t_{k-k_2}^\alpha t_{k_2}^\alpha \left[\sum_{n \geq 0} \frac{iT_\alpha \pi}{E + k_2\Omega + \epsilon + i\omega_n^\alpha} - \sum_{n \geq 0} \frac{iT_\alpha \pi}{E + k_2\Omega - \epsilon + i\omega_n^\alpha} \right] \\
&\quad + |11\rangle \langle 00| t_{k-k_2}^\alpha t_{k_2}^\alpha \left[\sum_{n \geq 0} \frac{iT_\alpha \pi}{E + k_2\Omega - \epsilon + i\omega_n^\alpha} - \sum_{n \geq 0} \frac{iT_\alpha \pi}{E + k_2\Omega + \epsilon + i\omega_n^\alpha} \right], \quad (6.3.7)
\end{aligned}$$

where summation over the double indices is assumed. The energy integral is closed in the upper half plane, such that the residues of the Matsubara frequencies as well as the bandwidth D are summed up, while the principal value of $\frac{1}{\bar{\omega}-z}$ with $z := -(E + k\Omega - k_1\Omega - H_{im} + H_{ln})$ yields no contribution. The symmetric part reads

$$\begin{aligned}
\Sigma^{s,k}(E) &= p_2 \gamma_1^s \delta_{1\bar{2}} G_{k_1,1}^{p_1} \Pi_{00}^{s_1}(E + k\Omega - k_1\Omega) G_{k_2,2}^{p_2} \delta_{k_1+k_2,k} \\
&= \lim_{D \rightarrow \infty} \int d\bar{\omega} \frac{D^2}{D^2 + \bar{\omega}^2} \frac{1}{E + k\Omega - k_1\Omega + \bar{\omega} - H_{im} + H_{ln}} \\
&\quad \times \frac{p_2}{2} \delta_{ln} \delta_{im} \delta_{1\bar{2}} \delta_{k_1+k_2,k} \langle rs | G_{k_1,1}^{p_1} | il \rangle \langle mn | G_{k_2,2}^{p_2} | pq \rangle \delta_{k_1+k_2,k} \\
&= \lim_{D \rightarrow \infty} \pi D \frac{1}{E + k\Omega - k_1\Omega + iD - H_{im} + H_{ln}} \\
&\quad \times \frac{p_2}{2} \delta_{ln} \delta_{im} \delta_{1\bar{2}} \delta_{k_1+k_2,k} \langle rs | G_{k_1,1}^{p_1} | il \rangle \langle mn | G_{k_2,2}^{p_2} | pq \rangle \delta_{k_1+k_2,k} \\
&= -i\pi \frac{p_2}{2} \delta_{ln} \delta_{im} \delta_{1\bar{2}} \delta_{k_1+k_2,k} \langle rs | G_{k_1,1}^{p_1} | il \rangle \langle mn | G_{k_2,2}^{p_2} | pq \rangle \delta_{k_1+k_2,k} \\
&= -i\pi \sum_{\alpha, k_2} t_{k-k_2}^\alpha t_{k_2}^\alpha (|00\rangle \langle 00| + |11\rangle \langle 11| - |00\rangle \langle 11| - |11\rangle \langle 00| + |10\rangle \langle 10| + |01\rangle \langle 01|). \quad (6.3.8)
\end{aligned}$$

6.3.2 Markov approximation in Floquet space

Separating the time scale of the kernel from the reduced density matrix by setting $\rho(t') \rightarrow \rho(t)$ is an often employed approximation in the time independent case [Sch94] or for time periodic system in the adiabatic limit, where it is enhanced by corrections to the order of Ω [Spl06]. In analogy to the time independent case, we call it Markov approximation, which needs to be contrasted to the approximation of setting the double time dependent tunneling rate $\Gamma(t, t')$ to $\Gamma(t)$ [Cav09, Win13].

Extending the approximation to the whole range of driving frequency seems to be crude, because the separation of the time scales is not justified anymore out of the adiabatic regime. In order to investigate the nature of this approach we employ it as follows

$$\begin{aligned}
 i\dot{\rho}(t) &= \int_{t_0}^t dt' \Sigma(t, t') \rho(t') \\
 &\stackrel{(Markov)}{=} \int_{t_0}^t dt' \Sigma(t, t') \rho(t) \\
 &= \int_{t_0}^t dt' \sum_k e^{-ik\Omega t} \int \frac{dE}{2\pi} e^{-iE(t-t')} \Sigma^k(E) \rho(t) \\
 &\approx \int d\tau \sum_k e^{-ik\Omega t} \int \frac{dE}{2\pi} e^{-iE\tau} \Sigma^k(E) \rho(t) \\
 &= \sum_k e^{-ik\Omega t} \Sigma^k(i0^+) \rho(t).
 \end{aligned} \tag{6.3.9}$$

This can be done analogously with the current kernel $\Sigma_{(\gamma)}$ leading to

$$\langle I_\gamma \rangle(t) = -i \text{Tr} \left(\sum_k e^{-ik\Omega t} \Sigma_\gamma^k(i0^+) \rho(t) \right). \tag{6.3.10}$$

The expression for the reduced density matrix becomes in this approximation

$$\begin{aligned}
 \rho_{s_1, s_2}(t) &= \sum_n e^{-in\Omega t} \frac{i}{2\pi} \int dE e^{-iE(t-t_0)} \sum_{s'_1, s'_2} \langle ns_1 s_2 | \left(\frac{1}{E - \hat{\underline{L}}(i0^+)} \right) | 0s'_1 s'_2 \rangle \rho_{s'_1 s'_2}(t_0) \\
 &= \sum_n e^{-in\Omega t} \frac{i}{2\pi} \int dE e^{-iE(t-t_0)} \sum_{k, s'_1, s'_2} \langle ns_1 s_2 | \frac{1}{E + k\Omega} | x_k(i0^+) \rangle \langle \bar{x}_k(i0^+) | 0s'_1 s'_2 \rangle \rho_{s'_1 s'_2}(t_0),
 \end{aligned} \tag{6.3.11}$$

where the spectral decomposition of $\hat{\underline{L}}(i0^+)$ is employed. For $t_0 \rightarrow -\infty$, the steady state is

$$\begin{aligned}
 \rho_{s_1, s_2}^{st}(t) &= \sum_{n, k, s'_1, s'_2} e^{-in\Omega t} e^{ik\Omega t} \langle ns_1 s_2 | x_k(i0^+) \rangle \langle \bar{x}_k(i0^+) | 0s'_1 s'_2 \rangle \rho_{s'_1 s'_2}(0) \\
 &= \sum_{n, s'_1} e^{-in\Omega t} \langle ns_1 s_2 | x_0(i0^+) \rangle \rho_{s'_1 s'_1}(0) \\
 &= \sum_n e^{-in\Omega t} \langle ns_1 s_2 | x_0(i0^+) \rangle,
 \end{aligned} \tag{6.3.12}$$

where we use the specific form of the left eigenvector. $\hat{\underline{L}}(i0^+)$ indicates that the initial eigenvalue equation for the upper right block

$$[i\Gamma_{0; n-n'}(E + n'\Omega) - n\Omega\delta_{nn'}] x_{n'00}^k(E) - i\Gamma_{1; n-n'}(E + n'\Omega) x_{n'11}^k = -k\Omega x_{n00}^k(E) \tag{6.3.13}$$

$$[i\Gamma_{1; n-n'}(E + n'\Omega) - n\Omega\delta_{nn'}] x_{n'11}^k(E) - i\Gamma_{0; n-n'}(E + n'\Omega) x_{n'00}^k = -k\Omega x_{n11}^k(E) \tag{6.3.14}$$

becomes

$$[i\Gamma_{0; n-n'}(i0^+) - n\Omega\delta_{nn'}] x_{n'00}^k(i0^+) - i\Gamma_{1; n-n'}(i0^+) x_{n'11}^k = -k\Omega x_{n00}^k(i0^+) \tag{6.3.15}$$

$$[i\Gamma_{1; n-n'}(i0^+) - n\Omega\delta_{nn'}] x_{n'11}^k(i0^+) - i\Gamma_{0; n-n'}(i0^+) x_{n'00}^k = -k\Omega x_{n11}^k(i0^+) \tag{6.3.16}$$

in the Markov approximation. We can deduce that only the eigenvector for the eigenvalue $\lambda = 0$ contributes to the stationary state in the Markov approximation and the higher harmonics of the probabilities $p_{0/1}$ are

$$p_0^m = x_{m00}^0(i0^+) \tag{6.3.17}$$

$$p_1^m = x_{m11}^0(i0^+). \tag{6.3.18}$$

6.3.3 Quantum Master equation in Floquet Space

Finally, the equations for the probabilities reduce to a quantum master equation in Floquet space

$$\begin{aligned}\dot{p}_s(t) &= \sum_{ks'} e^{-ik\Omega t} W_{ss'}^k p_{s'}(t), \\ &= \sum_{kns' \neq s} e^{-i(k+n)\Omega t} (W_{ss'}^k p_{s'}^n - W_{s's}^k p_s^n)\end{aligned}\quad (6.3.19)$$

$$\langle I_\gamma \rangle(t) = \sum_{knss'} e^{-i(k+n)\Omega t} W_{ss'}^{k,\gamma} p_{s'}^n, \quad (6.3.20)$$

where we have defined $-i\Sigma_{ss',s'}^{k,(\gamma)}(i0^+) = W_{ss'}^{k,(\gamma)}$ and $s, s' \in \{0, 1\}$. The entries of the (current) kernel are

$$\begin{aligned}W_{00}^k &= \Gamma_0^k & W_{00}^{k,\alpha} &= -\Gamma_0^{k,\alpha}/2 \\ W_{01}^k &= -\Gamma_1^k & W_{01}^{k,\alpha} &= \Gamma_1^{k,\alpha}/2 \\ W_{10}^k &= -\Gamma_0^k & W_{10}^{k,\alpha} &= -\Gamma_0^{k,\alpha}/2 \\ W_{11}^k &= \Gamma_1^k & W_{11}^{k,\alpha} &= \Gamma_1^{k,\alpha}/2\end{aligned}$$

with $\Gamma_{0/1}^k = \Gamma_{0/1}^{k,L} + \Gamma_{0/1}^{k,R}$ and with the rates calculated in Eqs. (6.3.7) and (6.3.8)

$$\begin{aligned}\Gamma_0^k &= \sum_{\alpha, k_2} t_{k-k_2}^\alpha t_{k_2}^\alpha \left[\sum_{n \geq 0} \frac{T_\alpha \pi}{k_2 \Omega + \epsilon + i\omega_n^\alpha} - \sum_{n \geq 0} \frac{T_\alpha \pi}{k_2 \Omega - \epsilon + i\omega_n^\alpha} - \pi \right], \\ \Gamma_1^k &= \sum_{\alpha, k_2} t_{k-k_2}^\alpha t_{k_2}^\alpha \left[\sum_{n \geq 0} \frac{T_\alpha \pi}{k_2 \Omega - \epsilon + i\omega_n^\alpha} - \sum_{n \geq 0} \frac{T_\alpha \pi}{k_2 \Omega + \epsilon + i\omega_n^\alpha} - \pi \right],\end{aligned}\quad (6.3.21)$$

with temperature T_α of reservoir $\alpha \in (L, R)$ and $\omega_n^\alpha = (2n+1)\pi T_\alpha$ are the respective fermionic Matsubara frequencies.

It is now equivalently to solve Eq. (6.3.16) or to rewrite Eq. (6.3.19) under the assumption of a time periodic form of the probability as well as by employing the symmetries $p_0^0 = 1 - p_1^0$; $p_0^n = -p_1^n$. Both way it leads to the following coupled expressions for the higher harmonics

$$p_0^0 = \frac{1}{\Gamma_1^0 + \Gamma_0^0} (\Gamma_1^0 - \sum_{k \neq 0} (\Gamma_1^k + \Gamma_0^k) p_0^{-k}), \quad (6.3.22)$$

$$p_1^0 = \frac{1}{\Gamma_1^0 + \Gamma_0^0} (\Gamma_0^0 - \sum_{k \neq 0} (\Gamma_1^k + \Gamma_0^k) p_1^{-k}), \quad (6.3.23)$$

$$p_0^m = -\frac{1}{-im\Omega + \Gamma_1^0 + \Gamma_0^0} \left(\sum_{k \neq 0} (\Gamma_1^k + \Gamma_0^k) p_0^{m-k} + \Gamma_0^m \right) \quad m \neq 0, \quad (6.3.24)$$

$$p_1^m = -\frac{1}{-im\Omega + \Gamma_1^0 + \Gamma_0^0} \left(\sum_{k \neq 0} (\Gamma_1^k + \Gamma_0^k) p_1^{m-k} + \Gamma_1^m \right) \quad m \neq 0. \quad (6.3.25)$$

The left mean current can be rewritten as

$$\begin{aligned}\langle I_{L,0} \rangle &= \sum_{nss'} W_{ss'}^{-n,L} p_{s'}^n \\ &= \sum_n \Gamma_1^{-n,L} p_1^n - \Gamma_0^{-n,L} p_0^n.\end{aligned}\quad (6.3.26)$$

This method is used to verify if the finite mean current of a single parameter pump can be captured already when employing the separation of time scales. The results are presented in Section 8.4.3.

Dynamics in Periodically Driven Quantum Dots

Chapter 7

Renormalization in Periodically Driven Quantum Dots

Contents

7.1	The equilibrium IRLM	64
7.2	The time independent non-equilibrium IRLM	65
7.3	The time dependent non-equilibrium IRLM	68
7.4	From transient behavior to the periodic steady state	69
7.5	Time periodically driven IRLM in the limit of small driving amplitude	70
7.5.1	Setup and Protocols	70
7.5.2	Keldysh Green's function in the limit of small driving amplitudes	71
7.5.3	Mean value: $k = 0$ component	73
7.5.4	Protocol 1: Time periodic $\tau_L(t)$	75
7.5.5	Protocol 2: Time periodic $\tau_L(t)$ and $\tau_R(t)$	79
7.5.6	Protocol 3: Time periodic $\epsilon(t)$	80
7.5.7	Protocol 4: Time periodic $\tau_L(t)$ and $\epsilon(t)$	84
7.6	Tuning the effective reservoir distribution function	85
7.6.1	Setup and Illustration of the physical situation	85
7.6.2	Effect on the Renormalization flow	86
7.7	Conclusion	88

In this chapter renormalization in the context of time periodically driven quantum dots is discussed. The interacting resonant level model (IRLM) used to model the quantum dot, is known to exhibit strong renormalization physics. In particular, intriguing is the way multiple energy scales compete in the renormalization group flow to act as an infrared cutoff [Sch80a, Doy07, Bou08, Bor07, Kar10c]. The physics reported in the literature about equilibrium, the time independent as well as the time dependent non-equilibrium IRLM is introduced in the first three sections. Subsequently, we compare the explicitly time dependent FRG to the one set up directly in Floquet space and elaborate in what sense the two can be viewed as complementary methods. Motivated by the known renormalization physics of the IRLM, we are interested in the role of the driving frequency Ω as an infrared cutoff of the renormalization flow. To study this, we first consider four different protocols with combinations of the hopping(s) and/or the onsite energy periodically varied in time. We focus on the limit of a small driving amplitude, since it allows to complement the full numerical solution of the truncated FRG flow equations with analytic expressions of the renormalization of the parameters. Secondly, a setup where only the onsite energy is driven time periodically is treated, considering an arbitrary driving amplitude and driving frequency. We elaborate that this scenario can be described in terms of an effective reservoir distribution function, which exhibits a multistep form, where position and height of the edges are defined by the ratio of driving amplitude and driving frequency. Taking advantage of the tunability of this function, its influence on the RG flow can be investigated and we

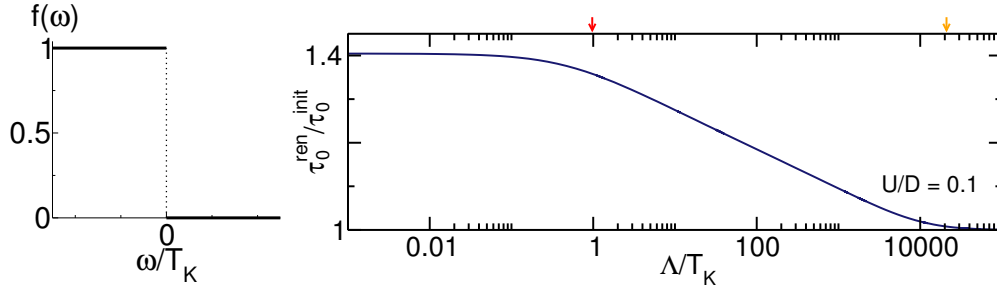


Figure 7.1: The reservoir distribution function in equilibrium (left panel) and the resulting renormalization group flow of the hopping (right panel) with $U/D = 0.1$, $T_K/D = 4.62 \cdot 10^{-5}$, $T = 0$ and $\epsilon = 0$. Yellow arrow indicates the bandwidth D , the red arrow marks the low energy scale T_K .

find that the energy scales defined by the positions of the sharp edges can be related to the infrared cutoffs of the flow.

The present chapter solely focuses on the renormalization of the dot parameters, which can be discussed in a transparent way. Subsequently, the acquired understanding is used to comprehend the resulting transport through the system, which is presented in the next chapter.

7.1 The equilibrium IRLM

The main physics of the equilibrium IRLM has been sketched shortly in Section 3.5 already when discussing the model, but is now illuminated further in the context of the functional renormalization group.

Calculating the first order contribution to the left (right) hopping for symmetric hoppings $\tau_{L,0} = \tau_{R,0} = \tau_0$ in perturbation theory in the interaction to the leading order of U/D reads¹ [Kar10c]

$$\begin{aligned} \tau_{L(R),0}^{\text{PT}} &= \tau_0 - U n_{12(23)} \\ &\stackrel{\mathcal{O}(\frac{1}{D})}{=} \tau_0 - \frac{U}{4\pi i} \int d\omega G_{11(23)}^{\text{ret}} \Sigma_{11(33)}^K G_{12(33)}^{\text{adv}} \\ &\stackrel{D \gg \tau_0}{=} \tau_0 - \frac{U}{\pi D} \frac{\tau_0}{D} \int_{-D}^D \frac{f_L(\omega) - 1/2}{\omega/D - 2i \frac{|\tau_0|^2}{D^2}} d\omega. \end{aligned} \quad (7.1.1)$$

The reservoir distribution function $f_L(\omega) = f_R(\omega) = \theta(-\omega)$ for $T = 0$ in the equilibrium (depicted in the left panel of Fig. 7.1) and thus has a sharp step at $\omega = 0$.

The step at $\omega = 0$ renders it necessary to rewrite the integral (we do not distinguish between left/right hopping anymore, since they are equivalent in the considered setup)

$$\tau_0^{\text{PT}} = \tau_0 - \frac{U}{\pi D} \frac{\tau_0}{D} \left[\frac{1}{2} \int_{-D}^0 \frac{1}{\omega/D - 2i \frac{|\tau_0|^2}{D^2}} d\omega - \frac{1}{2} \int_0^D \frac{1}{\omega/D - 2i \frac{|\tau_0|^2}{D^2}} d\omega \right]. \quad (7.1.2)$$

Evaluating the integral leads to

$$\begin{aligned} \tau_0^{\text{PT}} &= \tau_0 - \frac{U}{\pi D} \tau_0 \left[\ln \left(\frac{2\tau_0^2}{D^2} \right) - \ln \left(\sqrt{1 + \frac{4\tau_0^4}{D^2}} \right) \right] \\ &\stackrel{D \gg \tau_0}{=} \tau_0 - \frac{U}{\pi D} \tau_0 \ln \left(\frac{2\tau_0^2}{D^2} \right), \end{aligned} \quad (7.1.3)$$

which shows a logarithmic dependency on $2\tau_0^2/D^2$ resulting from the evaluation at $\omega = 0$ (as a consequence of the sharp Fermi edge). The expression diverges for $\tau_0/D \rightarrow 0$, such that the regime

¹The chosen integral borders $\pm D$ in the last step are a consequence of the approximation to only include the leading $\frac{1}{D}$ terms.

of approachable interaction vanishes in the wide band limit $D \rightarrow \infty$, as discussed in Section 3.5. This renders the usage of a RG method reasonable. The first order flow equation in the functional renormalization group for the equilibrium setup and with vanishing onsite energy is given by [Kar10c]

$$\partial_\Lambda \tau_0^\Lambda = -\frac{U}{\pi D} \frac{\tau_0^\Lambda/D}{(\Lambda/D)^2 + \Lambda/D + 2(\tau_0/D)^2}. \quad (7.1.4)$$

The respective renormalization flow of the hopping matrix element τ_0 is shown in the right panel of Fig. 7.1, where two scales become apparent to characterize the flow: The **ultraviolet cutoff** is the energy scale, where the flow starts to deviate from its initial value. Here the UV cutoff is given by the bandwidth D . The second scale is the infrared cutoff. An **infrared cutoff** is defined as the energy scale at which the renormalization flow stops, i.e. when the flow parameter Λ reaches the value of the infrared cutoff, the renormalization group flow levels off and the hopping saturates to its final value.

Solving the differential equation (7.1.4) analytically, results in

$$\frac{\tau_0^{\text{ren}}}{\tau_0^{\text{init}}} = \left[\frac{1 - \sqrt{1 - 8(\tau_0^{\text{init}}/D)^2}}{1 + \sqrt{1 - 8(\tau_0^{\text{init}}/D)^2}} \right]^{-\frac{U}{\pi D} [1 - 8(\tau_0^{\text{init}}/D)^2]^{-1/2}} \\ \stackrel{D \gg \tau_0^{\text{init}}}{=} \left(\frac{2\tau_0^{\text{init}2}}{D^2} \right)^{-\frac{U}{\pi D}}, \quad (7.1.5)$$

where the logarithmic divergency of perturbation theory is summed up within the renormalization flow, yielding the discussed power law (see Eq. (3.5.2)): In equilibrium τ_0 cuts its own flow, resulting in [Kar10c]

$$\frac{\tau_0^{\text{ren}}}{\tau_0^{\text{init}}} \sim \left(\frac{\tau_0^{\text{init}}}{D} \right)^{-\frac{2U}{\pi D} + \mathcal{O}(U^2)} \quad \text{for } |\epsilon| \ll T_K \ll D. \quad (7.1.6)$$

The final, renormalized value in turn depends on the infrared cutoff scale τ_0^{init} in a power-law fashion.

The emergent low energy scale T_K has been defined via the charge susceptibility (see Chapter 3, Eq. (3.5.4)), which directly reflects the power law. On the other hand, in the non-interacting case it is equivalent to define the low energy scale via

$$\tilde{T}_K = \frac{4|\tau_0^{\text{init}}|^2}{D}. \quad (7.1.7)$$

The bare hopping τ_0^{init} can now be substituted by τ_0^{ren} to incorporate the interaction and \tilde{T}_K can be identified as the infrared cutoff in Eq. (7.1.6). Both definitions of the low energy scale T_K are equivalent to the leading order in U and would be the same in the wide band limit $D \rightarrow \infty$. We thus do not distinguish between these definitions and suppress the tilde in the following.

The renormalization of the onsite energy ϵ shows also power law behavior in the limits $\epsilon \ll T_K$ and $\epsilon \gg T_K$. Taking the logarithmic derivative of the numerical solution of the FRG flow equation for ϵ (not shown) indicates that the exponent is of the order of U^2 in the scaling limit and hence cannot be determined correctly within the first order truncation [Kar10a]. Moreover, if $\epsilon^{\text{init}} = 0$, then it follows $\epsilon^{\text{ren}} = 0$ to all orders due to the particle hole symmetric structure of the respective flow equation. Equally the onsite energies of site 1 and 3 are only renormalized to order U^2 .

7.2 The time independent non-equilibrium IRLM

A well studied time independent, non-equilibrium setup in the IRLM, is one with an applied bias voltage V . Calculating the first order contribution to the left (right) hopping (with $\tau_{L,0} = \tau_{R,0} = \tau_0$)

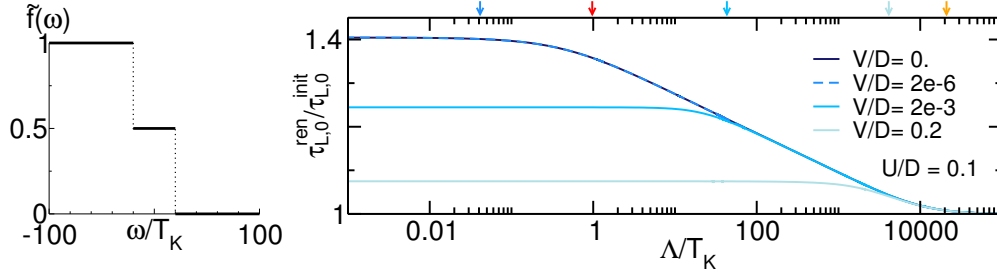


Figure 7.2: The effective reservoir distribution function (left panel) for a setup with a symmetrically applied bias voltage as well as vanishing onsite energy and the resulting renormalization group flows (right panel) of the renormalized hopping for different amount of applied bias voltage with $U/D = 0.1$ and $T_K/D = 4.62 \cdot 10^{-5}$. Red (yellow) arrow indicate the low energy scale T_K (the bandwidth D), the blue arrows mark color coded the voltage strength.

in perturbation theory in the interaction U/D for this non-equilibrium setup yields [Kar10c]

$$\begin{aligned} \tau_{L(R),0}^{\text{PT}} &= \tau_0 - Un_{12} \\ &\stackrel{\mathcal{O}(\frac{1}{D})}{=} \tau_0 - \frac{U}{4\pi i} \int d\omega G_{11(23)}^{\text{ret}} \Sigma_{11(33)}^K G_{12(33)}^{\text{adv}} \\ &\stackrel{D \gg \tau_0}{=} \tau_0 - \frac{U}{\pi D} \frac{\tau_0}{D} \int_{-D}^D d\omega \frac{\theta(-\omega + \mu_{L(R)}) - 1/2}{(\omega - \epsilon)/D - 2i \frac{|\tau_0|^2}{D^2}} \end{aligned} \quad (7.2.1)$$

where we have also included a finite onsite energy ϵ . The reservoir distribution function of the left (right) reservoir $f_{L(R)}(\omega)$ for $T = 0$ with a finite chemical potential $\mu_{L(R)}$ has been expressed in terms of a Heaviside function, which reveals the sharp step at $\mu_{L(R)}$. This expression can be recast to

$$\tau_{L(R),0}^{\text{PT}} \stackrel{D \gg \tau_0, \epsilon}{=} \tau_0 - \frac{U}{\pi D} \frac{\tau_0}{D} \int_{-D}^D d\omega \frac{\theta[-\omega + (\mu_{L(R)} - \epsilon)] - 1/2}{\omega/D - 2i \frac{|\tau_0|^2}{D^2}} \quad (7.2.2)$$

revealing $\mu_{L(R)} - \epsilon$ as the effective positions of the sharp edge. For a compact illustration of both relevant energy scales for the left and the right hopping, we define an effective reservoir distribution function. For this we consider the Keldysh reservoir self-energy of the effective one-dot structure (see Eq. (3.3.7))

$$\Sigma_{\text{res}}^K(\omega) = -2i\Gamma_{1d}[2 - 2f_L(\omega) - 2f_R(\omega)] = -4i\Gamma_{1d}[1 - 2\tilde{f}(\omega)], \quad (7.2.3)$$

such that the effective reservoir distribution function is defined as the sum of the left and right reservoir contribution

$$\tilde{f}(\omega) = \frac{1}{2} [f_L(\omega) + f_R(\omega)], \quad (7.2.4)$$

with a Fermi function $f_{L/R}$ that includes the onsite energy; $f_{L(R)} = \theta(\mu_{L(R)} - \epsilon - \omega)$ for $T = 0$. The resulting effective reservoir distribution function is depicted in the left panel of Fig. 7.2 for a symmetric applied bias voltage V and $\epsilon = 0$. It reveals the two sharp steps at $\omega = \pm V/2$, where the according energy scales (defined by these positions) affect the perturbation theory contribution of the left or right hopping, respectively. Equally as explained in the equilibrium setup, the integral of Eq. (7.2.2) is rewritten in two parts as a consequence of the step, and thus is evaluated at $\omega = \mu_{L/R} - \epsilon$ besides the integral borders $\omega = \pm D$. This yields for $\mu_L = -\mu_R = V/2$ and

$D \gg |\epsilon|, \tau_0, \mu_{L/R}$

$$\begin{aligned} \tau_{L(R),0}^{\text{PT}} &\approx \tau_0 - \frac{U}{2\pi D} \tau_0 \left\{ \ln \left[\frac{(V/2 \mp \epsilon)^2 + 4\tau_0^4/D^2}{D^2} \right] - \frac{1}{2} \ln \left[\left(1 + \frac{\epsilon}{D}\right)^2 + \frac{4\tau_0^4}{D^4} \right] \right. \\ &\quad \left. - \frac{1}{2} \ln \left[\left(1 - \frac{\epsilon}{D}\right)^2 + \frac{4\tau_0^4}{D^4} \right] \right\} \\ &\stackrel{D \gg \tau_0, \epsilon, \mu_{L(R)}}{\approx} \tau_0 - \frac{U}{2\pi D} \tau_0 \ln \left[\frac{(V/2 \mp \epsilon)^2 + 4\tau_0^4/D^2}{D^2} \right]. \end{aligned} \quad (7.2.5)$$

The resulting expression reveals a logarithmic dependency, where the argument depends on all energy scales present in this non-equilibrium setup: the difference between chemical potential and onsite energy $\mu_{L(R)} - \epsilon$ as well as the equilibrium, low energy scale T_K . In analogy to the equilibrium setup, the wide band limit renders the RG method necessary.

The according flow equation for a symmetrically applied bias voltage $\mu_L = -\mu_R = V/2$ is given by [Kar10c]

$$\partial_\Lambda \tau_{L(R),0}^\Lambda = -\frac{U}{\pi D} \frac{\tau_{L(R),0}^\Lambda}{D} \frac{\Lambda/D + (\tau_{L(R),0}^\Lambda/D)^2 + (\tau_{R(L),0}^\Lambda/D)^2}{[(V/2 \mp \epsilon)/D]^2 + [\Lambda/D + (\tau_{L(R),0}^\Lambda/D)^2 + (\tau_{R(L),0}^\Lambda/D)^2]^2}, \quad (7.2.6)$$

including a finite onsite energy ϵ (which is assumed to be independent of Λ , neglecting its weak renormalization (see previous section)). From this the renormalization flow of $\tau_{L,0}$ can be deduced, which is displayed in the right panel of Fig. 7.2 for several values of applied bias voltage and $\epsilon = 0$. It can be observed that the infrared cutoff is affected by both energy scales V and T_K , competing with each other. As a consequence, in the limit where one energy scale is much larger than the other, the larger one provides the infrared cutoff.

Solving the differential equation (7.2.6) analytically² yields to a regularized expression [Kar10c]

$$\frac{\tau_{L(R),0}^{\text{ren}}}{\tau_{L(R),0}^{\text{init}}} \stackrel{D \gg \tau_0}{=} \left[\frac{(V/2 \mp \epsilon)^2 + ((\tau_{L(R),0}^{\text{init}})^2/D + (\tau_{R(L),0}^{\text{init}})^2/D)}{D^2} \right]^{-\frac{U}{2\pi D}} \quad (7.2.7)$$

where the logarithmic divergency of Eq. (7.2.5) has been summed up throughout the RG flow. The result allows to identify three different regimes for the renormalized hopping exhibiting distinct power law behavior [Kar10c]

$$\frac{\tau_0^{\text{ren}}}{\tau_0^{\text{init}}} \sim \left(\frac{\tau_0^{\text{init}}}{D} \right)^{-\frac{2U}{\pi D} + \mathcal{O}(U^2)} \quad \text{for } |V|, |\epsilon| \ll T_K \ll D, \quad (7.2.8)$$

$$\frac{\tau_0^{\text{ren}}}{\tau_0^{\text{init}}} \sim \left(\frac{V}{D} \right)^{-\frac{U}{\pi D} + \mathcal{O}(U^2)} \quad \text{for } T_K, |\epsilon| \ll |V| \ll D, \quad (7.2.9)$$

$$\frac{\tau_0^{\text{ren}}}{\tau_0^{\text{init}}} \sim \left(\frac{\epsilon}{D} \right)^{-\frac{U}{\pi D} + \mathcal{O}(U^2)} \quad \text{for } T_K, |V| \ll |\epsilon| \ll D. \quad (7.2.10)$$

reflecting the respective infrared cutoff.

The above discussion indicates the following: The effective reservoir distribution function exhibits sharp edges, where the discontinuous jumps yield logarithmic divergencies in a perturbation theory calculation. The position of the sharp edges render $\mu_{L/R} - \epsilon$ the relevant energy scale or respectively with only a sharp edge at $\omega = 0$, the low energy scales emerges. The divergency present in the perturbation theory calculation is summed up within the RG flow, resulting in a regularized expression depending on all energy scales. If one energy scales is much larger than the others it provides the

²Only including the leading feedback, i.e. neglecting the feedback to τ_0 in the fraction.

infrared cutoff in the RG flow of the hopping. As a consequence, the renormalized hopping depends on the infrared cutoff in a power law fashion.

How the presented power laws are reflected in observables is discussed in the subsequent chapter, where we discuss transport.

7.3 The time dependent non-equilibrium IRLM

Choosing the parameters of the IRLM to be time dependent allows to study a very broad range of possible setups. One interesting problem is a quench, where the transient behavior for $t \geq t_0$ is investigated, when e.g. interaction and coupling to the reservoirs are switched on at t_0 abruptly. Those setups can be approached by several methods, among others by the explicitly time dependent FRG (t-FRG) [Ken12a, Ken12b, Ken13, Kas13] and the real time renormalization group (RTRG) [And11a, And11b, Ken13, Kas13].

We like to sketch shortly at this point the transient behavior of the hopping and the renormalization effects found in these quenched setup. The t-FRG has proven to capture the intriguing physics of these systems, where we only give a brief overview, a comprehensive discussion can be found in the according references and in [Ken14]. Several quench setups have been investigated, but we mainly focus on the interaction quench, as it yields the most intriguing physics [Ken13, Kas13]. These systems are very involved rendering it difficult to derive analytic expressions for the time dependent renormalization of the parameters from the FRG flow equations. As a consequence - despite the dominant route of the present chapter, where we nearly exclusively focus on the renormalization of the parameters - we here discuss the observable occupancy as well to give an impression on renormalization in a time dependent quench setup.

If an initially empty dot is considered and coupling to the leads and interaction is turned on at t_0 , the transient behavior of the three site system is expected to be equal to the field theoretical IRLM if $t \geq D^{-1}$. This scale corresponds to the time needed to fill the sites 1 and 3, which renders them proper reservoir sites.

If a bias voltage V is applied and $|\epsilon \pm V/2| \gg T_K$, the renormalized hoppings $\tau_{L(R)}^{\text{ren}}(t)$ begin to oscillate after a rather short time around the respective steady state value, where the left (right) hopping exhibits only the smaller frequency $\epsilon - V/2$ (the larger frequency $\epsilon + V/2$), i.e. they show different behavior characterized by the chemical potential of the respective side. The relaxation of the occupancy towards its stationary value is governed by two different (RTRG renormalized) decay rates $\tilde{\Gamma}$ and $\tilde{\Gamma}_\epsilon$, describing the broadening of the hybridization to the leads and the charge relaxation on the level, respectively. The frequency of the oscillatory behavior is given by $\epsilon \pm V/2$. This is accompanied by an exponential decay and a $1/t^{1-g}$ decay with an interaction dependent exponent $g = 2U/(\pi D) + \mathcal{O}(U^2)$ [And11a, And11b, Ken12a]. Similar behavior can be found when quenching the onsite energy ϵ to a value much larger than T_K , where ϵ defines the frequency of the oscillating contribution. While for small times weak oscillations above an exponential decay are observed, for longer times the oscillations become more dominant [Kas13]. Further quench setups are discussed in Ref. [Ken12b].

The most interesting physics is observed when quenching the interaction, for example from positive to negative interaction or vice versa. While the rough understanding of the time evolution of the dot occupancy indicates that the time evolution is coherent, i.e. damped oscillatory for $U/D > 0$ and incoherent, i.e. a purely decaying for $U/D < 0$, the discussion below reveals that this understanding needs to be refined [Ken13, Kas13].

In the short time regime $T_K t \ll 1$, the renormalization of the hopping term can be calculated by means of the flow equation [Ken14]

$$\frac{\partial_\Lambda \tau^\Lambda(t)}{\tau^\Lambda(t)} = U i \partial_\Lambda \left[\frac{i}{2D} \tilde{G}_0^{K,\Lambda}(t, t') - \int_{1/D}^\infty dt' \frac{1}{\pi D(t' - t)} \tilde{G}_0^{\text{adv},\Lambda}(t', t) \right], \quad (7.3.1)$$

where \tilde{G} are Green's functions obtained in the effective single dot structure and the index 0 indicates that the bare (time independent) value of τ is used in the calculation of the corresponding Green's

function. Solving this flow equation (see [Ken14] for the technical details) yields the expression

$$\frac{\tau_{L/R}^{\text{ren}}(t)}{\tau_{L/R}^{\text{init}}} = \left(\frac{\Gamma_{1d}}{D}\right)^{-\frac{U}{\pi D}} e^{-\frac{iU}{2D} \exp(-2\Gamma_{1d}t)} e^{-\frac{U}{\pi D} E_1(\Gamma_{1d}t)} \quad (7.3.2)$$

for an initially unoccupied dot, with the exponential integral $E_1(z) = \int_z^\infty \frac{e^{-t}}{t} dt$, $|\text{Arg}(z)| < \pi$. Using Eq. (4.6.1), the according dot occupancy can be calculated

$$n_2(t) \approx \frac{e^{g\gamma}}{2(g+1)} (T_K t)^{g+1}. \quad (7.3.3)$$

The interaction dependent exponent is given by $g = 2U/(\pi D) + \mathcal{O}(U^2)$, which can be extracted from the FRG to its leading order.

To consider the general times $t T_K$ it is necessary to complement the FRG results by RTRG results³. The comparison allows to derive analytic expressions, where it benefits from the different nature of the perturbative approaches. The resulting analytic expression for the transient dot occupancy [Ken13, Kas13]

$$n_2(t) = \frac{1}{2} + \frac{1}{2} (n_{\text{inc}}(t) + n_{\text{coh}}(t)) \quad (7.3.4)$$

consists of two parts, where n_{inc} constitutes the incoherent relaxation, while n_{coh} denotes the coherent relaxation. The two contributions are given by

$$n_{\text{inc}}(t) \approx \frac{1}{\pi} \text{Im} \left\{ e^{-\gamma t} E_1 \left(\left[\frac{1}{2} \Gamma_2^* - \gamma \right] t \right) \right\}, \gamma = e^{-i\pi g} t^g, \quad (7.3.5)$$

$$n_{\text{coh}}(t) \approx 2 \frac{1-g}{1+g} \cos(\omega t) e^{-\Gamma_1^* t} \Theta(g), \quad (7.3.6)$$

with the exponential integral $E_1(z)$, the decay rates Γ_n^* and the frequency ω of the oscillatory part

$$\Gamma_2^* \approx \left[\frac{\pi g}{2 \sin(\pi g)} \right]^{1/(1+g)}, \quad \omega + i\Gamma_1^* \approx e^{(i\pi + \ln 2)g/(1+g)}, \quad (7.3.7)$$

where the interaction dependent exponent $g = 2U/(\pi D) + \mathcal{O}(U^2)$ can be extracted from the FRG to its leading order. A detailed examination of these analytic expressions for the different U regimes reveal that the understanding of the different regimes of time evolution must be refined such that an $0 < U_c < 1$ can be specified, classifying three different regimes: asymptotically coherent time evolution for $1 \geq U > U_c$, partially coherent time evolution for $U_c > U > 0$ and incoherent time evolution for $U \leq 0$ [Ken14].

This is especially interesting as the IRLM can be mapped to the Ohmic spin-boson model (SBM) for small interactions, which relates the interaction U to the dimensionless coupling constant α (which couples the spin system to the phonon bath) and simultaneously the dot occupancy of the IRLM to the spin expectation value (SBM). As a consequence, it relates different magnitudes of spin-bath coupling to different regimes of time evolution for the spin expectation value [Ken13, Kas13].

7.4 From transient behavior to the periodic steady state

With the t-FRG arbitrary time dependent dot setups can be treated, including time periodically driven ones. Calculating the long time behavior of these systems with the t-FRG is possible, but each time step needs to be computed explicitly. The required computing time scales with the number of time steps to the power of 2, which becomes rather costly in the adiabatic limit, where the period

³The real time RG is a renormalization group method working in the Liouville space and perturbative in the interaction U and the tunneling rates Γ_{1d} . The method presented in chapter 6 lies the basic ground for the more involved RTRG. A didactical introduction to the method can be found in [Sch09].

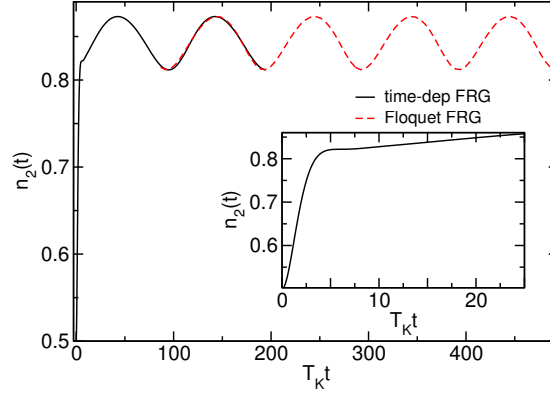


Figure 7.3: Comparison of the explicitly time dependent FRG procedure and the Floquet FRG: While only the first can describe the transient behavior as depicted in the inset, in the long time behavior both results coincide, displaying a dot occupancy that follows the oscillating onsite energy with the same period T . The onsite energy is driven as $\epsilon(t) = -T_K + \Delta\epsilon \cos(\Omega t)$ with $\Delta\epsilon/T_K = 0.2$, $\Omega/(2\pi T_K) = 100$ for $U/D = 0.2$ and $T_K/D = 7.93 \cdot 10^{-5}$.

$T \gg T_K$. The FRG set up in Floquet space takes advantage of the periodicity and is thus the more efficient choice of a basis. As a consequence, we have now two complementary methods at hand to consider the whole time regime: While the transient behavior is calculated by the t-FRG, the Floquet FRG is employed to calculate the long time behavior. This is exploited here to present the dot occupancy in the full time regime including the transient behavior and to compare the t-FRG results to the Floquet FRG results in the long time limit, depicted in Figure 7.3. The inset of the figure displays the increase of the occupancy from an initially half filled quantum dot due to the decrease of the onsite energy ($\epsilon_0 = -T_K$) compared to the initial state. This happens on a rather short time scale of $t_{\text{trans}} T_K \approx 5$. Subsequently the occupancy follows the periodically varying onsite energy and oscillates with the same period around a finite mean value. Once all transient behavior has died out, the explicit time dependent FRG can be compared to the FRG set up in Floquet space. The latter has been shifted for an appropriate comparison since the initial time $t_0 \rightarrow -\infty$ (rendering it independent of the initial setup (compare Eq. (4.1.36))). An excellent agreement of the results obtained with the two different methods is observed.

7.5 Time periodically driven IRLM in the limit of small driving amplitude

After understanding the power law behavior in the time independent or quenched setups, we like to investigate now periodically driven dot setups and the role of the newly introduced energy scale (inverse time scale) Ω in the renormalization flow, which might lead to a novel power law. Whereas we can consider arbitrary driving frequency and amplitude with the employed method, we now focus on the small driving amplitude since we like to complement our numerical results with analytic expressions. We still consider arbitrary driving frequency and the line shape of the applied signals can be of any form, as e.g. rectangular or sinusoidal form. We study four different protocols in this limit specified in the following.

7.5.1 Setup and Protocols

We aim at analytic expressions for the renormalization of the hoppings $\tau_{L/R}(t)$ and the onsite energy $\epsilon(t)$ in the time periodic interacting resonant level model in the limit of small driving amplitudes $\Delta\tau, \Delta\epsilon$ to gain an understanding of the underlying renormalization flow of our FRG approach and the role of the driving frequency Ω in it. We focus on left right symmetric mean hoppings

$\tau_{L,k=0} = \tau_{R,k=0} = \tau_0$ and the particle hole symmetric point $\epsilon_{k=0} = 0$. The left-right symmetry of the mean hoppings as well as the interaction simplifies the analytic expressions, but analogous consideration can be made for more general expression of asymmetric setups. We will consider four different protocols in the following:

- In protocol 1 only the left hopping $\tau_L(t)$ is chosen to be time periodic, while the right hopping $\tau_R(t)$ and the onsite energy $\epsilon(t)$ are assumed to be time independent, i.e. $\tau_R(t) = \tau_0$ and $\epsilon(t) = 0$.
- In protocol 2 the left and the right hopping $\tau_{L(R)}(t)$ are chosen to be time periodic, while the onsite energy $\epsilon(t)$ is assumed to be time independent and $\epsilon(t) = 0$.
- In protocol 3 the left and the right hopping are assumed to be time independent, i.e. $\tau_R(t) = \tau_L(t) = \tau_0$, while the onsite energy $\epsilon(t)$ is chosen to be time periodic.
- In protocol 4 the left hopping $\tau_L(t)$ and the onsite energy $\epsilon(t)$ are assumed to be time periodic, while the right hopping is assumed to be time independent with $\tau_R(t) = \tau_0$.

The flow equations of the hopping and the onsite energy are

$$\partial_\Lambda \tau_{L(R),k}^\Lambda = -\frac{U}{4\pi i} \partial_\Lambda^* \int d\omega G_{12(23);0k}^{K,\Lambda}(\omega), \quad (7.5.1)$$

$$\partial_\Lambda \epsilon_k^\Lambda = -\frac{Ui}{4\pi} \partial_\Lambda^* \int d\omega \left(G_{11;0k}^{K,\Lambda}(\omega) + G_{33;0k}^{K,\Lambda}(\omega) \right) \quad (7.5.2)$$

for time independent interaction U with the initial values

$$\tau_{L(R),k}^{\Lambda \rightarrow \infty} = \tau_{L(R),k}^{\text{init}}, \quad \epsilon_k^{\Lambda \rightarrow \infty} = \epsilon_k^{\text{init}}. \quad (7.5.3)$$

For the simplicity, we will suppress the superscript 'init' in the following and assume if not indicated otherwise the parameter to be the initial one.

7.5.2 Keldysh Green's function in the limit of small driving amplitudes

For the analytic description of $G^{K,\Lambda}(\omega)$ on the right hand side of the flow equation in the limit of small amplitudes, a dimensionless parameter $p = \frac{\tau_{k \neq 0}}{\tau_0} = \frac{\epsilon_{k \neq 0}}{T_K}$ is defined, which is kept small $p \ll 1$ for all calculations. The Keldysh Green's function is thus calculated perturbatively in p , where we keep only the leading order of p .

The inverse of the retarded reservoir dressed dot Green's function in Floquet space is defined as

$$(\underline{\underline{G}}^{\text{ret},\Lambda})^{-1} = \begin{pmatrix} \hat{H}_{-1-1} & \hat{H}_{-10} & 0 \\ \hat{H}_{0-1} & \hat{H}_{00} & \hat{H}_{01} \\ 0 & \hat{H}_{10} & \hat{H}_{11} \end{pmatrix}, \quad (7.5.4)$$

where only the Floquet indices k, k' are shown, while each $\hat{H}_{k,k'}$ is itself a matrix in real space. The infinite Fourier space is already truncated after the first higher harmonic i.e. only the subspace spanned by $k = 0, \pm 1$ is included. This is a consistent approximation to $\mathcal{O}(p)$ if we focus on the renormalization of the $k = 0, \pm 1$ coefficients.

The diagonal elements in the Fourier space $\hat{H}_{k,k}$ are the $k = 0$ components of the 'reservoir dressed' Floquet Hamiltonian defined in Eq. (4.3.3)

$$\hat{H}_{k,k} = \begin{pmatrix} \omega + k\Omega + i(D + \Lambda) & \tau_{L,0} & 0 \\ \tau_{L,0}^* & \omega + k\Omega - \epsilon_0 + i\Lambda & \tau_{R,0} \\ 0 & \tau_{R,0}^* & \omega + k\Omega + i(D + \Lambda) \end{pmatrix}, \quad (7.5.5)$$

the respective off-diagonal elements $\hat{H}_{k,k'}$ for $k \neq k'$ are

$$\hat{H}_{k,k'} = \begin{pmatrix} 0 & \tau_{L,k'-k} & 0 \\ \tau_{L,k'-k} & -\epsilon_{k'-k} & \tau_{R,k'-k} \\ 0 & \tau_{R,k'-k} & 0 \end{pmatrix}, \quad (7.5.6)$$

with the corresponding $k' - k$ Fourier coefficients as defined in Eq. (4.3.7). As we are interested in the left right symmetric case around the particle hole symmetric point, we set $\tau_{L,k=0} = \tau_{R,k=0} = \tau_0$ and $\epsilon_{k=0} = 0$ in the following.

Neglecting all terms $\mathcal{O}(p^2)$ the retarded Green's function is given by

$$\underline{\underline{G}}^{\text{ret},\Lambda} = \begin{pmatrix} \hat{H}_{-1-1}^{-1} & -\hat{H}_{-1-1}^{-1} \hat{H}_{01} \hat{H}_{00}^{-1} & 0 \\ -\hat{H}_{00}^{-1} \hat{H}_{10} \hat{H}_{-1-1}^{-1} & \hat{H}_{00}^{-1} & -\hat{H}_{00}^{-1} \hat{H}_{01} \hat{H}_{11}^{-1} \\ 0 & -\hat{H}_{11}^{-1} \hat{H}_{10} \hat{H}_{00}^{-1} & \hat{H}_{11}^{-1} \end{pmatrix}, \quad (7.5.7)$$

with only the Floquet indices shown and summation over the quantum numbers of the real space assumed and where we have already used that $\hat{H}_{10} = \hat{H}_{0-1}$. It shows a notably transparent structure: The diagonal elements only feature the inverse of the respective Hamiltonian entry and are not affected by any other entry. The off-diagonal elements with an effective (or physical) Fourier coefficient $k_1 = k - k' \neq 0$, depend on the k_1 th coefficient of the Hamiltonian as well as k and k' diagonal elements of the inverse Hamiltonian.

The respective entries of the inverse of the Hamiltonian (diagonal in Floquet space) in real space are given by

$$\begin{aligned} \hat{H}_{1,1;k,k}^{-1} &= \frac{1}{\mathbb{D}} \{ [\omega + k\Omega + i(\Lambda + D)] [\omega + k\Omega + i\Lambda] - |\tau_0|^2 \} \\ \hat{H}_{1,2;k,k}^{-1} &= \frac{1}{\mathbb{D}} \{ \tau_0 [\omega + k\Omega + i(D + \Lambda)] \} \\ \hat{H}_{1,3;k,k}^{-1} &= \frac{1}{\mathbb{D}} \{ \tau_0 \tau_0^* \} \\ \hat{H}_{2,1;k,k}^{-1} &= \frac{1}{\mathbb{D}} \{ \tau_0^* [\omega + k\Omega + i(\Lambda + D)] \} \\ \hat{H}_{2,2;k,k}^{-1} &= \frac{1}{\mathbb{D}} \{ [\omega + k\Omega + i(\Lambda + D)]^2 \} \\ \hat{H}_{2,3;k,k}^{-1} &= \frac{1}{\mathbb{D}} \{ \tau_0 [\omega + k\Omega + i(D + \Lambda)] \} \\ \hat{H}_{3,1;k,k}^{-1} &= \frac{1}{\mathbb{D}} \{ \tau_0^* \tau_0^* \} \\ \hat{H}_{3,2;k,k}^{-1} &= \frac{1}{\mathbb{D}} \{ \tau_0^* [\omega + k\Omega + i(D + \Lambda)] \} \\ \hat{H}_{3,3;k,k}^{-1} &= \frac{1}{\mathbb{D}} \{ [\omega + k\Omega + i(D + \Lambda)] [\omega + k\Omega + i\Lambda] - |\tau_0|^2 \} \end{aligned} \quad (7.5.8)$$

with

$$\mathbb{D} = [\omega + k\Omega + i(D + \Lambda)]^2 [\omega + k\Omega + i\Lambda] - 2|\tau_0|^2 [\omega + k\Omega + i(D + \Lambda)]. \quad (7.5.9)$$

The Keldysh reservoir self-energy is given in the $k = 0, \pm 1$ Fourier space as

$$\underline{\underline{\Sigma}}^K = \begin{pmatrix} \hat{\Sigma}_{-1-1}^K & 0 & 0 \\ 0 & \hat{\Sigma}_{00}^K & 0 \\ 0 & 0 & \hat{\Sigma}_{11}^K \end{pmatrix}, \quad (7.5.10)$$

where each $\hat{\Sigma}_{kk'}^K$ is again a matrix in \mathcal{R}

$$\hat{\Sigma}_{kk}^K = 4iD \begin{pmatrix} \theta[-(\omega + k\Omega)] - \frac{1}{2} & 0 & 0 \\ 0 & 0 & 0 \\ 0 & 0 & \theta[-(\omega + k\Omega)] - \frac{1}{2} \end{pmatrix}. \quad (7.5.11)$$

Utilizing Eq. (4.4.18) the Keldysh Green's function becomes to linear order in p

$$\underline{\underline{G}}^{K,\Lambda} = \begin{pmatrix} \hat{G}_{-1-1}^K & \hat{G}_{-10}^K & 0 \\ \hat{G}_{0-1}^K & \hat{G}_{00}^K & \hat{G}_{01}^K \\ 0 & \hat{G}_{10}^K & \hat{G}_{11}^K \end{pmatrix} \quad (7.5.12)$$

with

$$\begin{aligned}
\hat{G}_{-1-1}^K &= \hat{H}_{-1-1}^{-1} \hat{\Sigma}_{-1-1}^K (\hat{H}_{-1-1}^{-1})^* \\
\hat{G}_{-10}^K &= -\hat{H}_{-1-1}^{-1} \hat{\Sigma}_{-1-1}^K (\hat{H}_{00}^{-1})^* \hat{H}_{01} (\hat{H}_{-1-1}^{-1})^* - \hat{H}_{-1-1}^{-1} \hat{H}_{01} \hat{H}_{00}^{-1} \hat{\Sigma}_{00}^K (\hat{H}_{00}^{-1})^* \\
\hat{G}_{0-1}^K &= -\hat{H}_{00}^{-1} \hat{\Sigma}_{00}^K (\hat{H}_{-1-1}^{-1})^* \hat{H}_{10} (\hat{H}_{00}^{-1})^* - \hat{H}_{00}^{-1} \hat{H}_{10} \hat{H}_{-1-1}^{-1} \hat{\Sigma}_{-1-1}^K (\hat{H}_{-1-1}^{-1})^* \\
\hat{G}_{00}^K &= \hat{H}_{00}^{-1} \hat{\Sigma}_{00}^K (\hat{H}_{00}^{-1})^* \\
\hat{G}_{01}^K &= -\hat{H}_{00}^{-1} \hat{\Sigma}_{00}^K (\hat{H}_{11}^{-1})^* \hat{H}_{01} (\hat{H}_{00}^{-1})^* - \hat{H}_{00}^{-1} \hat{H}_{01} \hat{H}_{11}^{-1} \hat{\Sigma}_{11}^K (\hat{H}_{11}^{-1})^* \\
\hat{G}_{10}^K &= -\hat{H}_{11}^{-1} \hat{\Sigma}_{11}^K (\hat{H}_{00}^{-1})^* \hat{H}_{10} (\hat{H}_{11}^{-1})^* - \hat{H}_{11}^{-1} \hat{H}_{10} \hat{H}_{00}^{-1} \hat{\Sigma}_{00}^K (\hat{H}_{00}^{-1})^* \\
\hat{G}_{11}^K &= \hat{H}_{11}^{-1} \hat{\Sigma}_{11}^K (\hat{H}_{11}^{-1})^*
\end{aligned}$$

and $\hat{H}_{k,k}^{-1}$ defined as in Eq. (7.5.8). Again summation over suppressed real space quantum numbers is assumed.

A transparent structure of each of the elements becomes apparent, which allows to generalize the expression to

$$\hat{G}_{kk}^K = \hat{H}_{kk}^{-1} \hat{\Sigma}_{kk}^K (\hat{H}_{kk}^{-1})^*, \quad (7.5.13)$$

$$\hat{G}_{kk'}^K = -\hat{H}_{kk}^{-1} \hat{\Sigma}_{kk}^K \hat{H}_{k'k'}^{-1,*} \hat{H}_{kk'} \hat{H}_{kk}^{-1,*} - \hat{H}_{kk}^{-1} \hat{H}_{kk'} \hat{H}_{k'k'}^{-1} \hat{\Sigma}_{k'k'}^K \hat{H}_{k'k'}^{-1,*} \quad (7.5.14)$$

for all $k \neq k'$. Analyzing this structure leads to a key point in the analytic description: The diagonal elements of G^K only depend on diagonal elements with the same kk indices, whereas the off-diagonal elements with the effective Fourier coefficient $k_1 = k - k'$ depend on diagonal elements with coefficients kk or $k'k'$ and exclusively on off-diagonal elements with the same effective Fourier coefficient k_1 . Since any other contributions of a different higher harmonic would be of higher order in p , the different k channels decouple and hence can be considered independently. As a result, these expressions can be generalized from $k = 0, \pm 1$ to the entire Fourier space. These approximate $\hat{G}_{kk'}^K$ are inserted on the right hand side of the full flow equations to compute the renormalization analytically to the leading order of $\mathcal{O}(p)$ for each Fourier channel.

Before we proceed to consider the renormalization of each channel individually, we note the following: The Fourier series in general relates the driving frequency Ω directly to its factor m , such that the relevant energy scale (or inverse time scale) is $m\Omega$. This is trivial to understand by the fact that each T periodic function is also nT periodic, rendering it possible to decompose the series by Ω/n as well. The resulting prefactors for a certain signal form would be $m \cdot n$ in the according Fourier series, such that always only the combination $m\Omega$ appears. From the expression in Eq. (7.5.14) we can derive a stronger restriction on the Ω dependency in the limit of small driving amplitudes: The $\hat{G}_{kk'}^K$ with the effective $k_1 = k - k'$ Fourier coefficient depends on $k_1\Omega$ only. We thus can conclude that the renormalization of k th harmonic only depends on $k\Omega$ and is independent of the other higher harmonics.

7.5.3 Mean value: $k = 0$ component

To calculate the $k = 0$ component, i.e. the mean value of the parameters, we can consider any of the diagonal entries in Fourier space of the Keldysh Green's function G^K , as they are all equivalent. The zeroth channel is completely independent of the driving frequency and unaffected by higher harmonics and thus independent of the exact driving setup, i.e. it is the same for all four protocols.

We consider the mean values of the hopping matrix element. Sorting all contributions to the Keldysh Green's function by $\mathcal{O}(\frac{1}{D^n})$, we only include the leading order for a consistent expansion in $\frac{U}{D}$, which results in

$$G_{12(23);00}^K = \hat{H}_{1(2)l;00}^{-1} \hat{\Sigma}_{ll;00}^K \hat{H}_{l2(3);00}^{-1,*}. \quad (7.5.15)$$

Inserting it in the flow equation leads to

$$\partial_\Lambda \tau_0 = \partial_\Lambda^* \int d\omega \frac{Ui}{4\pi} \frac{\tau_0^\Lambda(\omega + i\Lambda)}{\omega + i(\Lambda + D)(\omega + i\Lambda) - 2|\tau_0|^2} \frac{4iD\theta(-\omega) - 2iD}{(\omega - i(\Lambda + D))(\omega - i\Lambda) - 2|\tau_0|^2}. \quad (7.5.16)$$

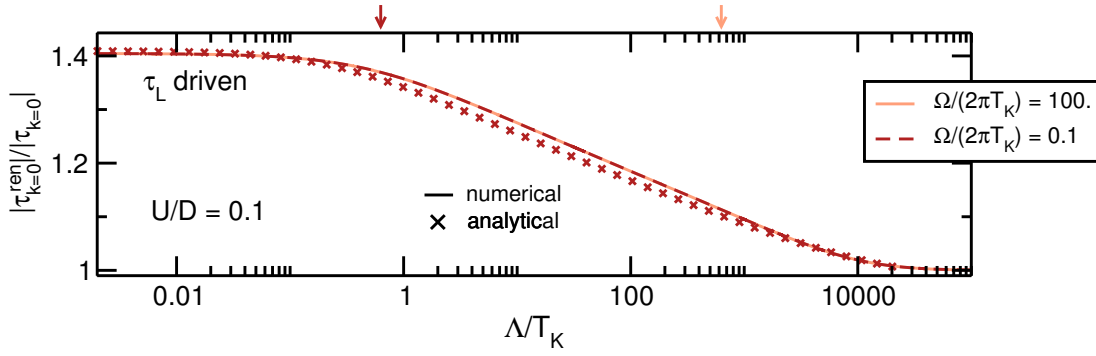


Figure 7.4: Renormalization flow of $\tau_{L,k=0}$ for any of the protocols (here obtained in protocol 1) for $U/D = 0.1$ and $T_K/D = 4.62 \cdot 10^{-5}$ for two different values of driving frequency. The flow is independent of the driving frequency or the exact form of the time dependence, but resembles the flow of the equilibrium, stationary setup. The analytic description (crosses) is in good agreement with the full numerical solution (solid line), where the difference arises from higher order corrections in U and p .

Next, the star derivative needs to be carried out. In order to only take the derivative of the explicit flow parameter, τ_0 in the denominator is set to its initial value and τ_0^Λ is moved in front of the derivative, which allows to substitute ∂_Λ^* by ∂_Λ

$$\partial_\Lambda \tau_0^\Lambda = -\frac{U \tau_0^\Lambda}{\pi D^2} \partial_\Lambda \int d\omega \frac{(\omega + i\Lambda)/D}{(\omega + i(\Lambda + D))/D (\omega + i\Lambda)/D - \frac{2|\tau_0|^2}{D^2}} \frac{\theta(-\omega) - \frac{1}{2}}{(\omega - i(\Lambda + D))/D (\omega - i\Lambda)/D - \frac{2|\tau_0|^2}{D^2}}. \quad (7.5.17)$$

Additionally all parameters are divided by D . Including all contributions to the order of $\frac{1}{D^2}$ in the denominator the expression can be evaluated to

$$\partial_\Lambda \tau_0^\Lambda = -\frac{U}{\pi D} \frac{\tau_0^\Lambda/D}{(\Lambda/D)^2 + \Lambda/D + 2(\tau_0/D)^2} \quad (7.5.18)$$

reproducing the differential equation for the time independent equilibrium setup [Kar10c]. Solving the differential equation analytically, results in the same power law as discussed in Sect. 7.1 for the stationary, equilibrium IRLM

$$\frac{\tau_0^{\text{ren}}}{\tau_0} \sim \left(\frac{\tau_0}{D}\right)^{-2\alpha_{k=0}}, \quad \alpha_{k=0} = \frac{U}{\pi D} + \mathcal{O}(U^2). \quad (7.5.19)$$

As depicted in Fig. 7.4 the flow is always cut by the low energy scale T_K independent of the applied driving frequency. The analytic result captures nicely the full numerical solution, where the differences results from higher order effects in p and $\frac{U}{D}$, which are beyond the scope of our analytics. In Fig. 7.7 the exponent $\alpha_{k=0}$ of the power law of the hopping is displayed (+ symbols). It has been extracted from the full numerical solution via a logarithmic derivative $d \ln(\tau_{L,0}^{\text{ren}})/d \ln(\tau_0)$, implemented as centered differences, which is a numerical very sensitive measure. The resulting exponent is in good agreement with the analytic prediction in the regime of small interactions. The deviation in the regime of larger interaction results from $(U/D)^2$ contributions.

An analogous consideration shows that the renormalization $\epsilon_{k=0}$ is also independent of Ω and unaffected by the time dependency. The resulting renormalization of order U^2 has been discussed in Section 7.1.

From this discussion, we derive that the driving frequency Ω does not provide an infrared cutoff for the $k = 0$ component of the hopping. This is consistent with the consideration we made at the end of the previous section that the effective scale for the k th component is $k\Omega$. The zeroth component is even completely unaffected by any time periodicity in the limit of small driving amplitudes, reproducing the steady state of the time independent, equilibrium IRLM and the according power law.

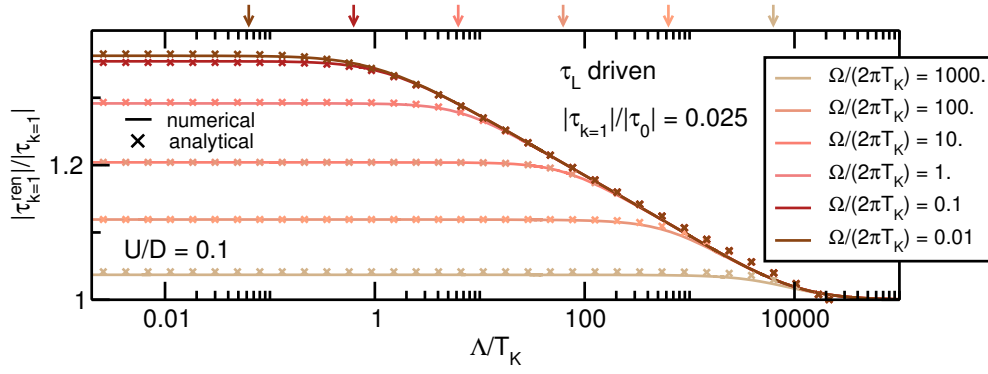


Figure 7.5: Renormalization flow of $\tau_{L,k=1}$ for protocol 1 with $U/D = 0.1$ and $T_K/D = 4.62 \cdot 10^{-5}$ for several values of driving frequency. Full numerical solution (solid lines) is compared to the analytic description (crosses). A clear dependency on the driving frequency Ω is observed: It provides the infrared cutoff as long as $\Omega \gg T_K$.

7.5.4 Protocol 1: Time periodic $\tau_L(t)$

In protocol 1 the left hopping is time periodically varied with an arbitrary signal shape, setting $\tau_{L,k \neq 0} \neq 0$, while $\epsilon_{k \neq 0} = \tau_{R,k \neq 0} = 0$. The analytic calculations in Sec. 7.5.2 showed that the Fourier components decouple from each other to the leading order in p , rendering it reasonable to consider the renormalization of each channel individually. In particular, a general expression for the Fourier components of the Keldysh Green's function (Eq. (7.5.14)) has been derived, revealing that the $k_1 = k - k'$ component has an effective, general dependence on $k_1 \Omega$ only.

The renormalization of $\tau_{L,k \neq 0}$ is described by the flow equation

$$\partial_\Lambda \tau_{L,k}^\Lambda = -\frac{U}{4\pi i} \partial_\Lambda^* \int d\omega G_{12;0k}^{K,\Lambda}(\omega). \quad (7.5.20)$$

Utilizing Eq. (7.5.14) to calculate the respective Keldysh Green's function on the right hand side, we take only contributions of the leading order of $\frac{1}{D}$ into account, which reads as

$$G_{12;0k}^{K,\Lambda}(\omega) = \frac{\tau_{L,k}^\Lambda(\omega + k\Omega - i(\Lambda + D))}{(\omega + k\Omega - i(D + \Lambda))(\omega + k\Omega - i\Lambda) - 2|\tau_0|^2} \frac{(\omega - i\Lambda)}{(\omega - i(D + \Lambda))(\omega - i\Lambda) - 2|\tau_0|^2} \frac{4iD[\theta(-\omega) - 1/2](\omega + i\Lambda)}{(\omega + i(D + \Lambda))(\omega + i\Lambda) - 2|\tau_0|^2}. \quad (7.5.21)$$

Weighting each parameter by dividing through the bandwidth D , only contributions to the order of $1/D^2$ need to be included consistently in the denominator. The star derivative is rewritten as in Eq. (7.5.17), which leads to

$$\partial_\Lambda \tau_{L,k \neq 0}^\Lambda = -\frac{U}{\pi D} \frac{\tau_{L,k}^\Lambda}{D} \partial_\Lambda \int d\omega \frac{(\omega - i\Lambda)/D [\theta(-\omega) - 1/2]}{-\frac{\omega + k\Omega - i\Lambda}{D} \frac{\omega - i\Lambda}{D} + \frac{2|\tau_0|^2}{D^2} i \left(\frac{\omega + k\Omega - i\Lambda}{D} + \frac{\omega - i\Lambda}{D} \right) + \frac{2|\tau_0|^4}{D^4}}. \quad (7.5.22)$$

The integral on the right hand side can be performed using the substitution $z = w - i\Lambda$ to cancel the integral and derivative, yielding

$$\partial_\Lambda \tau_{L,k \neq 0}^\Lambda = -\frac{U}{\pi D} \frac{\tau_{L,k}^\Lambda \Lambda/D^2}{\frac{\Lambda^2}{D^2} + \left(4\frac{|\tau_0|^2}{D^2} + \frac{ik\Omega}{D}\right) \frac{\Lambda}{D} + \frac{2i|\tau_0|^2 k\Omega}{D^3} + \frac{4|\tau_0|^4}{D^4}}. \quad (7.5.23)$$

The resulting differential equation describes the flow of all higher harmonics for a time periodically driven left hopping, showing a general functional dependence on $k\Omega$ for the k th harmonic. In Fig. 7.5 the analytic expression (symbols) is compared to the full numerical solution (solid line) for $\tau_{L,k=1}$. The analytic expression completely captures the full numerical solution and the role of $k\Omega$

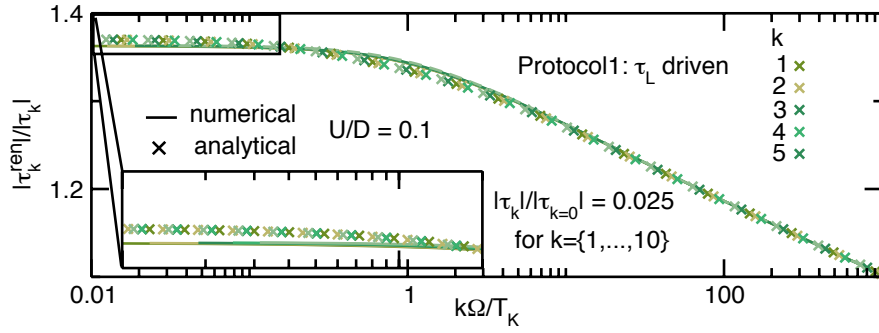


Figure 7.6: Renormalized $\tau_{L,k \neq 0}$ for protocol 1 with $U/D = 0.1$ and $T_K/D = 4.62 \cdot 10^{-5}$. The left hopping is periodically driven with a signal of the form $\tau_L = \tau_0 + \sum_{k=1}^{10} \Delta\tau \sin(k\Omega t)$, such that all higher harmonics have the same initial value. All solid lines (full numerical solution) lie on top of each other showing the same dependence on $k\Omega$. A comparison to the analytic description (crosses) shows excellent agreement especially in the large driving frequency limit. The inset shows that renormalization bends to a Ω independent value in the adiabatic limit.

as an infrared cutoff, such that the renormalization flow bends at the respective value $\Lambda \approx k\Omega$ (for $k\Omega \gg T_K$). The analytic description is improved by including the feedback of τ_0^{ren} , i.e. substituting the mean hopping matrix elements by their renormalized values of Eq. (7.5.19). This has no impact in the regime of $k\Omega > T_K$, but improves the agreement of the analytic description with the numerical solution of the full flow equation in the small frequency limit, where all components (including τ_0) are cut by T_K .

The differential equations for the higher harmonics can be solved analytically, yielding

$$\begin{aligned}
 \frac{\tau_{L,k \neq 0}^{\text{ren}}}{\tau_{L,k \neq 0}} &= e^{\frac{U}{2\pi D k \Omega} (2ik\Omega + \frac{4|\tau_0|^2}{D}) \arctan\left(\frac{k\Omega}{D+2|\tau_0|^2/D}\right)} \left(D + \frac{2|\tau_0|^2}{D}\right)^{\frac{2iU|\tau_0|^2}{\pi D^2 (k\Omega)}} \left[(k\Omega)^2 + \left(D + \frac{2|\tau_0|^2}{D}\right)^2 \right]^{\frac{U(k\Omega - 2i|\tau_0|^2/D)}{2\pi D k \Omega}} \\
 &\times e^{\frac{-U}{2\pi D k \Omega} (2ik\Omega + 4\frac{|\tau_0|^2}{D}) \arctan\left(\frac{k\Omega}{2|\tau_0|^2/D}\right)} \left(\frac{2|\tau_0|^2}{D}\right)^{\frac{-2iU|\tau_0|^2}{\pi D^2 k \Omega}} \left[(k\Omega)^2 + \left(\frac{2|\tau_0|^2}{D}\right)^2 \right]^{\frac{-U(k\Omega - 2i|\tau_0|^2/D)}{2\pi D k \Omega}} \\
 &\stackrel{D \gg T_K}{=} e^{\frac{-U}{2\pi D k \Omega} \frac{4|\tau_0|^2}{D} \arctan\left(\frac{k\Omega}{2|\tau_0|^2/D}\right)} \left[\frac{(k\Omega)^2 + 4(|\tau_0|^2/D)^2}{D^2} \right]^{-\frac{U}{2\pi D}} e^{-iU/(\pi D) \arctan\left(\frac{k\Omega}{2|\tau_0|^2/D}\right)} \\
 &\times \left[\frac{4(|\tau_0|^2/D)^2}{k^2 \Omega^2 + 4(|\tau_0|^2/D)^2} \right]^{\frac{U|\tau_0|^2/D}{\pi D k \Omega}} \quad (7.5.24)
 \end{aligned}$$

where in the last step we took advantage of the wide band limit. Substituting τ_0 by its renormalized value again, enhances the analytic description of the full numerical solution.

Two regimes can be identified, showing different power-law behavior

$$\frac{\tau_{L,k \neq 0}^{\text{ren}}}{\tau_{L,k \neq 0}} \sim \left(\frac{\tau_0}{D}\right)^{-2\alpha_{k=1}}, \quad \alpha_{k=1} = \frac{U}{\pi D} + \mathcal{O}(U^2), \quad |k\Omega| \ll T_K \quad (7.5.25)$$

$$\frac{\tau_{L,k \neq 0}^{\text{ren}}}{\tau_{L,k \neq 0}} \sim \left(\frac{k\Omega}{D}\right)^{-\alpha_\Omega}, \quad \alpha_\Omega = \frac{U}{\pi D} + \mathcal{O}(U^2), \quad |k\Omega| \gg T_K, \quad (7.5.26)$$

the small frequency regime of $k\Omega \ll T_K$ and the large frequency regime with $|k\Omega| \gg T_K$. In the small frequency regime the $\tau_{k \neq 0}$ are cut by the energy scale T_K , resulting in the same power law as for τ_0 . If the driving frequency $|k\Omega|$ is much larger than T_K , it provides the cutoff of the renormalization flow resulting in a power law in the driving frequency. Hence, as discussed in Sec. 7.2, both energy scales $k\Omega$ and T_K affect the infrared cutoff and compete with each other. In the limit of one energy scale much larger than the other, the larger one provides the infrared cutoff. This is immediately reflected in the power-law scaling of $\tau_{L,k}^{\text{ren}}$.

As a consequence the renormalized signal $\tau_L^{\text{ren}}(t)$ with several non-vanishing higher harmonics depends on both infrared scales, such that there is a crossover from Fourier coefficients, whose RG flow is cut by T_K to coefficients whose RG flow is cut by $k\Omega$. For $\Omega \gg T_K$, the low energy scale only provides the infrared cutoff for the zeroth component, whereas all higher harmonics are cut by $k\Omega$. The crossover is thus just between $k = 0$ and $k = \pm 1$. However, for a fixed small to intermediate Ω , there is a crossover of the infrared scale within the various Fourier coefficients. While the RG flows of all k th coefficients with $|k\Omega| \ll T_K$ are cut by T_K , there are higher harmonics in the same signal, where $|k\Omega| \gg T_K$ and therefore the according infrared cutoff is $k\Omega$. In this case it is a smooth crossover such that there are intermediate coefficients, which are cut by an infrared scale that depends on both energy scales T_K and $k\Omega$, which are about the same size.

In Fig. 7.7 the exponents of the power laws $\tau^{\text{ren}}(\tau_0)$ and $\tau^{\text{ren}}(\Omega)$ are displayed, which have been computed by a logarithmic derivative of the numerical solution of the full flow equation. Both exponents $\alpha_{k=1}$ and α_Ω show excellent agreement with the analytic prediction. The higher order corrections with increasing interaction strength are smaller for α_Ω than for $\alpha_{k=1}$.

The renormalized higher harmonics at the end of the flow are depicted as a function of $k\Omega$ in Fig. 7.6, where the analytic expression (crosses) is compared to the full numerical solution (solid line). Here the left hopping is designed as $\tau_L(t) = \tau_0 + \sum_{k=1}^{10} \Delta\tau \sin(k\Omega t)$ such that all non-vanishing Fourier coefficients have the same initial value. A universal dependence on $k\Omega$ is recognized for each k th harmonic, such that all shown solid lines lie on top of each other. We only display the first five Fourier coefficients for simplicity, but all higher harmonics have the same dependency. The inset shows the limit of small frequencies, where all curves level off to an Ω independent value due to the infrared scale T_K .

The dependency of the renormalization of the k th higher harmonic on $k\Omega$ has interesting implications for the renormalized signal $\tau_L^{\text{ren}}(t)$:

$$\frac{\tau_L^{\text{ren}}(t)}{\tau_{L,0}^{\text{ren}}} = \sum_k \frac{\tau_k^{\text{ren}}}{\tau_{L,0}^{\text{ren}}} e^{ik\Omega t} \sim \sum_k \tau_k^{\text{init}} \left(\frac{k\Omega}{T_K} \right)^{-\frac{U}{\pi D}} e^{ik\Omega t} \quad \text{for } |\Omega| \gg T_K \quad (7.5.27)$$

First, due to the k dependency, each of the component is renormalized differently. With increasing Floquet index k , the infrared cutoff grows, resulting in a weaker renormalization. The different strength of renormalization changes the ratio between the Fourier coefficients and thus modifies the line shape.

Second, the renormalization depends on the driving frequency Ω . While a positive sign of the interaction decreases the amplitude with increasing Ω , the opposite is true for a negative interaction. Thus, depending on the sign of the interaction, a rectification or amplification of the effective signal amplitude is observed.

To illuminate this further, we define three of the typical signal shapes by their dependencies on k with $s(t) = \sum_{k \text{ odd}} s_k e^{ik\Omega t}$

$$\begin{aligned} \text{sum of sinusoidal fcts. : } s_k^{\text{sin}} &= \frac{\text{sgn}(k)}{2i} \Delta s \\ \text{square fct. : } s_k^{\text{squ}} &= \frac{2\Delta s}{\pi i} \frac{\text{sgn}(k)}{k} \\ \text{triangular fct. : } s_k^{\text{tri}} &= (-1)^{\frac{k-1}{2}} \frac{4\Delta s}{\pi^2 i} \frac{\text{sgn}(k)}{k^2} . \end{aligned} \quad (7.5.28)$$

Assuming for example an initial signal of rectangular shape $\tau_k^{\text{init}} = s_k^{\text{squ}}$, the renormalized signal is

$$\tau_k^{\text{ren}} \sim s_k^{\text{squ}} (k\Omega)^{-\frac{U}{\pi D}} = g(\text{sgn}(k)) \Delta s \Omega^{-\frac{U}{\pi D}} k^{-1-\frac{U}{\pi D}} \sim \begin{cases} \frac{\Delta s / \Omega}{k^2} & \text{for } U/D = \pi \\ \Delta s \Omega & \text{for } U/D = -\pi \end{cases} . \quad (7.5.29)$$

For an interaction $U/D = \pm\pi$, there is a precise renormalization of one signal form into the other: For $U/D = \pi$ the renormalized signal is of triangular form with a rectified amplitude by the factor

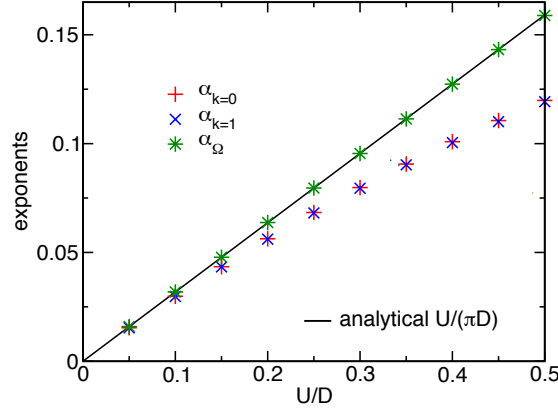


Figure 7.7: The exponents $\alpha_{k=0}$, $\alpha_{k=1}$, α_{Ω} are depicted. They are obtained via a logarithmic derivative of the full numerical solution. The deviation of the analytic description for the larger interaction U are higher order corrections.

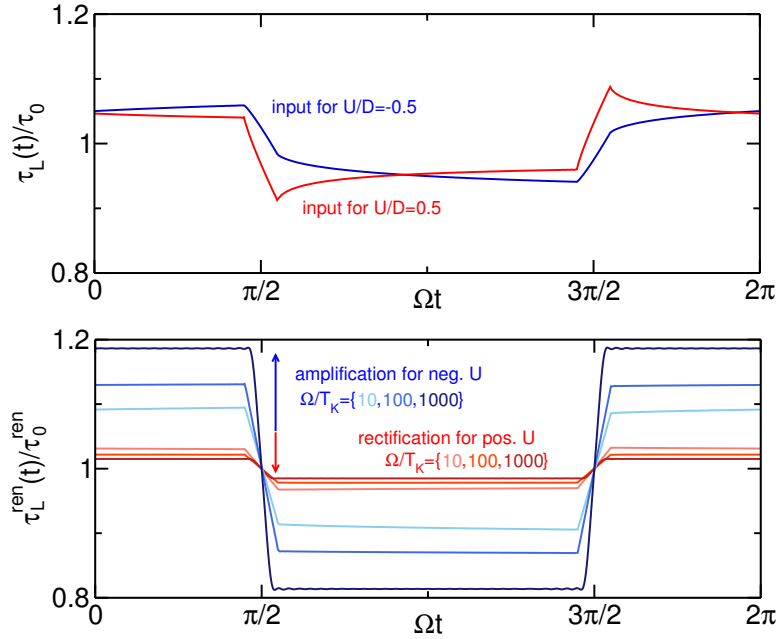


Figure 7.8: Two different input signals for positive and negative interaction are defined to illustrate the interesting implications of the $k\Omega$ dependent renormalization. $U/D = \pm 0.5$ and $T_K/D = 2.87 \cdot 10^{-4}$ as well as $T_K/D = 4.41 \cdot 10^{-7}$, respectively. The initial odd Fourier coefficients are defined as $\frac{\tau_k}{\tau_0} = \frac{0.1}{\pi} k \frac{U}{\pi D}^{-1}$ such that the renormalized signal is of rectangular shape. For positive interaction U the driving amplitude becomes rectified by the interaction, while for negative interaction the renormalized driving amplitude is amplified compared to the initial signal.

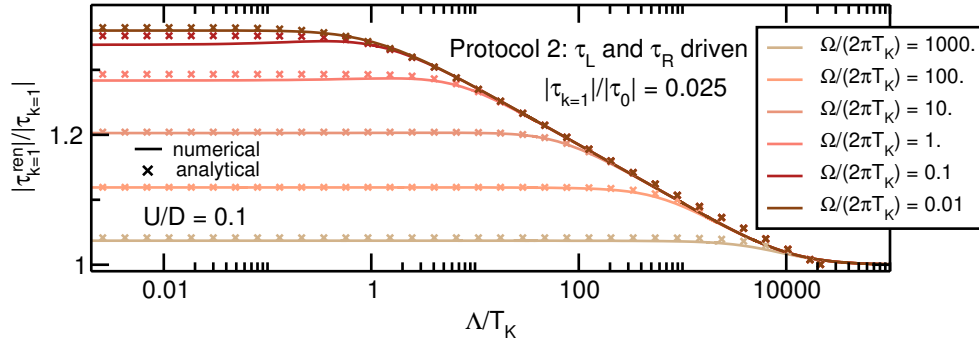


Figure 7.9: Full numerical solution (crosses) and analytic description (solid lines) of the renormalization flow of $\tau_{L,k=1}$ for protocol 2 with $U/D = 0.1$ and $T_K/D = 4.62 \cdot 10^{-5}$. The analytic description is the same as derived for protocol 1, because the feedback of $\tau_{R,k=1}$ into $\tau_{L,k=1}$ is of higher order and vice versa. These higher order effects are only observed in the adiabatic limit resulting in a deviation between analytical and numerical solution.

Ω^{-1} ($\Omega \gg T_K$). For $U/D = -\pi$, the k -dependency vanishes and the renormalized signal is a sum of sinusoidal functions with different frequencies $k\Omega$. The amplitude is enhanced by a factor of Ω ($\Omega \gg T_K$).

However, this interaction strength is beyond the accessible regime for our FRG approach, but the respective trends can be deduced for small to intermediate interactions: For $U/D > 0$ the amplitude is rectified by a factor of $\Omega^{-|U/(\pi D)|}$ and the effective k dependency is $k^{-1-|U/(\pi D)|}$, i.e. the effective signal tends towards a triangular form with increasing interaction. For $U/D < 0$ the amplitude is enhanced by a factor of $\Omega^{+|U/(\pi D)|}$, while the k dependency becomes $k^{-1+|U/(\pi D)|}$, tending to a sum of sinusoidal signals.

The respective opposite renormalization towards a square function also holds true, such that the trend of the renormalization can be summed up as:

$$\text{triangular function} \xrightarrow[U/D < 0]{U/D > 0} \text{square function} \xrightarrow[U/D < 0]{U/D > 0} \text{sum of sinusoidal functions}.$$

Knowledge of the described renormalization can be utilized to cancel its effect, i.e. the initial signal is designed such that the renormalized one is of the required form. In order to illustrate this we design the initial signal with odd Fourier coefficients as

$$\frac{\tau_k}{\tau_0} = \frac{0.1}{\pi} k^{\frac{U}{\pi D} - 1} \quad k \text{ odd} \quad (7.5.30)$$

for a renormalized signal of rectangular shape. The initial and renormalized signals are displayed in Fig. 7.8. As anticipated, the line shape of the signal is changed to a rectangular form and the driving amplitude is amplified for negative interaction and rectified for a positive interaction. In Section 8.5 the linear conductance is discussed for the bare and the renormalized signal shape.

Finally, we mention that the discussed power law in the regime of larger driving frequency is also reflected in an observable, the mean current J_0 of a single parameter pump. We postpone the detailed discussion to Section 8.4 in the next chapter, where transport is discussed in more detailed for several different setups.

7.5.5 Protocol 2: Time periodic $\tau_L(t)$ and $\tau_R(t)$

An analogous treatment as described in the previous section but for the setup of left and right hoppings driven periodically in time shows that there is no contribution of the higher harmonics of the right hopping to renormalization of the higher harmonics of the left hopping and vice versa to the order $\mathcal{O}(\frac{1}{D}, p, U)$. As a consequence, the flow of the left and right hoppings $\tau_{L(R),k}$ are described by

the same analytic expression as derived for $\tau_{L,k}$ in protocol 1. We compare this analytic description to the full numerical solution for $\tau_{L,k=1}$ of the setup, which is depicted in Fig. 7.9. The agreement in the large driving frequency regime is excellent and only in the adiabatic regime there is a deviation due to higher order effects. The Eqs. (7.5.23), (7.5.25) and (7.5.26) hold equally in this setup.

7.5.6 Protocol 3: Time periodic $\epsilon(t)$

In protocol 3 only the onsite energy ϵ is periodically varied in time. Since the renormalization of the higher harmonics of the hopping in this protocol turns out to be more involved, due to a complicated interplay of several energy scales, we here focus on a fairly simple signal of sinusoidal form and choose

$$\epsilon(t) = \Delta\epsilon \cos(\Omega t). \quad (7.5.31)$$

Renormalization of $\epsilon_{k=1}$

The flow equation of the first higher harmonic of the onsite energy is

$$\partial_\Lambda \epsilon_{k=1}^\Lambda = -\frac{U_i}{4\pi} \partial_\Lambda^* \int d\omega \left(G_{11;01}^{K,\Lambda}(\omega) + G_{33;01}^{K,\Lambda}(\omega) \right). \quad (7.5.32)$$

such that we need to evaluate

$$\hat{G}_{ij;01}^K = -\hat{H}_{il;00}^{-1} \hat{\Sigma}_{ll;00}^K (\hat{H}_{lm;11}^{-1})^* \hat{H}_{mn;01} (\hat{H}_{nj;00}^{-1})^* - \hat{H}_{io;00}^{-1} \hat{H}_{op;01} \hat{H}_{pq;11}^{-1} \hat{\Sigma}_{qq;11}^K (\hat{H}_{qj;11}^{-1})^* \quad (7.5.33)$$

at $i = j = 1$ and $i = j = 3$. Collecting all contributions of leading order $\frac{1}{D}$ once again, results in the following differential equation for $\epsilon_{k=1}^\Lambda$

$$\begin{aligned} \partial_\Lambda \epsilon_{k=1}^\Lambda = & \partial_\Lambda^* \int d\omega \frac{2U}{\pi D} \frac{\epsilon_{k=1}^\Lambda}{D} \\ & \left[\frac{(\omega + i\Lambda)/D}{i(\omega + i\Lambda)/D - 2|\tau_0|^2/D^2} \frac{|\tau_0|^2/D^2}{-i(\omega + \Omega - i\Lambda)/D - 2|\tau_0|^2/D^2} \frac{[\theta(-\omega) - 1/2]}{-i(\omega - i\Lambda)/D - 2|\tau_0|^2/D^2} \right. \\ & \left. + \frac{|\tau_0|^2/D^2}{i(\omega + i\Lambda)/D - 2|\tau_0|^2/D^2} \frac{[\theta(-\omega - \Omega) - 1/2]}{i(\omega + \Omega + i\Lambda)/D - 2|\tau_0|^2/D^2} \frac{(\omega + \Omega - i\Lambda)/D}{-i(\omega + \Omega - i\Lambda)/D - 2|\tau_0|^2/D^2} \right]. \end{aligned} \quad (7.5.34)$$

The differential equations 7.5.17 and 7.5.22 have been approximated to the order of $\frac{1}{D^2}$ in the denominator, which in turn allowed to simplify the right hand side by an appropriate substitution. This approximation is not possible here, but also not necessary. If we set all parameters on the right hand side of the flow equation to their respective initial values, the resulting expression can be integrated straight forwardly for $\Lambda = 0$ as it is not plagued by logarithmic divergencies. The resulting expression thus is a first order perturbation theory calculation

$$\epsilon_{k=1}^{\text{ren}}(\Omega) \stackrel{D \gg \tau_k/\Omega}{=} \frac{U}{\pi D} \frac{T_K}{2} \frac{\epsilon_{k=1}^{\text{init}}}{D} \frac{i(T_K/2 + i\Omega)/D}{\Omega/D(T_K + i\Omega)/D} \left[\ln \left(\frac{T_K^2}{T_K^2 + 4\Omega^2} \right) - 2i \arctan \left(\frac{2\Omega}{T_K} \right) \right], \quad (7.5.35)$$

where the feedback of the $k = 0$ channel has been included by substituting $\frac{4\tau_0^2}{D}$ by T_K . This analytic expression indeed captures the numerical solution of the full flow equation very well, as illustrated in the left panel of Fig. (7.10). While the imaginary part is mainly renormalized in the regime $\Omega \approx T_K$, the real part is renormalized for $\Omega \gtrsim T_K$; in both cases the renormalization is minor. This also holds for the higher harmonics of more general setups.

Replica picture

For the discussion of the renormalization of the first higher harmonic of $\tau_{L(R)}$ in this setup, we introduce the **replica picture** to consider time periodically driven systems [Shi65, Zel67, GL13]. The key idea is to make explicitly use of the infinite copies of the initial system which arise in the Floquet

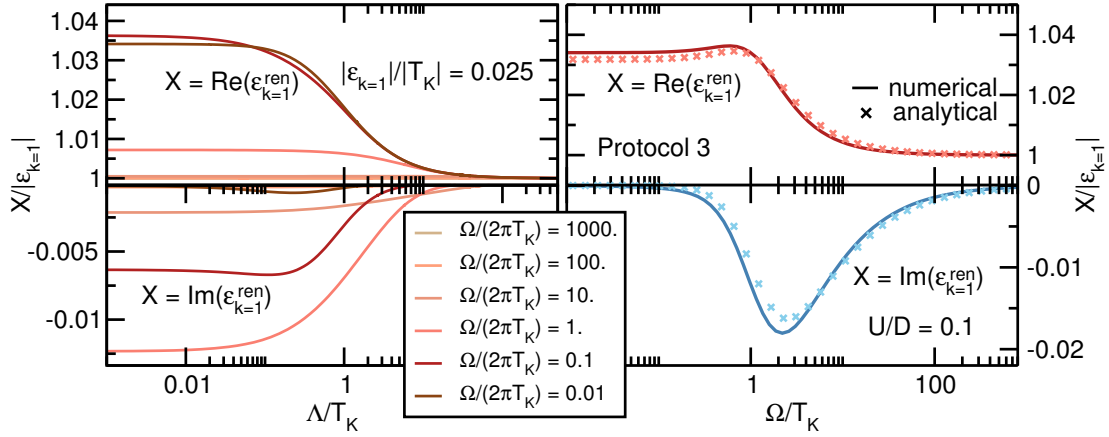


Figure 7.10: Renormalization of $\epsilon_{k=1}$ in Protocol 3: The left panel shows the respective renormalization flows, the right panel the renormalized real and imaginary part of $\epsilon_{k=1}$. The renormalization of the (initially non-vanishing) real part increases for intermediate Ω and is mainly renormalized in the adiabatic limit. The imaginary part vanishes in the large driving frequency limit as well as in the adiabatic limit. It is only finite in the intermediate regime. In any case the renormalization is minor and need not to be fed back in the analytic description of $\tau_{L(R),k=1}^{\text{ren}}$. All four panels are calculated with $U/D = 0.1$ and $T_K/D = 4.62 \cdot 10^{-5}$.

formalism, each indicated by the extra single particle like Floquet index. Treating the Floquet index as a spatial index and hence consider the Floquet channels as an extra spatial dimension, the non-interacting, time-periodically driven d dimensional system is mapped on a non-interacting, time independent $d + 1$ dimensional system with an infinite number of replicas of the system. All energy levels are shifted by $k\Omega$ for the k th replica, resulting in an effective chemical potential of $\mu = k\Omega$. The various replicas are coupled via the higher harmonics of the time periodic parameters, where the index k indicates the range of the coupling in the auxiliary direction. This means that two replicas k_1 and k_2 are coupled, if a finite Fourier coefficient $k_2 - k_1$ exists.

We demonstrate this with the specific case of interest here: In the top, left panel of Fig. 7.11 the replica picture is illustrated for the three site system with an harmonically driven onsite energy. Here the replicas $k = 0, \pm 1, \pm 2$ are displayed of the infinite numbers of copies. On the right hand side the effective chemical potentials $k\Omega$ of each of the replica is indicated. Within one replica the sites and reservoirs are coupled as known from the undriven system, neighbouring replicas are coupled at site 2 by $\epsilon_{k=1}$.

Renormalization of $\tau_{k=1}$

The calculation of the renormalization of $\tau_{L(R),k=1}$ is more interesting compared to $\epsilon_{k=1}^{\text{ren}}$: While their initial values are zero, they become finite throughout the renormalization flow. Due to the complicated interplay of several energy scales, which are not clearly separated anymore, it proofs to be more advantageous to calculate the renormalization in an effective model than following the procedure applied in Section 7.5.4 for the renormalization of the hopping.

Once again we focus on the left hopping, since due to the left-right symmetry of the setup, left and right hoppings are equivalent. $G_{12,01}^K$ is evaluated and shows that it does not depend on $\tau_{L,k=1}$ to the linear order in U . Thus, its feedback into its own flow equation is of order $\mathcal{O}(U^2)$, which is beyond our considerations. As a result the renormalization of $\tau_{L,k=1}$ is computed in a first order perturbation theory calculation in U

$$\tau_{L,k=1} = -Un_{12,k=1}, \quad (7.5.36)$$

where the replica idea is employed to calculate it in an effective, undriven model. The infinite replicas of the initial system are - due to the sinusoidal driving of the onsite energy - only coupled to neighboring copies at the central site via $\epsilon_{k=\pm 1}^A$. This is depicted in the left, upper panel of Fig. 7.11.

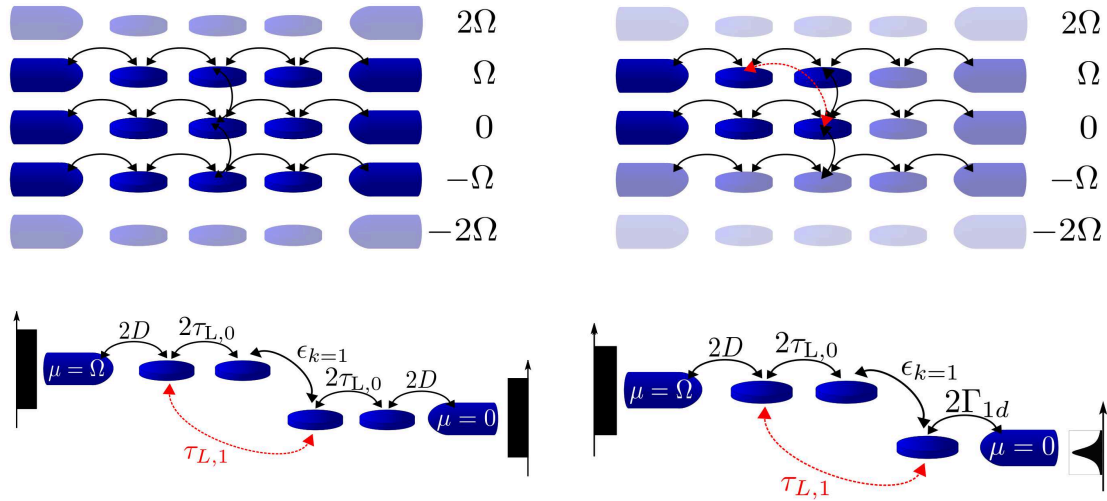


Figure 7.11: The time periodically driven one-dimensional system is mapped to an effective time-independent, two-dimensional system with replicas shifted by Ω . Neighboring replicas are coupled via $\epsilon_{k=1}$ for the setup with sinusoidally driven onsite energy. Main goal is the calculation of the renormalization of $\tau_{k=1}$, where only the zeroth and the first replica are of relevance to order $\mathcal{O}(p)$. The initially vanishing hopping $\tau_{L,k=1}$ is generated throughout the flow, here indicated by the red, dashed line. To realize the compact effective model (as depicted in the lower row), we take advantage of the left-right symmetry and finally include the first side into an effective reservoir in the $k = 0$ channel. The resulting effective model allows to set up the required lesser Green's function straight forwardly.

We focus on the first higher harmonic of the left hopping, which can be identified as the coupling between the first site of the $k = 1$ replica and the second site of the $k = 0$ channel. It is initially zero and only generated by the interaction (indicated by a dashed red line in the top right panel of Fig. 7.11). We can concentrate on the channels $k = 0, 1$ only (marked deep blue in the top right panel of Fig. 7.11), since contributions of the other channels would be of higher order in p . The afore discussed left-right symmetry allows to fold the system with respect to the central site, simplifying the system to a four site model of doubled parameters $2\tau_{L,0}$ and $2D$, respectively. The resulting setup is displayed in the left, lower panel of Fig. 7.11.

Within this four site model, the Λ dependent flow of the parameter is calculated, where the auxiliary reservoirs can be added to each of the four sites of the model. $\tau_{L,k=1}^\Lambda$ is then computed as

$$\tau_{L,k=1}^\Lambda = \tau_{14}^{\text{em}} = -U n_{14}^{\text{em}} = -\frac{U}{2\pi i} \int d\omega G_{14}^{<,\Lambda}(\omega), \quad (7.5.37)$$

with $\tau^{\text{em}}/n^{\text{em}}$ as hopping/occupation in the effective model. $G_{14}^{<,\Lambda}$ can be set up straightforwardly in the effective model with four sites and the ω integral is evaluated numerically for each value of Λ .

In the left panel of Fig. 7.12 the result of this perturbative calculation (crosses) is compared to the full numerical solution (solid line) for the renormalization flow of $\tau_{L,k=1}$. The flow diagram shows more structure compared to the afore discussed ones. The flow is affected by a complex interplay of Ω , $\epsilon_{k=1}$, T_K and the flow parameter Λ and thus does not depend on a single infrared cutoff. Three regimes can be identified: For large driving frequencies the hoppings are barely renormalized, resulting in minor renormalization of $\tau_{L(R),k=1}$. In the adiabatic regime on the contrary, the renormalization is sizable, but decreases again when the flow parameter reaches the regime $\Lambda \lesssim T_K$. In the regime of moderate driving frequency $\Omega \approx T_K$ (dark red line) renormalization is the strongest.

Finally, the renormalization at the end of the flow is calculated. For this, the fourth site of the central region is incorporated into the right reservoir. The effective model hence has a central region

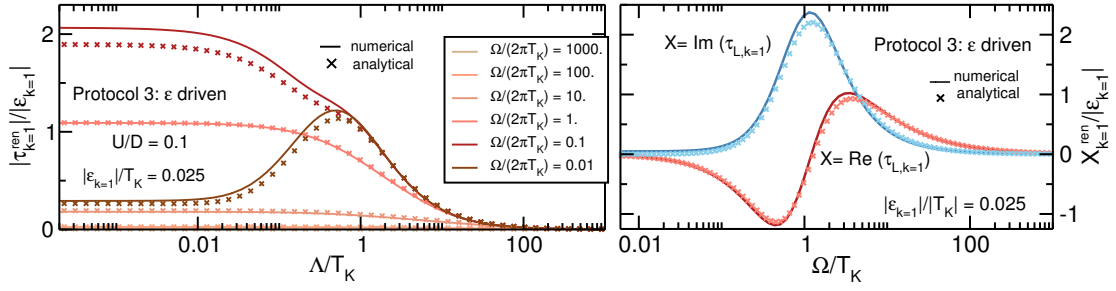


Figure 7.12: Renormalization of $\tau_{L,k=1}$ in protocol 3 with $U/D = 0.1$ and $T_K/D = 4.62 \cdot 10^{-5}$

Left panel: The renormalization flow shows a much more involved structure as a result of a complex interplay of the contributing energy scale, the flow hence does not feature a single infrared cutoff.

Right panel: Renormalized $\tau_{L,k=1}$ as a function of Ω . While in the limits of small and large driving frequency no renormalization is observed, in the regime $\Omega \approx T_K$ $\tau_{L,k=1}$ is renormalized prominently.

consisting of three sites, which is coupled on the one side to the reservoir with a flat density of states with the coupling $2D$ and on the other side, it is coupled with an effective hybridization $2\Gamma_{1d}$ to the right reservoir with an a Lorentzian shaped density of states. This is depicted in the lower, right panel of Fig. 7.11.

In this effective model,

$$\tau_{L,k=1}^{\text{ren}} = \tau_{13}^{\text{em}} = -Un_{13}^{\text{em}} = -\frac{U}{2\pi i} \int d\omega G_{13}^<(\omega) \quad (7.5.38)$$

with $\tau^{\text{em}}/n^{\text{em}}$ as hopping/occupation in the effective model. Thus $G_{13}^<(\omega)$ is set up in the effective non-interacting model

$$\begin{aligned} & \int d\omega G_{13}^<(\omega) \\ &= \int d\omega \frac{[(\omega - \Omega)(\omega + 2i\Gamma_{1d}) - \epsilon_{k=1}^2]2\tau_{L,0}\epsilon_{k=1}[4iD\Theta(-(\omega - \Omega))]}{(\omega - \Omega + 2iD)(\omega + 2i\Gamma_{1d})(\omega - \Omega) - (2\tau_{L,0})^2(\omega + 2i\Gamma_{1d}) - \epsilon_{k=1}^2(\omega - \Omega + 2iD)} \\ & \quad \times \frac{[(\omega - \Omega - 2iD)(\omega - \Omega) - 4\tau_{L,0}^2]2\tau_{L,0}\epsilon_{k=1}[4i\Gamma_{1d}\Theta(-\omega)]}{(\omega - \Omega - 2iD)(\omega - 2i\Gamma_{1d})(\omega - \Omega) - (2\tau_{L,0})^2(\omega - 2i\Gamma_{1d}) - \epsilon_{k=1}^2(\omega - \Omega - 2iD)} \\ & \stackrel{D \gg \tau_k}{=} \int d\omega \Theta(-\omega + \Omega) \frac{4i}{D} \frac{2\tau_{L,0}\epsilon_{k=1}}{D^2} \left[\frac{\omega - \Omega}{D} \frac{1}{2i(\omega - \Omega)/D - \frac{4\tau_{L,0}^2}{D^2}} \frac{1}{-2i(\omega - \Omega)/D - \frac{4\tau_{L,0}^2}{D^2}} \right] \\ & \quad + \Theta(-\omega) \frac{4i}{D} \frac{\Gamma_{1d}}{D} \frac{2\tau_{L,0}\epsilon_{k=1}}{D^2} \left[\frac{1}{(\omega - 2i\Gamma_{1d})/D} \frac{1}{(\omega + 2i\Gamma_{1d})/D} \frac{1}{2i(\omega - \Omega)/D - \frac{4\tau_{L,0}^2}{D^2}} \right] \end{aligned} \quad (7.5.39)$$

and integrating results in ($D \gg \tau_k, \Omega$)

$$\tau_{L(R),k=1}^{\text{ren}} \stackrel{D \gg \tau_k/\Omega}{=} -\frac{U}{2i\pi D} \frac{\tau_0^{\text{ren}}}{((T_K + i\Omega)/D)} \frac{\epsilon_{k=1}}{D} \left[-2i \arctan\left(\frac{T_K}{2\Omega}\right) + i\pi + \ln\left(\frac{T_K^2 + 4\Omega^2}{T_K^2}\right) \right], \quad (7.5.40)$$

where $4\Gamma_{1d}$ has been replaced by T_K , incorporating the feedback of τ_0 . The result has also been generalized to the right hopping element $\tau_{R,k=1}$ as the calculation holds equally true. The marginal renormalization of $\epsilon_{k=1}$ renders it unnecessary to include its feedback.

The renormalized hopping is shown in the right panel of Fig. 7.12, where the analytic expression (crosses) and the full numerical solution (solid line) are presented for $\tau_{L,k=1}$. The real and imaginary

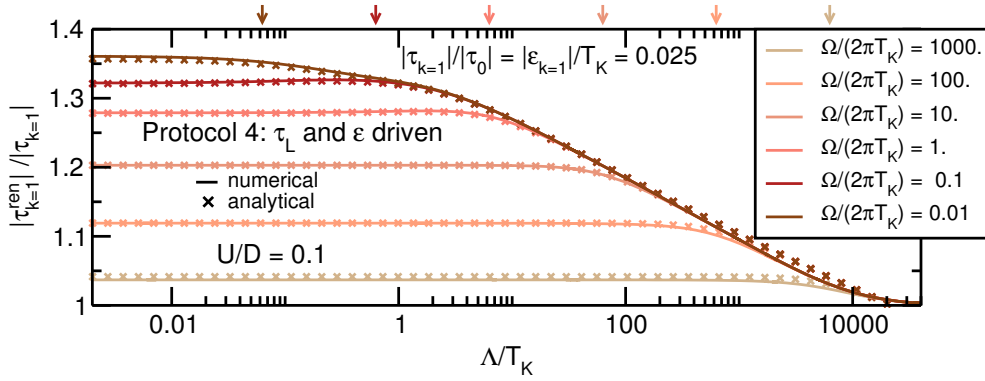


Figure 7.13: Renormalization flow for protocol 4 with $U/D = 0.1$ and $T_K/D = 4.62 \cdot 10^{-5}$. The analytic description is in excellent agreement with the full numerical solution. In the limit of large driving frequency the flow is mainly dominated by the renormalization due to the driven left hopping, while in the adiabatic limit the effect of the driven $\epsilon_{k=1}$ is apparent.

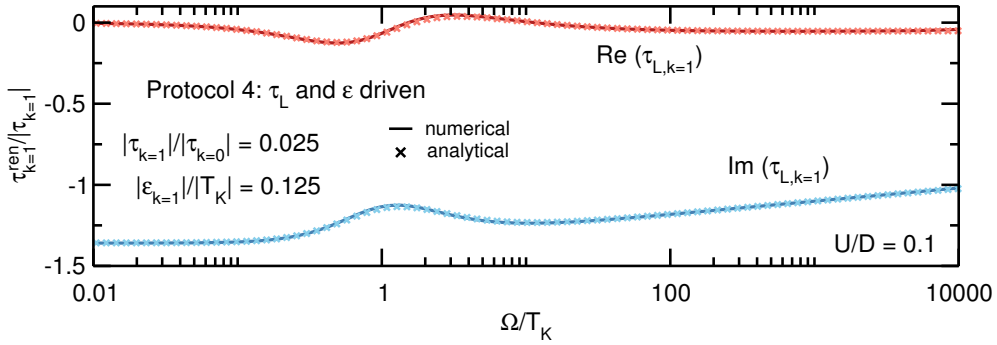


Figure 7.14: Renormalization of $\tau_{L,k=1}$ in protocol 4 and for $U/D = 0.1$ and $T_K/D = 4.62 \cdot 10^{-5}$. In the limiting cases of very large or very small driving frequency the renormalization is similar as observed for protocol 1, while in the regime $\Omega \approx T_K$ the influence of the driven onsite energy on the renormalization becomes visible. The driving amplitudes of both driven parameters have been chosen differently to emphasize the effect of $\epsilon_{k=1}$ on the renormalization.

parts are shown featuring the most prominent renormalization for $\Omega \approx T_K$ and no renormalization in the adiabatic ($\Omega \rightarrow 0$) as well as the antiadiabatic ($\Omega \rightarrow \infty$) limit. The difference between the analytic expression and the numerical data is of order $\mathcal{O}(U^2)$ and thus beyond the scope of our considerations.

7.5.7 Protocol 4: Time periodic $\tau_L(t)$ and $\epsilon(t)$

In protocol 4, we assume both left hopping and onsite energy to be time periodic

$$\begin{aligned}\tau_L(t) &= \tau_0 + \Delta\tau \sin(\Omega t), \\ \epsilon(t) &= \Delta\epsilon \cos(\Omega t).\end{aligned}$$

To describe the renormalization of $\tau_{L,k=1}$ in this protocol, we can combine the results of the protocols 1 and 3. Setting up the differential equations shows, that the renormalization to leading order in U , consists of the independent summation of the two contributions of both protocols. This is a consequence of the fact that the feedback of $\tau_{L,k=1}$ into its own renormalization is of order $\mathcal{O}(U^2)$ (and thus beyond the scope of our calculations) when only the onsite energy is driven periodically (as discussed for protocol 3). The renormalization of $\epsilon_{k=1}$ is the same as in protocol 3, since there is no contribution to it generated in protocol 1.

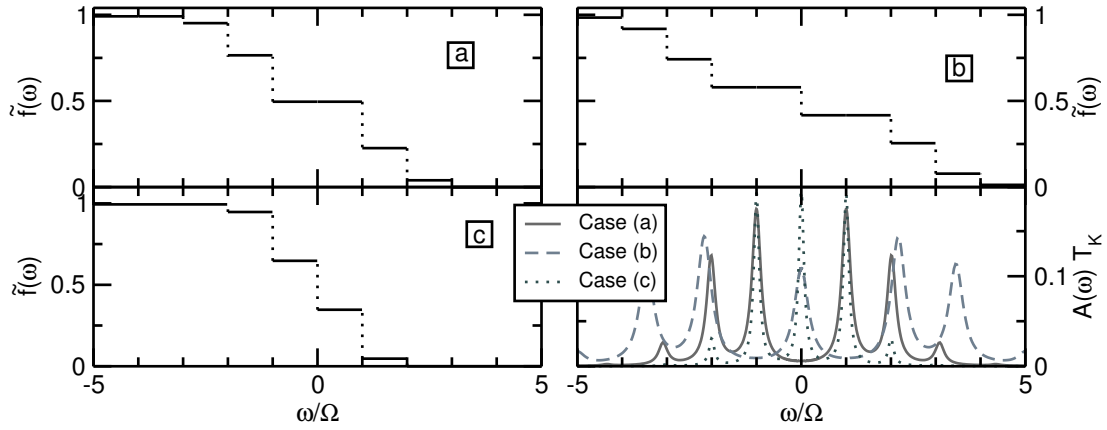


Figure 7.15: The effective reservoir distribution function for a time periodically varied onsite energy shows a multistep form. Three different cases are depicted here. Case (a): The edge at $\omega = 0$ is tuned to zero, such that the first effective reservoir distribution function resembles in the regime of small energies $|\omega|$ the form of a time independent setup with an applied bias voltage $V = 2\Omega$. Case (b): The edge at $\omega = \pm\Omega$ is tuned to zero. Case (c): The steps at $\omega = 0, \pm\Omega$ have equal height. The respective spectral function of the reservoir dressed dot for all three cases exhibit peaks at the position of the sharp edges in the reservoir distribution function.

The flow of the left hopping $\tau_{L,k=1}$ is depicted in Fig. 7.13, comparing the analytic expression (symbols) and the numerical solution (solid line). For large driving frequency the renormalization flow is mainly characterized by the contribution of protocol 1, featuring the driving frequency as the infrared cutoff. In contrast to this, the renormalization flows of $\Omega = 0.1 T_K$ and $\Omega = 0.01 T_K$ sheer off, reflecting pronouncedly the contribution to the renormalization induced by $\epsilon_{k=1}$.

In Fig. 7.14, the analytic expression and the full numerical solution of the renormalized $\tau_{L,k=1}$ is presented. In the limits $\Omega \rightarrow 0$ and $\Omega \rightarrow \infty$ the renormalization is defined by the contribution of the time periodic left hopping (from protocol 1), the contribution of the time periodic $\epsilon(t)$ manifests itself as a bump in the intermediate regime of $\Omega \approx T_K$.

7.6 Tuning the effective reservoir distribution function

In this section, a setup is discussed, where neither the driving amplitude nor the driving frequency are limited. It is shown that the effective reservoir function is influenced by the ratio of driving amplitude and driving frequency. At the beginning of this chapter we have discussed that we know from the equilibrium situation as well as the non-equilibrium situation that the sharp edges of the according reservoir distribution functions at vanishing temperature $T = 0$, result in logarithmic divergencies, which are summed up throughout the RG flow. The respective energy scales (defined by the position of the steps) are hence reflected in the infrared cutoff of the according renormalization flow. We here take advantage of the tunability of the reservoir distribution function in time periodically driven quantum dots to investigate its effect on the renormalization flow further. It allows to create a situation where the driving frequency appears as energy scale already in the zeroth component of the hopping $\tau_{k=0}$.

7.6.1 Setup and Illustration of the physical situation

The setup where only the onsite energy is varied time periodically

$$\epsilon(t) = \Delta\epsilon \cos(\Omega t) \quad (7.6.1)$$

around the particle-hole symmetric point, is considered again, but the driving amplitude can be of arbitrary size.

In order to illustrate the physical situation at hand the time dependency of the dot is shifted to the effective reservoir couplings $\tau(t) = \tau_0 \exp(i \int_{t_0}^t \Delta \epsilon \cos(\Omega t') dt')$ as described by Eq. (3.4.1) and in Refs. [Str05, Kwa10, Suz15]. This transformation is not performed for the numerical implementation but only serves for the demonstration. The Keldysh self-energy of the effective one dot structure is

$$\Sigma_{kk'}^K(\omega) = -2i\Gamma_{1d}[\delta_{kk'} - 2\tilde{f}_{kk'}(\omega)], \quad (7.6.2)$$

where the effective reservoir distribution function (also referred to as the generalized distribution function) from Eq.(7.2.4) is generalized to

$$\tilde{f}_{\alpha, kk'}(\omega) = \sum_{k_2} J_{k-k_2}^* \left(\frac{\Delta \epsilon}{\Omega} \right) f_{\alpha}(\omega + k_2 \Omega) J_{k'-k_2} \left(\frac{\Delta \epsilon}{\Omega} \right) \quad (7.6.3)$$

with $\tilde{f}_{\alpha, kk'}(\omega) = \sum_{\alpha} 1/2 \tilde{f}_{\alpha, kk'}(\omega)$. Here $J_m(x)$ is the m th Bessel function. We focus on the effect on the mean value of the hopping matrix elements and consider the $k = 0$ component of $\tilde{f}_{\alpha}(\omega)$, which is given as the weighted sum of the Fermi distribution function

$$\tilde{f}_{\alpha, 0}(\omega) = \sum_m \left[J_m \left(\frac{\Delta \epsilon}{\Omega} \right) \right]^2 f_{\alpha}(\omega + m\Omega), \quad (7.6.4)$$

where $f_{\alpha}(\omega) = (e^{\beta_{\alpha}\omega} + 1)^{-1}$. At $T = 0$ it shows a multistep structure with steps of width Ω and a height specified by the n th Bessel function

$$h_n = \left| J_n \left(\frac{\Delta \epsilon}{\Omega} \right) \right|^2 \quad (7.6.5)$$

at $\omega = n\Omega$ [Het95, Suz15, Bru94]. It is thus possible to tune the effective reservoir distribution by selecting a certain ratio of amplitude and driving frequency $q = \frac{\Delta \epsilon}{\Omega}$. We study here three different cases:

- Case (a): The ratio is fixed by $J_0(q) = 0$ ($q \approx 2.405$), i.e. no step at $\omega = 0$.
- Case (b): The ratio is fixed by $J_1(q) = 0$ ($q \approx 3.830$), i.e. no steps at $\omega = \pm\Omega$.
- Case (c): The ratio is fixed by $J_0(q) = J_1(q)$ with $q \approx 1.435$, i.e. equal height for the steps at $\omega = 0, \pm\Omega$.

7.6.2 Effect on the Renormalization flow

Case (a)

In case (a) the resulting effective reservoir distribution of the $k = 0$ channel (left top of Fig. 7.16) shows no step at $\omega = 0$, but steps at $\omega = \pm\Omega$. This way we have designed an effective reservoir function that resembles in the regime of small energies $|\omega|$ the form of the effective reservoir distribution of the time independent dot model with an applied bias voltage $V = 2\Omega$.

The renormalization group flow of the $k = 0$ component of the left hopping is depicted as the solid line in the upper panel of Fig. 7.16 for several values of the driving frequency. The flow is clearly characterized by an infrared cutoff at 2Ω as long as the driving frequency is larger than T_K . This follows from the positions of the steps in the reservoir distribution function located at the driving frequency in strict analogy to a time-independent setup with a driving bias voltage. The resulting divergencies at Ω are summed up to a cutoff in the infrared for the renormalization flow of the $k = 0$ coefficient of τ_L . The steps at larger ω do not affect the flow significantly due to their smaller heights.

Even though the present chapter is dedicated to the renormalization of the parameters solely, we like to shortly discuss an observable at this point to support the prior discussion. The charge susceptibility χ is determined by the renormalized hoppings, thus χ of case (a) and of a setup with an applied bias voltage as discussed in Ref. [Kar10c] are compared in the lower panel of Fig. 7.16. It shows equal behavior for both situations, which confirms the discussed similarity in the renormalization flows. The small difference arises from the influence of the other steps in the reservoir distribution function in the time periodic setup.

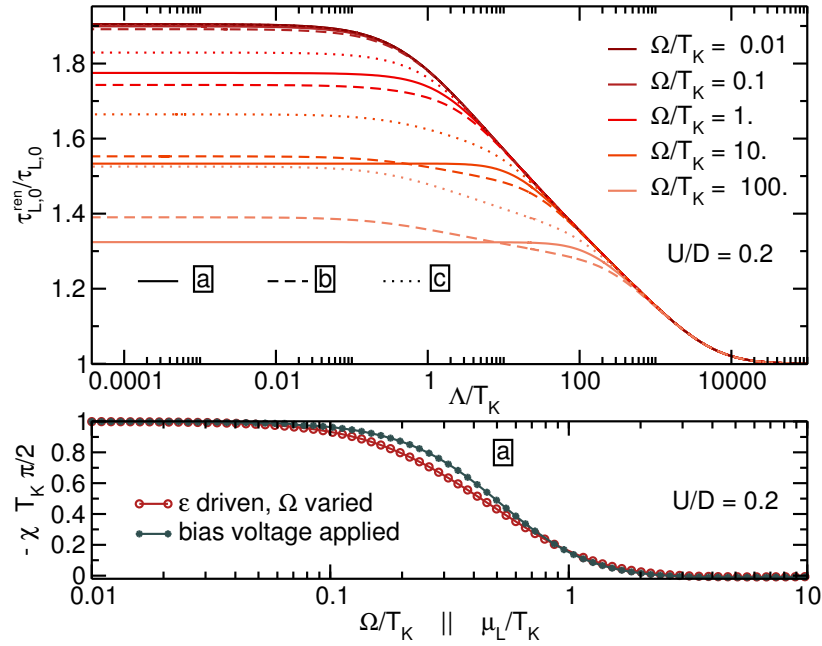


Figure 7.16: Upper panel: Renormalization flows of the zeroth component of τ_L demonstrating a transparent dependency on the driving frequency Ω for three different effective reservoir distribution function (shown in Fig. 7.15). Lower panel: Charge susceptibility in case (a) is compared to the charge susceptibility in (the time independent) case of an applied bias voltage. We choose $U/D = 0.2$ with $T_K/D = 7.93 \cdot 10^{-5}$.

Case (b)

The effective distribution function for case (b) is shown in the right top panel of Fig. 7.15. It features steps at $\omega = 0$ and $\omega = \pm 2\Omega$. Consequentially, the flow (dashed line in Fig. 7.16) exhibits two cut off scales, which is indicated by a change in the slope of the curve: It is first cut at the scale 2Ω reflecting the edge at $\omega = 2\Omega$ and then subsequently saturates around T_K , reflecting the edge at $\omega = 0$.

Case (c)

Finally, in case (c), the ratio q is chosen such that $J_0(q) = J_1(q)$ with $q \approx 1.435$, i.e. with edges at $\omega = 0, \pm\Omega$ with equal height. The resulting effective reservoir distribution function is displayed in the bottom left panel of Fig. 7.15. As a consequence of the equal heights, each of the equidistant edges contributes likewise and they are reflected as multiple, equally distant energy scales cutting the RG flow (dotted line). While the curve for $\Omega/T_K = 100$ features two changes in the slope, reflecting a cutoff at Ω and one by T_K , the other curves for smaller driving frequencies do not feature one pronounced infrared cutoff but are bend in a long tail as the several equal contributions are not resolved.

Here three different situations have been discussed to show the influence of the effective reservoir distribution function on the renormalization flow. The unbiased RG method we employ here is indeed capable to tackle this kind of question as no further assumptions have been made in the process of setting up the RG equations. Steps with a comparably high edge are reflected in the flow as infrared cutoff confirming the understanding known from the equilibrium and non-equilibrium situations. In this situation, the k th component of the hopping is no longer only defined by a dependency on $k\Omega$, but already $\tau_{k=0}$ reveals a dependency on Ω .

7.7 Conclusion

In this chapter the renormalization physics arising in the periodically driven interacting resonant level model has been discussed. It reveals that the energy scale Ω is reflected in the RG flows and depending on the exact conditions of the regarded setup, can play very different roles. We have focused solely on the renormalization of the parameters here, where we were able to provide analytic expressions in the small amplitude limit. Even beyond this limit, it is a reasonable route to first consider the renormalized parameters and only subsequently regard the transport, as it allows for a transparent path towards the rather involved observables.

New power law in small amplitude limit

First, four different protocols have been discussed in the small amplitude limit, where we have shown that the Floquet channels decouple and can be described independently. Moreover, the effective energy scale for the k th higher harmonic has been identified to be $k\Omega$. The considered limit made it feasible to find analytic expressions for the renormalization of $\tau_{L(R)}(t)$ and $\epsilon(t)$ in all four protocols, which show excellent agreement in comparison with the full numerical solution. The protocol of only one hopping element time periodically varied reveals a new power law in the higher harmonics depending on $k\Omega$, i.e. the renormalization in the high frequency regime depends not only on the driving frequency, but differs for the various higher harmonics. This allows to design the initial signals to be renormalized into a required form. In contrast to this, the periodically driven onsite energy exhibits a renormalization flow for $\tau_{L(R),k=1}$, which is affected by an involved interplay of several energy scales and not determined by a single infrared cutoff.

Influence of the effective reservoir distribution function on the RG flow

Second, we employed a setup, where only the onsite energy is varied time periodically, but driving amplitude and frequency are not restricted in any way. It has been discussed that the physical situation can be illustrated by an effective reservoir distribution function revealing a multistep function determined by the ratio of driving amplitude and frequency. It was elaborated that the sharp edges in the distribution function yield the logarithmic divergencies, which are summed up through the RG procedure and consequentially the energy scales defined by the positions of the edges are reflected as infrared cutoffs in the RG flow.

FRG reveals full potential

Since the approach presented here follows a transparent renormalization group procedure and is not biased by any assumption made in the process of setting up the RG equations, it is capable to tackle the questions presented in this chapter. Especially here the FRG can show its full potential. While unequivocal dependencies in the RG flow such as the $k\Omega$ dependency in the k th coefficient in the small amplitude limit might be captured by alternative RG methods, identifying dependencies, which result from a more involved interplay of cut-off scales, as observed for the driven onsite energy in the small amplitude limit as well as for arbitrary large driving amplitudes is a complicated task which can be approached by unbiased methods such as the FRG.

Acknowledgement

The data of the explicitly time dependent FRG has been provided by Dante Kennes.

References

The results discussed in this chapter (including the figures) were partly published in

A. K. Eissing, V. Meden, D. M. Kennes

'*Renormalization in Periodically Driven Quantum Dots*'

Phys. Rev. Lett. **116**, 026801 (2016)

A. K. Eissing, V. Meden, D. M. Kennes

'*Functional renormalization group in Floquet space*'

Phys. Rev. B **94**, 245116 (2016)

Chapter 8

Transport in Periodically Driven Quantum Dots

Contents

8.1	Transport in the time independent non-equilibrium IRLM	92
8.2	Transport in the adiabatic limit	92
8.2.1	Dot Occupancy	93
8.2.2	Current for a varying onsite energy	93
8.2.3	Parametric quantum pumps	94
8.3	Quantum pumps: Two parameter pump	95
8.4	Quantum pumps: Single parameter pump	98
8.4.1	Susceptibility	99
8.4.2	Pumping power	102
8.4.3	Perturbation Theory in Liouville space: Mean current	104
8.5	Current and Conductance of non-sinusoidal signals	105
8.6	Conclusion	108

The present chapter is dedicated to the discussion of the transport properties of time periodically driven quantum dots. The occupancy and the current are discussed in the time independent non-equilibrium setup to afterwards investigate which of their properties still hold true in the adiabatic limit of the periodic configuration. Subsequently, we review the known physics of parameter pumps as analyzed by Brouwer, in the limit of small driving amplitudes and frequency [Bro98, Spl07]. Based on this, we explore the pumped charge of the parameter pump beyond the adiabatic as well as the small amplitude limit. The phase difference between the two time periodically varied parameters is decreased to gradually evolve into an in-phase quantum pump, where both parameters are varied in phase. This is followed by a discussion of a single parameter pump, realized when only one hopping oscillates harmonically. The first higher harmonic of the charge susceptibility χ_1 and the pumping power J_0 are examined, looking for an observable that reflects the power law of $\tau_{k \neq 0}$ in the driving frequency Ω . The discussion of J_0 and its possible power law is supported by an analytic expression. A perturbation theory calculation of J_0 in Floquet-Liouville space is devised to examine the conditions of a finite pumping power in this setup. Finally, the current and conductance for non-sinusoidal signals are discussed, where among others the conductance for the designed signal of the preceding chapter is considered.

8.1 Transport in the time independent non-equilibrium IRLM

The steady state of the non-equilibrium IRLM in the wide band limit driven by an applied bias voltage V was studied in [Kar10c, And11a, And11b]. General expressions for the dot occupancy

[Kar10c, And11a, And11b]

$$\bar{n}_{22}^{\text{st}} = \frac{1}{2} + \frac{1}{\pi} \left[\frac{\Gamma_{1d,L}^{\text{ren}}}{\Gamma_{1d,L}^{\text{ren}} + \Gamma_{1d,R}^{\text{ren}}} \arctan \left(\frac{\mu_L - \epsilon^{\text{ren}}}{\Gamma_{1d,L}^{\text{ren}} + \Gamma_{1d,R}^{\text{ren}}} \right) + \frac{\Gamma_{1d,R}^{\text{ren}}}{\Gamma_{1d,L}^{\text{ren}} + \Gamma_{1d,R}^{\text{ren}}} \arctan \left(\frac{\mu_R - \epsilon^{\text{ren}}}{\Gamma_{1d,L}^{\text{ren}} + \Gamma_{1d,R}^{\text{ren}}} \right) \right] \quad (8.1.1)$$

as well as the current leaving the left reservoir [Kar10c, And11a, And11b]

$$J_L^{\text{st}} = \frac{2}{\pi} \frac{\Gamma_{1d,L}^{\text{ren}} \Gamma_{1d,R}^{\text{ren}}}{\Gamma_{1d,L}^{\text{ren}} + \Gamma_{1d,R}^{\text{ren}}} \left[\arctan \left(\frac{\mu_L - \epsilon^{\text{ren}}}{\Gamma_{1d,L}^{\text{ren}} + \Gamma_{1d,R}^{\text{ren}}} \right) - \arctan \left(\frac{\mu_R - \epsilon^{\text{ren}}}{\Gamma_{1d,L}^{\text{ren}} + \Gamma_{1d,R}^{\text{ren}}} \right) \right]. \quad (8.1.2)$$

have been derived. Here we take advantage of the effective non-interacting setup at the end of the flow. As discussed in Section 5.3.4 it allows us to use the non-interacting expressions and substitute the parameters by their renormalized ones. The renormalization behavior of $\Gamma_{1d,L(R)}$ can be derived from Eq. (7.2.7)

$$\frac{\Gamma_{1d,L(R)}^{\text{ren}}}{\Gamma_{1d,L(R)}} = \left(\frac{\tau_{L(R),k=0}^{\text{ren}}}{\tau_{L(R),k=0}} \right)^2 \sim \left[\frac{(V/2 \mp \epsilon)^2 + (T_K/2)^2}{D^2} \right]^{-\frac{U}{\pi D}} \quad (8.1.3)$$

where the infrared cutoff is influenced by all energy scales and in the according limits the largest energy scale provides the cutoff, as discussed in Section 7.2. Here already the emergent low energy scales has been used. Inserting it into Eq. (8.1.2), the power law behavior of the mean hopping matrix element manifests in an observable. Two interesting regimes of different behavior are identified in the limit of $|V| \gg T_K$ [Kar10a].

Zero impurity energy

For an onsite energy $|\epsilon| \ll |V|$ the renormalization of the left and the right hybridizations $\Gamma_{1d,L(R)}^{\text{ren}}$ is characterized by the infrared cutoff V and hence the current features the respective power law behavior [Kar10a, Kar10c]

$$\frac{J}{T_K} \sim \left(\frac{V}{T_K} \right)^{-2\alpha_J} \quad \alpha_J = \frac{U}{\pi D} + \mathcal{O}(U^2). \quad (8.1.4)$$

depending on the bias voltage.

Onsite energy at resonance

If the onsite energy is fixed on resonance, i.e. $\epsilon = \mu_{L(R)} = \pm V/2$, it results in different infrared cutoffs for the left and right effective hybridization $\Gamma_{1d,L(R)}$. Assuming e.g. the onsite energy to be at the left chemical potential $\epsilon = V/2$, $\epsilon - \mu_L = 0$, while $\epsilon - \mu_R = V$, such that $\Gamma_{1d,L}$ is cut by T_K , $\Gamma_{1d,R}$ is cut by the bias voltage. As a consequence, the factor of Eq. (8.1.2) combines two different power laws yielding the following behavior [Kar10a]

$$\frac{J}{T_K} \sim \frac{1}{1 + \left(\frac{V}{T_K} \right)^{2\alpha_{\text{res}}}} \quad \alpha_{\text{res}} = \frac{U}{\pi D} + \mathcal{O}(U^2) \quad (8.1.5)$$

for the current. It thus only features a power law for a very large bias voltage, orders of magnitude larger than necessary for the power law of Eq. (8.1.4). This is due to the additional constant in the denominator, which results from the two different energy cutoffs in the problem.

8.2 Transport in the adiabatic limit

Periodically driven quantum dots have been studied extensively in the limit of a driving frequency Ω much smaller than the characteristic energy scale of the system, the so called adiabatic limit. If additionally the driving amplitude is chosen to be small, the setup can be considered as quasi static. This allows to employ and generalize methods and some properties from the time independent steady state to the periodic one and consider the setup e.g. with a scattering method [Bro98].

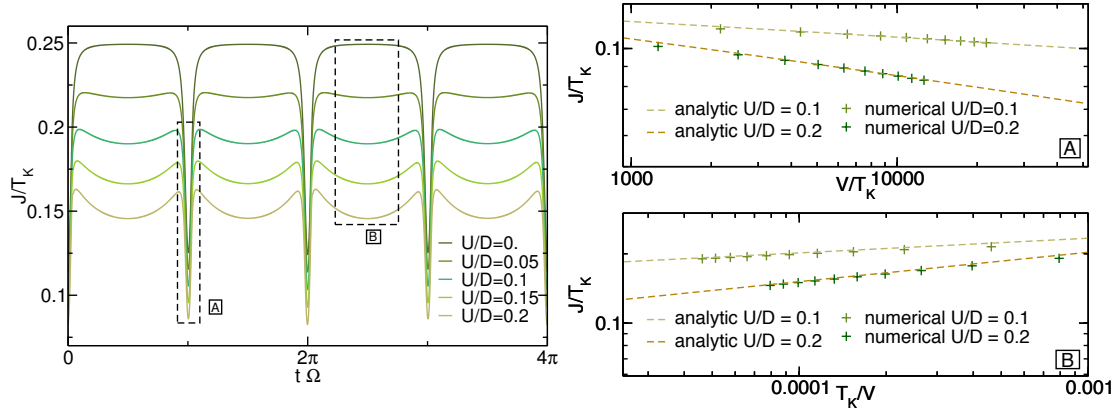


Figure 8.1: Onsite energy varying adiabatically between the resonances in a quantum dot with a symmetrically applied bias voltage for $U/D = \{0., 0.05, 0.1, 0.15, 0.2\}$ with $T_K/D = 2.5 \cdot 10^{-5}$, $T_K/D = 3.43 \cdot 10^{-5}$, $T_K/D = 4.62 \cdot 10^{-5}$, $T_K/D = 6.10 \cdot 10^{-5}$ and $T_K/D = 7.93 \cdot 10^{-5}$, respectively. In the left panel the current signal is depicted for several values of interaction U , the right panels show the power law behavior for $V \gg T_K$ at resonance (A) and around the particle hole symmetric point (B). The driving frequency is chosen to be $\Omega/(2\pi T_K) = 0.001$ and the applied bias voltage in the left panel is $V/T_K = 200$.

8.2.1 Dot Occupancy

As discussed in Section 8.1 the dot occupancy in the time independent IRLM can be described by Eq. (8.1.1). This expression can be generalized to describe the time periodic steady state dot occupancy in the adiabatic limit with small driving amplitudes by substituting the respective parameters by their time periodic ones,

$$\bar{n}_{22}^{\text{st}}(t) = \frac{1}{2} + \frac{1}{2\pi} \left[\arctan \left(\frac{\mu_L(t) - \epsilon^{\text{ren}}(t)}{\Gamma_{1d,L}^{\text{ren}}(t) + \Gamma_{1d,R}^{\text{ren}}(t)} \right) + \arctan \left(\frac{\mu_R(t) - \epsilon^{\text{ren}}(t)}{\Gamma_{1d,L}^{\text{ren}}(t) + \Gamma_{1d,R}^{\text{ren}}(t)} \right) \right]. \quad (8.2.1)$$

An analogous generalization of the current formula to the adiabatic time periodic setup is not possible

$$J_L^{\text{st}}(t) \neq \frac{2}{\pi} \frac{\Gamma_{1d,L}^{\text{ren}}(t) \Gamma_{1d,R}^{\text{ren}}(t)}{\Gamma_{1d,L}^{\text{ren}}(t) + \Gamma_{1d,R}^{\text{ren}}(t)} \left[\arctan \left(\frac{\mu_L(t) - \epsilon^{\text{ren}}(t)}{\Gamma_{1d,L}^{\text{ren}}(t) + \Gamma_{1d,R}^{\text{ren}}(t)} \right) - \arctan \left(\frac{\mu_R(t) - \epsilon^{\text{ren}}(t)}{\Gamma_{1d,L}^{\text{ren}}(t) + \Gamma_{1d,R}^{\text{ren}}(t)} \right) \right]. \quad (8.2.2)$$

We can directly read off that expression that there is no current for equal $\mu_L(t) = \mu_R(t)$, i.e. no current at all for configurations where the onsite energy and/or hybridization are varied periodic in time. While the expression at least describes the mean current correct for setups with a single parameter varied, the finite mean current of the parametric pump is not captured (see Section 8.2.3). Analogous expressions for the mean current and occupancy can be found in Ref. [Kwa10] for an harmonically driven onsite energy.

However, as we elaborate in the next part, in case of a finite bias voltage the mean current in the adiabatic limit shows the same behavior as derived from the static current expression (8.1.2).

8.2.2 Current for a varying onsite energy

In Section 8.1 the power law behavior of the current for $V \gg T_K$ for two level points has been discussed, where either the onsite energy is set to zero or the onsite energy is fixed to one of the chemical potentials, i.e. is on resonance. While in the regime of vanishing onsite energy a clear power law in the current can be observed, the on-resonance situation is characterized by the combination of two infrared scales featuring no clear power-law behavior.

Motivated by this, we vary the onsite energy time periodically between the left and right chemical potential adiabatically, and thus pass the two resonance positions as well the zero impurity energy

point. It is now examined whether the current in this situation exhibits the same behavior in the respective regimes as discussed for the time independent problem (see Section 8.1).

A bias voltage is applied symmetrically with $\mu_L = -\mu_R = V/2$ and a periodically varied onsite energy $\epsilon = \Delta\epsilon \cos(\Omega t)$, where $\Delta\epsilon = V/2$ and the driving frequency is chosen to be in the adiabatic limit $\Omega/(2\pi T_K) = 0.001$. The resulting current signal is depicted on the left hand side of Fig. 8.1 for several values of interaction U . The non-interacting setup exhibits a current that varies between a plateau around zero onsite energy and a sharp minimum at the resonance positions. A positive interaction levels down the plateau to a local minimum at the particle hole symmetric point and decreases the sharp minimum at the resonance positions further. In order to investigate whether we can extract the same behavior as known from the time independent situation at these two points, the time periodic setup is considered for a large range of the applied bias voltage. We then focus on the two special points A (ϵ at resonance) and B (zero onsite energy) accordingly marked in the time dependent current on the left hand side of Fig. 8.1. The respective values of the current at this point are then displayed as a function of voltage (situation A, at resonance) and as function of the inverse of voltage (situation B, zero onsite energy) to examine the respective behavior. The numerical solution (symbols) is compared to the analytic prediction (dashed line) on the right hand side of Fig. 8.1 to reveal that the current in both situations follows the behavior as predicted. The current when $\epsilon(t)$ passes adiabatically the resonance point shows the dependence on V as defined in Eq. (8.1.5) and the current when $\epsilon(t) \approx 0$ reveals power law behavior (Eq. (8.1.4)). This demonstrates that the adiabatic situation can be considered as a sequence of effectively time independent setups, where the mean current is only affected by the effective configuration at each point in time.

8.2.3 Parametric quantum pumps

The realization of a quantum pump is one of the main interest in the field of periodically driven quantum dots. In the adiabatic limit it can be achieved by varying two or more parameters periodically with a phase shift between the respective signals. The resulting parametric pump resembles the classic peristaltic pump. Accordingly, the transport mechanism of the electrons from one reservoir to the other can be understood in a completely classical picture, rendering no quantum mechanical property crucial for a finite pumped charge. It can be obtained in case of no interaction by a scattering approach, assuming an effective equilibrium situation at any point [Bro98]. For two traditional setups, where either one reservoir dot coupling and the onsite energy is varied or both reservoir dot couplings are varied, exact analytic expressions of the pumped charge can be derived from the Brouwer formula in the limit of small driving amplitudes (with $e = 1$) [Spl07]:

$$Q_{\Gamma_L, \Gamma_R} = \frac{2}{\pi} \eta(\Gamma_{1d,R}^{\text{ren}}, \Gamma_{1d,L}^{\text{ren}}) \frac{(\bar{\Gamma}_{1d,L}^{\text{ren}} + \bar{\Gamma}_{1d,R}^{\text{ren}})\bar{\epsilon}}{[\bar{\epsilon}^2 + (\bar{\Gamma}_{1d,L}^{\text{ren}} + \bar{\Gamma}_{1d,R}^{\text{ren}})^2]^2} \quad (8.2.3)$$

$$Q_{\Gamma_L, \epsilon} = \frac{2}{\pi} \eta(\Gamma_{1d,R}^{\text{ren}}, \epsilon) \frac{(\bar{\Gamma}_{1d,L}^{\text{ren}} + \bar{\Gamma}_{1d,R}^{\text{ren}})\bar{\Gamma}_{1d,R}^{\text{ren}}}{[\bar{\epsilon}^2 + (\bar{\Gamma}_{1d,L}^{\text{ren}} + \bar{\Gamma}_{1d,R}^{\text{ren}})^2]^2} \quad (8.2.4)$$

where $\bar{\Gamma}_{1d,(L(R))}^{\text{ren}} = \Gamma_{1d,L(R)}^{\text{ren}}, k=0$, $\bar{\epsilon} = \epsilon_{k=0}$ and η is the according directed, enclosed area in the phase space of one pumping cycle. While the expressions have been derived initially for the non-interacting case $U/D = 0$, where $\bar{\Gamma}_{1d,L(R)}^{\text{ren}}(U = 0) = \bar{\Gamma}_{1d,L(R)}^{\text{init}}$, the renormalized hybridizations are deployed already. Once again, the non-interacting expression can be generalized to the interacting case by substituting the parameters by their renormalized equivalents (as discussed in Section 5.3.4). The weak renormalization of ϵ can be neglected (compare Section 7.1).

In the simple cases of

$$\begin{aligned} \Gamma_{1d,L}(t) &= \bar{\Gamma}_{1d,L} + \Delta\Gamma_{1d} \sin(\Omega t) \\ \epsilon(t) &= \epsilon_0 + \Delta\epsilon \cos(\Omega t) \quad \text{or} \quad \Gamma_{1d,R}(t) = \bar{\Gamma}_{1d,R} + \Delta\Gamma_{1d} \cos(\Omega t) \end{aligned}$$

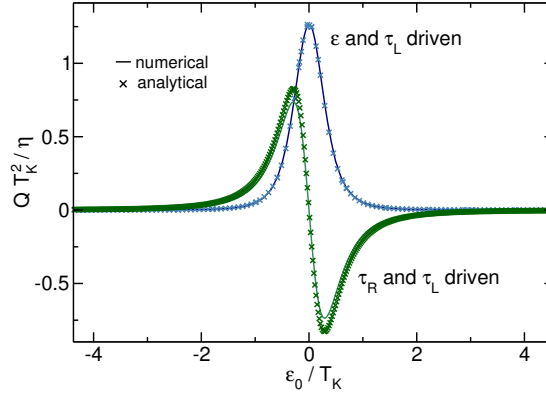


Figure 8.2: Pumped charge of the parametric pump with $\tau_L(t) = \tau_0 + \Delta\tau \sin(\Omega t)$ and $\epsilon(t) = \epsilon_0 + \Delta\epsilon \cos(\Omega t)$ in the adiabatic limit ($\Omega/(2\pi T_K) = 100$) and with small driving amplitudes $\Delta\tau/\tau_0 = 0.01$ and $\Delta\epsilon = 0.05 T_K$ with $T_K/D = 2.625 \cdot 10^{-7}$ for $U/D = 0.2$. The pumped charge of the interacting setup is described by the non-interacting analytic formula, when it is rescaled with T_K .

the respective η is calculated to

$$\begin{aligned}\eta(\Gamma_{1d,L}, \epsilon) &= \pi \Delta \Gamma_{1d,L} \Delta\epsilon \\ \eta(\Gamma_{1d,L}, \Gamma_{1d,R}) &= \pi \Delta \Gamma_{1d,L} \Delta \Gamma_{1d,R}.\end{aligned}$$

The analytic expressions are derived in the macroscopic model and accordingly depend on the hybridization Γ_{1d} . Nevertheless, within our approach the hoppings are periodically driven as

$$\begin{aligned}\tau_L(t) &= \tau_{L,0} + \Delta\tau \sin(\Omega t) \quad \text{and} \quad \epsilon(t) = \epsilon_0 + \Delta\epsilon \cos(\Omega t) \quad (\text{Protocol I}) \quad \text{or} \\ \tau_L(t) &= \tau_{L,0} + \Delta\tau \sin(\Omega t) \quad \text{and} \quad \tau_R(t) = \tau_{R,0} + \Delta\tau \cos(\Omega t) \quad (\text{Protocol II}).\end{aligned}$$

They are linked to the hybridization via Eq. (3.3.7), such that the latter varies sinusoidal to the leading order in the limit of small amplitudes as well. It renders the analytic expression still valid for this setup.

In Figure 8.2 the analytic expression (symbols) of the pumped charge Q as a function of the onsite energy ϵ_0 is compared to the numerical solution (solid line) of the interacting setup for both protocols of time periodically driven parameters. Both protocols are symmetric around the particle hole symmetric point. The combination of driven onsite energy and left hopping (Protocol I), results in a maximal pumped charge at zero onsite energy, which drops with increasing absolute value of ϵ_0 . For a finite pumped charge in the setup of both hoppings time periodically varied (Protocol II), the particle hole symmetry needs to be broken, featuring maximal pumping at $\epsilon = \pm \frac{T_K}{2\sqrt{3}}$. Both protocols result in no pumped charge for a large onsite energy.

The extension of the generalization of the analytic expression to the interacting setup proofs to be valid. We make use of the relation $4\Gamma_{1d}^{\text{ren}} = T_K$ (compare Eq. (7.1.7)) and scale Q with T_K^2/η , where the low energy scale captures the effect of the interaction in this setup. These pump setups are the starting point of our considerations of pumping out of the adiabatic and small driving amplitude limit, where we mainly concentrate on Protocol I.

8.3 Quantum pumps: Two parameter pump

The afore discussed traditional pump setup shows maximal pumped charge from the left to the right reservoir, if the signal of the left hopping is retarded by $\pi/2$ compared to the signal of the onsite energy. We want to examine a gradual evolution from this case into an in-phase quantum pump by decreasing the phase difference between the signals of the two periodically driven parameters in the whole regime of driving frequency with and without interaction. Starting with a maximal

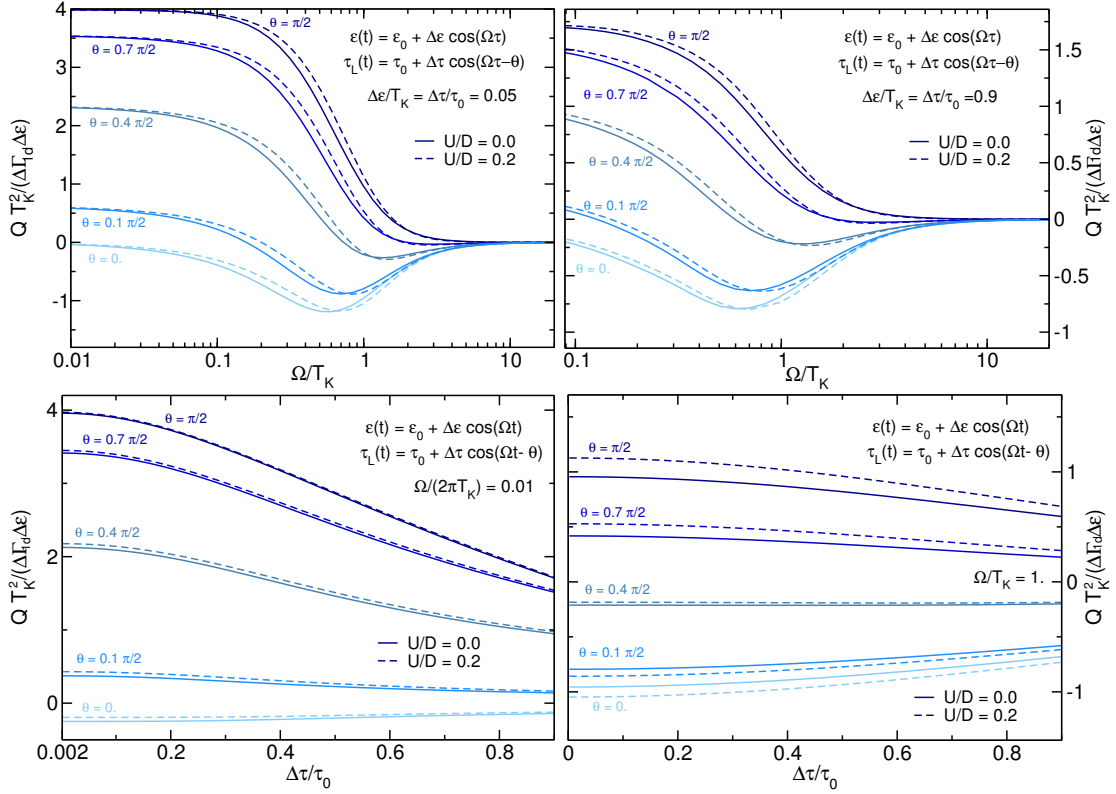


Figure 8.3: Top row: Comparison of the pumped charge Q for several phase differences gradually evolving into an in-phase quantum pump, for a small (left panel) and a large driving amplitude (right panel) for $U/D = \{0., 0.2, \}$ with $T_K/D = 2.5 \cdot 10^{-5}$ and $T_K/D = 7.93 \cdot 10^{-5}$, respectively. The qualitatively behavior is the same in both case, where the interaction only manifests in the renormalization of T_K . For the comparison the pumped charge is scaled per $\Delta\Gamma_d \Delta\epsilon$, showing that the relative pumped charge is even larger for the smaller driving amplitude. Bottom row: Pumped charge per $\Delta\Gamma_d \Delta\epsilon$ as a function of $\Delta\tau/\tau_0$ in the adiabatic limit (left panel) and for intermediate driving frequency (right panel).

phase difference $\theta = \pi/2$, θ is decreased gradually. For $\theta = 0$ we end up in an in-phase quantum pump with two time periodic parameters, which are varied with the same signal, i.e. oscillate in phase. The in-phase quantum pump is sometimes also called single parameter quantum pump in the literature [Cav09], since it might be realized by one periodically varying external field controlled by a single gate voltage experimentally [Kae08]. Here we use a different nomenclature, where a single parameter pump is defined by having only one time periodic model parameter. It will be discussed in the next section.

The whole range of driving frequency

The pumped charge Q is depicted for the whole range of possible driving frequency in the left, top panel of Fig. 8.3 for a small driving amplitude. Since the definition of η as the enclosed area in the phase space loses its meaning when leaving the small driving amplitude and frequency regime, for a useful comparison the pumped charge is scaled by the sinusoidal part of the amplitude of the effective coupling $\Delta\Gamma_{1d} = \frac{\Delta\tau}{2\tau_0} T_K$ and the amplitude of the onsite energy $\Delta\epsilon$.

For the maximal phase difference $\theta = \pi/2$, Q is maximal in the adiabatic limit and decreases monotonously and rapidly as the driving frequency Ω approaches the low energy scale T_K . Independent of the phase difference, no charge is pumped in the limit of large driving frequency, already at $\Omega = 10 T_K$ a negligibly small pumped charge is obtained. As θ decreases, the function becomes non-monotonic and establishes a minimum with a negative sign, such that for $\theta = 0$, maximal charge is pumped in the opposite direction for a moderate driving frequency of $\Omega \lesssim T_K$ [Cro12a]. The in-phase pump can no longer be understood in terms of a peristaltic pump but rather as a consequence of Ω being of the same scale as the hybridization Γ_{1d} , such that the pumped charge vanishes in the adiabatic limit. The consequence of the interaction on the behavior manifests mainly in the renormalization of the low energy scale T_K , since a finite pumped charge is only obtained in the small to intermediate regime, where Ω has no or only a small effect on the parameter renormalization.

Next, the pumped charge for the same setup is compared with a comparably large driving amplitude of $\Delta\tau/\tau_0 = \Delta\epsilon/T_K = 0.9$. The phase difference θ is decreased as before. This is depicted in the right, top panel of Fig. 8.3. Here we refrain from reducing the driving frequency below $\Omega/T_K = 0.1$ to avoid numerical instabilities. The pumped charge (scaled by the amplitudes as before) is diminished compared to the small amplitude limit for the same setup with a phase difference of $\theta = \pi/2$. The qualitative behavior is the same as before, exhibiting maximal pumping towards the adiabatic regime, which decreases with increasing Ω and no pumping is observed in the large Ω regime. With decreasing phase difference the same non-monotonic behavior is developed as before, where the in-phase setup shows maximal pumping in the opposite direction in the moderate driving frequency regime. The interaction manifests again in the renormalization of the low energy scale T_K , only.

The whole range of driving amplitude

The effect of the driving amplitude on the pumped charge is examined in the adiabatic limit for $\Omega/(2\pi T_K) = 0.01$ (left, bottom panel of Fig. 8.3) and for moderate driving frequency $\Omega/T_K = 1$. (right, bottom panel of Fig. 8.3). In the adiabatic limit the pumped charge per $\Delta\Gamma_{1d}\Delta\epsilon$ for $\theta = \pi/2$ decreases with increasing pumping amplitude, where the pumped charge is about half its initial value at around $\Delta\tau/\tau_0 = 0.8$. As the initial Q value in the small driving amplitude limit diminishes with decreasing phase difference θ , the negative slope reduces accordingly. For the in-phase quantum pump ($\theta = 0$), the initial value is negative (indicating the opposite direction of the pumped charge as discussed), the absolute value of pumped charge is lowered as well with increasing driving amplitude, but the respective slope is much smaller. The impact of the interaction is again covered by the correct scaling with the renormalized T_K . For a moderate driving frequency the pumped charge in the limit of small $\Delta\tau/\tau_0$ is smaller than observed for $\Omega/(2\pi T_K) = 0.01$. The pumped charge for the in-phase quantum pump equals the one for $\theta = \pi/2$ in the small driving amplitude (but in the opposite direction), where the pumped charge for the in-phase pump diminishes less strongly with increasing amplitude. The pumped charge for all phase differences between them is diminished accordingly. While the main interaction effect is still covered by the renormalization of T_K , this frequency regime shows the largest offset, as can be already observed in the panels of the upper

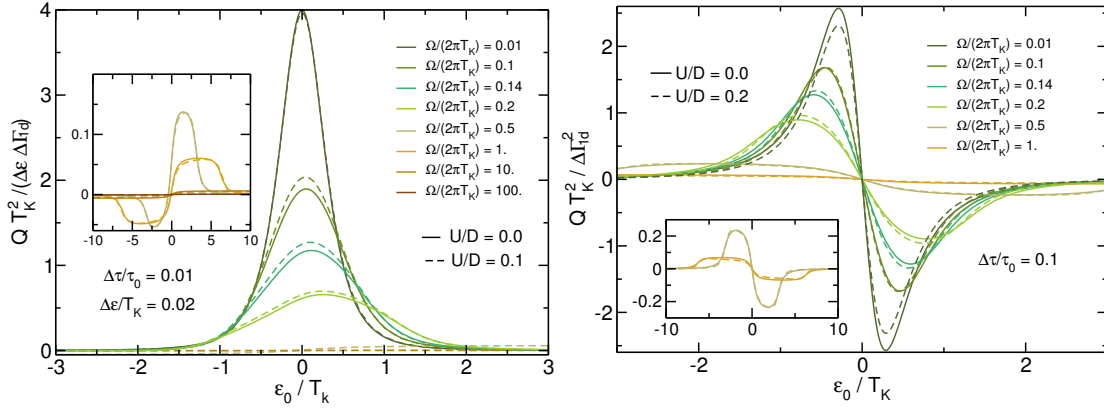


Figure 8.4: Pumped charge for both pump protocols plotted against the onsite energy for several values of driving frequency for $U/D = \{0, 0.1, 0.2, \}$ with $T_K/D = 2.5 \cdot 10^{-5}$, $T_K/D = 4.62 \cdot 10^{-5}$ and $T_K/D = 7.93 \cdot 10^{-5}$, respectively. With increasing Ω the maximal pumped charge for Protocol I (left panel) is decreased and shifted to positive onsite energy ϵ_0 . In intermediate frequency regimes maximums are developed non-symmetrically around the particle hole symmetric point. This is contrasted to pumped charge of Protocol II (right panel), which is decreased as well but stays symmetrically around the particle hole symmetric point.

row.

Off the particle hole symmetric point

All previous considerations are made at a zero mean onsite energy, as for the initial peristaltic pump it has been identified as maximal pumping point. Next, it is investigated if this still holds true out of the adiabatic regime. The pumped charge as a function of onsite energy for several values of Ω is depicted in the left panel of Fig.8.4. With increasing driving frequency the pumped charge decreases and the peak becomes broader, with the maximum slightly shifted towards positive onsite energies breaking the symmetry observed in the adiabatic limit. For intermediate driving frequencies $\Omega \approx T_K$ (see inset) small maximums away from the particle hole symmetric point are featured. In contrast to this, the right panel pictures the pumped charge for Protocol II, which equally reduces with increasing driving frequency, but stays symmetrical around ϵ_0 due to the symmetrical driving setup. Consistent with the previous observation the applied interaction has almost no effect on the pumped charge Q besides the renormalization of T_K .

8.4 Quantum pumps: Single parameter pump

A single parameter pump is realized here by driving only the left hopping with a sinusoidal signal as

$$\tau_L(t) = \tau_0 + \Delta\tau \sin(\Omega t) \quad (8.4.1)$$

at a finite $\epsilon \neq 0$. Left and right reservoir are held at the same chemical potential, such that a finite mean current only arises due to the periodic oscillation of the left hopping. All the renormalization of the parameters discussed for Protocol 1 in Section 7.5.4 of the previous chapter holds here, revealing one interesting question: Is there an observable reflecting the power law of the Fourier components of the hopping? Additionally an obvious key interest lies in the mean current flowing through the dot in order to check whether or not a pump is realized in this setup. This is supported by an analytic expression for the mean current derived in an effective model employing the replica picture. Finally, we like to better understand the conditions under which a finite mean current can be obtained in this setup by using an alternative method and supplement the previous findings with a perturbative treatment in Floquet-Liouville space.

8.4.1 Susceptibility

The renormalization and the resulting power law in the higher harmonics of the hopping matrix element have been discussed in Section 7.5.4. An obvious choice for an observable, where this power law might manifest in is the charge susceptibility χ , because we know from the time independent case that the respective power law of τ_0 is reflected in χ . To support this idea, the charge susceptibility is calculated to the leading order in p in the effective one site dot structure. This does not change the observed physics, but simplifies significantly the calculation, as the initial three by three matrix in the site indices reduces to a scalar. We thus only have to consider the Floquet index here. The retarded self-energy is calculated as $\Sigma_{L,01}^{\text{ret}}(\omega) = \tau_{L,0}g_{00}\tau_{L,1} + \tau_{L,1}g_{11}\tau_{L,0}$. In the one site dot structure the retarded and Keldysh self-energy in the $k = 0, \pm 1$ subspace are

$$\begin{aligned}\Sigma_{L,00}^{\text{ret}}(\omega) &= \Sigma_{L,11}^{\text{ret}} = \Sigma_{L,-1-1}^{\text{ret}} = -i\Gamma_{1d} \\ \Sigma_{L,01}^{\text{ret}}(\omega) &= \Sigma_{L,-10}^{\text{ret}}(\omega) = -2i\Gamma_{1d} \frac{\tau_{L,1}}{\tau_{L,0}} \\ \Sigma_{L,10}^{\text{ret}}(\omega) &= \Sigma_{L,0-1}^{\text{ret}}(\omega) = -2i\Gamma_{1d} \frac{\tau_{L,-1}}{\tau_{L,0}}\end{aligned}\quad (8.4.2)$$

and accordingly

$$\begin{aligned}\Sigma_{L,00}^K(\omega) &= 4i\Gamma_{1d} [\Theta(-\omega) - 1/2] \\ \Sigma_{L,11}^K(\omega) &= 4i\Gamma_{1d} [\Theta(-\omega - \Omega) - 1/2] \\ \Sigma_{L,-1-1}^K(\omega) &= 4i\Gamma_{1d} [\Theta(-\omega + \Omega) - 1/2] \\ \Sigma_{L,01}^K(\omega) &= \Sigma_{L,-10}^K(\omega + \Omega) = 4i\Gamma_{1d} \frac{\tau_{L,1}}{\tau_{L,0}} [\Theta(-\omega) - 1/2] + 4i\Gamma_{1d} \frac{\tau_{L,1}}{\tau_{L,0}} [\Theta(-\omega - \Omega) - 1/2] \\ \Sigma_{L,10}^K(\omega) &= \Sigma_{L,0-1}^K(\omega - \Omega) = 4i\Gamma_{1d} \frac{\tau_{L,-1}}{\tau_{L,0}} [\Theta(-\omega) - 1/2] + 4i\Gamma_{1d} \frac{\tau_{L,-1}}{\tau_{L,0}} [\Theta(-\omega - \Omega) - 1/2] .\end{aligned}\quad (8.4.3)$$

With these, the retarded Green's functions

$$\begin{aligned}G_{00}^{\text{ret}}(\omega) &= (\omega - \epsilon_0 - 2i\Gamma_{1d})^{-1} \\ G_{11}^{\text{ret}}(\omega) &= (\omega + \Omega - \epsilon_0 - 2i\Gamma_{1d})^{-1} \\ G_{-1-1}^{\text{ret}}(\omega) &= (\omega - \Omega - \epsilon_0 - 2i\Gamma_{1d})^{-1} \\ G_{01}^{\text{ret}}(\omega) &= G_{-10}^{\text{ret}}(\omega + \Omega) = -(\omega - \epsilon_0 - 2i\Gamma_{1d})^{-1} \left(-2i\Gamma_{1d} \frac{\tau_{L,1}}{\tau_{L,0}} \right) (\omega + \Omega - \epsilon_0 - 2i\Gamma_{1d})^{-1} \\ G_{10}^{\text{ret}}(\omega) &= G_{0-1}^{\text{ret}}(\omega - \Omega) = -(\omega + \Omega - \epsilon_0 - 2i\Gamma_{1d})^{-1} \left(-2i\Gamma_{1d} \frac{\tau_{L,-1}}{\tau_{L,0}} \right) (\omega - \epsilon_0 - 2i\Gamma_{1d})^{-1}\end{aligned}\quad (8.4.4)$$

and the Keldysh Green's functions

$$\begin{aligned}G_{00}^K(\omega) &= (\omega - \epsilon_0 - 2i\Gamma_{1d})^{-1} \{8i\Gamma_{1d} [\Theta(\omega) - 1/2]\} (\omega - \epsilon_0 + 2i\Gamma_{1d})^{-1} \\ G_{11}^K(\omega) &= (\omega + \Omega - \epsilon_0 - 2i\Gamma_{1d})^{-1} \{8i\Gamma_{1d} [\Theta(-\omega - \Omega) - 1/2]\} (\omega + \Omega - \epsilon_0 + 2i\Gamma_{1d})^{-1} \\ G_{-1-1}^K(\omega) &= (\omega - \Omega - \epsilon_0 - 2i\Gamma_{1d})^{-1} \{8i\Gamma_{1d} [\Theta(-\omega + \Omega) - 1/2]\} (\omega - \Omega - \epsilon_0 + 2i\Gamma_{1d})^{-1} \\ G_{01}^K(\omega) &= G_{-10}^K(\omega + \Omega) = -\frac{8i\Gamma_{1d} [\Theta(-\omega) - 1/2]}{\omega - \epsilon_0 - 2i\Gamma_{1d}} \frac{1}{\omega + \Omega - \epsilon_0 + 2i\Gamma_{1d}} \frac{-2i\Gamma_{1d}}{\omega - \epsilon_0 - 2i\Gamma_{1d}} \frac{\tau_{L,1}}{\tau_{L,0}} \\ &\quad - \frac{\{8i\Gamma_{1d} [\Theta(-\omega - \Omega) - 1/2]\}}{\omega - \epsilon_0 - 2i\Gamma_{1d}} \frac{1}{\omega + \Omega - \epsilon_0 + 2i\Gamma_{1d}} \frac{-2i\Gamma_{1d}}{\omega + \Omega - \epsilon_0 - 2i\Gamma_{1d}} \frac{\tau_{L,1}}{\tau_{L,0}} \\ G_{10}^K(\omega) &= G_{0-1}^K(\omega - \Omega) = -\frac{8i\Gamma_{1d} [\Theta(-\omega) - 1/2]}{\omega - \epsilon_0 - 2i\Gamma_{1d}} \frac{1}{\omega + \Omega - \epsilon_0 + 2i\Gamma_{1d}} \frac{-2i\Gamma_{1d}}{\omega - \epsilon_0 - 2i\Gamma_{1d}} \frac{\tau_{L,-1}}{\tau_{L,0}} \\ &\quad - \frac{\{8i\Gamma_{1d} [\Theta(-\omega - \Omega) - 1/2]\}}{\omega - \epsilon_0 - 2i\Gamma_{1d}} \frac{1}{\omega + \Omega - \epsilon_0 + 2i\Gamma_{1d}} \frac{-2i\Gamma_{1d}}{\omega + \Omega - \epsilon_0 - 2i\Gamma_{1d}} \frac{\tau_{L,-1}}{\tau_{L,0}}\end{aligned}\quad (8.4.5)$$

are calculated.

The first higher harmonic of the charge susceptibility is defined as

$$\chi_1 = \lim_{\epsilon_0 \rightarrow 0} \frac{dn_1}{\epsilon_0}. \quad (8.4.6)$$

The respective harmonic of the onsite energy is calculated in the one site dot structure to the order p ,

$$\begin{aligned} n_1 &= \frac{1}{4\pi i} \int d\omega G_{01}^K(\omega) \\ &= \frac{1}{4\pi i} \int d\omega \left\{ -\frac{8i\Gamma_{1d}[\Theta(-\omega) - 1/2]}{\omega - \epsilon_0 - 2i\Gamma_{1d}} \frac{-2i\Gamma_{1d}}{\omega + \Omega - \epsilon_0 + 2i\Gamma_{1d}} \frac{1}{\omega - \epsilon_0 + 2i\Gamma_{1d}} \frac{\tau_{L,1}}{\tau_{L,0}} \right. \\ &\quad \left. - \frac{8i\Gamma_{1d}[\Theta(-\omega - \Omega) - 1/2]}{\omega - \epsilon_0 - 2i\Gamma_{1d}} \frac{-2i\Gamma_{1d}}{\omega + \Omega - \epsilon_0 - 2i\Gamma_{1d}} \frac{1}{\omega + \Omega - \epsilon_0 + 2i\Gamma_{1d}} \frac{\tau_{L,1}}{\tau_{L,0}} \right\} \\ &= \frac{8\Gamma_{1d}}{4\pi i} \frac{\tau_{L,1}}{\tau_{L,0}} \left\{ \frac{3i}{2\pi(4i\Gamma_{1d} + \Omega)} \frac{1}{4i\Gamma_{1d}} - \frac{i}{2\pi\Omega(4i\Gamma_{1d} + \Omega)} + \frac{i}{2\pi(4i\Gamma_{1d}\Omega)} \right. \\ &\quad + \frac{1}{(4i\Gamma_{1d} + \Omega)4i\Gamma_{1d}} [\ln(-\epsilon_0 - 2i\Gamma_{1d}) - \ln(-\epsilon_0 + 2i\Gamma_{1d})] \\ &\quad + \frac{1}{(4i\Gamma_{1d} + \Omega)\Omega} [\ln(-\epsilon_0 + \Omega + 2i\Gamma_{1d}) - \ln(-\epsilon_0 - \Omega - 2i\Gamma_{1d})] \\ &\quad \left. - \frac{1}{4i\Gamma_{1d}\Omega} [\ln(-\epsilon_0 + 2i\Gamma_{1d}) - \ln(-\epsilon_0 - 2i\Gamma_{1d})] \right\}. \end{aligned} \quad (8.4.7)$$

Taking the derivative with respect to the onsite energy ϵ_0 and employing the limit $\epsilon_0 \rightarrow 0$, leads to

$$\chi_1 = \frac{2\Gamma_{1d}^2}{i\pi} \frac{\tau_{L,1}}{\tau_{L,0}} \left[\frac{-1}{4\Gamma_{1d}^2} \left(\frac{1}{4i\Gamma_{1d} + \Omega} + \frac{1}{\Omega} \right) - \frac{2}{2i\Gamma_{1d} + \Omega} \frac{1}{\Omega(4i\Gamma_{1d} + \Omega)} \right] \quad (8.4.8)$$

to the leading order in p .

In the large driving limit of $\Omega \gg \Gamma_{1d}$, this yields

$$\chi_1 \approx -\frac{1}{\pi i} \frac{\tau_{L,1}^{\text{ren}}}{\tau_{L,0}^{\text{ren}}} \frac{1}{\Omega}, \quad (8.4.9)$$

where the parameter are substituted by the renormalized one in the last step. The resulting expression suggests that the power law behavior of $\tau_{L,1}$ is directly reflected in the first higher harmonic of the charge susceptibility.

In the upper panel of Fig. 8.5 the logarithmic derivative of the full numerical solution of χ_1 (solid line) is depicted together with the analytic prediction (dashed line) color coded for the different values of U . Even though for small absolute values of the interaction ($|U/D| \leq 0.1$) the logarithmic derivative shows a constant value over an order of magnitude of Ω indicating power law behavior, its value does not coincide with the analytic prediction. Furthermore, the plateau vanishes with increasing interaction. Thus, the numerical solution does not exhibit the predicted power law. This renders a further discussion of the analytic expression necessary.

The lower panel of Figure 8.5 shows the absolute value of χ_1 comparing the numerical solution (solid line) and the analytic description (symbols) in the high driving frequency and adiabatic limit (inset). The analytic expression is shown here in three different ways: (A) The numerical calculated τ_k are inserted in the analytic expression (circles). (B) The analytic expression is used with the analytic expressions for all renormalized τ_k (pluses). (C) The analytic expressions is used where τ_0 is not fed back by its analytic expression but via T_K calculated from the equilibrium charge susceptibility (filled dots).

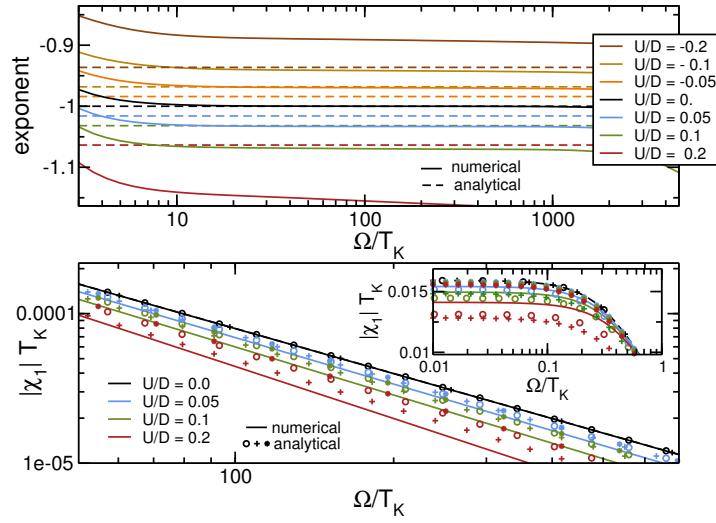


Figure 8.5: Analytic expression (symbols) and numerical solution (solid line) of the first Fourier coefficient of the charge susceptibility are compared revealing no power law behavior in χ_1 for $U/D = \{-0.2, -0.1, -0.05, 0, 0.05, 0.1, 0.2\}$ with $T_K/D = 5.54 \cdot 10^{-6}$, $T_K/D = 1.24 \cdot 10^{-5}$, $T_K/D = 1.78 \cdot 10^{-5}$, $T_K/D = 2.5 \cdot 10^{-5}$, $T_K/D = 3.43 \cdot 10^{-5}$, $T_K/D = 4.62 \cdot 10^{-5}$ and $T_K/D = 7.93 \cdot 10^{-5}$, respectively. The upper panel shows the logarithmic derivative of the full numerical solution not exhibiting the power law as predicted by the analytic expression (see main text for details). The lower panel compares full numerical solution and analytic prediction for $|\chi_1|$. While the non-interacting curve is full captured by the analytic expression, with increasing interaction U higher order corrections become relevant and spoil the analytic description. See main text for the description of the distinct analytic expressions.

The full numerical solution includes the leading order of U correctly due to the chosen truncation, but also partially includes higher order corrections. For the small driving amplitude limit no assumptions are made in the numerical flow equation, i.e. p is included to all orders. On the other hand, the analytic expressions is correct to the leading order of U and p . Furthermore, for its derivation an effective one site dot structure is employed.

For the noninteracting case the analytic expression captures the numerical solution, exemplifying the mere expression to be correct. In this case the different analytic approaches coincide. With increasing interaction nevertheless the analytic description becomes poorer, revealing higher order corrections in U to play a not negligible role. Hence three different approaches are used: While the purely analytic expressions ((B), pluses) captures the leading order U , the expressions (A) (circles) and (C) (filled dots) include the (partial) higher corrections (of the full flow equation) through the numerically determined τ_k or respectively T_K . These two further demonstrate the subtle higher order corrections in U for the definitions of T_K (compare Eqs. (3.5.5) and (7.1.7)). As a consequence, the different analytic approaches lead to the same qualitative behavior, but different quantitative values.

From the analytic description, where the numerically calculated τ_k are fed back ((A), circles) we can derive that the mismatch between analytic description and full numerical solution not only arises from higher order corrections in U to τ_k itself, but also to higher order corrections in Up to the one site effective model.

We thus deduce that the higher order corrections in Up to the first higher harmonic of the charge susceptibility are not negligible here, such that the analytic calculations employed does not capture the numerical solution. Higher order calculations in p would be required to clarify their contribution, but moreover higher order calculations in U would be necessary to investigate whether the correct exponent of $|\chi_1|$ includes higher order contributions in U with a large factor.

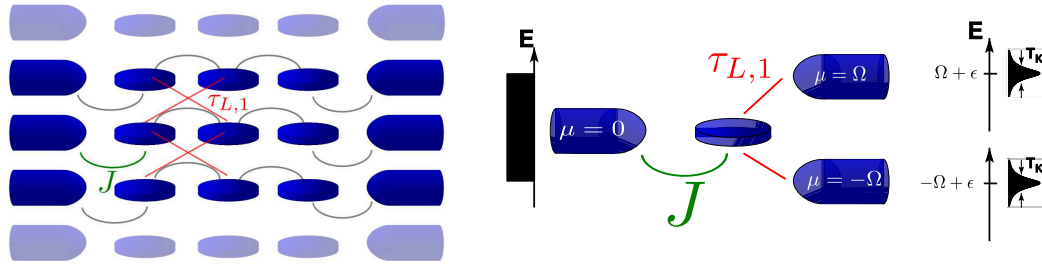


Figure 8.6: For the derivation of an analytic expression of the current the replica picture is employed (left panel). Identifying the main contribution to the current flowing from the left reservoir into the dot, the system can be condensed to be an effective three terminal setup as depicted in the right panel. Applying the Landauer - Büttiker formula to this situation leads to the correct analytic description.

8.4.2 Pumping power

A single parameter pump is realized if a non-vanishing pumped charge is observed even though only a single parameter is varied periodically in time and no bias voltage is applied. We start with the derivation of an analytic expression for the mean current in this setup employing the replica picture and subsequently examine the numerical solution for power law behavior.

Current formula

The main goal is to find an analytic expression for the pumping power $J_{L,k=0}$ to order p^2 and in the high driving frequency regime. The replica picture as discussed in Section 7.5.6 is employed for the derivation where the Floquet index k takes the role of an additional spatial index. It maps the initial, time periodically driven, one-dimensional system to a two-dimensional static system, where an infinite number of replicas are included. With the sinusoidal driving of $\tau_L(t)$ solely $\tau_{L,\pm 1}$ is non-zero, which thus couples only neighboring replicas. The mapping is sketched in the left panel of Fig. 8.6.

For the analytic description of the current J_L leaving the left reservoir through the central channel $k = 0$ of the mapped system to the order p^2 , only the replicas $k = \pm 1$ are of relevance, all other replicas can be neglected. There is no mean current to the order p^0 , because the left and right reservoirs are held at the same chemical potential. A finite mean current only arises due to the periodic oscillation of the left hopping and hence results from temporary excursions of the particles in the $k = \pm 1$ channels (and back) leading to a contribution of $\mathcal{O}(p^2)$.

For a finite current, the particle hole symmetry needs to be broken (by a finite onsite energy) and only those processes contribute, which break left right symmetry. Only a single process can be identified to fulfill this: The particle tunnels from the first side of the $k = 0$ channel to the second side of the $k = \pm 1$ channel and back. Additionally the first side of the $k = 0$ channel is coupled much stronger to the left reservoir $\sim D$ than to the right, central site ($\sim \tau_0^2/D$), which allows to neglect the coupling to the right side. As a result the effective model is condensed to the three terminal setup depicted in the right panel of Figure 8.6. The (former first) site of the central channel is coupled on the left hand side to the reservoir with chemical potential $\mu = 0$ and a flat density of states and on the right hand side to two reservoirs with chemical potentials $\mu = \pm\Omega$ and a Lorentzian shaped density of states.

Using the standard Landauer-Büttiker formula for multi-terminal scattering problems [Lan96,

Büt86], one now finds

$$\begin{aligned}
 J_{L,k=0} &= \frac{1}{2\pi} \int_{-\infty}^{\infty} dE [f(E) - f(E - \Omega)] \frac{2}{D} \frac{|\tau_{L,1}|^2 T_K/2}{(E - \epsilon - \Omega)^2 + (T_K/2)^2} \\
 &\quad + \frac{1}{2\pi} \int_{-\infty}^{\infty} dE [f(E) - f(E + \Omega)] \frac{2}{D} \frac{|\tau_{L,1}|^2 T_K/2}{(E - \epsilon + \Omega)^2 + (T_K/2)^2}
 \end{aligned} \tag{8.4.10}$$

for $|\epsilon| \ll \Omega \ll D$ and $|\tau_{L,1}| = |\tau_{L,-1}|$ and where $T_K = 4\tau_0^2/D$.

For $T = 0$ this simplifies to

$$\begin{aligned}
 J_{L,k=0} &= \frac{1}{2\pi} \int_{-\infty}^{\infty} dE [\Theta(-E) - \Theta(-E + \Omega)] \frac{2}{D} \frac{|\tau_{L,1}|^2 T_K/2}{(E - \epsilon - \Omega)^2 + (T_K/2)^2} \\
 &\quad + \frac{1}{2\pi} \int_{-\infty}^{\infty} dE [\Theta(-E) - \Theta(-E - \Omega)] \frac{2}{D} \frac{|\tau_{L,1}|^2 T_K/2}{(E - \epsilon + \Omega)^2 + (T_K/2)^2} \\
 &= \frac{1}{2\pi} \left(\frac{|\tau_{L,1}|}{\tau_0} \right)^2 T_K \left[\arctan \left(\frac{2\epsilon}{T_K} \right) + \frac{1}{2} \arctan \left(\frac{2\Omega - 2\epsilon}{T_K} \right) - \frac{1}{2} \arctan \left(\frac{2\Omega + 2\epsilon}{T_K} \right) \right]
 \end{aligned} \tag{8.4.11}$$

An expansion in the limit of small driving frequency Ω yields the leading contribution $\sim \epsilon \Omega^2$, which shows that an adiabatic approach is insufficient to describe the pumped charge and thus underlines the relevance of the non-adiabatic physics at play. In the opposite limit of large driving frequency $\Omega \gg |\epsilon|$, plugging in the renormalized values for $\tau_{L,0}$ and $\tau_{L,1}$ yields

$$J_{L,k=0} \stackrel{\Omega \gg \epsilon}{\approx} \frac{1}{2\pi} \left(\frac{|\tau_{L,1}^{\text{ren}}|}{\tau_{L,0}^{\text{ren}}} \right)^2 T_K \arctan \left(\frac{2\epsilon}{T_K} \right). \tag{8.4.12}$$

Note the role of the onsite energy ϵ in the resulting expression: It is similar to the steady state expression for the time independent non-equilibrium system of an applied bias voltage (Eq. (8.1.2)), where the onsite energy takes the role of the bias voltage, such that no dc current flows without a finite onsite energy.

Finite pumping power and Power law

The power law in the driving frequency of the higher harmonics then manifests through $\tau_{L,1}^{\text{ren}}$ in the pumping power as

$$\frac{J_{L,k=0}}{T_K} \sim \left(\frac{\Omega}{T_K} \right)^{-2\alpha_J} \quad \alpha_J = \frac{U}{\pi D} + \mathcal{O}(U^2) \quad \Omega \gg T_K. \tag{8.4.13}$$

In the upper left panel of Fig. 8.7 the full numerical solution of the pumping power is depicted as a function of the driving frequency Ω . The finite value shows that a single parameter pump is realized by this setup already for a vanishing interaction. The current in case of finite interaction shows clear power law behavior as it increases/decreases with increasing Ω with U dependent slopes. For a more rigorous confirmation the logarithmic derivative is computed as $d \ln(J_{L,k=0})/d \ln(\Omega)$ and depicted in the lower left panel. The constant effective exponents over orders of magnitudes of Ω confirms a clear power law. The resulting exponent α_J is also shown on the right hand side as a function of the interaction and compared to the exponents of the previous chapter. Equally as observed for $\alpha_{k=1}$ the agreement with the analytic prediction is excellent, showing hardly any higher order corrections in U .

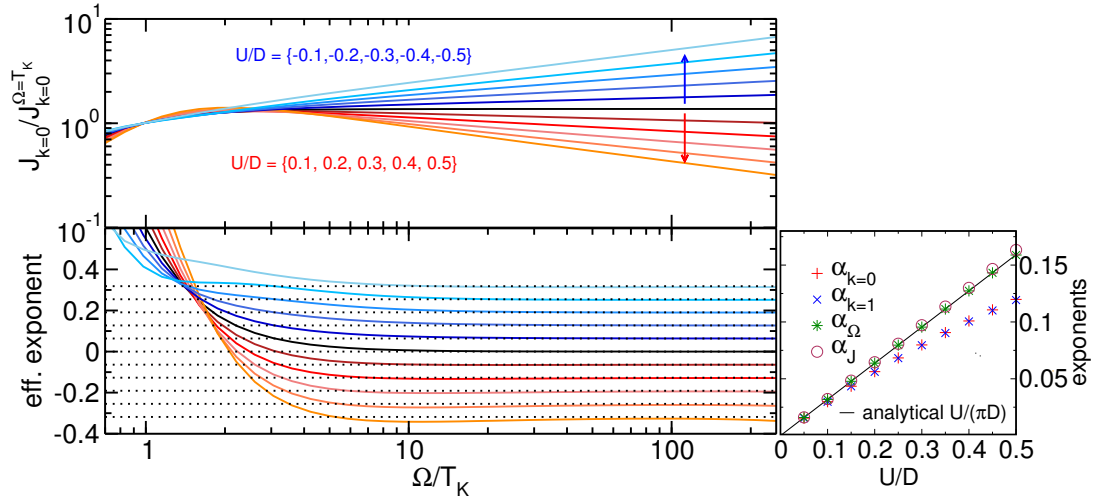


Figure 8.7: A single parameter pump is realized by sinusoidal variation of the left hopping for $U/D = \{-0.5, -0.4, -0.3, -0.2, -0.1, 0., 0.1, 0.2, 0.3, 0.4, 0.5\}$ with $T_K/D = 4.41 \cdot 10^{-7}$, $T_K/D = 8.4 \cdot 10^{-7}$, $T_K/D = 2.2 \cdot 10^{-6}$, $T_K/D = 5.54 \cdot 10^{-6}$, $T_K/D = 1.24 \cdot 10^{-5}$, $T_K/D = 2.5 \cdot 10^{-5}$, $T_K/D = 4.62 \cdot 10^{-5}$, $T_K/D = 7.93 \cdot 10^{-5}$, $T_K/D = 1.28 \cdot 10^{-4}$, $T_K/D = 1.96 \cdot 10^{-4}$ and $T_K/D = 2.86 \cdot 10^{-4}$, respectively. The upper left panel shows the finite mean current as a function of the driving frequency for $\Omega > T_K$ at $\epsilon_0 = 0.4 T_K$. The mean current reflects the power law behavior of $\tau_{L,k=1}$. The lower left panel shows the logarithmic derivative of the current revealing the power law behavior. On the right hand side, the exponents are shown as a function of the interaction U/D compared to the ones discussed for the renormalized parameters in the previous chapter.

8.4.3 Perturbation Theory in Liouville space: Mean current

The afore discussed finite current in this setup cannot be obtained by methods, which rely on tunneling rates (hybridization, Eq. (3.3.7)) with a single time argument as e.g. used in Ref. [Cav09] for the regime $\Omega \lesssim \Gamma_{1d}$. The single time dependency neglects the temporary excursions of the electron to the $k = \pm 1$ Floquet channel, which lead to the finite pump current, as discussed in the previous section. A different approach was put forward in Ref. [Bra08]. The authors consider the two-time structure of tunneling in and out, but integrate out one time argument using time scale separation in the anti-adiabatic limit. This approach allows to compute a finite current in a spinful single level setup in the anti-adiabatic limit for the same protocol as considered here.

In order to relate to these results and understand our setup in the context of quantum master equations, where the time scale of the kernel and the density matrix are separated, the master equation are set up in Floquet space. They have been introduced in Chapter 6, where the kernel $W_{ss'}^k$ is computed to the first order in tunneling rates (see Section 6.3.1). The mean value of the left current (Eq. (6.3.26)) is calculated numerically in this setup for the case of no interactions and the whole range of driving frequency Ω .

These results (solid lines) are compared in the left panel of Fig. 8.8 to the analytic formula (dashed line) obtained via Landauer-Büttiker formalism in the replica picture (Eq. (8.4.10)), which is valid for finite temperature as long as $T < \Omega$. The left mean current as a function of onsite energy is displayed. The quantum master equation is indeed able to reproduce the finite mean current with a correct qualitative behavior. The perturbative expansion in the tunneling rates improves with increasing temperature leading to a good agreement in the regime $T > T_K$, where the tunneling rate can be considered as a small parameter. Since the discussion of the renormalization in the previous chapter has shown that the relevant energy scale is $k\Omega$ and hence the mean value of the involved parameters is not influenced by Ω , a large temperature is still required for a correct perturbative treatment even in the limit $\Omega \gg T_K$.

The right panel of Fig. 8.8 compares the quantum master equation results to the analytic formula

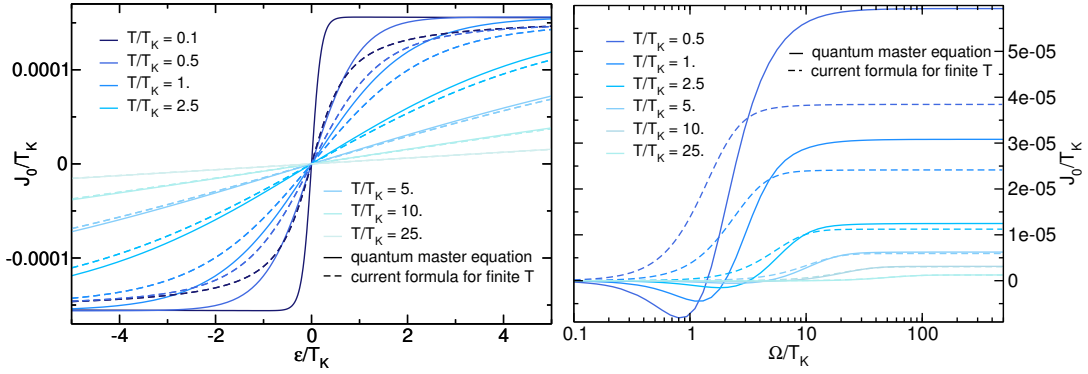


Figure 8.8: Mean left current of the non-interacting single parameter pump calculated perturbatively (in Γ) in Floquet Liouville space compared to the analytic expression (Eq. (8.4.10)) for $T_K = 0.01$. The left panel shows the results as a function of the onsite energy at a driving frequency $\Omega/(2\pi T_K) = 200$. The perturbative calculation obtains qualitatively good results, which with increasing temperature are in compliance with the analytic expression Eq. (8.4.10). The right panel shows the dependence on the driving frequency for $\epsilon_0 = 0.4T_K$, where a finite current can only be obtained in the high frequency limit. The perturbative calculation in the small temperature regime cannot be trusted for the whole range of driving frequency.

as a function of the driving frequency Ω . It needs to be noted that also the analytic expression might not be correct in the limit $T \gg \Omega$, it still can be used as a rough estimate. Again we observe that the compliance between the analytic expression and the numerical results increases with increasing temperature. The results of the quantum master equation in the small temperature regime do not only not coincide with the quantitative prediction in the high frequency regime, but even yield unreasonable results in the small to intermediate regime of a mean current that flows in the opposite direction.

8.5 Current and Conductance of non-sinusoidal signals

As discussed in Section 7.5.4 the renormalization of $\tau_L(t)$ leads to a changed effective lineshape and amplitude. We here discuss how this affects transport observables resulting from a non-sinusoidal signal for $\tau_L(t)$.

Designed signal

In the upper panel of Fig. 8.9 the conductance for the bare, i.e. non-interacting setup are considered for the designed input signals with

$$\tau_L(t) = \tau_0 + \sum_{k=-250}^{250} \frac{\Delta\tau}{\pi} k^{(-1+U/(\pi D))} e^{ik\Omega t} \quad (8.5.1)$$

for k , $\Delta\tau/\tau_0 = 0.1$. The initial signal is designed to cancel the renormalization effect and therefore U dependent, such that the renormalized signal is of rectangular form as it has been discussed in Sect. 7.5.4. The bare conductance reflects the form of the initial signal (compare Figure 7.8). The renormalized conductance signal shows a weak amplification ($U/D < 0$) or rectification ($U/D > 0$) in the high frequency regime, as discussed for the renormalized signal itself.

Triangular signal

The left hopping is varied as

$$\tau_L(t) = \tau_0 + \frac{4\Delta\tau}{i\pi^2} \sum_{k=-200}^{200} \text{sgn}(k)(-1)^{|k| \bmod 2} \frac{1}{k^2} e^{ik\Omega t} \quad (8.5.2)$$

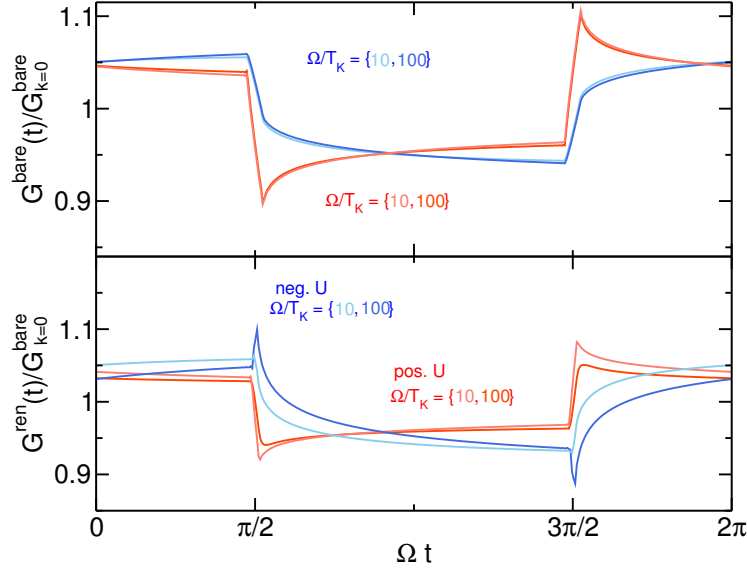


Figure 8.9: Conductance signal for the initial hopping (upper panel) with the line shape defined in Eq. (8.5.1) and the respective renormalized one (lower panel). The different initial signals depending on the sign of the interaction are reflected in the bare conductance. The renormalized conductance shows weak amplification or rectification in the anti-adiabatic frequency regime. The interaction is chosen to be $U/D = \pm 0.5$ with the emergent low energy scales $T_K/D = 4.41 \cdot 10^{-7}$ and $T_K/D = 2.865 \cdot 10^{-4}$, respectively.

i.e. with a triangular signal. The RG flow suppresses (enhances) higher harmonics of the signal with respect to the initial harmonics, resulting in a different line shape as discussed in Section 7.5.4. The renormalized signal is presented in the first panel of Fig. 8.10 for several values of positive and negative interaction. While the amplification (for $U/D < 0$) and rectification (for $U/D > 0$) of the signal amplitude is very pronounced, the change of line shape is only minor, it is still mainly characterized by a triangular form.

The linear conductance is considered for the same setup, where the static bias is chosen to be so small not to interfere with the renormalization as discussed. The resulting conductance is displayed in the middle panel of Fig. 8.10 for positive and negative interactions and compared to the bare conductance (black line) for no interaction. The line shape of the conductance for an intermediate interaction of $U/D = \pm 0.2$, only differs very little from the bare conductance, for positive interaction more than for negative interaction. However, for large interaction values of $U/D = \pm 0.5$ the difference is quite prominent, where especially the negative interaction demonstrates already a very distinct line shape. While the amplification/rectification effect of the renormalized signal is enhanced by the scaling with the renormalized mean value, this effect is less pronounced in the conductance as the mean value of the conductance is not renormalized at the particle hole symmetric point [Kar10c]. For large absolute values of the interaction, the amplitude of the renormalized conductance signal is reduced compared to the bare one independent of the sign of the interaction. This is consistent with the behavior the individual higher harmonics exhibit, which is discussed in the next section.

Next, the current is calculated for a finite mean onsite energy $\epsilon_0 = 0.4 T_K$ and displayed in the two lowest panel of Fig. 8.10. We observe a finite mean current of $J_0/T_K = 4.47 \cdot 10^{-5}$ for $U/D = 0$ ($J_0/T_K = \{2.81 \cdot 10^{-4}, 9.75 \cdot 10^{-5}, 2.07 \cdot 10^{-5}, 6.47 \cdot 10^{-6}\}$ for $U/D = \{-0.5, -0.2, 0.2, 0.5\}$) due to the finite onsite energy, where the current amplitudes are orders of magnitudes larger. The curves for positive and negative interaction have been separated to better illustrate the effects of the renormalization (note the different y-axis scales). It exhibits a strong renormalization of the amplitude reflecting the renormalization of the underlying hopping signal. Equally as the line shape

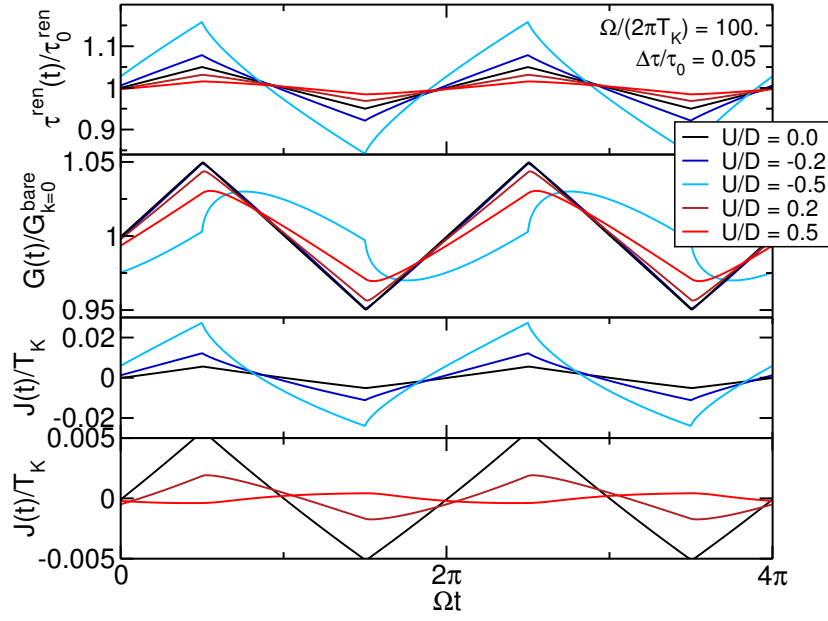


Figure 8.10: Renormalized signal $\tau^{\text{ren}}(t)$, conductance $G(t)$ and current $J(t)$ for a triangular signal for $\tau_L(t)$ for $U/D = \{-0.5, -0.2, 0., 0.2, 0.5\}$ with $T_K/D = 4.41 \cdot 10^{-7}$, $T_K/D = 5.54 \cdot 10^{-6}$, $T_K/D = 2.5 \cdot 10^{-5}$, $T_K/D = 7.93 \cdot 10^{-5}$ and $T_K/D = 2.86 \cdot 10^{-4}$, respectively. The current is calculated for a finite $\epsilon = 0.4 T_K$, renormalized signal and conductance for $\epsilon = 0$.

of the hopping signal, also the shape of the current signal is renormalized. While for the negative interaction the effective line shape of the current seems to resemble the form of the corresponding hopping signal, for positive interaction, a difference of the effective line shape to the bare signal is a little more pronounced, moreover a pronounced phase shift is observed for $U/D = 0.5$.

Nevertheless, we can only discuss our observation of the numerical results here, the complexity of the observables, where the current and conductance signal depends in a non-trivial way on the corresponding hopping signal, prevents us from a derivation of an analytic description of the according relation.

Scalability in the Conductance

Finally, we consider each of the higher harmonics of the renormalized conductance individually for two different applied signal forms of the left hopping

$$\begin{aligned} \tau_L(t) &= \tau_0 + \Delta\tau \sum_{k=0}^{10} \sin(k\Omega t) & (i) \\ \tau_L(t) &= \tau_0 + \Delta\tau \sum_{k=-250}^{250} \pi k^{(-1+U/(\pi D))} e^{ik\Omega t} \text{ for } k \text{ odd} & (ii) \end{aligned} \quad (8.5.3)$$

such that the first has even and odd higher harmonics, which are all of the same size, while the second, designed signal has only odd higher harmonics, which are separated by $\sim k^{-1+U/(\pi D)}$. The resulting higher harmonics of the conductance for $U/D = \{-0.2, 0, 0.2, 0.5\}$ are displayed in Fig. 8.11. Here we can benefit from the discussion of the renormalization of the Fourier coefficients of the hopping $\tau_{L,k}$ in Section 7.5.4, from which we know that the respective, effective energy scales is $k\Omega$. We hence multiply the k th coefficient's argument by a factor k . To compensate the $k^{-1+U/(\pi D)}$ dependency of the higher harmonics of the initial signal (ii), the higher harmonics are multiplied by $k^{1-U/(\pi D)}$ accordingly. In both cases the higher harmonics collapse, i.e. are completely rescaled by these multiplications. Despite the involved dependence on the dot parameters, the

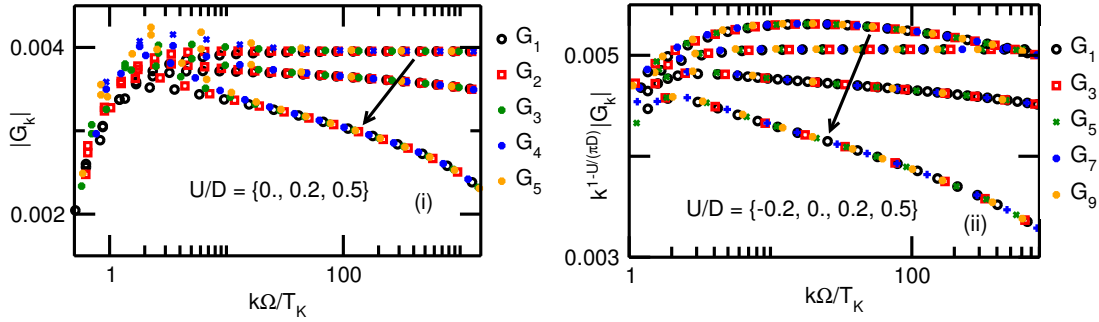


Figure 8.11: Higher harmonics of the resulting conductance if $\pi_L(t)$ is driven with two different signals (defined in Eq. (8.5.3)) with $\Delta\tau/\tau_0 = 0.05$. We choose $U/D = \{0., 0.2, 0.5\}$ with $T_K/D = 5.54 \cdot 10^{-6}$, $T_K/D = 2.5 \cdot 10^{-5}$, $T_K/D = 7.93 \cdot 10^{-5}$ and $T_K/D = 2.86 \cdot 10^{-4}$, respectively. A universal dependency on $k\Omega$ is observed.

coefficients thus depend on the energy scale $k\Omega$ in a universal way and the initial k dependency of the Fourier coefficients of the hopping is preserved in the renormalized higher harmonics of the linear conductance. Hence, we observe also for the time periodic case a universal scaling as observed in earlier, time independent setups of the interacting resonant level model [Doy07, Bor07, Bou08, Kar10c]. While the curves for a positive interaction ease off with increasing interacting, the curve for $U/D = -0.2$ in the right panel of Fig. 8.11 shows that the dependency is composed of more than one contribution, as it first increases with increasing $k\Omega$, but exhibits a maximum around $k\Omega \approx 20 T_K$ and then decreases. The coefficients seem to be a superposition of several contributions, which add up for $U/D > 0$, but generate the more involved dependency for $U/D < 0$. This is also consistent with the diminished amplitude of the renormalized conductance signal for $U/D = -0.5$, discussed in the previous section. Taking the logarithmic derivative of the numerical solution confirms that there is no power law in the higher harmonics of the conductance (not shown).

If the signal initially only consists of odd higher harmonics, whose initial value decreases for increasing Fourier index (as e.g. in the designed signal depicted in the right panel of Fig. 8.11), we see universal scaling even beyond the high frequency regime. This needs to be contrasted to the sum of sinusoidal functions (shown in the left panel of Fig. 8.11), where all (even and odd) higher harmonics are of the same initial size. The various higher harmonics interfere with each other around $\Omega \approx T_K$ yielding non-universal bumps in this regime (left panel of Fig. 8.11).

8.6 Conclusion

Transport within the steady state of the periodically driven interacting resonant level model has been discussed in this chapter. Based on the known transport of the time independent non-equilibrium for finite interaction, we have started with transport in the adiabatic limit with small amplitudes of the driven parameters creating quasi-static configurations. The known expression for the static, steady state occupancy have been extended to the periodic steady state by substituting the parameters by their time periodic ones for adiabatic driving. For a symmetrically applied bias voltage and an onsite energy adiabatically oscillating between the two chemical potentials, we have observed that the mean current at each point in time is characterized by the effectively static situation. As a consequence, the dependency of the mean current on the applied bias voltage, when the onsite energy either vanishes or is tuned to be on resonance with one of the chemical potentials, has been reproduced in the periodic setup as known from the time independent case.

Two parameter pumps in the whole regime of driving frequency and amplitude

One major interest in the time periodic setups focuses on quantum pumps, which are realized by two or more oscillating parameters where the according signals are phase shifted. The known adiabatic expressions for the pumped charge in two different traditional setups have been compared to our

results when including interaction. The analytic expressions have been generalized to the interacting setup by substituting the parameters in the relation by their renormalized ones, i.e. rescaling it with the renormalized low energy scale T_K . Starting from this, the pumped charge has been calculated in the protocol, where onsite energy and left hopping are varied periodically in time. The whole range of driving frequency and amplitude have been studied and results of the non-interacting and the interacting regime are compared. Additionally, the phase difference θ between both signals is gradually diminished towards an in-phase quantum pump with $\theta = 0$. For a meaningful comparison the pumped charge is divided by the driving amplitudes of the effective hybridization and the onsite energy.

The adiabatic limit with a small driving amplitude leads to the largest pumped charge per driving amplitude for a phase difference $\theta = \pi/2$. Increasing the driving frequency reduces the relative pumped charge, such that no pumped charge is observed in the high frequency regime. Decreasing the phase differences a non-monotonically reduction of Q as a function of driving frequency is observed. This yields up to an maximal pumped charge of the in-phase pump in the opposite direction (compared to the pump direction of the parametric pump) in the intermediate regime $\Omega \lesssim T_K$. This behavior is observed independent of the amount of the driving amplitude, but increasing the driving amplitude yields to a reduced pumped charge per driving amplitude.

Since a finite pumped charge is only obtained in the small to intermediate driving frequency regime, the main effect of the interaction is covered by the renormalization of the low energy scale T_K . When rescaling the pumped charge Q accordingly, the interacting and non-interacting curves coincide.

Pumping power in the single parameter pump reflects power law in Ω

Subsequently, a single parameter pump has been examined, which is realized by an harmonically varied left hopping. The first higher harmonics of the charge susceptibility has been computed analytically to the order $\mathcal{O}(p)$, which suggests to reflect the power law depending on the driving frequency. The full numerical solution however does not show this predicted power law behavior indicating that higher orders in Up , which are not captured by the analytic solution, but included in the numerical result, play a non-negligible role in this observable.

Next, the finite pumping power has been analyzed to demonstrate that indeed already without interaction a single parameter pump is achieved. An effective model has been employed, where it has been used explicitly that within the Floquet formalism a time periodic d -dimensional system can be mapped to $d + 1$ -dimensional system with an infinite number of copies of the initial system. The temporary excursions of the electrons to replicas of higher order Floquet channels have been identified to yield the finite dc current. It renders the pump of true quantum nature. An analytic expression of the mean current to the leading order of $\mathcal{O}(p^2)$ has been derived by condensing the system to a three-terminal setup, which has been treated by Landauer-Büttiker formalism. The resulting expression reveals that the pumping power reflects the Ω dependent power law in $\tau_{k \neq 0}$. The FRG results have been complemented by a calculation of the mean current in the same setup (but $U/D = 0$) with perturbation theory in Floquet Liouville space. Here the approximation of separated time scales of the kernel and the density operator is assumed. We have demonstrated that a finite mean current can already be obtained within this approach, where the mean current is in good agreement with the analytic expression obtained in the effective model for a finite temperature.

Current and conductance for non-sinusoidal signals: Scalability

In the last section current and conductance for non-sinusoidal signal forms have been discussed. Renormalized signal as well as resulting current and linear conductance have been discussed for an initial bare line shape of triangular form. Linear conductance has been considered for the designed signal that compensates the renormalization effect for an effective square signal, discussed in the previous chapter. The discussed amplification/rectification for the hopping is reflected minorly in the conductance, but the various higher harmonics show universal scaling when considered as a function of $k\Omega$.

References

Parts of the results discussed in this chapter were published in

A. K. Eissing, V. Meden, D. M. Kennes

'*Renormalization in Periodically Driven Quantum Dots*'

Phys. Rev. Lett. **116**, 026801 (2016)

A. K. Eissing, V. Meden, D. M. Kennes

'*Functional renormalization group in Floquet space*'

Phys. Rev. B **94**, 245116 (2016)

Conclusion & Outlook

Chapter 9

Conclusion & Outlook

The thesis at hand presents the methodical extension of the functional renormalization group method to Floquet space. It enabled us to describe the steady state of an interacting quantum dot with time periodic parameters. Introducing Floquet-Green's functions allowed for a transformation of the explicit time dependent flow equation to Floquet space. This way the FRG has been set up in a convenient basis to tackle the long time behavior in the whole regime of driving frequency and amplitude of interacting quantum dots.

The approach has been applied to the interacting resonant level model to tackle the following two main questions: What role does the driving frequency play in the renormalization group procedure as a possible infrared cutoff? And how does the interaction affect transport in these periodically driven systems?

Renormalization in the time periodically driven IRLM

We have started by examining the renormalization of the dot parameters in the limit of a small driving amplitude. The full numerical solution has been complemented by an analytic description of the renormalization, which has been calculated perturbatively to the leading order of the ratio of driving amplitude over its mean value. It has been shown that the Floquet channels decouple in this limit and thus can be considered independently. This allowed for an analytic treatment of all Fourier components of the renormalized parameters $\tau^{\text{ren}}(t)$ and $\epsilon^{\text{ren}}(t)$. Four different protocols have been examined, where different combinations of the hoppings and/or the onsite energy are chosen to be time periodic. $k\Omega$ has been identified to be the effective energy scale in these systems, rendering the mean value independent of the driving frequency. Moreover, it has been demonstrated that the renormalization of the mean value is described by the same differential equation as known for the steady state of the static, equilibrium situation. As a consequence, the same power law behavior was observed. The renormalization of the $k = 0$ component is thus completely independent of any time dependency regardless of the explicit protocol.

The most interesting effects have been observed in the setup, where only one hopping is chosen to be time periodic with an arbitrary signal. An analytic expression for the renormalized Fourier coefficients has been found. In the high frequency limit $k\Omega$ provides the infrared cutoff of the respective k th harmonic yielding a new power law in the argument $k\Omega$. It has interesting implications on the renormalized $\tau^{\text{ren}}(t)$: On the one hand each of the higher harmonics is renormalized differently (as a consequence of the dependency on k), which results in a renormalized signal of modified shape compared to the bare (non-interacting) one. Knowing the renormalization, the initial signal can be designed to cancel the interaction effect, such that the renormalized one is of desired form. On the other hand, the dependency on Ω of the infrared cutoff leads - depending on the sign of the interaction - to rectified or amplified signal amplitudes.

This can be contrasted to the protocol, where only the onsite energy is driven periodically in time with a sinusoidal signal. While the higher harmonic of the onsite energy itself is only weakly renormalized,

the renormalization flow of $\tau_{k=1}$ reveals an interesting and involved interplay of several energy scales not featuring a single infrared cutoff anymore. Even though this renders the analytic description slightly more complicated, an expression for its renormalization has been found in an effective model.

The renormalization for the two protocols, where either left and right hopping or left hopping and onsite energy are chosen to be time periodic, have been deduced from the two protocols where only a single parameter is periodic in time. The respective contributions have been added up, since there is no feedback of the involved parameters into each other to the considered order of U and p .

Renormalization beyond the small amplitude limit has been treated for an harmonically driven onsite energy. An effective reservoir distribution function has been defined in this setup. It is a sum of weighted Fermi function with arguments shifted by $k\Omega$. The resulting staircase appearance is specified by the ratio of driving amplitude and driving frequency and allowed us to examine the influence of the effective reservoir distribution function on the renormalization flow. We have focused on the renormalization of the $k = 0$ coefficient, where considering three different configurations it has been demonstrated that the energy scales set by the positions of the sharp edges are reflected as infrared scales in its RG flow. As a consequence, in this setup the driving frequency acts as an infrared cutoff already in the zeroth component in contrast to the small amplitude limit.

The functional renormalization group provides us with an unbiased RG procedure capable to tackle renormalization in the whole regime of driving frequency and amplitude. While the infrared cutoff $k\Omega$ in the small amplitude limit might be approachable by less general RG methods, FRG shows its full potential in those setups, where there is not a single infrared cutoff, but the flow is characterized by a combination of several energy scales.

Transport in the time periodically driven IRLM

A good knowledge of the renormalization of the parameters lays the foundation to the understanding of the transport in time periodically driven quantum dots. The starting point is the well studied adiabatic regime, where the driving frequency is chosen to be much smaller than any other energy scale. The resulting time dependent system can be considered as a sequence of effectively static situations. It allows to extend the static dot occupancy expression [And11a, And11b] to the time periodic steady state. Also the mean current has been observed to show similar behavior as a function of the bias voltage as known from the time independent steady state [Kar10c]. It has been shown that the known analytic expression of the pumped charge for the non-interacting parametric pump [Spl07] is still valid, when substituting the parameters by their renormalized ones.

Based on this, the parametric pump setup with the hopping and the onsite energy varied periodic in time has been examined out of the adiabatic and small amplitude limit. Here the phase differences between the applied signals is gradually reduced, leading up to an 'in-phase pump', where both parameters are varied in phase. The reduction of the phase difference yields a non-monotonic function in Ω , which when the phase difference vanishes, establishes a negative bump at around $\Omega \lesssim T_K$, i.e. leads to pumping in the opposite direction compared to the parametric pump. This qualitative behavior is observed for small as well as for large driving, where with increasing amplitude the relative pumped charge (per driving amplitude) reduces. Since a finite pumped charge is only observed in the small to intermediate regime of the driving frequency, the main renormalization effect is covered by the rescaling with the renormalized low energy scale T_K .

Next, a single parameter pump has been treated, realized by an harmonically driven hopping in the small amplitude limit. From the consideration of the renormalization in this setup, the power law behavior of the Fourier coefficients is known, motivating us to study the first higher harmonic of the charge susceptibility. It has been revealed that the observable cannot be described sufficiently by a first order calculation in the ratio of the amplitude and the mean value. While the analytic description predicts the charge susceptibility to reflect the power law of $\tau_{k=1}^{\text{ren}}$, this has not been

confirmed by the full numerical solution. It includes partially higher order contribution in U and all orders of p , which here have been demonstrated to play a non-negligible role.

However, the pumping power J_0 of the single parameter pump not only has been proven to be finite in the anti-adiabatic limit, but also reflects the power law dependency on the driving frequency. This has been confirmed by an analytic calculation of the mean current in an effective model of the time periodic systems. To investigate the prerequisites of a finite current in such a setup, it has been calculated with quantum master equations in the Floquet Liouvillian space for a finite temperature. Despite the approximation of a separated time scale for kernel and density matrix, a finite current has been obtained in the high driving frequency regime which is consistent with our analytic prediction for larger temperatures.

Finally, non-sinusoidal signals for the time periodic hopping have been applied and the resulting current and conductance in this setup were considered. While the involved dependency of the observables on the dot parameters prevents us from presenting analytic relations, the amplification/rectification as well as the change of the line shape is partially reflected in the renormalized signal of the current and the conductance. In addition, an universal dependency of the higher harmonics of the conductance on $k\Omega$ has been found.

The presented Floquet FRG has been proven to be a powerful tool to tackle the time periodic systems revealing interesting renormalization physics as well as making it feasible to consider transport in the interaction setup, where the frequency and the amplitude are unlimited.

Outlook

In this work we focused exclusively on the application of the developed method on the interacting resonant level. However, since the approach follows from a straightforward transformation of the explicitly time dependent flow equation [Ken12a] without any further assumptions, the method can be applied to other low-dimensional systems. Among others time periodically driven one-dimensional lattices constitute systems of particular interest, where the FRG has been vital in understanding, e.g. the boundary and impurity physics of Luttinger liquids in [Med08, Met12] and out-of [Jak07] equilibrium. This possible further route is already followed by Dante Kennes [Kenb].

Additionally, the presented approach relies on the lowest order truncation of the hierarchy of flow equations of the FRG. An extension to higher order truncation scheme is possible with a more general transformation to Floquet space [Tsu08] to treat the four time dependent two-particle vertex function. Nevertheless, the numerical effort to include the resulting full frequency dependency and a sufficient number of Fourier channels, is rather high rendering it necessary to use e.g. ladder approximations as presented in Ref. [Kar08, Jak10a] to keep it numerically manageable.

The perturbative (in Γ) calculation in Floquet-Liouville space has been set up under the assumption of the separation of the time scales of the kernel and the density operator which simplifies the calculation significantly. A full perturbation theory calculation including the search for the correct poles and branch cuts in the complex plane would be a next step. For a more comprehensive study and to include interaction, the real time renormalization group could be set up in Floquet space to complement the FRG results accordingly. First steps on this route have been pursued by Herbert Schoeller and Dante Kennes.

Supplements

Bibliography

- [Ale98] I. L. Aleiner and A. V. Andreev. *Adiabatic Charge Pumping in Almost Open Dots*. Phys. Rev. Lett. **81**, 1286 (1998).
- [And11a] S. Andergassen, M. Pletyukhov, D. Schuricht, H. Schoeller, and L. Borda. *Renormalization group analysis of the interacting resonant-level model at finite bias: Generic analytic study of static properties and quench dynamics*. Phys. Rev. B **83**, 205103 (2011).
- [And11b] S. Andergassen, M. Pletyukhov, D. Schuricht, H. Schoeller, and L. Borda. *Renormalization group analysis of the interacting resonant-level model at finite bias: Generic analytic study of static properties and quench dynamics - Erratum, Original article: [\[And11a\]](#)*. Phys. Rev. B **84**, 039905 (2011).
- [Arr05] L. Arrachea. *Green-function approach to transport phenomena in quantum pumps*. Phys. Rev. B **72**, 125349 (2005).
- [Arr06] L. Arrachea and M. Moskalets. *Relation between scattering-matrix and Keldysh formalisms for quantum transport driven by time-periodic fields*. Phys. Rev. B **74**, 245322 (2006).
- [Bor07] L. Borda, K. Vladár, and A. Zawadowski. *Theory of a resonant level coupled to several conduction-electron channels in equilibrium and out of equilibrium*. Phys. Rev. B **75**, 125107 (2007).
- [Bor08] L. Borda, A. Schiller, and A. Zawadowski. *Applicability of bosonization and the Anderson-Yuval methods at the strong-coupling limit of quantum impurity problems*. Phys. Rev. B **78**, 201301 (2008).
- [Bou08] E. Boulat, H. Saleur, and P. Schmitteckert. *Twofold Advance in the Theoretical Understanding of Far-From-Equilibrium Properties of Interacting Nanostructures*. Phys. Rev. Lett. **101**, 140601 (2008).
- [Bra08] M. Braun and G. Burkard. *Nonadiabatic Two-Parameter Charge and Spin Pumping in a Quantum Dot*. Phys. Rev. Lett. **101**, 036802 (2008).
- [Bro98] P. W. Brouwer. *Scattering approach to parametric pumping*. Physical Review B **58** 16, R10135 (1998).
- [Bru94] C. Bruder and H. Schoeller. *Charging effects in ultrasmall quantum dots in the presence of time-varying fields*. Phys. Rev. Lett. **72**, 1076 (1994).
- [Bru97] P. Brune, C. Bruder, and H. Schoeller. *Photon-assisted transport through ultrasmall quantum dots: Influence of intradot transitions*. Phys. Rev. B **56**, 4730 (1997).
- [Buk15] M. Bukov, L. D'Alessio, and A. Polkovnikov. *Universal high-frequency behavior of periodically driven systems: from dynamical stabilization to Floquet engineering*. Advances in Physics **64** 2, 139 (2015).
- [Büt86] M. Büttiker. *Four-Terminal Phase-Coherent Conductance*. Phys. Rev. Lett. **57**, 1761 (1986).

- [Büt94] M. Büttiker, H. Thomas, and A. Prêtre. *Current partition in multiprobe conductors in the presence of slowly oscillating external potentials*. Zeitschrift für Physik B Condensed Matter **94** 1, 133 (1994).
- [Cav09] F. Cavaliere, M. Governale, and J. König. *Nonadiabatic Pumping through Interacting Quantum Dots*. Phys. Rev. Lett. **103**, 136801 (2009).
- [Cit03] R. Citro, N. Andrei, and Q. Niu. *Pumping in an interacting quantum wire*. Phys. Rev. B **68**, 165312 (2003).
- [Cro12a] A. Croy and U. Saalman. *Nonadiabatic rectification and current reversal in electron pumps*. Phys. Rev. B **86**, 035330 (2012).
- [Cro12b] A. Croy, U. Saalman, A. R. Hernández, and C. H. Lewenkopf. *Nonadiabatic electron pumping through interacting quantum dots*. Phys. Rev. B **85**, 035309 (2012).
- [Dir33] P. A. M. Dirac. *The Lagrangian in Quantum Mechanics*. Physikalische Zeitschrift der Sowjetunion **3**, 64 (1933).
- [DiV95] D. P. DiVincenzo. *Quantum Computation*. Science **270** 5234, 255 (1995).
- [Doy07] B. Doyon. *New Method for Studying Steady States in Quantum Impurity Problems: The Interacting Resonant Level Model*. Phys. Rev. Lett. **99**, 076806 (2007).
- [Eid13] E. Eidelstein, D. Goberman, and A. Schiller. *Crossover from adiabatic to antiadiabatic phonon-assisted tunneling in single-molecule transistors*. Phys. Rev. B **87**, 075319 (2013).
- [Fey48] R. P. Feynman. *Space-Time Approach to Non-Relativistic Quantum Mechanics*. Rev. Mod. Phys. **20**, 367 (1948).
- [Fey49] R. P. Feynman. *Space-Time Approach to Quantum Electrodynamics*. Phys. Rev. **76**, 769 (1949).
- [Fey50] R. P. Feynman. *Mathematical Formulation of the Quantum Theory of Electromagnetic Interaction*. Phys. Rev. **80**, 440 (1950).
- [Fil81] V. Filyov, A. Tzvelik, and P. Wiegmann. *Thermodynamics of the s-d exchange model (Kondo problem)*. Physics Letters A **81** 2, 175 (1981).
- [Flo83] G. Floquet. *Sur les équations différentielles linéaires á coefficients périodiques*. Annales scientifiques de l'É.N.S. **2e série** tome 12, 47 (1883).
- [Gen15] M. Genske and A. Rosch. *Floquet-Boltzmann equation for periodically driven Fermi systems*. Phys. Rev. A **92**, 062108 (2015).
- [GL13] A. Gómez-León and G. Platero. *Floquet-Bloch Theory and Topology in Periodically Driven Lattices*. Phys. Rev. Lett. **110**, 200403 (2013).
- [Gri98] M. Grifoni and P. Hänggi. *Driven Quantum tunneling*. Phys Rep. **304**, 229 (1998).
- [Han07] R. Hanson, L. P. Kouwenhoven, J. R. Petta, S. Tarucha, and L. M. K. Vandersypen. *Spins in few-electron quantum dots*. Rev. Mod. Phys. **79**, 1217 (2007).
- [Hau13] F. Haupt, M. Leijnse, H. L. Calvo, L. Classen, J. Splettstoesser, and M. R. Wegewijs. *Heat, molecular vibrations, and adiabatic driving in non-equilibrium transport through interacting quantum dots*. physica status solidi (b) **250** 11, 2315 (2013).
- [Her09] A. R. Hernández, F. A. Pinheiro, C. H. Lewenkopf, and E. R. Mucciolo. *Adiabatic charge pumping through quantum dots in the Coulomb blockade regime*. Phys. Rev. B **80**, 115311 (2009).

-
- [Het95] M. H. Hettler and H. Schoeller. *Anderson Model Out of Equilibrium: Time-Dependent Perturbations*. Phys. Rev. Lett. **74**, 4907 (1995).
 - [Hil10] B. Hiltscher, M. Governale, and J. König. *Interference and interaction effects in adiabatic pumping through quantum dots*. Phys. Rev. B **81**, 085302 (2010).
 - [Hil11] B. Hiltscher, M. Governale, J. Splettstoesser, and J. König. *Adiabatic pumping in a double-dot Cooper-pair beam splitter*. Phys. Rev. B **84**, 155403 (2011).
 - [Jak07] S. G. Jakobs, V. Meden, and H. Schoeller. *Nonequilibrium Functional Renormalization Group for Interacting Quantum Systems*. Phys. Rev. Lett. **99**, 150603 (2007).
 - [Jak09] S. Jakobs. *Functional renormalization group studies of quantum transport through mesoscopic systems*. Ph.D. thesis, RWTH Aachen (2009).
 - [Jak10a] S. G. Jakobs, M. Pletyukhov, and H. Schoeller. *Nonequilibrium functional renormalization group with frequency-dependent vertex function: A study of the single-impurity Anderson model*. Phys. Rev. B **81**, 195109 (2010).
 - [Jak10b] S. G. Jakobs, M. Pletyukhov, and H. Schoeller. *Properties of multi-particle Green's and vertex functions within Keldysh formalism*. Journal of Physics A: Mathematical and Theoretical **43** 10, 103001 (2010).
 - [Jak14] S. G. Jakobs. *Keldysh formalism for nonequilibrium transport through quantum systems*. In *45th IFF Spring School: Computing Solids - Models, ab-initio methods and supercomputing* [Lec14].
 - [Kae08] B. Kaestner, V. Kashcheyevs, S. Amakawa, M. D. Blumenthal, L. Li, T. J. B. M. Janssen, G. Hein, K. Pierz, T. Weimann, U. Siegner, and H. W. Schumacher. *Single-parameter nonadiabatic quantized charge pumping*. Phys. Rev. B **77**, 153301 (2008).
 - [Kae15] B. Kaestner and V. Kashcheyevs. *Non-adiabatic quantized charge pumping with tunable-barrier quantum dots: a review of current progress*. Reports on Progress in Physics **78** 10, 103901 (2015).
 - [Kam00] A. Kaminski, Y. V. Nazarov, and L. I. Glazman. *Universality of the Kondo effect in a quantum dot out of equilibrium*. Phys. Rev. B **62**, 8154 (2000).
 - [Kar06] C. Karrasch. *Transport Through Correlated Quantum Dots - A Functional Renormalization Group Approach -*. Master's thesis, Georg-August Universität Göttingen (2006).
 - [Kar08] C. Karrasch, R. Hedden, R. Peters, T. Pruschke, K. Schönhammer, and V. Meden. *A finite-frequency functional renormalization group approach to the single impurity Anderson model*. Journal of Physics: Condensed Matter **20** 34, 345205 (2008).
 - [Kar10a] C. Karrasch. *The Functional Renormalization Group for Zero-Dimensional Quantum Systems in and out of Equilibrium*. Ph.D. thesis, RWTH Aachen (2010).
 - [Kar10b] C. Karrasch, S. Andergassen, M. Pletyukhov, D. Schuricht, L. Borda, V. Meden, and H. Schoeller. *Non-equilibrium current and relaxation dynamics of a charge-fluctuating quantum dot*. EPL (Europhysics Letters) **90** 3, 30003 (2010).
 - [Kar10c] C. Karrasch, M. Pletyukhov, L. Borda, and V. Meden. *Functional renormalization group study of the interacting resonant level model in and out of equilibrium*. Phys. Rev. B **81**, 125122 (2010).
 - [Kas12] O. Kashuba, H. Schoeller, and J. Splettstoesser. *Nonlinear adiabatic response of interacting quantum dots*. EPL **98** 5, 57003 (2012).

- [Kas13] O. Kashuba, D. M. Kennes, M. Pletyukhov, V. Meden, and H. Schoeller. *Quench dynamics of a dissipative quantum system: A renormalization group study*. Phys. Rev. B **88**, 165133 (2013).
- [Kena] D. M. Kennes. *Personal communication*.
- [Kenb] D. M. Kennes. *to be published*.
- [Ken11] D. M. Kennes. *A Renormalization Group Approach to the Time Evolution of Correlated Quantum Dots*. Master's thesis, RWTH Aachen (2011).
- [Ken12a] D. M. Kennes, S. G. Jakobs, C. Karrasch, and V. Meden. *Renormalization group approach to time-dependent transport through correlated quantum dots*. Phys. Rev. B **85**, 085113 (2012).
- [Ken12b] D. M. Kennes and V. Meden. *Quench dynamics of correlated quantum dots*. Phys. Rev. B **85**, 245101 (2012).
- [Ken13] D. M. Kennes, O. Kashuba, M. Pletyukhov, H. Schoeller, and V. Meden. *Oscillatory Dynamics and Non-Markovian Memory in Dissipative Quantum Systems*. Phys. Rev. Lett. **110**, 100405 (2013).
- [Ken14] D. M. Kennes. *Dynamics in Low-Dimensional Correlated Quantum Systems*. Ph.D. thesis, RWTH Aachen (2014).
- [Koh05] S. Kohler, J. Lehmann, and P. Hänggi. *Driven quantum transport on the nanoscale*. Phys. Rep. **406** 6, 379 (2005).
- [Kwa10] T. Kwapinski, S. Kohler, and P. Hänggi. *Dynamically broken symmetry in periodically gated quantum dots: charge accumulation and dc current*. Ukrainian Journal of Physics **55** 1 (2010).
- [Lan96] R. Landauer. *Spatial variation of currents and fields due to localized scatterers in metallic conduction (and comment)*. J. Math. Phys. **37** (1996).
- [Lar75] A. Larkin and Y. Ovchinnikov. *Nonlinear conductivity of superconductors in the mixed state*. Sov.Phys.JETP **41** 5 (1975).
- [Lec14] *45th IFF Spring School: Computing Solids - Models, ab-initio methods and supercomputing*. Forschungszentrum Jülich (2014).
- [Med02] V. Meden. *Funktionale Renormierungsgruppe* (2002).
- [Med08] V. Meden, S. Andergassen, T. Enss, H. Schoeller, and K. Schönhammer. *Fermionic renormalization group methods for transport through inhomogeneous Luttinger liquids*. New Journal of Physics **10** 4, 045012 (2008).
- [Mei92] Y. Meir and N. S. Wingreen. *Landauer Formula for the Current through an Interacting Electron Region*. Phys. Rev. Lett. **68**, 2512 (1992).
- [Met12] W. Metzner, M. Salmhofer, C. Honerkamp, V. Meden, and K. Schönhammer. *Functional renormalization group approach to correlated fermion systems*. Rev. Mod. Phys. **84**, 299 (2012).
- [Mos02] M. Moskalets and M. Büttiker. *Floquet scattering theory of quantum pumps*. Phys. Rev. B **66**, 205320 (2002).
- [Mos04a] M. Moskalets and M. Büttiker. *Adiabatic quantum pump in the presence of external ac voltages*. Phys. Rev. B **69**, 205316 (2004).

- [Mos04b] M. Moskalets and M. Büttiker. *Floquet scattering theory for current and heat noise in large amplitude adiabatic pumps*. Phys. Rev. B **70**, 245305 (2004).
- [Neg88] J. W. Negele. *Quantum many particle systems*. Addison-Wesley (1988).
- [Noz69] P. Nozières and C. T. de Dominicis. *Singularities in the X-Ray Absorption and Emission of Metals. III. One-Body Theory Exact Solution*. Phys. Rev. **178**, 1097 (1969).
- [Pek13] J. P. Pekola, O.-P. Saira, V. F. Maisi, A. Kemppinen, M. Möttönen, Y. A. Pashkin, and D. V. Averin. *Single-electron current sources: Toward a refined definition of the ampere*. Rev. Mod. Phys. **85**, 1421 (2013).
- [Pla04] G. Platero and R. Aguado. *Photon-assisted transport in semiconductor nanostructures*. Physics Reports **395** 1–2, 1 (2004).
- [Pol84] J. Polchinski. *Renormalization and effective lagrangians*. Nuclear Physics B **231** 2, 269 (1984).
- [Pot92] H. Pothier, P. Lafarge, C. Urbina, D. Esteve, and M. H. Devoret. *Single-Electron Pump Based on Charging Effects*. EPL (Europhysics Letters) **17** 3, 249 (1992).
- [Ren14] J. F. Rentrop, S. G. Jakobs, and V. Meden. *Nonequilibrium transport through a Josephson quantum dot*. Phys. Rev. B **89**, 235110 (2014).
- [Riw10] R.-P. Riwar and J. Splettstoesser. *Charge and spin pumping through a double quantum dot*. Physical Review B **82** 20, 205308 (2010).
- [Riw13] R.-P. Riwar, J. Splettstoesser, and J. König. *Zero-frequency noise in adiabatically driven interacting quantum systems*. Phys. Rev. B **87**, 195407 (2013).
- [Roc13] B. Roche, R.-P. Riwar, B. Voisin, E. Dupont-Ferrier, R. Wacquez, M. Vineta, M. Sanquer, J. Splettstoesser, and X. Jehl. *A two-atom electron pump*. Nature Communication **4**, 1581 EP (2013).
- [Sch80a] P. Schlottmann. *Simple spinless mixed-valence model. I. Coherent-hybridization states versus virtual-bound states*. Phys. Rev. B **22**, 613 (1980).
- [Sch80b] P. Schlottmann. *Simple spinless mixed-valence model. II. Solution of the isolated f -level problem*. Phys. Rev. B **22**, 622 (1980).
- [Sch82a] P. Schlottmann. *The Kondo problem. I. Transformation of the model and its renormalization*. Phys. Rev. B **25**, 4815 (1982).
- [Sch82b] P. Schlottmann. *The Kondo problem. II. Crossover from asymptotic freedom to infrared slavery*. Phys. Rev. B **25**, 4828 (1982).
- [Sch82c] P. Schlottmann. *The Kondo problem. III. The susceptibility and relaxation rate*. Phys. Rev. B **25**, 4838 (1982).
- [Sch94] H. Schoeller and G. Schön. *Mesoscopic quantum transport: Resonant tunneling in the presence of a strong Coulomb interaction*. Phys. Rev. B **50**, 18436 (1994).
- [Sch09] H. Schoeller. *A perturbative nonequilibrium renormalization group method for dissipative quantum mechanics*. The European Physical Journal Special Topics **168** 1, 179 (2009).
- [Sch11] H. Schoeller. *Lecture on Quantum statistics in nonequilibrium*. unpublished (2011).
- [Sch12] H. Schoeller. *Lecture on Real-time Renormalization Group and Application to Nonequilibrium Phenomena and Time Dynamics in Open Quantum Systems*. unpublished (2012).

- [Sch14] H. Schoeller. *Dynamics of Open Quantum Systems*. In *45th IFF Spring School: Computing Solids - Models, ab-initio methods and supercomputing* [Lec14].
- [Shi65] J. H. Shirley. *Solution of the Schrödinger Equation with a Hamiltonian Periodic in Time*. Phys. Rev. **138**, B979 (1965).
- [Spl05] J. Splettstoesser, M. Governale, J. König, and R. Fazio. *Adiabatic Pumping through Interacting Quantum Dots*. Phys. Rev. Lett. **95**, 246803 (2005).
- [Spl06] J. Splettstoesser, M. Governale, J. König, and R. Fazio. *Adiabatic pumping through a quantum dot with coulomb interactions: A perturbation expansion in the tunnel coupling*. Physical Review B **74** 8, 085305 (2006).
- [Spl07] J. Splettstoesser. *Adiabatic Pumping through Quantum Dots*. Ph.D. thesis, Scuola Normale Superiore and Ruhr-Universität Bochum (2007).
- [Ste08] G. Stefanucci, S. Kurth, A. Rubio, and E. K. U. Gross. *Time-dependent approach to electron pumping in open quantum systems*. Phys. Rev. B **77**, 075339 (2008).
- [Str05] M. Strass, P. Hänggi, and S. Kohler. *Nonadiabatic Electron Pumping: Maximal Current with Minimal Noise*. Phys. Rev. Lett. **95**, 130601 (2005).
- [Suz15] T. J. Suzuki and T. Kato. *Effects of Coulomb interaction on photon-assisted current noise through a quantum dot*. Phys. Rev. B **91**, 165302 (2015).
- [Swi99] M. Switkes, C. M. Marcus, K. Campman, and A. C. Gossard. *An Adiabatic Quantum Electron Pump*. Science **283** 5409, 1905 (1999).
- [Tay72] J. R. Taylor. *Scattering theory*. Wiley (1972).
- [Tho83] D. J. Thouless. *Quantization of particle transport*. Phys. Rev. B **27**, 6083 (1983).
- [Tsu08] N. Tsuji, T. Oka, and H. Aoki. *Correlated electron systems periodically driven out of equilibrium: Floquet + DMFT formalism*. Phys. Rev. B **78**, 235124 (2008).
- [Weg73] F. J. Wegner and A. Houghton. *Renormalization Group Equation for Critical Phenomena*. Phys. Rev. A **8**, 401 (1973).
- [Wet93] C. Wetterich. *Exact evolution equation for the effective potential*. Physics Letters B **301** 1, 90 (1993).
- [Wie88] C. Wiecekowsky. *Symanzik's improved actions from the viewpoint of the renormalization group*. Communications in Mathematical Physics **120** 1, 149 (1988).
- [Wil74] K. G. Wilson and J. Kogut. *The renormalization group and the expansion*. Physics Reports **12** 2, 75 (1974).
- [Win93] N. S. Wingreen, A.-P. Jauho, and Y. Meir. *Time-dependent transport through a mesoscopic structure*. Phys. Rev. B **48**, 8487 (1993).
- [Win13] N. Winkler, M. Governale, and J. König. *Theory of spin pumping through an interacting quantum dot tunnel coupled to a ferromagnet with time-dependent magnetization*. Phys. Rev. B **87**, 155428 (2013).
- [Wu08] B. H. Wu and J. C. Cao. *A Floquet-Green's function approach to mesoscopic transport under ac bias*. Journal of Physics: Condensed Matter (2008).
- [Zel67] Y. B. Zel'dovich. *The quasienergy of a quantum-mechanical system subjected to a periodic action*. Sov. Phys. JETP **24** 5 (1967).

List of Publications

- [1] A. K. Eissing, V. Meden, D. M. Kennes
'*Renormalization in Periodically Driven Quantum Dots*'
Phys. Rev. Lett. **116**, 026801 (2016)

- [2] A. K. Eissing, V. Meden, D. M. Kennes
'*Functional renormalization group in Floquet space*'
Phys. Rev. B **94**, 245116 (2016)

Curriculum Vitae

Anna Katharina Eissing

born on May 6th 1988 in Papenburg, Germany



Academic record:

07/2007	Abitur Gymnasium Papenburg, Germany
10/2007 – 07/2010	Bachelor Studies of Physics Ludwig-Maximilians-Universität, Germany
09/2008 – 02/2009	Bachelor Studies of Physics Universidad de Sevilla, Spain
04/2010 – 07/2010	Bachelor Thesis Institute for Experimental Quantum Physics, Ludwig-Maximilians-Universität, Germany <i>'Aufbau und Charakterisierung eines Lasersystems zur Ionisation von Rubidiumatomen'</i> Advisor: Harald Weinfurter
10/2010 – 04/2013	Master Studies of Physics Ludwig-Maximilians-Universität, Germany
01/2011 – 06/2011	Master Studies of Physics Stellenbosch University, South Africa Project thesis <i>'Polarons in a suspended nanotube'</i> Advisor: Izak Snyman
04/2012 – 04/2013	Master's Thesis Chair of Theoretical Solid State Physics, Ludwig-Maximilians-Universität, Germany <i>'Functional Renormalization Group Applied to a Multimode Quantum Point Contact'</i> Advisor: Jan von Delft
since 07/2013	Ph.D. studies Institut für Theorie der Statistischen Physik, RWTH Aachen University, Germany Advisor: Volker Meden

Thank You!

An dieser Stelle möchte ich mich bei den Menschen bedanken, die mich während meiner Doktorarbeit auf vielfältige Art und Weise unterstützt haben.

Zuerst sei mein Doktorvater Volker Meden genannt: Vielen Dank für die gute Betreuung, bei der ich das Gefühl hatte sehr selbstständig und frei arbeiten zu können, aber immer die Tür offen stand für Fragen.

Gleichermaßen danken möchte ich Dante Kennes für die vielen Stunden der Diskussion und der unendlichen Begeisterung, die er für die Probleme der theoretischen Physik zeigt und gerne teilt.

Außerdem möchte ich der ganzen Arbeitsgruppe danken für die herzliche Aufnahme in Aachen als ich gerade erst hergezogen war. Hier gilt mein Dank insbesondere meinen damaligen Bürokollegen Stefan Göttel und Dante Kennes: Für lange Debatten über Physik und die Welt, die unter anderem zur Entdeckung des Gödel Knödels und des van Eising Effekts führten (in einschlägiger Literatur auch als Eising Smiley zu finden). Ebenso sei auch der aktuellen Besetzung der Arbeitsgruppe für eine tolle Arbeitsatmosphäre gedankt.

Auch meinen Freunden bin ich dankbar für all die unterstützenden Worte, Abgabe- und Adventskalender für den Endspurt, für durchtanzte Nächte im Apollo, lange Spieleabende und ganz großartige WG-Parties. Meret, Ike, Kathi, Michi, Stefan, Felix, Alex, Jonas, Neni, Jennifer, Dante, Stefan, Andreas, Kristina, Tobi, Veronika, Theresa, Ana, Achim, Marlene, die Meiers, Sarah, Marie, Andreia, Buri, Sarah und Eddie.

Und schließlich, ganz besonders herzlich möchte ich meiner Familie danken: Meinen Eltern Manuela und Hans-Bernd Eissing, Marie-Lena und Philipp und Oma H. Danke, dass ihr so unerschütterlich an mich glaubt.

Erklärung

Hiermit erkläre ich eidesstattlich, dass ich die vorliegende Arbeit selbständig verfasst und dabei nur die angegebenen Quellen verwendet habe. Ferner erkläre ich, dass durch die Veröffentlichung der Arbeit keine Urheberrechte verletzt werden und dass ich bisher keine Promotionsanträge gestellt habe.

Aachen, den 1. März 2017